

AD-A197 632

THE THIRD CONFERENCE ON THE ENVIRONMENTAL CHEMISTRY OF HYDRAZINE FUELS

D.A. STONE, F.L. WISEMAN

HAZARDOUS MATERIALS TECHNICAL CENTER
P.O. BOX 8168
ROCKVILLE MD 20856-8168

JANUARY 1988

FINAL REPORT

15 SEPTEMBER 1987 - 17 SEPTEMBER 1987

DTIC
ELECTE
JUL 13 1988
S E D

APPROVED FOR PUBLIC RELEASE: DISTRIBUTION UNLIMITED



ENGINEERING AND SERVICES LABORATORY
AIR FORCE ENGINEERING AND SERVICES CENTER
TYNDALL AIR FORCE BASE, FLORIDA 32403

NOTICE

PLEASE DO NOT REQUEST COPIES OF THIS REPORT FROM
HQ AFESC/RD (ENGINEERING AND SERVICES LABORATORY).
ADDITIONAL COPIES MAY BE PURCHASED FROM:

NATIONAL TECHNICAL INFORMATION SERVICE
5285 PORT ROYAL ROAD
SPRINGFIELD, VIRGINIA 22161

FEDERAL GOVERNMENT AGENCIES AND THEIR CONTRACTORS
REGISTERED WITH DEFENSE TECHNICAL INFORMATION CENTER
SHOULD DIRECT REQUESTS FOR COPIES OF THIS REPORT TO:

DEFENSE TECHNICAL INFORMATION CENTER
CAMERON STATION
ALEXANDRIA, VIRGINIA 22314

1-2-87 632

REPORT DOCUMENTATION PAGE

Form Approved
OMB No. 0704-0188

1a. REPORT SECURITY CLASSIFICATION UNCLASSIFIED			1b. RESTRICTIVE MARKINGS		
2a. SECURITY CLASSIFICATION AUTHORITY			3. DISTRIBUTION/AVAILABILITY OF REPORT Approved for Public Release Distribution Unlimited		
2b. DECLASSIFICATION/DOWNGRADING SCHEDULE					
4. PERFORMING ORGANIZATION REPORT NUMBER(S) ESL-TR-87-74			5. MONITORING ORGANIZATION REPORT NUMBER(S)		
6a. NAME OF PERFORMING ORGANIZATION Hazardous Materials Technical Center		6b. OFFICE SYMBOL (If applicable)	7a. NAME OF MONITORING ORGANIZATION Defense Electronic Supply Center DESC-PSC		
6c. ADDRESS (City, State, and ZIP Code) P.O. Box 8168 Rockville, MD 20856-8168			7b. ADDRESS (City, State, and ZIP Code) 1507 Wilmington Pike Dayton, OH 45444-5208		
8a. NAME OF FUNDING / SPONSORING ORGANIZATION HQ AFESC		8b. OFFICE SYMBOL (If applicable) RDVS	9. PROCUREMENT INSTRUMENT IDENTIFICATION NUMBER Modification P00074 to Contract No. DLA900-82-C-4426		
8c. ADDRESS (City, State, and ZIP Code) HQ AFESC Tyndall AFB FL 32403-6001			10. SOURCE OF FUNDING NUMBERS		
			PROGRAM ELEMENT NO. 6.2 6.4	PROJECT NO. 1900 2054	TASK NO. 9999 9999
			WORK UNIT N/A N/A	ACCESSION NO. N/A N/A	
11. TITLE (Include Security Classification) The Third Conference on the Environmental Chemistry of Hydrazine Fuels					
12. PERSONAL AUTHOR(S) Daniel A. Stone and Floyd L. Wiseman					
13a. TYPE OF REPORT Proceedings		13b. TIME COVERED FROM 15Sep87 TO 17Sep87		14. DATE OF REPORT (Year, Month, Day) January 1988	
15. PAGE COUNT 320					
16. SUPPLEMENTARY NOTATION Availability of this report is specified on reverse of front cover.					
17. COSATI CODES			18. SUBJECT TERMS (Continue on reverse if necessary and identify by block number)		
FIELD	GROUP	SUB-GROUP	Hydrazine fuels; Gas Phase Kinetics, Models; Soil Studies;		
21	09	01	Matrix Isolation Studies; Disposal Studies; Detection;		
07	04		Monitoring; Toxicology. (inquiry) ←		
19. ABSTRACT (Continue on reverse if necessary and identify by block number)					
<p>The third conference on the environmental chemistry of hydrazine fuels consisted of the following five general sessions: gas-phase kinetics and models; soil, surface, and matrix isolation studies; hydrazine disposal studies; detection and monitoring; and toxicology. Researchers in these areas of hydrazine fuels chemistry gave short lectures and afterwards entertained questions. The plenary lecture, entitled "100 Years of Hydrazine Chemistry," was given by Dr Eckart W. Schmidt.</p> <p>The first session dealt with gas-phase kinetics and models and included results from studies of the atmospheric reactions of hydrazine fuels with atmospheric pollutants, decay studies in Teflon chambers, and the interaction of hydrazine fuels with metals and metal oxides. Results show that hydrazine in the vapor state does not react with oxygen at atmospheric conditions, but does react with commonly occurring pollutants, such as ozone, nitrogen oxides, and sulfur oxides. Hydrazine can be oxidized by certain metals and metal oxides, including aluminum and cupric oxide.</p>					
20. DISTRIBUTION/AVAILABILITY OF ABSTRACT <input checked="" type="checkbox"/> UNCLASSIFIED/UNLIMITED <input type="checkbox"/> SAME AS RPT. <input type="checkbox"/> DTIC USERS			21. ABSTRACT SECURITY CLASSIFICATION UNCLASSIFIED		
22a. NAME OF RESPONSIBLE INDIVIDUAL Daniel A. Stone			22b. TELEPHONE (Include Area Code) (904) 283-4298		22c. OFFICE SYMBOL AFESC/RDVS

The second session, soil, surface, and matrix isolation studies, dealt with hydrazine fuels interactions with soil constituents, mineral surfaces, aqueous solutions, and soil microbes, and included matrix isolation studies, soil transport, and fate modeling. These studies indicate that hydrazine fuels have a strong tendency to adsorb onto soil constituents and intercalate between clay mineral surfaces. Vibrational studies show there can be strong chemical interactions between hydrazine fuels and the polar functional groups on soil and mineral substances, as well as certain metals. Hydrazine fuels can degrade in aqueous media, the rate of degradation being dependent upon the presence of certain metal ions, the pH, the temperature, the presence of dissolved oxygen, the type of container used, and the presence of certain microbes.

The third session, hydrazine disposal studies, dealt with various chemical methods for disposing of hydrazine fuels. Studies show hydrazine fuels can be degraded by hypochlorite neutralization and ozonation. However, depending upon the reaction conditions, undesirable intermediates and products can be found, most notably nitrosamines. The degree to which these nitrosamines form depends upon pH and temperature, but cannot be eliminated entirely.

The fourth session, detection and monitoring, dealt with various chemical and analytical techniques for measuring low levels of vapor-phase hydrazines. Microsensors which depend upon pattern recognition techniques have been developed, as well as chemiluminescence methods. Chemical methods have been developed for measuring the concentration of hydrazine fuels in soils. A very sensitive photoacoustic detector has been developed for detecting ppb levels of vapor-phase hydrazine fuels.

The fifth session, toxicology, dealt with results of case studies and animal clinic studies for determining tolerable levels of vapor-phase hydrazine fuels in work areas. Results of these studies actually indicate that present EPA requirements for vapor-phase hydrazine fuels are probably too stringent. However, case studies are few and have not been followed up; hence, knowledge of the hazardous effects of hydrazine fuels on humans is sketchy.

Following the technical sessions, there was an informal panel discussion. Participants from each session were asked to give their recommendations for areas of future research on hydrazine fuels. These recommendations are summarized as the final section of the report.

PREFACE

This report was prepared by the Air Force Engineering and Services Center (AFESC), Engineering and Services Laboratory, Tyndall Air Force Base FL 32403-6001. The conference was sponsored by AFESC, with administrative support from the Hazardous Materials Technical Center, Dynamac Corp., P.O. Box 8168, Rockville, MD 20856-8168. Dr Daniel A. Stone and 1Lt Floyd L. Wiseman (AFESC/RDVS) were the government project officers. The report presents the proceedings of The Third Conference on the Environmental Chemistry of Hydrazine Fuels which was held at Panama City Beach, FL from 15 through 17 September 1987. The papers contained in this report are printed as submitted, without further editing.

This report has been reviewed by the Public Affairs Office and is releasable to the National Technical Information Service (NTIS). At NTIS, it will be available to the general public, including foreign nationals.

This technical report has been reviewed and is approved for publication.

Daniel A. Stone
DANIEL A. STONE, Ph.D.
Research Chemist

Floyd L. Wiseman
FLOYD L. WISEMAN, 1Lt, USAF
Chemistry R&D Project Officer

Kenneth T. Denbleyker
KENNETH T. DENBLEYKER, Maj, USAF
Chief, Environmental Sciences Branch

Thomas J. Walker
THOMAS J. WALKER, Lt Col, USAF, BSC
Chief, Environics Division

Lawrence D. Hokanson
LAWRENCE D. HOKANSON, Col, USAF
Director, Engineering and Services
Laboratory



Accession For	
NTIS GRA&I	<input checked="" type="checkbox"/>
DTIC TAB	<input type="checkbox"/>
Unannounced	<input type="checkbox"/>
Justification	
By	
Distribution/	
Availability Codes	
Dist	Avail and/or Special
A-1	

TABLE OF CONTENTS

Section	Title and Authors	Page
I	INTRODUCTION.....	1
II	PLENARY LECTURE.....	3
	ONE HUNDRED YEARS OF HYDRAZINE CHEMISTRY E. W. Schmidt, Rocket Research Company, Olin Defense Systems Group, Redmond, WA.....	4
III	GAS-PHASE KINETICS AND MODELS.....	17
1	ATMOSPHERIC CHEMISTRY OF THE FUEL HYDRAZINES E. C. Tuazon and W. P. L. Carter, Statewide Air Pollution Research Center, Univ. of California, Riverside, CA.....	18
2	SURFACE-CATALYZED AIR OXIDATION OF HYDRAZINES: ENVIRONMENTAL CHAMBER STUDIES Jan E. Kilduff and Dennis D. Davis, Lockheed-EMSCO, and Steven L. Koontz, NASA, White Sands Test Facility, Las Cruces, NM.....	38
3	AN ATMOSPHERIC PRESSURE FLOW REACTOR: GAS-PHASE KINETICS AND MECHANISM IN TROPOSPHERIC CONDITIONS WITHOUT WALL EFFECTS Steven L. Koontz, NASA, Dennis D. Davis and Merrill Hansen, Lockheed-EMSCO, White Sands Test Facility, Las Cruces, NM.....	50
4	THE BEHAVIOR OF HYDRAZINE VAPOR IN AN ENVIRONMENTAL CHAMBER UNDER SIMULATED ATMOSPHERIC CONDITIONS D. A. Stone and F. L. Wiseman, AFESC/RDVS, Tyndall AFB, FL.....	66
5	MODELING OF HYDRAZINE SURFACE INTERACTIONS IN ENVIRONMENTAL REACTION CHAMBERS F. L. Wiseman and D. A. Stone, AFESC/RDVS, Tyndall AFB, FL.....	76
6	TRACE METAL CATALYSIS OF HYDRAZINE DECOMPOSITION: THE ROLE OF CHROMIUM J. M. Bellerby, Royal Military College of Science, Shrivenham, England.....	86

TABLE OF CONTENTS
(Continued)

Section	Title and Authors	Page
IV	SOIL, SURFACE, AND MATRIX ISOLATION STUDIES.....	93
1	INTERACTION OF HYDRAZINES WITH COLLOIDAL CONSTITUENTS OF SOILS M. H. B. Hayes, K. Y. Chia, and T. B. R. Yormah Department of Chemistry, University of Birmingham, England.....	94
2	HYDRAZINE FATE AND TRANSFORMATIONS IN NATURAL WATERS AND SOILS J. J. Street and A. M. Moliner, Soil Science Department, Univ. of Florida, Gainesville, FL.....	108
3	VIBRATIONAL SPECTROSCOPIC STUDY OF THE KAOLINITE-HYDRAZINE INTERCALATION COMPLEX C. T. Johnston and L. A. Applewhite, Department of Soil Science, Univ. of Florida, Gainesville, FL, and D. A. Stone, AFESC/RDVS, Tyndall AFB, FL.....	118
4	SURFACE-CATALYZED AIR OXIDATION REACTIONS OF HYDRAZINES: TUBULAR REACTOR STUDIES Jan E. Kilduff and Dennis D. Davis, Lockheed-EMSCO, and Steven L. Koontz, NASA, White Sands Test Facility, Las Cruces, NM.....	128
5	A MATRIX ISOLATION FT-IR STUDY OF HYDRAZINE T. Tipton, W. B. Person, K. Kubulat, and M. Vala, Department of Chemistry, University of Florida, Gainesville, FL, and D. A. Stone, AFESC/RDVS, Tyndall AFB, FL.....	138
6	LOW-TEMPERATURE SPECTROSCOPY OF HYDRAZINE AND AMMONIA COMPLEXES WITH THE NEUTRAL TRANSITION METALS, Cu AND Fe M. Vala, M. Szczesniak, J. Szczepanski, and W. B. Person, Department of Chemistry, University of Florida, Gainesville, FL.....	145
7	A DIFFUSE REFLECTANCE INFRARED FOURIER TRANSFORM SPECTROSCOPIC STUDY OF ADSORBED HYDRAZINES Dennis D. Davis and Jan E. Kilduff, Lockheed-EMSCO, and Steven L. Koontz, NASA, White Sands Test Facility, Las Cruces, NM.....	154
8	THE SOIL MICROBIOLOGY OF HYDRAZINES L.-T. Ou and J. J. Street, Soil Science Department, University of Florida, Gainesville, FL.....	167

TABLE OF CONTENTS
(Continued)

Section	Title and Authors	Page
9	NUMERICAL SIMULATION OF HYDRAZINE TRANSPORT IN A SANDY SOIL R. S. Mansell, S. A. Bloom and W. C. Downs, Soil Science Department, University of Florida, Gainesville, FL.....	177
V	HYDRAZINE DISPOSAL STUDIES.....	191
1	THE CHEMISTRY OF THE HYPOCHLORITE NEUTRALIZATION OF HYDRAZINE FUELS Kenneth L. Brubaker, Argonne National Laboratory, Argonne, IL.....	192
2	OZONATION OF HYDRAZINES AND THEIR ASSOCIATED IMPURITIES B. Jody and P. Kosenka, IIT Research Institute, Chicago, IL, S. Lewis, H. Takimoto, and H. Judeikis, Aerospace Corp., Los Angeles, CA, and J. Petschard, USAF Space Division, Los Angeles, CA	202
3	MODELING THE OZONOLYSIS OF HYDRAZINES WASTEWATER H. S. Judeikis, The Aerospace Corporation, Los Angeles, CA.....	216
4	FUEL NEUTRALIZATION BY OZONE OXIDATION A. B. Swartz, R. E. Agathe, I. D. Smith, and J. P. Mulholland, Lockheed-EMSCO, White Sands Test Facility, Las Cruces, NM.....	225
VI	DETECTION AND MONITORING.....	243
1	MICROSENSOR AND PATTERN RECOGNITION TECHNIQUES IN HYDRAZINE DETECTION S. L. Rose-Pehrsson and J. W. Grate, Naval Research Laboratory, Washington, DC.....	244
2	HYDRAZINE DOSIMETRY P. A. Taffe, J. H. Callahan, and K. P. Crossman, GEO-CENTERS, INC., Ft. Washington, MD, and S. L. Rose-Pehrsson, Naval Research Laboratory, Washington, DC.....	252
3	DESCRIPTION OF A CHEMILUMINESCENCE DETECTOR SYSTEM SPECIFICALLY DESIGNED FOR MONITORING AIRBORNE HYDRAZINE AND OXIDIZER PROPELLANT VAPORS F. Fraim, D. Rounbehler, J. Buckley, and P. Nama, Thermedics, Inc., Woburn, MA.....	261

TABLE OF CONTENTS
(Concluded)

Section	Title and Authors	Page
4	MEASUREMENT OF HYDRAZINE CONTAMINATION IN SOILS C. S. Leasure and E. L. Miller, Lockheed-EMSCO, White Sands Test Facility, Las Cruces, NM.....	276
5	LOW PPB LEVEL DETECTION OF TOXIC COMPOUNDS WITH A FULLY AUTOMATED CO ₂ LASER PHOTOACOUSTIC DETECTOR S. M. Beck, M. L. Takayama, R. L. Corbin, and G. L. Loper, The Aerospace Corporation, Los Angeles, CA.....	286
VII	TOXICOLOGY.....	299
1	OCCUPATIONAL SAFETY CONSIDERATIONS WITH HYDRAZINE Harvey J. Clewell, III, James N. McDougal, Marilyn E. George, and Melvin E. Andersen, Aerospace Medical Research Laboratory, Wright-Patterson AFB, OH.....	300
VIII	RECOMMENDATIONS FOR FUTURE RESEARCH.....	309

SECTION I

INTRODUCTION

A. OBJECTIVE

The objective of this technical report is to provide a summary of the main areas of research relating to the environmental chemistry of hydrazine fuels. It is not intended to be an exhaustive review of all such research, but rather is designed to acquaint both scientist and manager with some of the key issues and research in this unique field.

B. BACKGROUND

Since its inception as a separate organizational branch at Kirtland AFB, NM, the environmental chemistry research group, now located at the Air Force Engineering and Services Center (AFESC), Tyndall Air Force Base, FL, has been involved in research concerning the environmental fate and effects of hydrazine fuels. In the interest of promoting the exchange of engineering and fundamental research results among those who are involved with hydrazine fuels, AFESC has sponsored three conferences on the environmental chemistry of these fuels. This technical report contains the papers presented at the third, and most recent of these conferences.

This third conference was designed to cover all of the major areas of interest of those who use hydrazines as fuels. Consequently it addressed the environmental issues associated with these fuels. It was divided into an overview, plenary lecture and five technical sessions which ran in sequence.

C. SCOPE

The conference covered a range of topics. It began with a plenary lecture noting the discovery and uses of hydrazines in the past 100 years. This was followed by technical presentations in five general areas: (1) Gas-phase kinetics and models, (2) Soil, surface, and matrix isolation studies, (3) Hydrazine disposal studies, (4) Detection and Monitoring, and, (5) Toxicology. The conference was concluded with a panel discussion where recommendations for future research were discussed and noted for each area.

SECTION II
PLENARY LECTURE

ONE HUNDRED YEARS OF HYDRAZINE CHEMISTRY

E. W. Schmidt, Senior Staff Scientist
Rocket Research Company, Olin Defense Systems Group
11441 Willows Rd. N.E., Redmond, WA 98052-1012

ABSTRACT

During the hundred years since the discovery of hydrazine by T. Curtius in 1887, hydrazine has developed into a useful rocket propellant and industrial chemical. Likewise, many organic hydrazine derivatives (some of which actually were known to chemists prior to the discovery of the parent compound hydrazine itself), have come to be used as rocket propellants and industrial intermediates. Like many other household and industrial chemicals, hydrazine and its derivatives are potentially hazardous and the occupational hygiene and environmental safety of hydrazines require careful study.

Hydrazine itself, the major topic of this paper, has found application as a rocket propellant and gas generant for aerospace and marine applications, boiler feed water additive, chemical intermediate for plastic foam blowing agents, pesticides, and pharmaceutical products. It can serve as a source of energy in rockets, airplanes, submarines, and fuel cells.

Whereas it was initially thought that environmental problems with hydrazines were unique to man-made synthesized hydrazines, it has been only recently recognized that certain hydrazines, including one used as rocket propellant, are naturally occurring in glucosidic bonds in mushrooms. The implications of this discovery require additional study.

1. INTRODUCTION

This paper is not so much a year-by-year account of the history of hydrazine chemistry as it tries to put current hydrazine applications in perspective. Therefore, more emphasis is placed on the most recent decades of hydrazine usage. Also, with the professional background of the author being,

in hydrazine applications and not as a full-time occupational hygienist and environmental safety officer, this paper will emphasize the key position played by hydrazines as fuels in the current space program and offer means how safety questions can be addressed with adequate levels of priority. The current status of hydrazine chemistry has been sufficiently summarized in the literature (Reference 1).

2. HYDRAZINE FUELS

It may be very useful at this point to provide a summary of rocket and gas generator applications of hydrazines. Rocket applications are as bipropellant fuels and as monopropellants in catalytic and electrothermal rocket engines. Gas generator applications are for auxiliary power in the Space Shuttle Auxiliary Power Unit (APU) and for emergency power in the F-16 fighter.

The hydrazine fuels of interest as rocket propellants and gas generators include:

Hydrazine, N_2H_4

Methylhydrazine, CH_3NHNH_2 ("Monomethylhydrazine, MMH")

1,1-Dimethylhydrazine, $(CH_3)_2NNH_2$ ("unsymmetrical dimethylhydrazine, UDMH")

In this paper, we refer to this group of chemicals in the plural case, "hydrazines". In terms of total quantity produced, UDMH may actually outweigh the amount of anhydrous hydrazine, in particular if the total quantity is summed up worldwide. It must be emphasized that, although there are far more publications on the toxicity of 1,2-dimethylhydrazine ("SDMH") in the literature of the past decade than on all other hydrazines combined, symmetrical dimethylhydrazine is not used as a rocket propellant and there are no known industrial uses of this chemical. The toxic nature of the various hydrazines is sufficiently different that hydrazines as a group should not be summarily judged by the highly toxic (in this case carcinogenic) properties of one of its members. It may be difficult to justify additional work on SDMH only because its isomer happens to be used as a rocket propellant.

3. PRODUCTION OF HYDRAZINE PROPELLANTS

The processes for the production of hydrazine fuels are summarized in Table 1.

TABLE 1 METHODS FOR PRODUCTION OF HYDRAZINES.

Designation	Formula	Abbreviation	Method of Manufacture
Hydrazine (anhydrous) by way of hydrazine hydrate	N_2H_4	AH	Raschig process. Ketazine process. Peroxide process.
Methylhydrazine ("Monomethylhydrazine")	$H_3C-NH-NH_2$	MMH	Raschig process with methylamine
1,1-Dimethylhydrazine	$(H_3C)_2N-NH_2$	UDMH	Reduction of N-nitrosodimethylamine. Raschig process with dimethylamine. Reductive methylation of acethydrazide.

After hydrazine hydrate was discovered in 1887, it remained a laboratory curiosity for a long time and not very many applications for it were known for several decades afterwards. The first sample of anhydrous hydrazine was prepared by Lobry DeBruyn in 1893. The method for preparation of hydrazine hydrate by the Raschig process was discovered in 1907 and cleared the way for the production of hydrazine hydrate in industrial quantities. In some installations and with a few process modifications, the Raschig process is still used nowadays for preparation of hydrazine hydrate. The majority of hydrazine hydrate is now prepared by the ketazine process.

Hydrazine starts its life cycle as hydrazine hydrate which contains only 64% hydrazine, and has to be dehydrated to 99+% N_2H_4 to be useful as a rocket propellant. The dehydration is now achieved in industrial quantities by azeotropic distillation with aniline as an auxiliary fluid.

MMH and UDMH are now made in the USA by a modified Raschig process. For the production of UDMH, this avoids the use of the very toxic dimethyl-nitrosamine (N-nitrosodimethylamine) as an intermediate as was done in the fifties and sixties until the carcinogenic hazards of this intermediate became better known.

When examining the change of the use pattern of hydrazine (hydrate) in the United States from 1964 to 1982 (Figure 1), it becomes apparent that whereas more than half of all hydrazine was used as a rocket propellant in the 60's, in the meantime many other industrial applications are taking the major share of all hydrazine (hydrate) produced. For the occupational hygiene and environmental safety community that means that whereas in the sixties the handling of hydrazine could have been considered a potential problem mostly

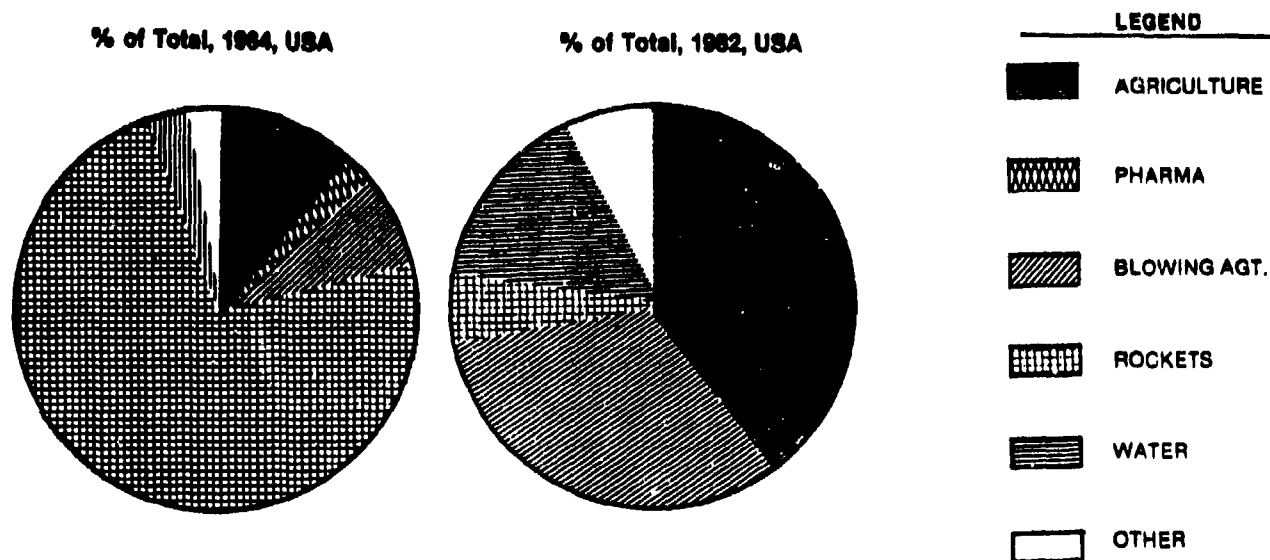


Figure 1. Shift of Hydrazine Use Pattern from 1964 to 1982, U.S.A.

for the armed forces, in the meantime many other industrial users have learned how to handle hydrazine safely (although some use it only as a dilute aqueous solution or as an intermediate in the preparation of other chemicals).

During the same time period, from 1964 to 1982, the worldwide production of hydrazine (as measured by installed capacity) has more than doubled (Figure 2). As can be seen from this figure, the USA still has a lead in installed capacity, but other countries have been increasing their share of the world market.

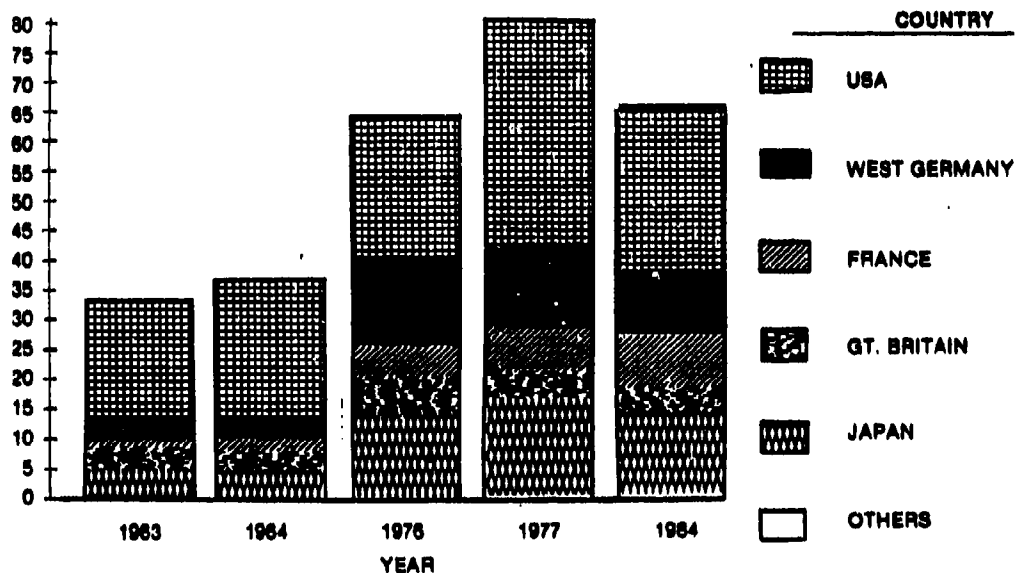


Figure 2. Chronological Evolution of Installed Hydrazine Hydrate Capacity; Noncommunist Countries, Expressed as Million lbs N_2H_4

4. USE OF HYDRAZINES AS ROCKET PROPELLANTS

4.1 MONOPROPELLANTS AND BIPROPELLANTS

When reviewing the uses of hydrazine as a rocket propellant, one must recognize the difference between hydrazine use as a monopropellant and as a bipropellant. In a monopropellant system, as illustrated in Figure 3, hydrazine by itself is injected into a reaction chamber and its decomposition is initiated by contact with a catalyst. Hydrazine is an exothermic compound

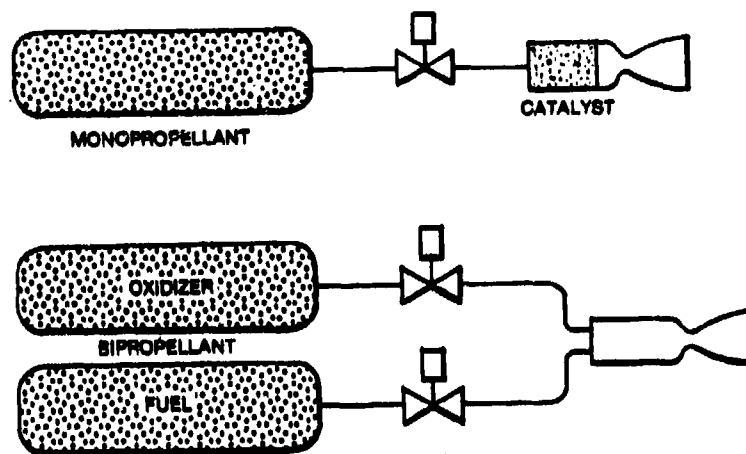


Figure 3. Schematic of Hydrazine Monopropellant and Bipropellant Systems.

that can decompose spontaneously and many of its handling hazards are caused by this property. In bipropellant systems, such as those used in the Orbital Maneuvering System (OMS) on the Space Shuttle, a hydrazine fuel (MMH) is injected simultaneously with an oxidizer and ignition takes place on contact of the two hypergolic fluids. Bipropellant systems are typically used where total impulse requirements are high. For small impulse requirements, such as for attitude control and orbit maintenance of satellites, monopropellant systems are lighter and more reliable because they require only a single tank, a single pressurization system, and a single control valve, whereas the dry weight of a bipropellant system with dual sets of tanks and flow controls would be less favorable. However, the specific impulse of monopropellant hydrazine is lower than that of bipropellant combinations. Whereas the specific impulse of monopropellant hydrazine is typically 2313 N s/kg ($236 \text{ lb}_f \text{ s/lb}_m$), that of bipropellant combinations (NTO/MMH) is 38% higher.

As a means of increasing the specific impulse beyond that of hydrazine, and also in order to widen the liquid range (hydrazine has an undesirably high freezing point, like water), additives have been added to hydrazine resulting in the formation of hydrazine blends. New hydrazine blends that are currently being tested are those containing hydrazinium nitrate and water.

In the case of the Aerozine-50 blend, UDMH was added to hydrazine to make it safe to use as a regenerative coolant and to lower its freezing point. This blend is only used as a bipropellant fuel.

4.2 HISTORY OF HYDRAZINE USE AS A ROCKET PROPELLANT

The evolution of hydrazine as an industrial chemical has been closely tied to its use as a rocket propellant. As far as we can trace it back, the first recorded use of hydrazine hydrate as a rocket propellant was in a rocket plane, the Me-163B, in Germany in 1937. A mixture of hydrazine hydrate and methanol was used as a hypergolic fuel with hydrogen peroxide as the oxidizer in a bipropellant rocket engine. The mixture consisted of 30% hydrazine hydrate, 57% methanol and 13% water and the code-name for it was "C-Stoff". The large-scale production of hydrazine hydrate as part of the German war effort opened the way to other industrial uses of hydrazine and hydrazine chemicals. The first use of anhydrous hydrazine as a monopropellant was demonstrated at the Jet Propulsion Laboratory in Pasadena in 1954 and the first production of anhydrous hydrazine started in the United States in the late 50's. Hydrazine production capacity in the U.S. saw an enormous increase in the 60's when a 50:50 blend of UDMH and hydrazine was used to fuel the TITAN-II and TITAN-III missiles and satellite launchers.

For hydrazine monopropellant use, a key milestone was the development of the Shell 405 catalyst under a contract from NASA-Jet Propulsion Laboratory in 1963. This spontaneous catalyst allowed almost unlimited restart capability and opened the way for new hydrazine applications. As a result, most military, commercial and scientific satellites in earth orbit now use hydrazine propulsion systems for attitude control and orbit maintenance (stationkeeping for GEO).

4.2.1 Satellites

Figure 4 shows a chronology of unclassified satellites launched carrying hydrazine and a breakdown of the total number by satellite task. The most pronounced growth is in the area of commercial communication satellites and this trend is expected to continue with the advent of direct broadcast satellites that allow reception of TV signals with parabolic dish antennas small enough not to constitute an eyesore to your neighborhood backyard. Some of these antennas may even fit indoors on top of the TV console.

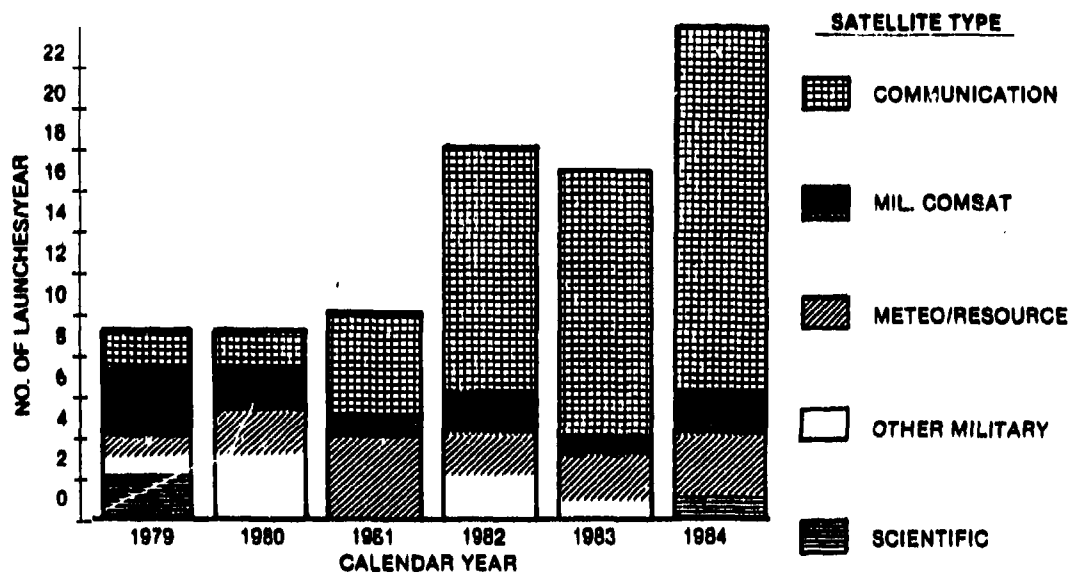


Figure 4. Satellites Launched Carrying Hydrazine, 1979 through 1984.

4.2.2 Spaceprobes

Many of the spectacular unmanned space missions have used hydrazine propulsion. The more successful ones include the Viking landers on Mars, the Pioneer and Voyager spaceprobes to Jupiter, Saturn, and Uranus, and the Giotto space probe to the comet Halley.

4.2.3 Upper Stages

In addition to satellites, hydrazine thrusters are used extensively for upper stage propulsion, either for nutation control, thrust centralization during solid rocket motor burns or for impulse corrections after the solid rocket motor burn is complete and for circularization of the interim orbits. Upper stages of satellite launch vehicles using hydrazine thrusters are Transtage, IUS, PAM-D, Voyager TJI and more recently also TITAN-II, Centaur and OMV. In the strategic arena, hydrazine thrusters are to be used for post-boost propulsion on the Small ICBM third stage and on a foreign submarine-launched missile.

4.3 ELECTRIC ROCKET PROPULSION USING HYDRAZINE

In a more recent development, the use of hydrazine has been expanded beyond the simple catalytic decomposition by augmenting the energy of hydrazine decomposition products with resistojet or arcjet heaters. Whereas the specific impulse of conventional catalytic thrusters was of the order of 2313 N s/kg (236 lb_f s/lb_m), it was possible to increase this to 3335 N s/kg (340 lb_f s/lb_m) for resistance-heated augmentors and to 7100 N s/kg (730 lb_f s/lb_m) for arc-heated augmentors. Augmented catalytic thrusters (ACT) of the resistojet type are already in flight use on 5 commercial spacecraft and many more are planned. Similar resistojets (HIPEHT) using electrothermal instead of catalytic hydrazine decomposition were used on a number of INTELSAT-V spacecraft. Hydrazine arcjets are still under development and have so far not yet found flight applications. A NASA-sponsored arcjet flight experiment is planned for late 1990 on a commercial satellite.

5. HYDRAZINE GAS GENERATOR APPLICATIONS

Current hydrazine gas generator applications are for rotary power and for pneumatic power. For rotary power, anhydrous hydrazine is used in the Auxiliary Power Unit (APU) on both the Space Shuttle orbiter and on the two Solid Rocket Boosters (SRBs). As shown in Figure 5, there are three gas generators on the orbiter vehicle and two gas generators on each SRB. Hydrazine decomposition gases at very high pressures are capable of expelling ballast water from submarine ballast tanks in emergency situations. Such systems are now in use on several NATO submarines. Hydrazine systems weigh only a fraction of comparable compressed gas systems.

6. FUTURE APPLICATIONS OF HYDRAZINE FUELS

The current use pattern for hydrazine fuels is likely to continue for at least another decade. Although electric propulsion systems (e.g., ion thrusters without the use of hydrazine) are being developed that offer specific impulses an order of magnitude better than monopropellant hydrazine, these electric thrusters are not likely to replace monopropellant hydrazine or bipropellant NTO/MMH in their current applications.

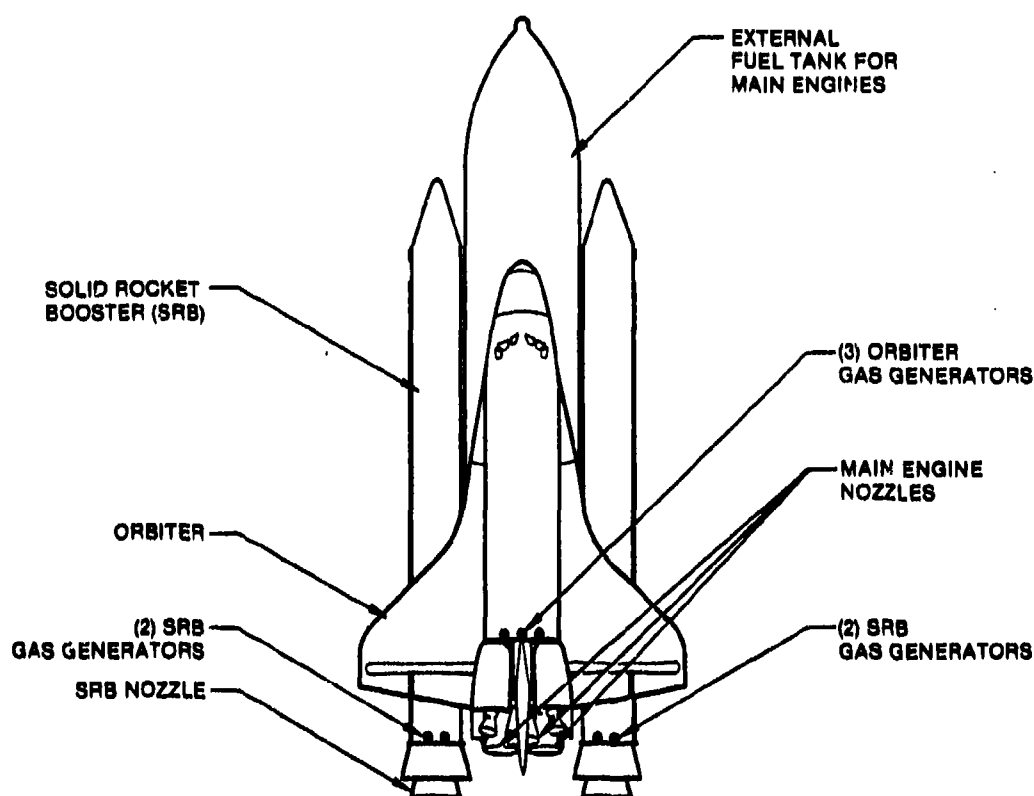


Figure 5. Location of Hydrazine Gas Generators on Space Shuttle Vehicle.

7. ENVIRONMENTAL CHEMISTRY OF HYDRAZINE FUELS

The main topic of the current conference is the environmental chemistry of hydrazine fuels. There is an impressive amount of work being presented at this conference dealing with the occupational hygiene and environmental safety of hydrazine fuels. This work is all very desirable in order to better understand the environmental ramifications of hydrazine fuels and to arrange for the safe disposal of these chemicals. However, as several of the studies will show, hydrazines are not very persistent and are readily detoxified in the environment. As such, they are in a totally different category compared to chlorinated pesticides or PCB transformer oils. We consider it important that this difference be made public when reports on occasional incidents involving spills of hydrazines are released to the news media.

8.1 OCCUPATIONAL HYGIENE AND EPIDEMIOLOGICAL STUDIES OF HYDRAZINE WORKERS

Based on animal test data published to date, it appears that the response to hydrazine and methylhydrazines is very much dependent on the path of ingestion. Typical animal feeding studies with hydrazine in the drinking water cannot truly simulate the common industrial exposure condition where the most likely path of ingestion is by inhalation. In spite of the thousands of animals exposed to hydrazine by all paths of administration, the carcinogenicity of hydrazine itself for humans is not clearly proven and still subject of discussion. It is currently listed as an "animal carcinogen" and "suspected carcinogen" on the A2 list of the American Conference of Governmental Industrial Hygienists (ACGIH) Threshold Limit Value (TLV) booklet (Reference 2). It has been proposed to classify it as a "weak animal carcinogen".

Repeated epidemiological studies of workers routinely exposed to hydrazine vapors at the place of employment have failed to reveal any increased incidence of any form of cancer or any abnormal mortality in the group of workers tested (Reference 3). It is recommended that such studies be continued and updated periodically. The difficulty with industrial exposure and worker epidemiological studies is that the workers are usually exposed to more than one chemical in the course of their career. Nevertheless, if hydrazine was as hazardous as some try to make it appear, adverse health effects would have shown up in workers even with shorter periods of exposure and at lower concentrations than those routinely tolerated in the early years of hydrazine industrial usage (Reference 4).

8.2 SIGNIFICANCE OF HERP INDEX IN HAZARD EVALUATION

We all have been frustrated by the inability of extrapolating from animal tests to human exposure and by the difficulty of setting human exposure limits based on animal test data.

A recent publication by the renowned biochemist Bruce Ames (Reference 5) introduces a new index for the assessment of carcinogenic risks in the environment. The Human Exposure dose/Rodent Potency dose ratio (HERP) can be

of value when discussing industrial exposure versus exposure that exists naturally as part of the human environment. The HERP is expressed as the ratio of human exposure to the daily dose rate TD_{50} that is capable of cutting in half the number of tumor-free animals at the end of a standard lifetime. Ames cautions that "It would be a mistake to use our HERP index as a direct estimate of human hazard". However, lacking any other more accurate method and lacking many of the animal test data needed to complete the HERP evaluation, the HERP method should be applied to hydrazines as well and we hope that someone will submit a paper on this subject at one of the future hydrazine environmental conferences. Likewise, the significance of hydrazine derivatives in crop residues of growth retardants should be compared to other sources of hydrazines.

8.3 RECOMMENDATIONS

The occupational hygiene and environmental safety scientific community is fortunate to have found a sponsor in the NASA and Armed Services laboratories and to receive continued funding. If one summarized all funding devoted to toxicity and environmental questions of hydrazines, that number would be a multiple of funding devoted to all other properties of hydrazine combined. Why is that so? It appears that toxicity has gained a disproportionate amount of attention. What has been overlooked is that hydrazines as energetic chemicals are inherently dangerous and to this date many of the engineering safety properties (e.g., adiabatic compression, vapor detonations, electrostatic discharge sensitivity, thermal stability, corrosion) have been insufficiently investigated to allow a complete evaluation of handling hazards. Although the probability of accidents is very low, chances are that in the coming decades more propellant handling personnel will be injured through mechanical and engineering malfunctions involving hydrazine than through intoxication. What is needed is a hydrazine fuels engineering property and handling safety research program to complement the excellent work that has been done on hydrazines toxicity. The engineering property program should be on an equal footing with the toxicity effort in terms of funding and centralized coordination. The result of such an effort could be a hydrazine fuels handling and design safety manual that would be made available to all propulsion system designers and flight test and propellant handling personnel.

REFERENCES

1. Schmidt, E. W., Hydrazine and Its Derivatives, Wiley Interscience, New York, ISBN 0-471-891170-3, 1984.
2. American Conference of Governmental Industrial Hygienists, Threshold Limit Values for 1986-1987, Cincinnati, OH, 1986, ISBN 0-936712-69-4.
3. Roe, F. J. C., "Hydrazine", Ann. Occup. Hyg., vol. 21, pp. 323-326, 1978.
4. Wald, N., et al., "Occupational Exposure to Hydrazine and subsequent Risk of Cancer", Brit. J. Ind. Med., vol. 41, pp. 31-34, 1984.
5. Ames, B. N., R. Magaw, and L. S. Gold, "Ranking Possible Carcinogenic Hazards", Science, 17 April 1987, pp. 271-280.

SECTION III

GAS-PHASE KINETICS AND MODELS

ATMOSPHERIC CHEMISTRY OF THE FUEL HYDRAZINES

E. C. Tuazon, Research Chemist, and W. P. L. Carter, Research Chemist
Statewide Air Pollution Research Center
University of California
Riverside, CA 92521

ABSTRACT

Selected gas phase reactions of hydrazine (N_2H_4), monomethyl hydrazine (MMH), and unsymmetrical dimethyl hydrazine (UDMH) have been investigated under simulated atmospheric conditions in ~3800 and 6400-liter Teflon® reaction chambers by FT-IR spectroscopy. Their reactions with ozone and nitrogen dioxide were extensively studied, and data were also obtained concerning their reactions with formaldehyde and nitric acid. The results of these experiments are summarized, and possible mechanisms for the reactions of these hydrazines with O_3 and NO_2 are discussed.

INTRODUCTION

Hydrazine (N_2H_4) and its alkyl derivatives, monomethylhydrazine (MMH) and 1,1-dimethylhydrazine (unsymmetrical dimethylhydrazine or UDMH) are employed in large quantities as fuels for military and space propulsion systems. Information concerning their atmospheric transformations is essential in evaluating the possible adverse impact of their releases into the atmosphere stemming from storage, transfer, and venting operations.

Photolysis and reactions with O_3 and the OH radical are the major chemical loss processes of most compounds released into the clean atmosphere, with reactions with species such as NO_x , HNO_3 , $HCHO$, etc., being additional possible removal routes in the case of a polluted troposphere (Reference 1). For the fuel hydrazines, photolysis is not expected to be an important atmospheric removal process since these compounds do not significantly absorb in the actinic region (>290 nm), but the other atmospheric loss processes should be considered.

In exploratory investigations of the atmospheric reactions of the fuel hydrazines, we utilized in situ long-pathlength Fourier transform infrared (FT-IR) spectroscopy in environmental chamber simulations (References 2-4) and a flash photolysis-resonance fluorescence technique (Reference 5) to investigate the gas-phase reactions of these compounds, and observed that they react very rapidly with O_3 (References 2-4) and the OH radical (Reference 5). More recently, we carried out more detailed studies in large-volume environmental chambers at parts-per-million concentrations of the reactants in an effort to determine the products, rates, and salient features of the mechanisms of the gas-phase reactions of these hydrazines with O_3 , OH radical, NO_x (NO and NO_2), as well as with HNO_3 and $HCHO$ (Reference 6). This paper gives a summary of results from this more recent research.

EXPERIMENTAL

All experiments were carried out in environmental chambers constructed from 50- μm thick Dupont FEP Teflon® film, heat-sealed at the seams, and held semirigidly inside rectangular aluminum frames. Provisions for injection and sampling of gases consisted of glass tubes with sealed fittings and a Teflon® disperser tube. Teflon®-coated fans were used for initial mixing of the reactants. Initial experiments were conducted in an ~6400 L chamber (Figure 1); later experiments were carried out in a similar but smaller ~3800 L chamber. Known pressures of the reactants in calibrated 2 L and 5 L bulbs were flushed into the chamber with measured flows of N_2 and stirred. The mixing time was ≤ 30 seconds for either chamber size, which was limited more by the speed of sample injection than by the efficiency of the mixing fan.

All reactants and products were monitored in situ by FT-IR spectroscopy at pathlengths of ~68-102 m. The 2.13-m basepath White optical system housed in the chamber consisted of gold-coated mirrors with Teflon®-coated mounting hardware. The FT-IR spectrometer employed a liquid- N_2 -cooled HgCdTe detector to monitor the 700-3000 cm^{-1} region of interest. All spectra were recorded at 1 cm^{-1} resolution. Each spectral record consisted of 6 to 64 averaged scans, with midpoint times of 0.1 to 0.8 min, respectively, depending upon the speed of the reaction being monitored.

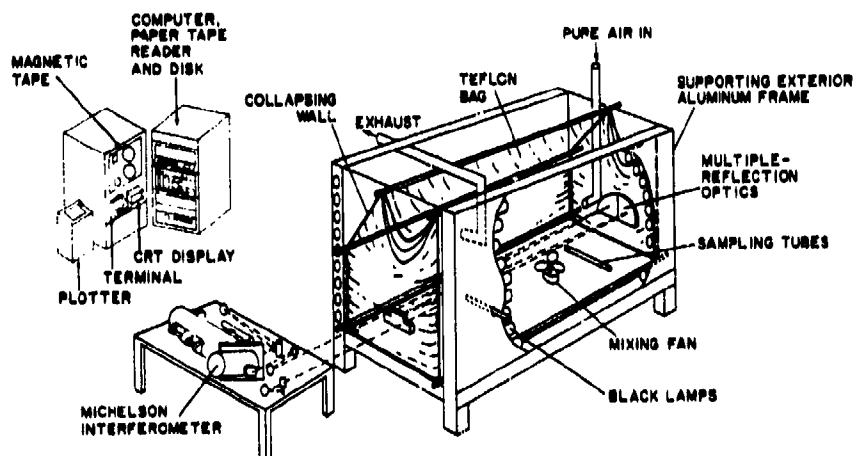


Figure 1. Schematic Diagram of the ~6400 L Teflon® Reaction Chamber with Long Pathlength FT-IR Spectrometer.

RESULTS

THE REACTIONS OF HYDRAZINES WITH OZONE

The reactions of ozone with the fuel hydrazines were studied in air at low relative humidities (<25%), at 20-25°C and ~740 torr total pressure under conditions of excess hydrazine, near equimolar reactant concentrations, and excess ozone. The initial reactant concentrations ranged from ~4 to ~20 ppm. To investigate the participation of OH radicals in the ozone + hydrazine reactions, additional experiments were carried out in the presence and absence of ~270 ppm of n-octane as a "radical trap" to suppress OH radicals. Separate runs were conducted with ~0.2 ppm each of n-octane and hexamethylethane present as "tracers" to obtain integrated OH radical levels from the relative rates of their disappearance, as monitored by GC techniques. The low amounts of the tracers had no effect on the hydrazine and ozone reaction rates and the products formed.

Results of the Hydrazine + Ozone Experiments

The results of the $\text{N}_2\text{H}_4 + \text{O}_3$ experiments are summarized in Table 1. The major products were hydrogen peroxide (H_2O_2) and diazene (N_2H_2), though small increases in the levels of the ammonia (NH_3) impurity were observed during the course of the reactions, and nitrous oxide (N_2O) was observed as a minor product in the runs without the radical trap. Representative reactant and product spectra are shown in Figures 2 and 3.

TABLE 1. SUMMARY OF RESULTS OF THE $\text{N}_2\text{H}_4 + \text{O}_3$ CHAMBER EXPERIMENTS WITH AND WITHOUT RADICAL TRAPS.

		Excess N_2H_4	Equimolar	Excess O_3
Initial Concentration (ppm)				
N_2H_4		16	10	4
O_3		4	10	16
Apparent $k(\text{O}_3 + \text{N}_2\text{H}_4)$ ($\text{ppm}^{-1} \text{ min}^{-1}$)				
	No Trap	0.09		>0.4
	Trap	0.06		0.04
Yield/ $\Delta[\text{N}_2\text{H}_4]$				
$-\Delta[\text{O}_3]$	No Trap	0.8	1.0	1.4
	Trap	1.0	1.4	1.9
$[\text{H}_2\text{O}_2]$	No Trap	0.6	0.5	0.4
	Trap	0.2	0.08	<0.04
$[\text{N}_2\text{H}_2]$	No Trap	0.7	0	0
(Absorbance/ppm) ^a	Trap	0.4	0	0
Integrated [OH] (10^{-6} ppm-min)				
	No Trap	0.7	2.5	4.9

^aAbsorbance of the 1276.7 cm^{-1} Q branch at 1 cm^{-1} resolution and 68.3 meter path.

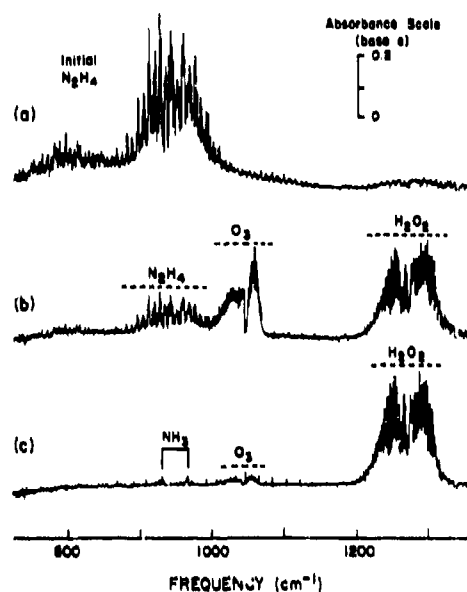


Figure 2. Spectra from an $\text{N}_2\text{H}_4 + \text{O}_3$ Equimolar Run. (a) Initial N_2H_4 , (b) Mixture at $t=1.4$ min, (c) Mixture at $t=20.8$ min.

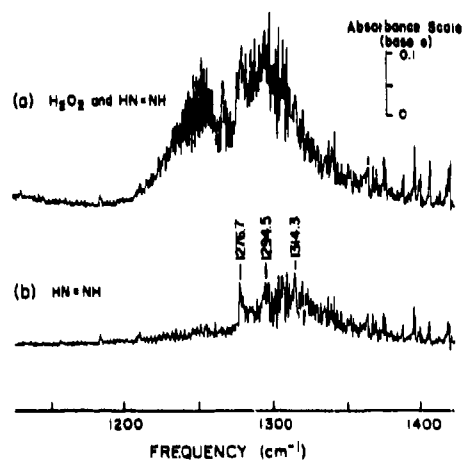


Figure 3. Detection of Diazene in $\text{N}_2\text{H}_4 + \text{O}_3$ Run with Excess Hydrazine. (a) Products at $t=1.4$ min, (b) $\text{HN}=\text{NH}$ Spectrum after Subtraction of H_2O_2 Absorptions.

Table 1 shows that the hydrazine-ozone stoichiometry and the product yields were affected by the initial reactant ratio. As the initial $[O_3]/[N_2H_4]$ reactant ratio increased, the amount of O_3 consumed per N_2H_4 reacted increased, and the relative yield of N_2H_2 decreased markedly. The N_2H_2 remained at the end of the reaction only in the excess hydrazine runs, and was observed as a transient intermediate at very low levels in the equimolar runs and the excess O_3 runs. In addition, when O_3 was added to a reacted mixture already containing N_2H_2 , the latter species rapidly disappeared, indicating a fast reaction between O_3 and N_2H_2 . The H_2O_2 yields were far less sensitive to the initial $[O_3]/[N_2H_4]$ ratio in the runs without the radical trap than in experiments with the radical trap present.

The sets of experiments with added radical tracers and radical traps both indicated the role of OH radicals in the $O_3 + N_2H_4$ reaction. The tracer data showed an increase in the integrated OH levels with increasing initial $[O_3]/[N_2H_4]$. The presence of the radical trap resulted in more O_3 consumed per N_2H_4 reacting, in significantly lower H_2O_2 yields, and in lower apparent rates of reaction, as measured by the O_3 decay rate in the presence of excess N_2H_4 or the N_2H_4 decay rate in excess O_3 . The radical trap had the greatest effect on the product yields and reaction rates in the experiments with excess O_3 , which is consistent with the higher integrated OH levels indicated by the tracer data under those conditions.

Results of the MMH + Ozone Experiments

The results of the MMH + O_3 experiments are summarized in Table 2. The major products observed were CH_3OOH , CH_3NNH , $HCHO$, CH_2N_2 , and H_2O_2 , with lower yields of CH_3OH , CO , and $HCOOH$; traces of NH_3 and N_2O were also formed. Representative spectra are shown in Figure 4.

The results in Table 2 show that, as in the $N_2H_4 + O_3$ system, the reactant stoichiometry and the products formed in the MMH + O_3 system depended on the ratio of initial reactants and on the presence of radical traps. Indeed, within the experimental uncertainties the relative amounts of hydrazine and ozone consumed were in most cases essentially the same as those in analogous $N_2H_4 + O_3$ experiments. The yields of CH_3NNH (like its analogue, N_2H_2 , formed

TABLE 2. SUMMARY OF RESULTS OF THE MMH + O₃ CHAMBER EXPERIMENTS WITH AND WITHOUT RADICAL TRAPS.

		Excess MMH	Equimolar	Excess O ₃
Initial Concentration (ppm)				
	MMH	18	10	4
	O ₃	5	10	16
Yield/Δ[MMH]				
-Δ[O ₃]	No Trap	0.9	1.0	1.3
	Trap	0.7	1.2	1.9
[H ₂ O ₂]	No Trap	0.2	0.15	0.13
	Trap	0.08	0.04	0.07
[CH ₃ NNH]	No Trap	0.4	0.15	0
	Trap	0.3	0.23	0
[CH ₃ OOH]	No Trap	0.4	0.5	0.6
	Trap	0.3	0.3	0.3
[HCHO]	No Trap	<0.03	0.14	0.3
	Trap	0.09	0.18	0.5
[CH ₃ OH]	No Trap	0.03	0.06	0.09
	Trap	0.03	0.09	0.19
[CH ₂ N ₂]	No Trap	0.13	0.11	0.01
	Trap	0.13	0.3	0.16
Integrated [OH]				
(10 ⁻⁶ ppm-min)	No Trap	0.2	1.0	7.1

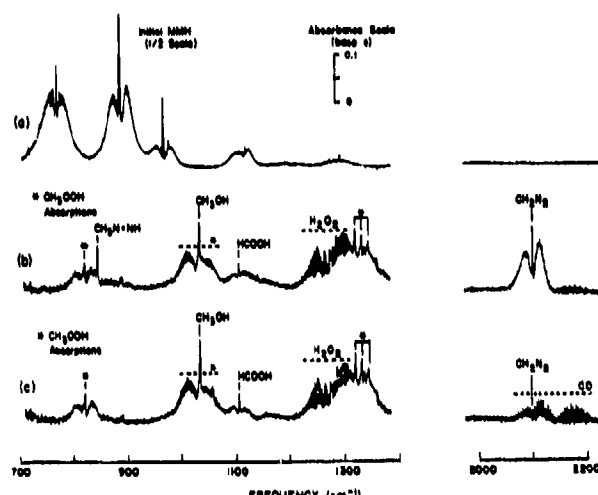


Figure 4. Spectra from an MMH + O₃ Equimolar Run. (a) Initial MMH, (b) Mixture at t=1.4 min after First O₃ Injection, (c) Mixture at t=1.4 min after Second O₃ Injection.

in the N₂H₄ + O₃ system) decreased markedly as the [O₃]/[MMH] ratio increased, and it was not observed when O₃ was in excess. The observation that CH₃NNH already present in a reacted mixture rapidly disappeared after excess O₃ was added can be attributed to a rapid reaction between CH₃NNH and O₃. The CH₂N₂ yields were also observed to decrease as the [O₃]/[MMH] ratio increased, indicating that this product also reacted with O₃. The reduced CH₃NNH and CH₂N₂ yields in the higher O₃ runs were offset primarily by increased yields of HCHO and CH₃OOH, with HCHO not being observed in the excess MMH runs, but becoming a major product in excess O₃.

The radical trap and tracer results indicated the role of OH radicals in the MMH + O₃ system. As with the N₂H₄ system, the integrated OH levels increased as the initial [O₃]/[hydrazine] increased, and the radical trap suppressed the H₂O₂ yields. The radical trap also suppressed the yields of CH₃OOH, but resulted in increased yields of CH₃OH, HCHO, and CH₂N₂.

Results of the UDMH + Ozone Experiments

The results of the UDMH + O₃ experiments are summarized in Table 3. The major product formed was (CH₃)₂NNO (N-nitrosodimethylamine or NDMA), with CH₃OOH, CH₃NNH, and H₂O₂, minor yields of CH₃OH, CO, HCOOH, HONO, NO₂, and NH₃, and traces of CH₂N₂ also being observed. The NDMA yields were generally 60-70% of the UDMH consumed. The UDMH + O₃ system differed from those of the other hydrazines in that HONO was produced and that significantly lower yields of H₂O₂ were observed.

Representative spectra obtained from the UDMH + O₃ experiment with equimolar initial reactants are shown in Figure 5. The absorption bands of NDMA are seen to be the dominant features of the product spectrum (Figure 5b). An unidentified product, with its strongest absorption at ~976 cm⁻¹, was detected upon subtraction of the NDMA absorptions (Figure 5c). This unknown product was observed to form in all experiments conducted in the absence of the radical trap.

The radical trap and tracer data indicated that OH radicals were also generated in the UDMH + O₃ system. As with the other hydrazines, the integrated radical levels increased with increasing [O₃]/[hydrazine] ratio. The radical trap caused increased yields of NDMA, but lower yields of all the other products.

REACTIONS OF HYDRAZINES WITH OXIDES OF NITROGEN

The reactions of the hydrazines with oxides of nitrogen were carried out under conditions of excess hydrazine, excess NO₂, and excess NO. The summary of data from these reactions are given in Tables 4-6. N₂H₄, MMH, and UDMH all reacted at significant rates in the gas phase with NO₂, with the rates of reaction being the lowest for N₂H₄ and the highest for UDMH. However, none of these hydrazines reacted with NO alone at measurable rates, although some NO was consumed when NO₂ and the hydrazines reacted in its presence.

The reaction of NO₂ with N₂H₄ resulted in the formation of HONO in high yields, hydrazinium nitrate [N₂H₄·HNO₃], N₂H₂ (in excess N₂H₄ only), N₂O, and

TABLE 3. SUMMARY OF RESULTS OF THE UDMH + O₃ CHAMBER EXPERIMENTS WITH AND WITHOUT RADICAL TRAPS.

		Excess UDMH	Equimolar	Excess O ₃
Initial Concentration (ppm)				
UDMH		8-16	10	5
O ₃		4	10	17
Yield/Δ[UDMH]				
-Δ[O ₃]	No Trap	1.4	1.4	1.8
	Trap	1.7	1.5	a
[(CH ₃) ₂ NNO]	No Trap	0.6	0.6	0.7
	Trap	0.7	0.7	a
[HCHO]	No Trap	0.13	0.16	0.24
	Trap	<0.05	0.09	a
[CH ₃ OOH]	No Trap	<0.15	0.12	0.21
	Trap	<0.17	<0.06	a
[CH ₃ NNH]	No Trap	0.09	0.05	0
	Trap	<0.03	0.03	a
[H ₂ O ₂]	No Trap	0.05	0.08	0.09
	Trap	<0.06	0.03	a
[HONO]	No Trap	0.04	0.04	0.01
	Trap	0.01	0.01	a
Integrated [OH]				
(10 ⁻⁶ ppm-min)	No Trap	0.4	1.0	2.4

^aNo data.

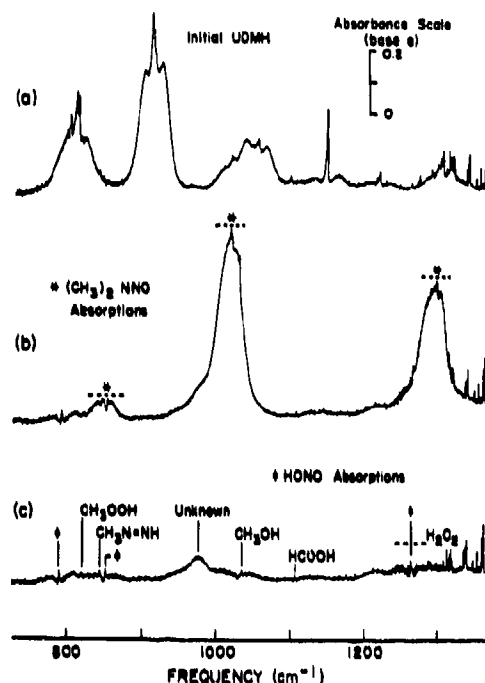


Figure 5. Spectra from a UDMH + O₃ Equimolar Run. (a) Initial UDMH, (b) Products at t=1.4 min, (c) from (b) with (CH₃)₂NNO Bands Subtracted.

NH₃ (Table 4). Analogous products were formed when NO₂ and MMH reacted, namely HONO (in high yields), monomethylhydrazinium nitrate [CH₃NHNH₂·HNO₃], CH₃NNH, and traces of N₂O, and NH₃ (Table 5). In addition, in the MMH + NO₂ system, CH₃OOH (in excess MMH only), CH₃OH, and two unknown products were observed, and peroxyntiric (HOONO₂) was formed as a transient intermediate in the absence of NO, indicating the intermediacy of HO₂ radicals. In both N₂H₄ and MMH cases, the reactant stoichiometry, product yields and (for N₂H₄) apparent reaction rates depended on reaction conditions.

The reaction of NO₂ with UDMH in the absence of NO appears to be simpler than is the case with the other hydrazines. The only products observed were HONO and tetramethyltetrazene-2 (TMT), with the product yields and reactant stoichiometries being consistent with the overall process being UDMH + 2 NO₂ → 2 HONO + 1/2 TMT, independent of the initial [NO₂]/[UDMH] ratio. In addition, the apparent reaction rates were also unaffected by the initial reactant

TABLE 4. SUMMARY OF RESULTS OF THE $\text{N}_2\text{H}_4 + \text{NO}_2$ CHAMBER EXPERIMENTS.

	Excess N_2H_4	Excess NO	Excess NO_2
Initial Concentration (ppm)			
N_2H_4	8	4	4
NO		19	
NO_2	2	4	20
Apparent $k(\text{NO}_2 + \text{N}_2\text{H}_4)$ ($10^{-4} \text{ ppm}^{-1} \text{ min}^{-1}$)			
	15		3.5
Yield/ $\Delta[\text{N}_2\text{H}_4]^a$			
$-\Delta[\text{NO}_2]$	1.1	1.3^b	1.8
[HONO]	0.6	0.9	1.4
$[\text{N}_2\text{H}_4 \cdot \text{HNO}_3 \text{ Salt}]^c$	0.13	0.2	0.4
$[\text{N}_2\text{O}]$	0.04	0.15	0.2
$[\text{NH}_3]$	0.08	0.2	0.3
N_2H_2 Detected?	yes	no	no

^a $\Delta[\text{N}_2\text{H}_4]$ corrected for N_2H_4 dark decay in the chamber.

^b $\Delta[\text{NO}_2]$ corrected by subtracting the estimated amount of NO_2 formed from the reaction $\text{NO} + \text{NO} + \text{O}_2 \rightarrow 2 \text{NO}_2$.

^c Calibration from a separate $\text{N}_2\text{H}_4 + \text{HNO}_3$ run.

TABLE 5. SUMMARY OF RESULTS OF THE MMH + NO₂ CHAMBER EXPERIMENTS.

	Excess MMH	Excess NO	Excess NO ₂
Initial Concentration (ppm)			
MMH	9	4	4
NO		19	
NO ₂	5	2	19
Apparent k(NO ₂ + MMH) (10 ⁻³ ppm ⁻¹ min ⁻¹)			
	4		3
Yield/Δ[MMH] ^a			
-Δ[NO ₂]	1.3	0.8 ^b	2.9
[HONO]	1.0	1.4	1.4
[CH ₃ NNH]	0.2	0.2	0.3
[CH ₃ OOH]	0.4	<0.1	<0.1
[CH ₃ OH]	0.03	0.02	0.03
[N ₂ O]	<0.01	0.05	0.01
[NH ₃]	0.03	0.02	0.02
Relative Yield/Δ[MMH]			
Unknown 1	1	1	13
Unknown 2	0	2	1
HOONO ₂ Observed?	yes	no	yes

^aΔ[MMH] corrected for MMH dark decay in the chamber.

^bΔ[NO₂] corrected by subtracting the estimated amount of NO₂ formed from the reaction NO + NO + O₂ → 2 NO₂.

TABLE 6. SUMMARY OF RESULTS OF THE UDMH + NO₂ CHAMBER EXPERIMENTS.

	Excess UDMH	Excess NO	Excess NO ₂
Initial Concentrations (ppm)			
UDMH	10	3	4
NO		15	
NO ₂	4	3	19
Apparent k(NO ₂ + UDMH)			
(10 ⁻² ppm ⁻¹ min ⁻¹)	3.5 ^a		3.6
Yield/Δ[UDMH]			
-Δ[NO ₂]	2.1	2.0 ^b	2.1
[HONO]	2.1	1.7	2.1
[(CH ₃) ₂ NNNN(CH ₃) ₂]	0.5	0.2	0.5
[(CH ₃) ₂ NNO]	0	0.05	0
[N ₂ O]	<0.02	0.17	<0.01
Relative Yield/Δ[UDMH]			
Unknown	<0.04	1	<0.02

^aCorrected using a stoichiometric factor of 2 when relating NO₂ decay to the reaction rate.

^bΔ[NO₂] corrected by subtracting the estimated amount of NO₂ formed from the reaction NO + NO + O₂ → 2 NO₂.

concentrations. On the other hand, in the presence of NO, the yields of TMT and (to a lesser extent) HONO were reduced, and the formation of N₂O, NDMA, and an unknown product were observed, indicating that NO reacts with the intermediate(s) involved in TMT formation.

REACTIONS OF HYDRAZINES WITH NITRIC ACID AND FORMALDEHYDE

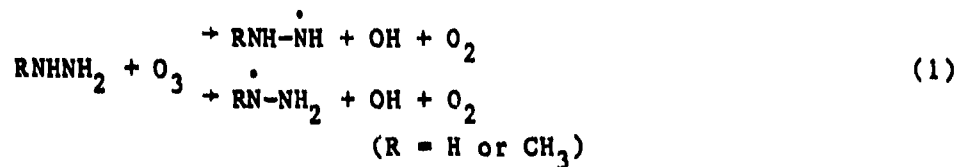
Several experiments were also conducted to investigate the reactions of the fuel hydrazines with HNO_3 and HCHO . All three hydrazines were observed to react with HNO_3 at rates too fast to measure, forming the corresponding monobasic salts. (No similar reactions with HONO were evident). N_2H_4 and UDMH were also observed to react with HCHO in the gas phase, with 1:1 reactant stoichiometry, to form the corresponding formaldehyde hydrazones $[\text{H}_2\text{N}=\text{NCH}_2$ and $(\text{CH}_3)_2\text{NN}=\text{CH}_2]$. However, the concentration-time profiles were not consistent with these reactions being simple second order processes, and the mechanism may be in part heterogeneous. A transient intermediate, possibly $\text{NH}_2\text{NHCH}_2\text{OH}$, was observed in the $\text{HCHO} + \text{N}_2\text{H}_4$ system, though no such intermediate was evident in the UDMH case. The MMH + HCHO reaction was not studied.

DISCUSSION

REACTIONS OF HYDRAZINES WITH OZONE

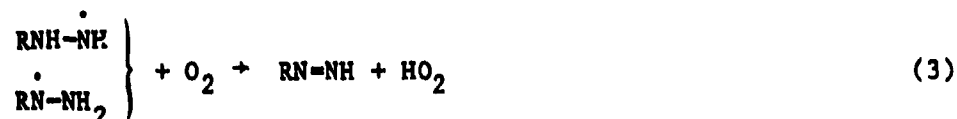
The results of our experiments suggest that the mechanisms of O_3 reactions with N_2H_4 and MMH may be similar in their overall features, but that there are distinct differences in the case of the UDMH + O_3 reaction. In the case of N_2H_4 and MMH, the observed dependencies of stoichiometry, product yields and integrated OH radical levels or initial reactant ratios are consistent with the following processes where OH, hydrazyl radicals ($\text{H}_2\text{N}-\dot{\text{N}}\text{H}$ or $\text{CH}_3\text{NH}-\dot{\text{N}}\text{H}$), and the diazenes ($\text{HN}=\text{NH}$ or $\text{CH}_3\text{N}=\text{NH}$) act as the chain carriers.

Initiation:



Propagation:

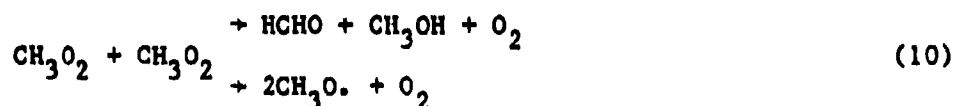




Termination:



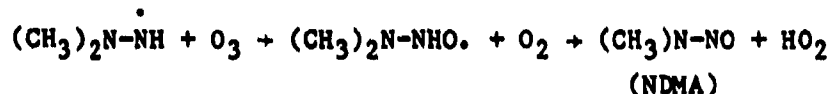
Product formation:



This mechanism is consistent with most of results for the N_2H_4 and MMH systems, except that it does not account for the observed formation of diazomethane in the MMH + O_3 system. The fact that diazomethane formation is not suppressed by the addition of radical traps indicates that it is not due to an OH radical reaction as we had initially proposed (References 2 and 3). Diazomethane is most likely a product of the reaction of ozone with methyldiazene, although the details of its formation are uncertain.

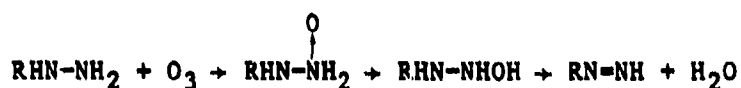
UDMH differs from the other hydrazines in that the hydrazyl radical, presumed to be formed in the initial reactions of UDMH with O_3 or OH radicals,

cannot react with O_2 to form a diazene. The most reasonable mechanism is that the radical instead reacts with ozone, resulting in the ultimate formation of the observed products NDMA and H_2O_2 [the latter being formed from HO_2 via reaction (8), above].



The other products observed can be attributed to subsequent reactions of NDMA with OH radicals, since the yields of these products decreased while that of NDMA increased in the presence of radical traps. However, this mechanism does not account for the fact that the H_2O_2 yields are much lower in the UDMH system than for the other hydrazines.

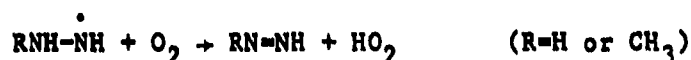
Although reasonable, the above mechanisms must still be regarded as uncertain, since the possibility of other processes being significant, e.g., reactions of HO_2 with the hydrazines, cannot be ruled out. Moreover, the initial ozone + hydrazine reaction is itself uncertain, since there is an alternative possibility involving O-atom transfer, forming an N-oxide intermediate, which presumably would undergo subsequent rearrangement and elimination of H_2O , resulting in the eventual formation (in the N_2H_4 or MMH systems) of the observed diazene products.



There is evidence that N-oxides are intermediates in the reactions of $O(^3P)$ atoms with amines and hydrazines (References 7 and 8), and the results of our $N_2H_4 + O_3$ and $MMH + O_3$ experiments are not inconsistent with a mechanism involving N-oxide intermediates. On the other hand, it is difficult to rationalize our UDMH + O_3 results based on such a mechanism, and thus for UDMH the mechanism discussed earlier is preferred.

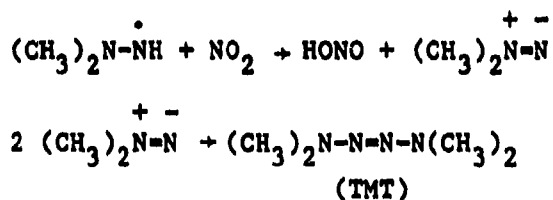
REACTIONS OF THE HYDRAZINES WITH NO₂

The most likely initial process in the reactions of the hydrazines with NO₂ is H-atom abstraction, forming the nitrous acid and a hydrazyl radical, with the latter (in the case of N₂H₄ and MMH) subsequently reacting with oxygen to form the corresponding diazene:



Diazene and methyldiazene apparently react with NO₂, with the reaction of the former probably being faster. However, we are unable to reconcile all of our results in the NO₂ + N₂H₄ and NO₂ + MMH systems with a satisfactory reaction mechanism. Particular uncertainties concern the fates of HO₂ and CH₃O₂ radicals in these systems (if indeed they are formed), and the source of HNO₃ which is a precursor to the observed nitrate salts when they are formed in the absence of NO.

In contrast to the NO₂ + N₂H₄ and the NO₂ + MMH systems, the NO₂ + UDMH system appears to be much simpler. In the absence of NO, the only significant products formed were HONO and tetramethyltetrazene-2 (TMT), with the reactant stoichiometries and product yields being consistent with the following subsequent reactions of the initially formed (CH₃)₂N-NH radicals



When NO is present, it could react with the hydrazyl radical to form the nitrosohydrazine, with the latter undergoing a secondary reaction with NO₂ to ultimately give rise to N₂O and N-nitrosodimethylamine. This is discussed in detail elsewhere (Reference 9).

CONCLUSIONS

A major overall conclusion which can be drawn from this and previous studies of the fuel hydrazines is that these compounds are extremely labile, that they can undergo a wide variety of reactions under atmospheric conditions, and that in some cases these reactions involve the formation of products which are more hazardous than the hydrazines themselves. Examples of these products are N-nitrosodimethylamine from UDMH and diazomethane from MMH. Thus, an understanding of the consequences of and appropriate responses to accidental releases of these hydrazines into the atmosphere requires not only the ability to predict their atmospheric lifetimes, but also to predict the nature, formation rates, and fates of their reaction products. This in turn requires an understanding of the details of the atmospheric reaction mechanisms of these hydrazines and amines in general, as well as those of their major oxidation products.

The results of our chamber studies of the fuel hydrazines have provided important clues concerning the mechanisms of the reactions of these compounds with O_3 and NO_2 in the dark, and indirect information concerning their reactions with OH radicals, the latter being probably a significant loss process of the hydrazines in sunlight. However, our chamber experiments do not represent the full range of conditions under which these hydrazines might react in the atmosphere, and many significant uncertainties remain concerning their reaction mechanisms even for the relatively limited sets of conditions which we have studied. Much more research of fundamental nature is needed before we can predictively model the consequences of the release of the fuel hydrazines into the atmosphere.

REFERENCES

1. Finlayson-Pitts, B.J. and J.N. Pitts, Jr., Atmospheric Chemistry, Wiley and Sons, New York, 1986.
2. Pitts, J.N., Jr., E.C. Tuazon, W.P.L. Carter, A.M. Winer, G.W. Harris, R. Atkinson, and R.A. Graham, Atmospheric Chemistry of Hydrazines: Gas Phase

Kinetics and Mechanistic Studies, ESL-TR-80-39, Air Force Engineering and Services Center, Tyndall AFB, FL 32403, August 1980.

3. Tuazon, E.C., W.P.L. Carter, A.M. Winer, and J.N. Pitts, Jr., "Reactions of Hydrazines with Ozone under Simulated Atmospheric Conditions," Environmental Science and Technology, vol. 15, pp. 823-828, 1981.
4. Carter, W.P.L., E.C. Tuazon, A.M. Winer, and J.N. Pitts, Jr., N-Nitroso Compounds, R.A. Scanlan and S.R. Tannenbaum (eds.), ACS Symposium Series, American Chemical Society, Washington, D.C., No. 174, pp. 117-131.
5. Harris, G.W., R. Atkinson, and J.N. Pitts, Jr., "Kinetics of the Reactions of the OH Radical with Hydrazine and Methylhydrazine," Journal of Physical Chemistry, vol. 83, pp. 2557-2559, 1979.
6. Tuazon, E.C., W.P.L. Carter, R.V. Brown, R. Atkinson, A.M. Winer, and J.N. Pitts, Jr., Atmospheric Reaction Mechanisms of Amine Fuels, ESL-TR-82-17, Air Force Engineering and Services Center, Tyndall AFB, FL 32403, March 1982.
7. Slagle, I.R., J.F. Dudich, and D. Gutman, "Identification of Reactive Routes in the Reactions of Oxygen Atoms with Methylamine, Dimethylamine, Trimethylamine, Ethylamine, Diethylamine, and Triethylamine," Journal of Physical Chemistry, vol. 83, pp. 3065-3070, 1979.
8. Foner, S.N. and S.L. Hudson, "Mass spectrometric studies of Atom-Molecule Reactions using High-Intensity Crossed Molecular Beams," Journal of Chemical Physics, vol. 53, pp. 4377-4386, 1970.
9. Tuazon, E.C., W.P.L. Carter, R.V. Brown, A.M. Winer, and J.N. Pitts, Jr., "Gas-Phase Reaction of 1,1-Dimethylhydrazine with Nitrogen Dioxide," Journal of Physical Chemistry, vol. 87, pp. 1600-1605, 1983.

**SURFACE-CATALYZED AIR OXIDATION OF HYDRAZINES:
ENVIRONMENTAL CHAMBER STUDIES**

**Jan E. Kilduff, Scientist
Lockheed-EMSCO
White Sands Test Facility
Las Cruces, NM 88004**

**Dennis D. Davis Senior Scientist
Lockheed-EMSCO
White Sands Test Facility
Las Cruces, NM 88004**

**Steven L. Koontz, Project Scientist
NASA
White Sands Test Facility
Las Cruces, NM 88004**

ABSTRACT

The surface-catalyzed air oxidation reactions of fuel hydrazines were studied in a 6500-liter fluorocarbon-film chamber at 80 to 100 ppm concentrations. First-order rate constants for the reactions catalyzed by aluminum, water-damaged aluminum ($\text{Al}/\text{Al}_2\text{O}_3$), stainless steel 304L, galvanized steel and titanium plates with surface areas of 2 to 24 m^2 were determined. With 23.8 m^2 of $\text{Al}/\text{Al}_2\text{O}_3$ the surface-catalyzed air oxidation of hydrazine had a half-life of 2 hours, diimide (N_2H_2) was observed as an intermediate and traces of ammonia were present in the final product mixture. The $\text{Al}/\text{Al}_2\text{O}_3$ catalyzed oxidation of monomethylhydrazine yielded methyldiazene ($\text{HN}=\text{NCH}_3$) as an intermediate and traces of methanol. Unsymmetrical dimethylhydrazine gave no detectable products. The relative reactivities of hydrazine, MMH and UDMH were 130 : 7.3 : 1.0, respectively.

The rate constants for $\text{Al}/\text{Al}_2\text{O}_3$ -catalyzed oxidation of hydrazine and MMH were proportional to the square of the surface area of the plates. Mechanisms for the surface-catalyzed

oxidation of hydrazine and diimide and the formation of ammonia are proposed.

INTRODUCTION

Hydrazine and its alkyl-substituted derivatives are important members of the high energy fuels used in military and aerospace applications. The toxicity of the hydrazine fuels (Reference 1) have generated considerable interest in their environmental fate. In an effort to assess the environmental impact of accidental or intentional spills of the fuel hydrazines, their gas phase decomposition rates are required. Previous workers (References 2 - 5) have noted that surface reactions interfere with gas phase studies by dramatically effecting the decomposition kinetics. Increasing the size of the reaction vessel decreases the surface to volume ratio thus minimizing the effects of container walls. This work involved the use of a fluorocarbon film chamber with a surface to volume ratio of 3.39 m^{-1} to determine the effects of common metal surfaces on the gas phase hydrazine decomposition kinetics with minimal chamber wall interferences.

EXPERIMENTAL

APPARATUS

A fluorinated-ethylene propylene (FEP) polymer film chamber, $2.44 \text{ m} \times 2.44 \text{ m} \times 1.22 \text{ m}$, was constructed from 0.13 cm (5 mil) sheets. The joints were heat-sealed and reinforced with poly(tetrafluoroethylene) (TFE) pressure-sensitive tape. The chamber was supported by an outside metal framework and the framework covered by a 0.025 cm (10 mil) thick poly(ethylene) liner. A 5 cm purgeable air space between the inner FEP and outer poly(ethylene) liner provided thermal and mechanical protection. A 250 mL gas sampling bulb, wrapped in heating tape, acted as an injector system where the hydrazine fuel could be vaporized and transferred into the chamber by nitrogen flow. The chamber could be vented through a 5 cm TFE pipe-exhaust stack. A $1.22 \text{ m} \times .91 \text{ m}$ FEP door, sealed with TFE tape and covered with poly(ethylene) sheet, provided access to the chamber interior.

The chamber was also fitted with a 30.5 cm TFE-coated variable-speed fan to provide mixing.

Changes in reactant and product concentrations were monitored using a Mattson Sirius 100 Fourier transform infrared spectrometer with a remote HgCdTe detector and a multiple-path optical system (White cell) of 74.9 m pathlength. The White cell consisted of two 20.3 cm field mirrors and an in-focus mirror with 2.45 cm ZnSe windows. The mirrors were gold coated and held in TFE-coated frames. Except for the ZnSe windows and the gold mirror surfaces, the entire interior surface of the chamber was FEP or TFE Teflon. Data collection was carried out at 1 cm^{-1} resolution.

MATERIALS

Hydrazine and monomethylhydrazine (MMH) were propellant grades (Olin) analyzed according to MIL-P-26536-C and MIL-P-2740413. Unsymmetrical dimethylhydrazine (UDMH), (Aldrich), was reagent grade and used as received. Sheets of .16 cm (20 gauge) stainless steel 304-L, hot dipped galvanized steel (zinc), titanium 6Al-4V and aluminum 6061-T6 were cut into .46 m x .46 m plates. Serendipity provided the $\text{Al}/\text{Al}_2\text{O}_3$ sample when a lot of aluminum was left in the bed of an open pick-up truck during a rain storm. A white crystalline aluminum oxide formed which encrusted the water damaged aluminum sheets. Surface areas reported here refer to mensurated, not actual surface areas.

PROCEDURE

In a typical experiment, the requisite number of metal plates were placed vertically in TFE racks in the FEP environmental chamber which was then purged with clean air for 6 hours at 300 L/min to provide 17 turnovers of the 6500L chamber atmosphere. The inner purge was then halted and the liner purged at 150 L/min. A background reference spectrum was taken followed by vaporization of 0.5 to 1.75 mL (60 - 100 ppm) of hydrazine fuel into the chamber. High speed stirring with the mixing fan was carried out during injection followed by low speed stirring during actual data collection. Immediately after vaporization of

fuel was completed, data acquisition was started via automatic program such that sample spectra were acquired at specified intervals.

The hydrazine loss rate was determined by integrating suitable analytical infrared bands as the reaction occurred. A plot of the $\log(\text{area})$ versus time was treated by least squares analysis, the slope yielding the first-order rate constant.

RESULTS

The first-order background rate constants (k_{bkg}) in the FEP chamber for hydrazine, MMH and UDMH are 4.78×10^{-6} , 10.2×10^{-6} , and $3.19 \times 10^{-6} \text{ sec}^{-1}$, respectively. Plots of the $\log(\text{area})$ versus time were linear and followed first-order kinetics except for hydrazine, for which a non-linear portion was observed in the first 6 to 8 hours. This portion of the decay curve was not included in the calculation of the background rate. Stone and others have ascribed these background loss rates to physical, not chemical, processes and the initial curvature has been discussed in detail elsewhere (References 6 -7). The average half-life for hydrazine background loss was 40.3 hrs.

Rates for the disappearance of the fuel hydrazines in the presence of Al/Al₂O₃, titanium, 304-L SS, zinc and aluminum plates (Tables 1 and 2) were 2 to 100 times faster than the background rates in the empty chamber. The most reactive surface proved to be the Al/Al₂O₃ plates and the least reactive was aluminum. The surface-catalyzed rate constants (k_{cat}) for hydrazine decomposition shown in Tables 1 and 2 were determined by subtracting k_{bkg} from k_{obs} .

In the presence of high surface area (23.83 m^2) of Al/Al₂O₃ the appearance of new bands at 3180 - 3050 and 1380 - 1275 cm^{-1} were observed and identified as diimide, H-N=N-H (Reference 8). Diimide reached a maximum concentration approximately 1.5 hours after the start of the run (Figure 1). After 10 hours no hydrazine or diimide remained, however approximately 3 to 5 percent of the initial hydrazine concentration was present as ammonia. Ammonia was never seen in the background runs. With

TABLE 1. RATE CONSTANTS FOR THE AIR CATALYZED OXIDATION OF HYDRAZINE ON METAL SURFACE AREAS, 22 ± 3 °C

Metal	Area m ²	k _{obs} sec ⁻¹ (x 10 ⁻⁵)	k _{cat} sec ⁻¹ (x 10 ⁻⁵)
Al/Al ₂ O ₃	23.83	50.80	50.40
"	"	63.90	63.40
"	23.83	53.90	53.40
"	13.37	10.50	9.99
"	"	8.33	7.86
"	6.69	3.24	3.24
"	3.34	1.33	0.86
Zinc	21.32	1.38	0.91
"	19.23	1.33	0.86
Titanium	2.11	0.69	0.22
SS 304-L	20.91	0.99	0.52
Aluminum	20.90	1.00	0.52
"	"	0.87	0.40
Blank	0.00	0.48	-

smaller surface areas of Al/Al₂O₃ or with other metals the buildup of detectable concentrations of diimide was not observed. Numerical analysis of appearance/disappearance curves for diimide, treated as two consecutive first-order reactions, gives 9.7×10^{-5} sec⁻¹ and 3.3×10^{-4} sec⁻¹ as the formation and decay rate constants. The maximum concentration is estimated to be 18 percent.

The background rate for MMH loss (Table 2) from the FEP chamber was faster than either hydrazine or UDMH with an average half-life of 18.9 hours. The Al/Al₂O₃ metal plates again exhibited the greatest reactivity with MMH, however at high surface area the observed rate was only four-fold faster than the background rate. Methanol (3 - 9 percent of the initial MMH concentration) and traces of methyldiazene (Reference 9) were the

TABLE 2. RATE CONSTANTS FOR THE AIR CATALYZED OXIDATION OF MMH AND UDMH ON METAL SURFACE AREAS, 26 ± 3 °C

Metal	Area m ²	k _{obs} sec ⁻¹ (x 10 ⁻⁵)	k _{cat} sec ⁻¹ (x 10 ⁻⁵)
Al/Al ₂ O ₃	23.83	3.33	2.32
"	"	4.06	3.04
"	"	4.17	3.15
"	12.12	1.94	0.93
"	11.70	1.81	0.79
SS 304-L ^a	20.91	3.58	2.57
" ^a	"	3.86	2.85
Zinc	20.90	1.79	0.77
"	"	1.76	0.75
Aluminum	20.90	1.31	0.29
"	"	1.17	0.15
Blank	0.00	1.02	-
Al/Al ₂ O ₃ ^b	23.83	0.75	0.43
" ^b	"	0.53	0.21
Blank ^b	0.00	0.32	-

^a Temperature 31 ± 2 °C

^b UDMH at 100 ppm

only products observed in the presence of metal plates. A smaller (2 percent of the initial MMH concentration) yield of methanol was observed in background runs.

The slowest background rate (Table 2) was observed for UDMH disappearance with an average half-life of 60.3 hours. No products were observed. Lack of reactivity was evidenced by a mere doubling of k_{obs} in the presence of 23.83 m² of Al/Al₂O₃ and no further experiments were conducted.

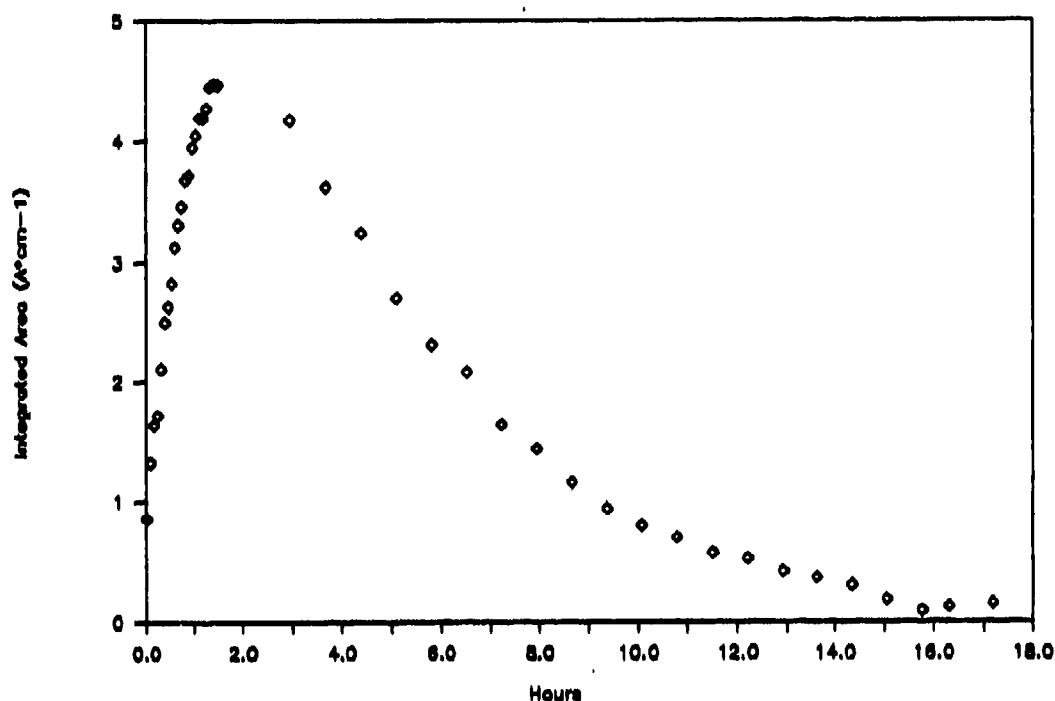


Figure 1. Diimide Concentration as Integrated Area (1350 - 1210 $\text{A}\cdot\text{cm}^{-1}$) Versus Time for Hydrazine and $23.8 \text{ m}^2 \text{ Al/Al}_2\text{O}_3$

DISCUSSION

The rate data for hydrazine and MMH oxidation with various numbers of $\text{Al/Al}_2\text{O}_3$ plates indicates that k_{cat} increases as the square of the surface area. A plot of $\log(k_{\text{cat}})$ against $\log(\text{area})$ for both hydrazine and MMH shows the data close to theoretical lines of slope 2, (Figure 2). The rate expression for the disappearance of hydrazine or MMH is:

$$\text{rate} = k [\text{hydrazine}] [\text{surface area}]^2$$

The observed rate expression is consistent with a kinetic scheme involving equilibrium adsorption of hydrazine and oxygen on different sites followed by an irreversible bimolecular reaction.

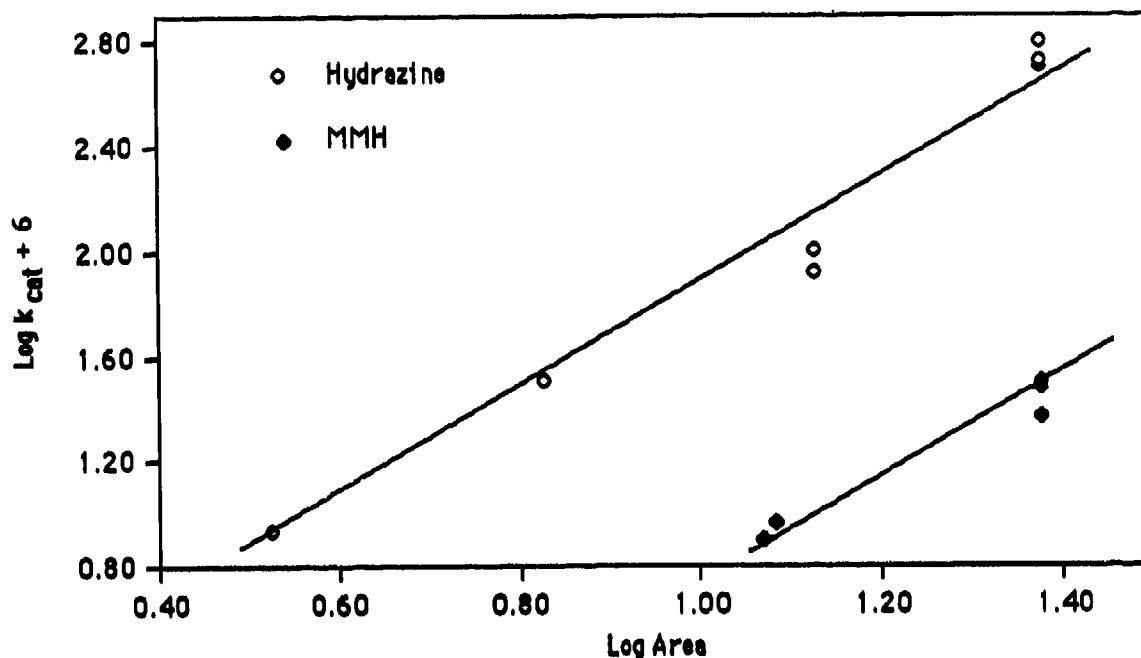


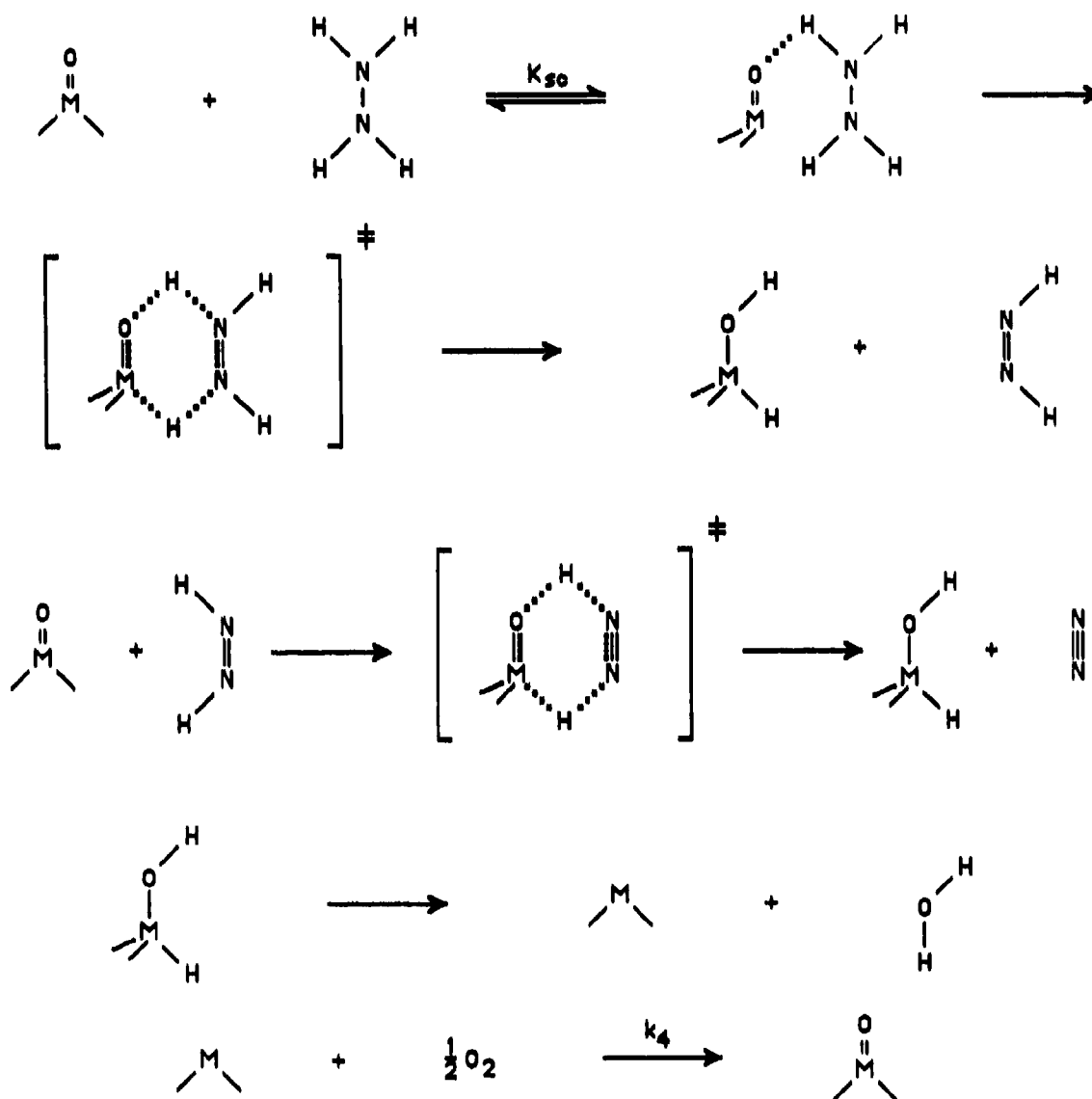
Figure 2. $\text{Log}(k_{cat})$ Versus $\text{Log}(\text{Area})$ for Hydrazine and MMH on 23.8 m^2 of $\text{Al}/\text{Al}_2\text{O}_3$. Lines Shown Have a Slope of 2

The relative reactivities of the fuel hydrazines toward $\text{Al}/\text{Al}_2\text{O}_3$ are:

$$\begin{array}{ccccc} \text{hydrazine} & > & \text{MMH} & > & \text{UDMH} \\ 130 & & 7.3 & & 1 \end{array}$$

The disappearance of hydrazine and the appearance of the intermediate diimide catalyzed by a metal surface in air can be described by the mechanism shown in Scheme 1. Hydrazine vapor is adsorbed onto the metal oxide surface via hydrogen bonding. An oxidative dehydrogenation proceeding through a 6 membered-ring transition state yields diimide and a metal hydroxy hydride. Similarly, diimide can further react, after desorption/adsorption, through the same type of transition state to yield nitrogen and another surface hydroxy hydride. The hydride molecules can undergo reductive elimination to yield a reduced surface and water. Since these reactions occur in air the reduced surface is re-oxidized from that source.

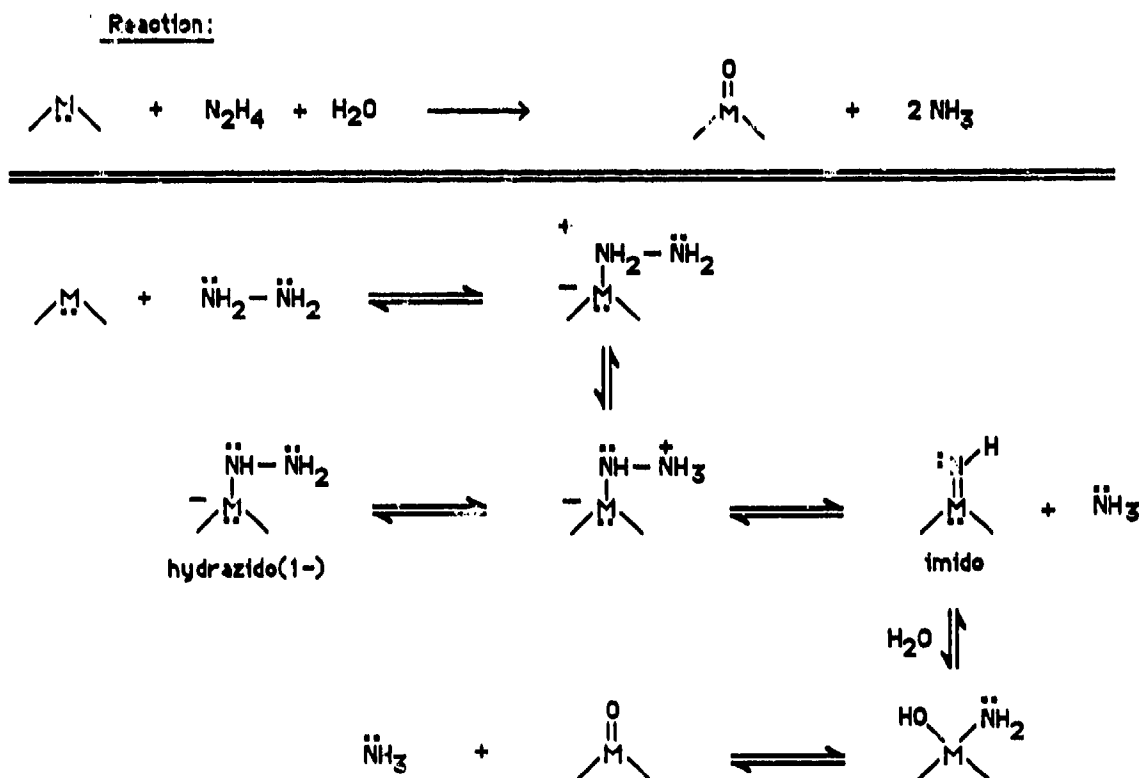
SCHEME 1



In our experiments, ammonia was noted as a trace (< 5 percent) product only when active metal surfaces were present. Other workers (Reference 2) have detected its formation in blank runs, but some exposed metal surfaces were present in their chambers. This mechanistically significant reduction product deserves deeper consideration in view of its importance in hydrazine decompositions in general, and its role as final

product in nitrogen fixation. A mechanism accounting for the overall reaction in which hydrazine and water react with a metal surface to yield two ammonia molecules and oxidized metal surface is shown in Scheme 2. The initially formed Lewis acid adduct undergoes a proton transfer and the resulting intermediate partitions between two reaction routes: one resulting in the formation of a hydrazido(1-) complex, which is a precursor to diazenido-complexes; or the other undergoing an ammonia elimination concomitant with formation of an imido structure. Water can react with the imido compound to form a surface-bound hydroxy amide. Reductive elimination from the hydroxy amide leads to ammonia and metal oxide. The putative intermediates shown in Scheme 2 are similar to those incorporated in general nitrogen fixation schemes (Reference 10).

SCHEME 2



Although the low reactivity of MMH makes it difficult to study in the environmental chamber, the chamber results are consistent with those derived from flow reactor studies at higher temperatures. Mechanistically, our proposals are similar, drawing upon several common structures (Reference 11), where even the observed activity order was the same.

Assuming that the environmentally important surface area of a metal plate is its mensurated area, the relative environmental reactivities of the hydrazine fuels toward exposed metal surfaces (per unit surface area²) can be calculated and a ranking of the metals obtained:

Hydrazine

Al/Al ₂ O ₃	>	Titanium	>	Zinc	>	Aluminum, 304L SS
74		46		2		1

MMH

Al/Al ₂ O ₃	>	Zinc	>	Aluminum
11		4		1

It is interesting to note that aluminum with its normal smooth oxide coat is catalytically unnotable, however any process leading to a thickening of the oxide coating results in a very catalytically active surface. The white crystalline material which encrusted the water damaged aluminum and apparently resulted in the dramatic activity, may be due to a large microscopic surface area.

REFERENCES

1. Langa, R.E., Editor The Sigma-Aldrich Library of Chemical Safety Data, Edition I, Sigma-Aldrich Corporation, Milwaukee, WI, 1985.
2. Stone, A.D. The Autooxidation of Hydrazine Vapor, CEEDO-TR-78-17, Civil and Environmental Engineering Office, Tyndall AFB, FL 32403, January 1978.
3. Stone, A.D. The Autooxidation of Monomethylhydrazine Vapor, ESL-TR-79-10, Engineering and Services Laboratory, Tyndall AFB, FL 32403, January 1979.
4. Stone, A.D. The Autooxidation of Unsymmetrical Dimethylhydrazine and 50 Percent Unsymmetrical Dimethylhydrazine-50 Percent Hydrazine Mixtures, ESL-TR-80-21, Engineering and Services Laboratory, Tyndall AFB, FL 32403, April 1980.
5. Tuazon, E.C., Carter, W.P., Brown, R.V., Atkinson, R., Winer, A.M., Pitts, J.N. Jr., Atmospheric Reaction Mechanisms of Amine Fuels, ESL-TR-82-17, Engineering and Services Laboratory, Tyndall AFB, FL 32403, March 1982.
6. Stone, D.A. Hydrazine Decay in a Teflon Film Reaction Chamber, Proceedings of the Third Conference on the Environmental Chemistry of Hydrazine Fuels, Panama City, FL, September 1987, this volume.
7. Wiseman, F.L. Modeling the Decay of Hydrazine in Teflon Film Reaction Chambers, Proceedings of the Third Conference on the Environmental Chemistry of Hydrazine Fuels, Panama City, FL, September 1987, this volume.
8. Back, R.A. Rev. Chem. Intermediates, 1984, 5, 293.
9. Ackermann, M.N., Burdge, J.J., Craig, N.C. J. Chem. Phys., 1973, 58, 203 - 215.
10. Henderson, R.A., Leigh, G.J., Pickett, C.J. Adv. Inorg. Radiochem., 1983, 27, 197.
11. Kilduff, J.E., Davis, D.D., Koontz, S.K. Surface-Catalyzed Air Oxidation of Hydrazines: Tubular Reactor Studies, Proceedings of the Third Conference on the Environmental Chemistry of Hydrazine Fuels, Panama City, FL, September 1987, this volume.

**AN ATMOSPHERIC PRESSURE FLOW REACTOR: GAS PHASE KINETICS
AND MECHANISM IN TROPOSPHERIC CONDITIONS WITHOUT WALL EFFECTS**

Steven L. Koontz, Project Scientist

NASA/White Sands Test Facility

Las Cruces, NM 88004

Dennis D. Davis, Senior Scientist

Lockheed-EMSCO/White Sands Test Facility

Las Cruces, NM 88004

Merrill Hansen, Engineer

Lockheed-EMSCO/White Sands Test Facility

Las Cruces, NM 88004

ABSTRACT

A new type of gas phase flow reactor, designed to permit the study of gas phase reactions near 1 atm of pressure, is described. A general solution to the flow/diffusion/reaction equations describing reactor performance under pseudo-first-order kinetic conditions is presented along with a discussion of critical reactor parameters and reactor limitations. The results of numerical simulations of the reactions of ozone with monomethylhydrazine and hydrazine are discussed, and performance data from a prototype flow reactor are presented.

INTRODUCTION

Accurate rate and mechanism data are needed for a wide variety of gas phase chemical reactions, both to further our basic understanding of Earth's atmosphere and to comply with regulations designed to protect the public from manmade air pollution (References 1 and 2). A wide variety of experimental techniques for the study of gas phase chemical processes has been described and applied to atmospheric problems (References 2 and 3). Flow reactors (References 4 and 5), flash photolysis and pulse radiolysis instruments (References 6 and 7), and environmental chambers (Reference 8) have all been used to further our understanding of the atmosphere and have well-known

advantages and disadvantages as applied to particular reactions.

The flow reactors used for gas phase kinetic studies, often referred to as fast-flow systems, operate under laminar flow conditions at pressures on the order of 1 torr (Reference 9). Because the rate constants of many reactions depend on the total pressure (References 2, 4, and 5), rate data taken at 1 torr may be very misleading if used to estimate the rate of processes at or near 760 torr. Additionally, while the reactants are well-mixed by molecular diffusion, wall reactions are often a significant and not easily corrected source of experimental error (References 10 - 12).

This paper presents a new type of flow reactor designed to circumvent some of the limitations of the fast-flow systems. The White Sands Test Facility (WSTF) flow reactor is designed to operate at or near 760 torr of pressure, in order to provide experimental conditions representative of the troposphere. In addition, design of the flow and reactant introduction systems has reduced or eliminated significant wall reactions. Reactants are still mixed by molecular diffusion, perhaps with some assistance from local small-scale turbulence. The diffusion coefficient depends on total pressure and is much smaller at 1 atm than at 0.001 atm. The rate of diffusion transport to the reactor walls is thus much smaller. In this case, however, concentration profiles are not uniform across the reactor cross section, and equations describing the flow/diffusion/reaction process must be solved to obtain kinetic data from the experiment.

BACKGROUND

OVERVIEW OF THE PROTOTYPE FLOW REACTOR

A concept drawing of the flow reactor is shown in figure 1. A diffuser is located behind flow-straightening screens to eliminate turbulence, providing a flat, uniform, laminar flow field for an inert carrier-gas containing the first reactant.

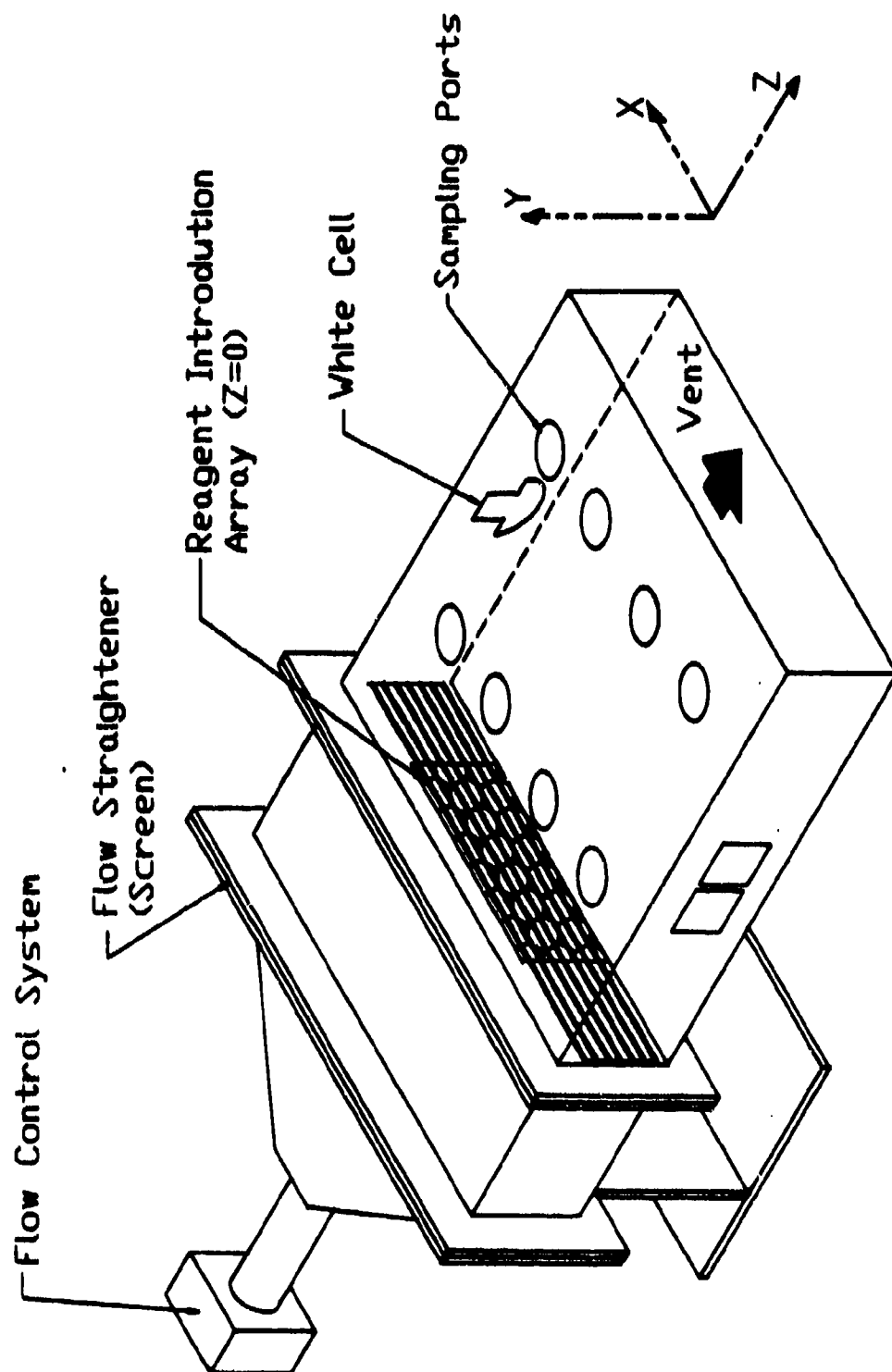


Figure 1. Concept Drawing of Prototype Flow Reactor

The second reactant is delivered as a vapor in carrier gas and is introduced by an array of small-diameter porous tubes. The small diameter of these tubes prevents the formation of wake vortices (Reference 13). These tubes are oriented perpendicularly to the flow velocity vector, and the reactant/carrier-gas mixture is forced out of the porous delivery tubes with a small positive pressure. Since the second reactant is introduced only by the portion of the tube array indicated in figure 1, this reactant does not contact the walls. The remaining tubes, as well as those parts of the delivery tubes close to the reactor duct walls, serve only to maintain a uniform flow field.

The reactants are mixed by molecular diffusion, possibly augmented by microscale turbulence generated by the delivery array. However, the reactants are not mixed uniformly, and the reactant concentration is a function of position in the duct. Reactant, intermediate, and product concentrations are observed downstream of the delivery array using a White Cell-FTIR spectrometer system (Reference 14).

GENERAL FLOW REACTOR THEORY

For the case of dilute reactants in an inert carrier-gas, the flow/diffusion/reaction process (References 15 - 18) can be described by

$$\frac{\delta C_a}{\delta t} + \vec{v} \cdot \vec{\nabla} C_a = D_{ab} \vec{\nabla}^2 C_a - [\sum_i k_i C_i] C_a \quad \text{eqn. 1}$$

where:

- C_a = the concentration of a species, a, as a function of the spatial coordinates and time
- \vec{v} = the velocity of the flowing carrier-gas stream in the laboratory reference frame
- $\vec{\nabla}$ = the grad operator
- $\vec{\nabla}^2$ = the Laplacian operator
- C_i = the concentration of a species, i, which reacts with the species, a

k_1 = the rate constant for the reaction between a and 1

D_{ab} = the diffusion coefficient for the species a in the carrier gas

The physical significance of each term in equation 1 is as follows. $\delta C_a / \delta t$ is the rate of change of C_a at some fixed point in the reactor (at steady state $\delta C_a / \delta t = 0$). The change in C_a with position resulting from carrier-gas flow (forced convection) is given by $v \cdot \nabla C_a$. $D_{ab} \nabla^2 C_a$ is the change in C_a with position resulting from molecular diffusion. Finally, $\sum_1 k_1 C_1 C_a$ is the change of C_a with position resulting from chemical reaction. The solution function $C_a(x, y, z, t)$ for a particular reactor configuration allows rate constants to be obtained from experimental data.

In the following general solution to equation 1 under steady state conditions, Cartesian coordinates are used and pseudo-first-order reaction conditions are assumed. Laminar flow is assumed with a constant flow velocity. An important simplifying assumption is that diffusion along the z-axis is negligible compared to convective transport. With these assumptions, equation 1 becomes equation 2:

$$v \frac{\delta C_a}{\delta z} = D_{ab} \left[\frac{\delta^2 C_a}{\delta x^2} + \frac{\delta^2 C_a}{\delta y^2} \right] - [\sum_1 k_1 C_1] C_a \quad \text{eqn. 2}$$

Solution of equation 2 is facilitated by substituting the trial function $C_a = C_a' \exp(-\sum_1 k_1 C_1 / v) z$ (References 15 and 19), which yields equation 3, a pure flow/diffusion problem. Formally, equation 3 is identical to a large class of transient diffusion problems for which solutions exist when $C_a'(x, y, z)$ is an analytic function at some value of $z = z_0$ and when one or more other constraining (boundary) conditions are given (References 19 and 20).

$$v \frac{\delta C_a'}{\delta z} = D_{ab} \left[\frac{\delta^2 C_a'}{\delta x^2} + \frac{\delta^2 C_a'}{\delta y^2} \right] \quad \text{eqn. 3}$$

Fortunately C_a' does not need to be determined explicitly. Equation 3 can be solved by separating variables (Reference 21) to produce a solution of the form $C_a'(x,y,z) = X(x)Y(y)Z(z)$. The complete solution is of the form

$$C_a(x,y,z) = X(x)Y(y)Z(z)\exp(-\sum k_1 C_1/v)z$$

If C_1 is varied systematically, plots of $\ln(C_a(x,y,z,C_1)/C_a(x,y,z,C_1=0))$ against C_1 return k_1/v as the slope. The C_a' terms cancel identically.

If a spectrometer cell is used to measure C_a , the situation is more complex. In this case the measured quantity is the average value of C_a in the spectrometer cell, C_{aave} , and is given by

$$C_{aave} = \frac{1}{V_C} \int_{V_C} C_a(x, y, z,) dV_C$$

where V_C is the cell volume.

In equation 4, the $X(x)$ and $Y(y)$ components of C_a' cancel identically, but a more explicit expression for $Z(z)$ is required. In general, $Z(z)$ is of the form $Z(z) = B\exp(-p^2z)$ (Reference 19) where p^2 and B are separation constants to be determined by application of the boundary and initial ($z = 0$) conditions. The expression for C_{aave} can now be integrated for the case of a single reactant, C_1 , to give

$$\begin{aligned} \frac{C_{aave}(C_1)}{C_{aave}(C_1=0)} &= \frac{A(C_1)}{A(C_1=0)} \\ &= \frac{p^2}{p^2 + \frac{k_1 C_1}{v}} \left[\frac{\frac{e^{-k_1 C_1 z_1}}{v} - \frac{e^{-k_1 C_1 z_2}}{v}}{\frac{e^{-p^2 z_1}}{v} - \frac{e^{-p^2 z_2}}{v}} \right] \end{aligned} \quad \text{eqn. 4}$$

Rate constants can be obtained by plotting $(C_{aave}(C_1)/C_{aave}(C_1=0)) = (A(C_1)/A(C_1=0))$ where A is the absorbance signal. The separation constant B cancels identically, and both the rate constant, k_1 , and the remaining separation

constant, p , can be determined by graphic or nonlinear modeling methods.

APPROACH

These flow reactor concepts were developed and evaluated by numerical simulation of and performance measurements on the prototype WSTF flow reactor design. The numerical simulation was designed to better understand how the ideal prototype reactor would perform. The performance measurements to date were made to see if the prototype reactor can produce a carrier-gas velocity field that is uniform, laminar, and flat, as required. Understanding the fluid flow characteristics of the reactor is prerequisite to obtaining valid kinetic measurements.

RESULTS AND DISCUSSION

EVALUATION BY SIMULATION

Numerical Simulation of Flow Reactor Performance

The theoretical treatment presented above shows that rate data can, in principle, be obtained from a flow/diffusion/reaction system. However, this treatment provides little insight into reactor performance or reactor limitations.

For the case of diffusion from a point source in a uniform velocity field, a simple closed-form analytical solution to equation 3 can be found (References 13 and 22). In the prototype reactor, the reactant, a , is introduced into a uniform carrier flow containing one reactant at a uniform concentration, C_1 . We will consider only the net disappearance of reactant a .

The reactant introduction system is designed to resemble an array of point sources that produces only a minimal disturbance of the flow field. As a result, the prototype flow reactor can be represented to good approximation by a linear combination of point source solutions (Reference 19). The linear combination of point sources provides an explicit expression for C_a' . $C_a = C_a' \exp(k_1 C_1 / v)$ as before (axial

diffusion was not neglected in the point source solution; use of the exponential reaction term is an approximation).

The configuration of the reactor to be simulated with this approach is shown in figure 1. At $z = 0$ an array of point sources can be described as a stack of nine source lines symmetrical about $y = 0$, $x = 0$. Each source line is composed of 401 points. The location of the array corresponds to the location of the reactant introduction system in the prototype reactor.

The point source solution is given by

$$C_a'P(x,y,z) = \frac{W_a}{4 \pi D_{ab} \sqrt{x^2 + y^2 + z^2}} e^{-\frac{v}{2 D_{ab}} [\sqrt{x^2 + y^2 + z^2} - z]}$$

where W_a is the rate of introduction of species a in moles/second. The expression for a single line of point sources along the x-axis is

$$C_a'L(x,y,z) = \sum_m C_a'P(x - mb, y, z)$$

$$b = 0.1 \text{ cm,}$$

$$m = -200, -199 \dots 200$$

which describes a line of point sources 40 cm long with 0.1 cm spacing. The expression for the final array is given by

$$C_a'A(x,y,z) = \sum_n C_aL(x,y - nd, z)$$

$$d = 0.32 \text{ cm} \quad \text{eqn. 5}$$

$$n = -4, -3, \dots 3$$

which describes an array of nine line sources symmetrical about $y = 0$ with 0.32 cm between lines.

The reactor simulation was carried out on an IBM PC-XT by direct calculation of equation 5 using the Math Cad software package from Math Soft, Inc. (Reference 23). Concentration profiles were calculated for the hydrazine - ozone reaction and the monomethylhydrazine (MMH) - ozone reaction. In addition, C_{aave} for a hypothetical spectrometer white cell was estimated

for several different ozone concentrations, in effect simulating an actual kinetic experiment. The carrier flow velocity was 10 cm/sec, and the reaction rate constants were those measured or estimated by Tuazon et al (Reference 24): $1 \times 10^{-16} \text{ cm}^3 \text{ molecule}^{-1} \text{ sec}^{-1}$ for hydrazine and $1 \times 10^{-15} \text{ cm}^3 \text{ molecule}^{-1} \text{ sec}^{-1}$ for MMH. The diffusion coefficients used were $0.39 \text{ cm}^2/\text{sec}$ for hydrazine and $0.15 \text{ cm}^2/\text{sec}$ for MMH.*

Calculated hydrazine and MMH concentrations in the $x = 0$ plane are plotted for several different values of z in figures 2 and 3. Ozone is assumed to be present at $3.0 \times 10^{-8} \text{ mol/cc}$. Diffusion results in a rapid smoothing of the concentration profile and rapid achievement of reasonable pseudo-first-order kinetic conditions. Direct calculation also shows that the hydrazine or MMH concentrations at the reactor walls are effectively zero throughout the kinetic measurement section. Hydrazine and MMH both decay rapidly along the z -axis when ozone is present. Figure 4 shows the decay of hydrazine and MMH along the z -axis under the same conditions as those assumed in calculating figures 2 and 3. The decay curves show that hydrazine or MMH concentration in the spectrometer cell depends on $k_1 C_1$ and the flow velocity, v .

Calculated values of C_{ave} and the corresponding peak absorbance values as a function of ozone concentration are shown for hydrazine and MMH in table 1. Reasonable absorbance values can be obtained over a range of ozone concentrations which permits recovery of the net disappearance rate constants for MMH and hydrazine.

* The MMH diffusion coefficient was derived from measurements made at White Sands Test Facility using gas chromatography (results to be published). The diffusion coefficient for hydrazine was derived from the data of R.L. Johnson and P.G. Bhuta in the TRW Systems (One Space Park, Redondo Beach, California) final report 07282-6032-R0-00, August 15, 1969.

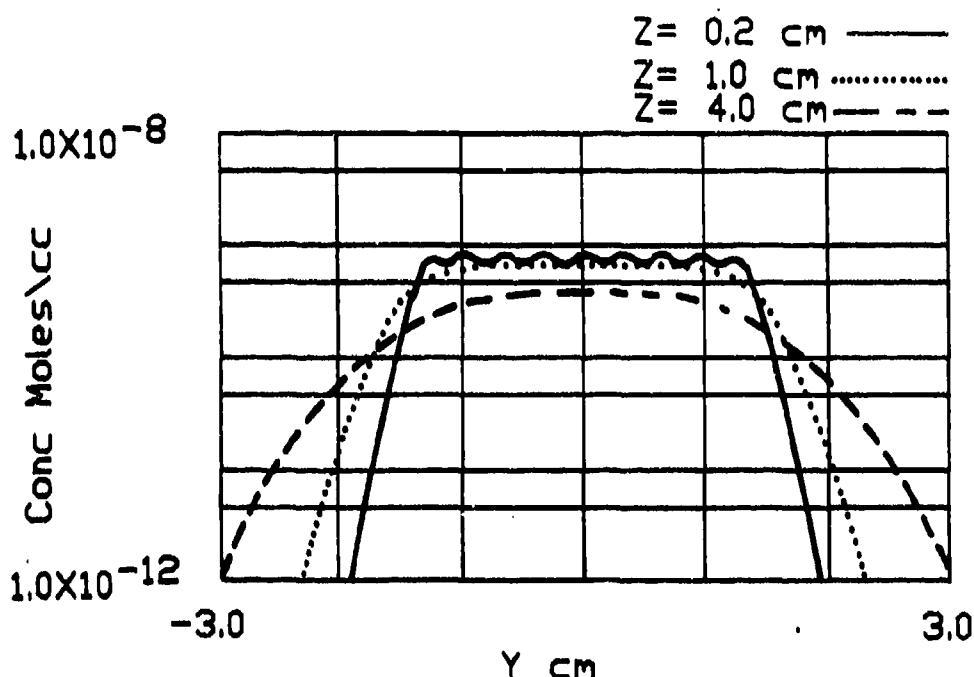


Figure 2. Calculated Hydrazine Concentration
 Hydrazine concentration as a function of the y-coordinate for $x = 0$ and three different values of z downstream of the introduction array. Conditions: $P = 760$ torr, $T = 300$ K, $v = 10$ cm/sec, $O_3 = 3.0 \times 10^{-8}$ moles/cc, hydrazine/MMH introduction rate is constant

Critical Parameters and Limitations of Flow Reactors

The quantity $(k_1 C_1 / v)^{-1}$ is the characteristic reaction length for this system. The precision and sensitivity of the technique used to measure the C_a interacts with the range of useful flow velocities through the reaction length expression to determine the range of values of the rate constants that can be measured with a given piece of equipment. If the minimum useful absorbance value is 0.01 AU cm^{-1} , then rate constants between 10^{-17} and $10^{-14} \text{ cm}^3 \text{ molecule}^{-1} \text{ sec}^{-1}$ should be measurable if useful flow velocities (between 10 and 100 cm/sec) can be achieved. The data in table 1 can be recalculated directly using the reaction decay term to show this. Extension to rates greater than $10^{-14} \text{ cm}^3 \text{ molecule}^{-1} \text{ sec}^{-1}$ may only be achieved by reductions in C_1 (i.e., better

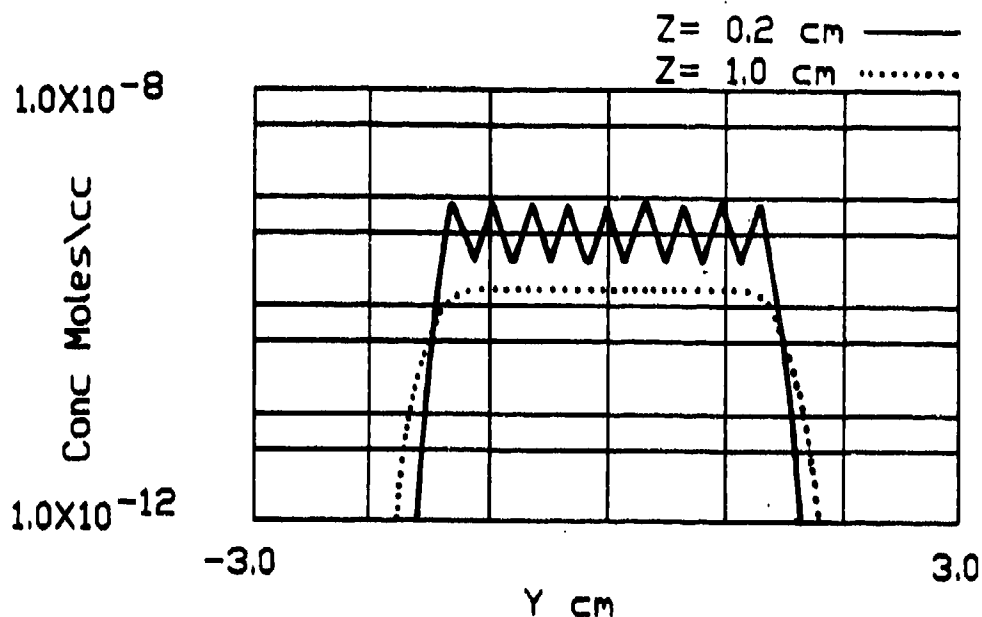


Figure 3. Calculated MMH Concentration
MMH concentration as a function of the y-coordinate for $x = 0$ and two different values of z downstream of the introduction array. Conditions: $P = 760$ torr, $T = 300$ K, $v = 10$ cm/sec, $O_3 = 3.0 \times 10^{-8}$ moles/cc, hydrazine/MMH introduction rate is constant

measurement sensitivity) combined with further increases in flow velocity (limited by the onset of turbulence).

EVALUATION OF ACTUAL PERFORMANCE

Design of the Prototype Flow Reactor

The prototype flow reactor was provided by Kurz Instruments of Carmel California. The flow reactor consists of a mass flow meter, a precision flow control valve, an expansion - diffuser section, a set of microetched screens designed to eliminate turbulence, and the chemical kinetics flow section. The data obtained from the mass flow meter are used to regulate the flow control valve through control and display electronics.

The flow reactor provides a uniform, constant, laminar carrier-gas flow (i.e., a flow field described by a single velocity vector, v) by applying well-known principles of fluid

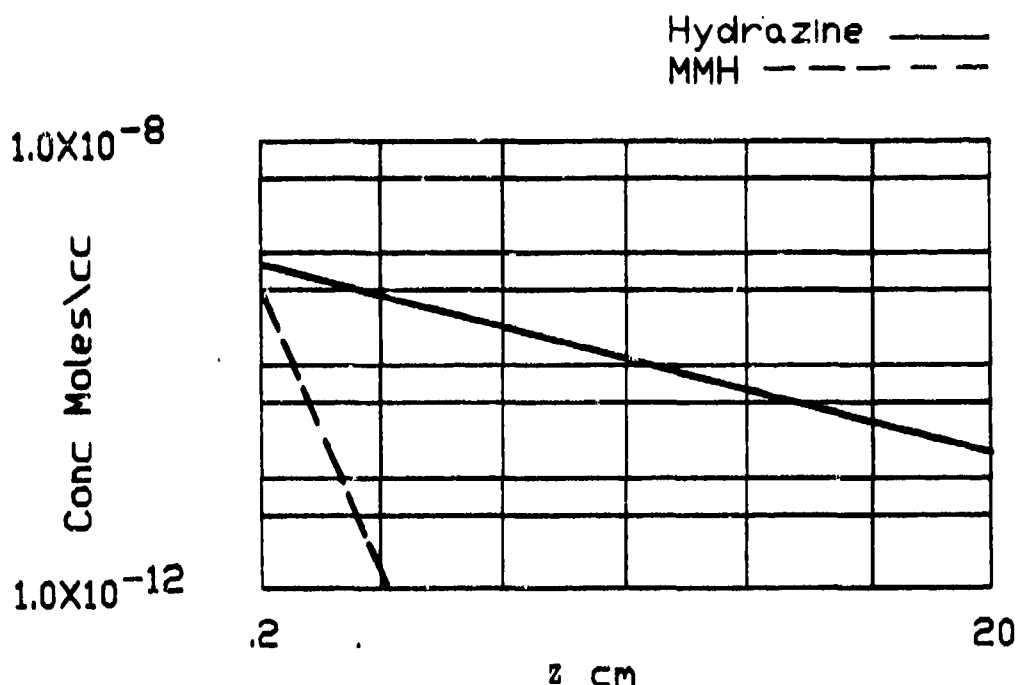


Figure 4. Calculated Hydrazine and MMH Concentration Decay
Hydrazine and MMH concentrations at $x = 0$, $y = 0$ as a
function of z downstream from the introduction array.
Conditions: $P = 760$ torr, $T = 300$ K, $v = 10$ cm/sec, $O_3 =$
 3.0×10^{-8} moles/cc, hydrazine/MMH introduction rate is
constant

dynamics (References 22, 25, 26, and 27). The Point Source Method of measuring diffusion coefficients (Reference 22) uses many of the same principles as the flow reactor described in this paper and achieves the necessary uniform, laminar, constant flow fields. Diffusion coefficients were measured with accuracy and repeatability on the order of 2 percent.

Turbulence in the kinetic measurement section of the prototype reactor is prevented by the use of an expansion section in front of flow-smoothing screens that are located between the flow control valve and the kinetic measurement section. The development of a parabolic velocity profile is prevented by working at high Reynolds numbers so that the entry length, L_e , of the kinetic measurement section is much greater than the physical length, L (Reference 13).

TABLE 1. NUMERICAL SIMULATION OF HYDRAZINE AND MMH KINETICS
AT VARYING OZONE CONCENTRATIONS^a

O ₃ Concentration (moles/cc)	Hydrazine		MMH	
	C _{ave} ^b (moles/cc)	Absorbance (AU)	C _{ave} ^b (moles/cc)	Absorbance (AU)
0	3.7 x 10 ⁻¹⁰	0.11	3.6 x 10 ⁻¹⁰	0.13
8 x 10 ⁻⁹	2.9 x 10 ⁻¹⁰	0.082	1.2 x 10 ⁻¹⁰	0.036
1.6 x 10 ⁻⁸	2.2 x 10 ⁻¹⁰	0.063	5.3 x 10 ⁻¹¹	0.015
2 x 10 ⁻⁸	1.9 x 10 ⁻¹⁰	0.056	3.7 x 10 ⁻¹¹	0.011
2.4 x 10 ⁻⁸	1.7 x 10 ⁻¹⁰	0.049	2.7 x 10 ⁻¹¹	0.008

^a P = 760 torr, T = 300 K, v = 10 cm/sec, hydrazine/MMH
introduction rate is constant

^b Average concentration in the spectrometer cell

Performance Data for the Prototype Flow Reactor

The velocity field in the flow reactor was measured at Reynolds numbers (Re) of 1380 and 2100 with a hot wire anemometer. The average value and variance for 48 different sampling positions uniformly distributed within the kinetic flow section were obtained. The flowing gas was nitrogen at 0.84 atm (ambient pressure at WSTF). The average velocity at a Reynolds number of 1380 was 15 cm/sec with a variance of ± 0 ; the average velocity at a Reynolds number of 2100 was 20 cm/sec with a variance of ± 1 .

No evidence of turbulence was obtained, and the variance in the velocity at the higher Reynolds number was probably small enough to permit accurate chemical kinetic measurements (References 25 through 26 suggest that velocity variance on the order of 10 percent has no adverse effects on the measurement of diffusion constants to 2 percent accuracy). The variation in velocity may be further reduced by changing the number and type of flow-smoothing screens.

CONCLUSIONS

Both general theoretical considerations and numerical simulation show that chemical kinetic measurements can be made near 1 atm of pressure with no contribution from wall effects. The chemical reaction is not homogeneous (i.e., the reactant concentrations are not uniform in the duct), but solution of the flow/diffusion/reaction equation allows determination of reaction rate constants and/or diffusion constants from experimental data if certain conditions are maintained. The most important conditions are the following: (1) uniform, constant, laminar carrier-gas flow; (2) pseudo-first-order reaction conditions; and (3) pressures near 1 atm to maintain small diffusion coefficients ($0.1 \text{ cm}^2 \text{ sec}^{-1}$). The prototype WSTF kinetic flow system was shown to maintain the first condition readily. Work is in progress to determine the rates and mechanisms of decay of the hydrazine fuels in the troposphere using this new type of flow reactor.

REFERENCES

1. Chamberlain, J.W., Theory of Planetary Atmospheres, Academic Press, New York, 1978.
2. Finlayson-Pitts, B.J. and J.N. Pitts, Atmospheric Chemistry, John Wiley and Sons, New York, 1986.
3. Pearson, R.G. and J.W. Moore, Kinetics and Mechanism, John Wiley and Sons, New York, 1981.
4. Poirier, R.V. and R.W. Carr, J. Phys. Chem., 1971 (75:10), p. 1593.
5. Keyser, L.F., J. Phys. Chem., 1984 (88), pp. 4750.
6. Gutman, D., N. Saunders, and J.E. Butler, J. Chem. Phys., 1982 (86), p. 66.
7. Jonah, C.D., W.A. Mulac, P. Zeglinski, J. Phys. Chem., 1984 (88), p. 4100.
8. Finlayson-Pitts and Pitts, Atmospheric Chemistry, ch. 6, 1986.
9. Howard, C.J., J. Chem. Phys., 1979 (83), p. 3.
10. Clyne, M.A.A. and W.P. Nip, Int. J. Chem. Kinet., 1977 (10), p. 397.
11. Anderson, J.G., J.G. Margitan, and F. Kaufman, J. Chem. Phys., 1974 (60), p. 3310.
12. Debley, P.E., Rev. Sci. Instrum., 1970 (41), p. 1290.
13. Bird, B.R., W.E. Stewart, and E.N. Lightfoot, Transport Phenomena, pp. 173-174, John Wiley and Sons, New York, 1960.
14. Griffiths, P.R., Chemical Infrared Fourier Transform Spectroscopy, p. 35, John Wiley and Sons, New York, 1975.
15. Ogren, P.J., J. Chem. Phys., 1975 (79), p. 1749.
16. Brown, R.L., J. Res. Natl. Bur. Stand. (US), 1978 (83), p. 1.
17. Bolden, R.C., R.S. Hemsworth, M.J. Shaw, and N.D. Twiddy, J. Phys. B: Atom. Molec. Phys., 1970 (3), p. 45.
18. Farragher, A.L., Faraday Soc. Trans., 1970 (66), p. 1411.
19. Crank, J., The Mathematics of Diffusion, 2nd Ed., Oxford University Press, Oxford, Eng., 1975.

20. Kreyszig, E., Advanced Engineering Mathematics, Ch. 10, John Wiley and Sons, 1972.
21. Carrier, G.F. and C.E. Pearson, Partial Differential Equations, Academic Press, New York, 1976.
22. Walker R.E. and A.A. Westenberg, J. Chem. Phys., 1958 (29), p. 1139.
23. MathSoft, Inc., One Kendall Square, Cambridge, Mass.
24. Tuazon, E.C., W.P.L. Carter, R.V. Brown, R. Atkinson, A.M. Winer, and J. N. Pitts, Atmospheric Reaction Mechanisms of Amine Fuels, Final Report ESL-TR-82-17 AFESC, Tyndall AFB, Fla.
25. Walker, R.E. and A.A. Westenberg, J. Chem. Phys., 1958 (29:5), p. 1147.
26. Walker, R.E. and A.A. Westenberg, J. Chem. Phys., 1960 (32:5), p. 1314.
27. Walker, R.E. and A.A. Westenberg, J. Chem. Phys., 1959 (31:2), p. 519.

THE BEHAVIOR OF HYDRAZINE VAPOR IN AN ENVIRONMENTAL CHAMBER
UNDER SIMULATED ATMOSPHERIC CONDITIONS

D. A. Stone, Research Chemist
Headquarters Air Force Engineering and Services Center
Engineering and Services Laboratory
Tyndall Air Force Base, FL 32403-6001

F. L. Wiseman, Research Chemist

ABSTRACT

A series of experiments has been conducted to determine the decay kinetics of hydrazine vapor under simulated atmospheric conditions. These experiments were carried out in a 320-1 environmental simulation chamber. Conditions studied included dry and humid air, and dry and humid nitrogen. The concentration of hydrazine was monitored with long-path FT-IR spectroscopy. In contrast to earlier studies in glass vessels, there was no detectable difference in the decay rate of hydrazine in dry air or in dry nitrogen. The rate of decay of hydrazine in humid air or humid nitrogen was also essentially identical, but was four to five times faster than in dry air or dry nitrogen. Adsorption and permeation appear to be the major controlling factors in the decay of hydrazine in this chamber.

INTRODUCTION

Hydrazine is used extensively in small thrusters for satellites, as a fuel cell reactant, in emergency power generating units and as a liquid rocket fuel component. Both routine handling operations and accidental spills can produce fuel vapors which constitute a substantial health risk. Hydrazine is classified as an animal carcinogen (Reference 1) and a suspect human carcinogen (Reference 2). This toxicity is reflected in its low threshold limit value, 0.1 ppm (Reference 3), and has prompted numerous studies of its eventual fate in both atmospheric and terrestrial environments.

The autoxidation of hydrazine vapor has been the subject of several previous studies. These have included studies in glass containers (References 4-10), in small (less than 500 liter) Teflon[®] or Tedlar[®] bags (References 13-16) and large (greater than 3000 liter) Teflon[®] film chambers (References 11,12). Generally, these studies have shown that the reaction between hydrazine and oxygen proceeds by a multi-step process with several radical intermediates. These investigations have also noted that the rate of the reaction depended on the surface area and composition of the reaction vessel. The overall observed stoichiometry in these studies, however, was shown to be the simple relation,



It is clear from the findings of previous studies that the relative magnitudes of humidity, adsorption, permeation, surface-to-volume ratio and actual oxidation as factors affecting the decay of hydrazine in various types of reaction chambers are still very much in question. This study was undertaken to further investigate these effects with the aim of attempting to clarify the relative importance of these various loss processes.

EXPERIMENTAL

Complete descriptions of the reaction chamber, pure air system, FT-IR spectrometer, long-path optics, sample inlet system, and experimental methods are published in other reports (References 12 and 17). Briefly, the studies were conducted in a 320-l chamber constructed from .005-in FEP Teflon[®] film (Figure 1). The chamber was suspended within an aluminum frame and the frame was covered with Plexiglas[®]. The gas distribution system had outlets for both the inside of the chamber and the annular space between the chamber and the Plexiglas[®] cover. This allowed control of the environment both inside and outside the chamber.

A typical experimental run was conducted by purging the chamber and its support area with the matrix gas under study. The chamber mixing fan was operated continuously during this time. The hydrazine sample was injected into an exterior, heated glass bulb and flushed into the chamber with

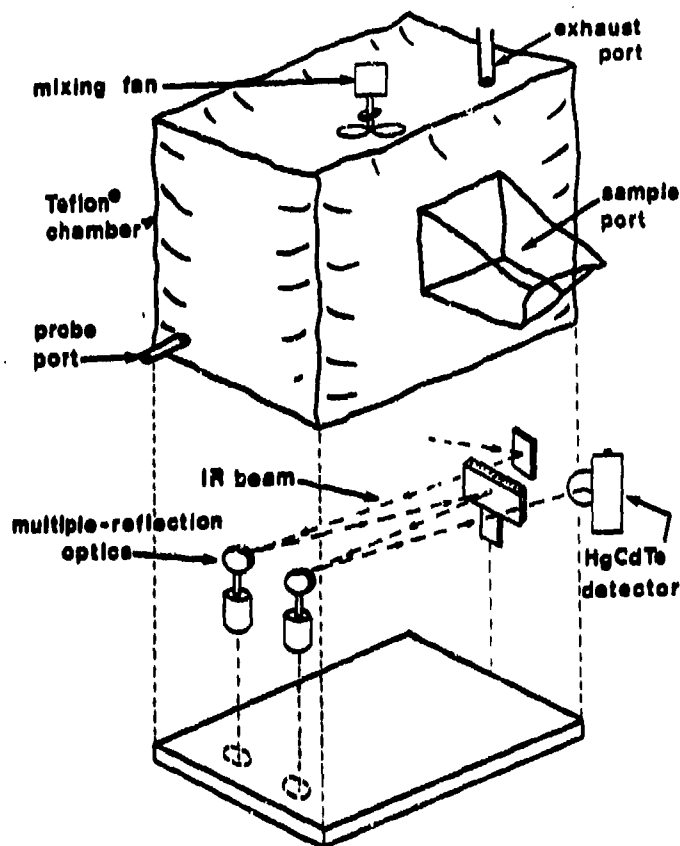


Figure 1. Environmental Chamber and Internal Reflection Optics

matrix gas. Then the mixing fan was shut off and the concentration of the hydrazine was monitored with the FT-IR spectrometer.

RESULTS AND DISCUSSION

THE STABILITY OF INTERNAL STANDARDS IN THE ENVIRONMENTAL CHAMBER

Both methane (CH_4) and sulfur hexafluoride (SF_6) were used to test the stability of inert gases in the environmental chamber. Numerous experimental runs were conducted where these gases were introduced into the chamber under a variety of experimental conditions. Methane was used as the internal standard for most of the hydrazine runs so that any major changes in chamber leak rate could be detected and repaired. Typical SF_6 and CH_4 stability curves are shown in Figure 2.

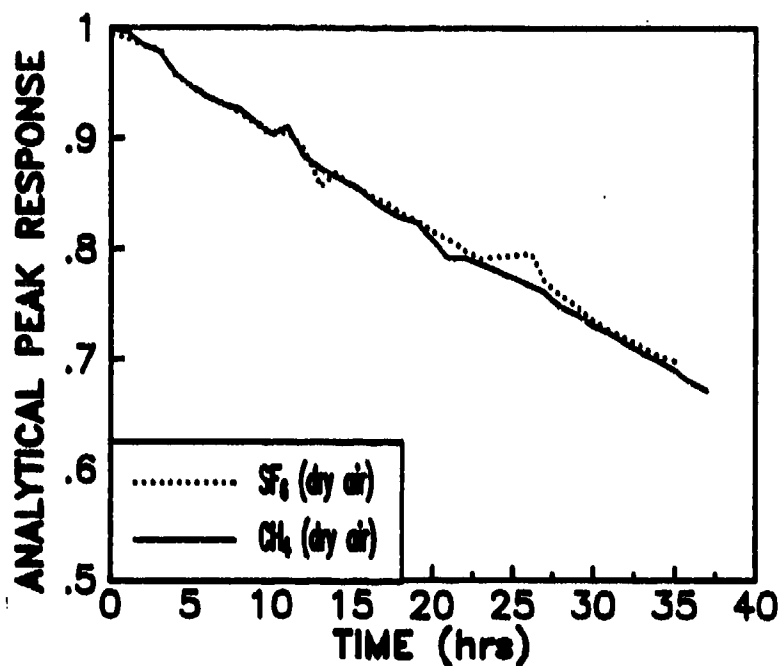


Figure 2. Decay of SF_6 and CH_4 in the Environmental Reaction Chamber

As the experiments were conducted, a concurrent effort was underway to develop a mathematical model of the processes which appeared to occur in the chamber. During the first few months of these experiments, it became clear that oxidation was only a minor process, if it occurred at all on the time scale of the observed disappearance of hydrazine. Thus, the model was developed to include the physical loss processes of adsorption/conditioning and permeation. It became clear that the experimental decay curves for any gas which had been used in the chamber could be duplicated very well with this type of model. The model and its development are discussed in a companion paper in this volume (Wiseman and Stone).

THE BEHAVIOR OF HYDRAZINE IN THE CHAMBER

Hydrazine in Dry Nitrogen

A total of five different experiments were conducted. The runs were normalized to a starting absorbance of one for the hydrazine analytical band at 958 cm^{-1} and plotted on one graph in Figure 3. Four of the runs fall on nearly the same decay curve, while one (the 10-12 Jan 86 run) is

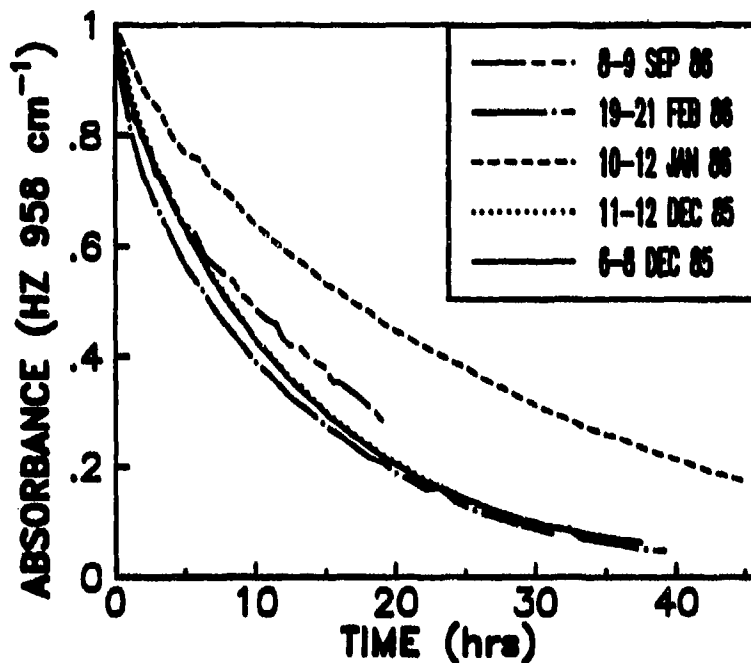


Figure 3. Hydrazine Decay in Dry Nitrogen

considerably slower. This slowest run was the third in a sequence of runs conducted within one week; apparently the first two runs served to condition the chamber causing the third run to exhibit a significantly longer half life. The other runs were all conducted after fairly long periods (two to four weeks) of no chamber activity. This apparently allowed the chamber enough time to de-condition and resulted in a shorter decay period.

Hydrazine in Dry Air

A total of 18 different experiments were conducted. These runs were separated into three groups (according to experimental time sequence) and normalized to a starting absorbance of one for comparison with each other. One set of runs is plotted in Figure 4. This set represents the final series of hydrazine/dry air runs which were conducted. To verify the chamber conditioning hypothesis, these runs were conducted in sequence, with no purging of the chamber in between runs. As anticipated they show a half-life which increases and reaches a maximum. This is consistent with a chamber conditioning process with a half-life of a few days.

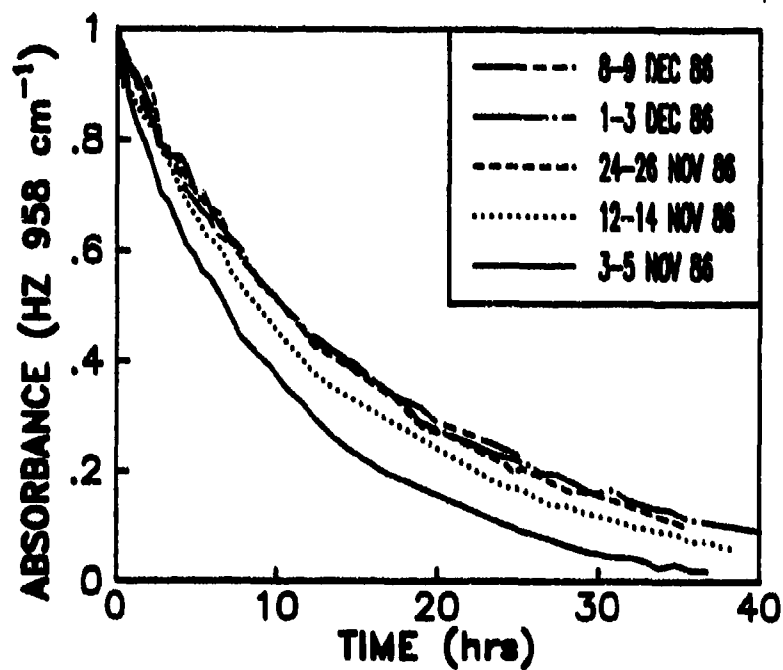


Figure 4. Hydrazine Decay in Dry Air, A Series of Five Sequential Runs

A comparison of hydrazine decay in dry nitrogen versus dry air under similar chamber conditioning is shown in Figure 5.

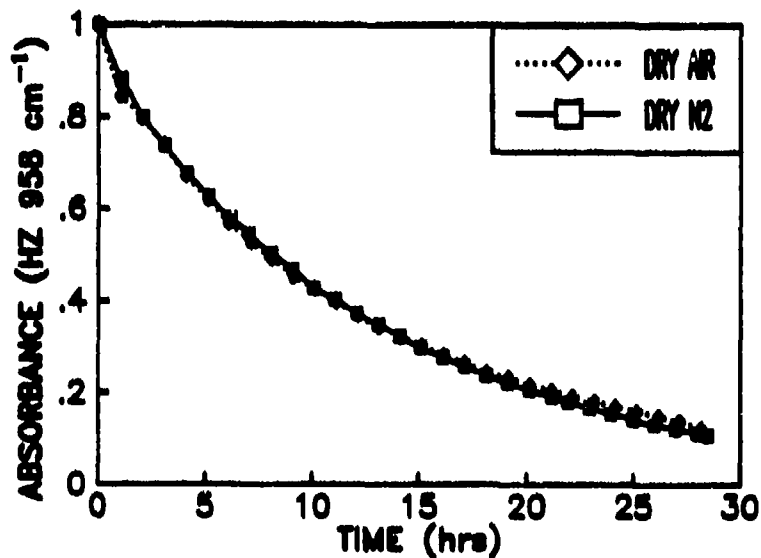


Figure 5. Comparison of Hydrazine Decay in Dry Nitrogen versus Dry Air
Hydrazine in Humid Nitrogen

Hydrazine in Humid Nitrogen

Because of experimental limitations, only a single run was conducted under these conditions. The decay curve is shown in Figure 6. Several observations were apparent in this system: (1) The decay was not pseudo-first-order, (2) The decay rate was much more rapid, and (3) There was a fairly significant amount of ammonia produced (≈ 4 ppm).

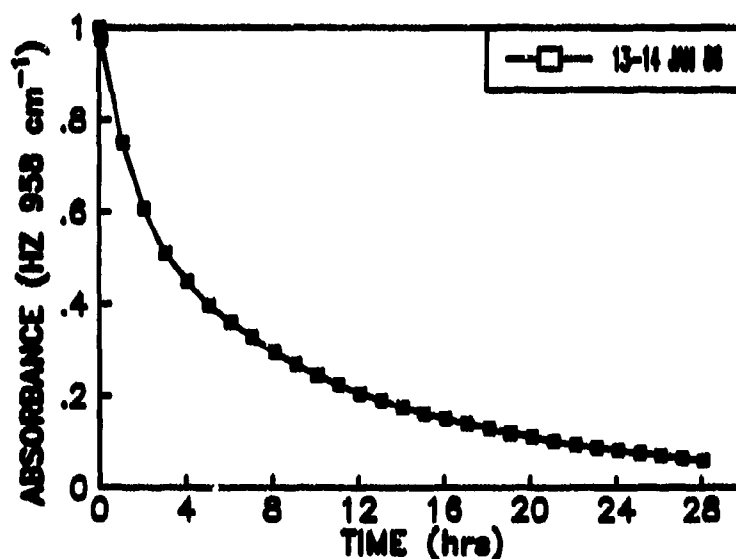


Figure 6. Decay of Hydrazine in Humid Nitrogen

The explanation for these dramatic differences in the decay curves for this system versus the hydrazine/dry nitrogen system appears to lie in the ability of Teflon® to readily adsorb and allow permeation of both hydrazine and water. In all likelihood, all of the "active sites" (both surface sites and microvoids in the film itself) on the Teflon® chamber surface are occupied by water in a high humidity experiment. In addition, the adsorbed water appears to catalyze the formation of ammonia.

Hydrazine in Humid Air

A total of 12 runs were completed in humid air. The final series were conducted in sequence, with no purging in between, to determine the chamber conditioning effects at high humidity levels. These six runs were

normalized to a beginning absorbance of one and are plotted in Figure 7.

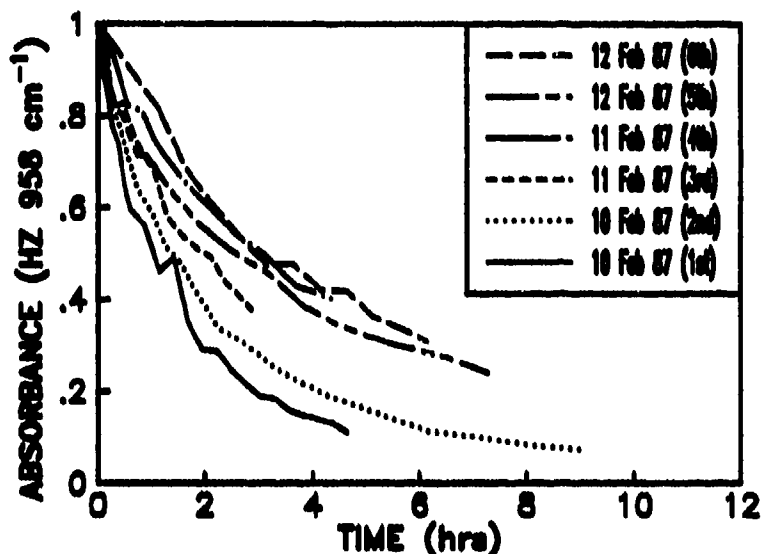


Figure 7. Decay of Hydrazine in Humid Air, a Series of Six Sequential Runs

Generally, the same type of conditioning response is noted in the first four runs. Runs 5 and 6 show no additional conditioning over run 4. Again, there is no readily discernible difference between the run conducted in humid nitrogen and those conducted under roughly similar conditions in humid air.

CONCLUSIONS

The decay of hydrazine vapor in an environmental simulation chamber is the result of physical loss processes, primarily adsorption followed by permeation. In dry air or nitrogen, the decay process is pseudo-first-order with a half life which depends on the degree of chamber conditioning which precedes any given experiment. The presence of water vapor causes a marked acceleration in the observed hydrazine decay rate, a departure from pseudo-first-order kinetics, and the production of additional ammonia. These results suggest that the homogeneous air oxidation of hydrazine should be studied in a rigid, evacuable chamber with a minimum of surface interactions and the lowest possible surface-to-volume ratio.

REFERENCES

1. Sotaniemi, E., J. Hirvonen, H. Isomake, J. Takkunen, and J. Kaila, "Hydrazine Toxicity in the Human: Report of a Fatal Case," Annals of Clinical Research, vol. 3, pp. 30-33, 1971.
2. Back, K. C. and A. A. Thomas, "Aerospace Problems in Pharmacology and Toxicology," Annual Reviews of Pharmacology, vol. 10, pp. 393-412, 1970.
3. Hannum, J. A. E., ed., Hazards of Chemical Rockets and Propellants, Volume III, "Liquid Propellants", Chemical Propulsion Information Agency, CPIA Publication 394, The Johns Hopkins University, Applied Physics Laboratory, Laurel, MD, September 1984.
4. Bowen, E. J. and A. W. Birley, "The Vapour Phase Reaction between Hydrazine and Oxygen," Faraday Society Transactions, vol. 47, pp. 380-383, 1951.
5. Winning, W. I. H., "The Thermal Oxidation of Hydrazine Vapour," Chemical Society Journal, pp. 926-931, 1954.
6. Stone, D. A., The Autoxidation of Hydrazine Vapor, Report No. GEEDO-TR-78-17, Civil and Environmental Engineering Development Office, Tyndall AFB, FL 32403, January 1978.
7. Stone, D. A., The Autoxidation of Monomethylhydrazine Vapor, Report No. ESL-TR-79-10, Air Force Engineering and Services Center, Tyndall AFB, FL 32403, April 1979, pp. 39-42 ("Additional Work on Hydrazine Autoxidation").
8. Bellerby, J. M., The Autoxidation of Hydrazine and Alkyl Substituted Hydrazine Vapours, Memorandum 92, Propellants, Explosives and Rocket Motor Establishment. Westcott, Aylesbury, Bucks. May 1980.
9. Bellerby, J. M., The Effect of Reaction Vessel Surfaces on the Vapour Phase Autoxidation of Hydrazines at Ambient Temperature, Memorandum 117, Propellants, Explosives and Rocket Motor Establishment. Westcott, Aylesbury, Bucks. August 1980.
10. Moody, K. N., The Vapour Phase Oxidation of Hydrazine, Ph.D. Thesis, The University of Leeds, April 1985.
11. Naik, D. V. and D. A. Stone, Air Oxidation of Hydrazine - A Kinetic Study, Final Report, USAF-SCEEE Summer Faculty Research Program, Tyndall AFB, FL 32403, September 1984.
12. Stone, D. A., M. V. Henley, and D. V. Naik, The Effects of Surfaces on the Air Oxidation of Hydrazine, Chemical Propulsion Information Agency Publication No. 436, November 1985, pp. 151-159.
13. Lin, S. F., The Decay of Hydrazine in Air, Final Report, USAF-SCEEE Research Initiation in Science Program, North Carolina Central University, Durham, NC, January 1985.

14. Naik, D. V., Kinetics of Homogeneous Gas Phase Oxidation of Hydrazine in Air, Final Report, USAF-SCEEE Research Initiation in Science Program, Monmouth College, West Long Branch, NJ, March 1986.
15. Pitts, J. N., Jr., E. C. Tuazon, W. P. L. Carter, A. M. Winer, G. W. Harris, R. Atkinson, and R. A. Graham, Atmospheric Chemistry of Hydrazines: Gas Phase Kinetics and Mechanistic Studies, Report No. ESL-TR-80-39, Air Force Engineering and Services Center, Tyndall AFB, FL 32403, August 1980.
16. Tuazon, E. C., W. P. L. Carter, R. V. Brown, R. Atkinson, A. M. Winer, and J. N. Pitts, Jr., Atmospheric Reaction Mechanisms of Amine Fuels, Report No. ESL-TR-82-17, Air Force Engineering and Services Center, Tyndall AFB, FL 32403, March 1982.
17. Stone, D. A. and F. L. Wiseman, Hydrazine Loss Processes in a Teflon® Film Reaction Chamber, Technical Report (to be published), Air Force Engineering and Services Center, Tyndall AFB, FL 32403-6001.

MODELING OF HYDRAZINE SURFACE INTERACTIONS IN ENVIRONMENTAL REACTION CHAMBERS

F. L. Wiseman and D. A. Stone
Headquarters Air Force Engineering and Services Center
Tyndall AFB, Florida

ABSTRACT

Hydrazine vapor loss data generated from Teflon[®] film reaction chambers have been successfully modeled. The data do not fit a simple first-order rate equation, but do fit a model which allows for surface adsorption, desorption, and permeation through the Teflon[®] film. This implies that the reaction between hydrazine vapor and oxygen is insignificant, and that surface interactions of hydrazine vapor are the significant avenues for hydrazine vapor losses in Teflon[®] film chambers. In humid conditions, hydrazine vapor losses are more rapid and more deviant from first-order behavior than in dry conditions. This has been modeled by assuming a hydrazine-hydrate formation. At this point it is not known whether the hydrate forms in the vapor or on the Teflon[®] film surface. The results of these studies were presented at the 1987 Joint Army Navy NASA Air Force (JANNAF) Safety and Environmental Protection Subcommittee held at Cleveland, Ohio^{1,2}.

INTRODUCTION

Hydrazine gas-phase processes have been studied for many years³⁻⁷. The air oxidation of hydrazine vapor has been proposed to go by the simple reaction⁸⁻¹¹:



However, recent studies have shown that air oxidation is not the major loss process of vaporous hydrazine in ambient conditions (room temperature and pressure). Evidence for this includes the fact that the hydrazine vapor decay rate is essentially unchanged in nitrogen-enriched environments and that nonreactive species, such as oxygen, water, methane, and sulfur

hexafluoride, exhibit similar kinetic behavior in Teflon[®] chambers. In addition, the hydrazine vapor loss rate is greatly enhanced in humid air¹¹. This phenomenon is difficult to account for in terms of a radical mechanism. A more likely explanation for this enhancement is that the excess water in the chamber environment is facilitating hydrazine hydrate formation, either in the gas phase or on the surface.

The kinetic model presented in this report incorporates surface adsorption and desorption reactions, permeation through the Teflon[®] film, chemical reactions, and leakages through very small holes¹². The model is more inclusive than required by this work, but was designed for future work, as well as this work. Condensed versions of this model fit the data much better than the pseudo-first-order rate equation required to describe Equation (1).

The experimental work for this report has been aptly described by Stone and Wiseman in a previous report¹ and will not be given in this report.

MODELING OF HYDRAZINE VAPOR LOSS

The model presented below takes into account all processes described above. Hereafter, the leakage process will be referred to as effusion, which is a term describing a gas molecule having a long mean-free path compared to the area of the hole through which it leaks. It can be shown that leakage of this type yields a first-order decay law for the gas in a container. Although the condition of the long mean-free path may not be met in these experimental conditions, it is assumed that leakage through holes can still be described by a simple first-order process. The model assumes the Teflon[®] film has pores throughout its entire thickness and the adsorbed molecules can migrate from one pore "layer" to another until they reach the outside pore layer. The molecules can then desorb and be lost from the system. This migration process is illustrated in Figure 1. The processes leading to loss of hydrazine from the chamber system are effusion, permeation, and irreversible chemical reactions. Adsorption onto surface materials placed inside the chamber or adsorption onto nonpermeable sites on the Teflon[®] film of the chamber do not lead to loss of hydrazine from the

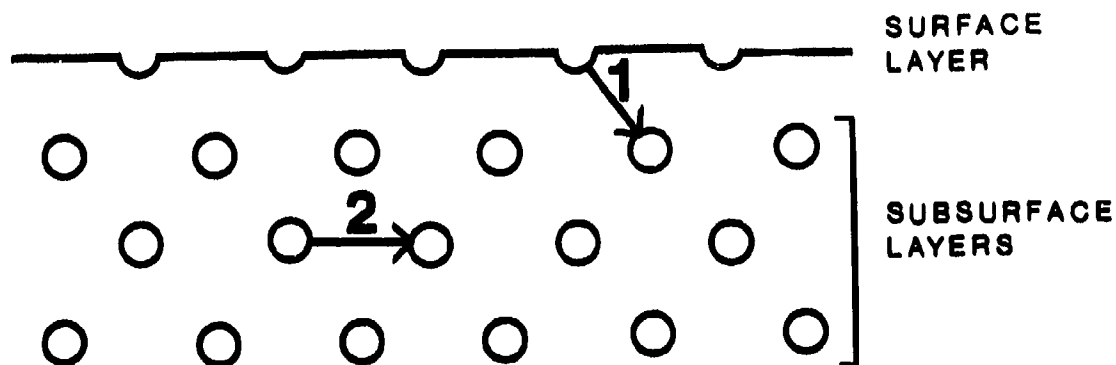
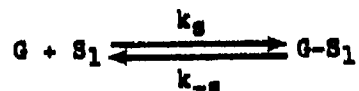


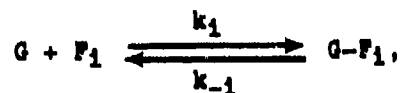
Figure 1. Diagram showing how a molecule can permeate within and through a polymeric film. Molecules can jump from one pore layer to another (arrow 1) or from one pore site to another within the same layer (arrow 2).

system but only to loss of hydrazine vapor. This model is not restricted to hydrazine and can be applied to any gas emitted into an environmental chamber.

Any gas, G, might interact with the chamber environment according to the following processes:



For $i = 1$ to f ;

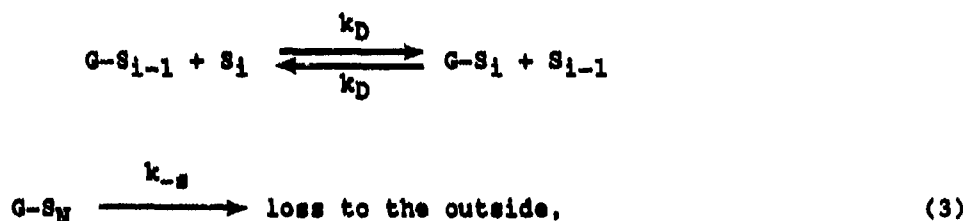


For $i = 1$ to p ;



in which k_e is the effusion rate constant, S_1 is the first pore layer on the inside surface of the Teflon[®] film, k_s and k_{-s} are the adsorption and desorption rate constants, respectively, for S_1 , $G-S_1$ is the adsorption complex on the first pore layer, f is the number of surfaces other than Teflon[®], F_i is the i th surface other than Teflon[®], $G-F_i$ is the i th adsorption complex on surface F_i , k_i and k_{-i} are the i th adsorption and desorption rate constants, respectively, for F_i , p is the number of gaseous species which can react with G , P_i is the i th species which reacts irreversibly with G in a second-order reaction, and k_{pi} is the rate constant for this reaction. Once $G-S_1$ is formed, the adsorbed molecules can either desorb or migrate to the next pore layer, S_2 . The molecules can then migrate to either S_1 or S_3 , the third pore layer. This process continues until some molecules have permeated to the last pore layer, S_N , in which N is the total number of pore layers. This process is modeled simply as:

For $i = 2$ to N ;



in which S_i is the i th pore layer, $G-S_i$ is the complex at the i th pore layer, and k_D is the diffusion rate constant. It is assumed that molecules desorbing off the outside pore layer, S_N , diffuse fast enough away from the chamber wall that outside adsorption does not take place. The differential rate equations describing the processes shown in Equations (2) and (3) are:

$$\begin{aligned}
 d[G]/dt = & -(k_s + k_s[S] + \sum_{i=1}^f k_i[F_i] + \sum_{i=1}^p k_{pi}P_i)[G] + \\
 & k_{-s}[G-S_1] + \sum_{i=1}^f k_{-i}[G-F_i]
 \end{aligned}$$

$$d[G-S_1]/dt = k_s[S][G] - k_{-s}[G-S_1] + k_D[S]([G-S_2] - [G-S_1])$$

For $i = 2$ to $N - 1$;

$$d[G-S_i]/dt = k_D[S]([G-S_{i-1}] + [G-S_{i+1}] - 2[G-S_i]),$$

$$d[G-S_N]/dt = k_D[S]([G-S_{N-1}] - [G-S_N]) - k_g[G-S_N]$$

For $i = 1$ to f ;

$$d[G-F_i]/dt = k_i[G][F_i] - k_{-i}[G-F_i],$$

in which the brackets refer to the concentrations, and $[S]$ is the pore layer concentration for each and every pore layer. If N is equal to 2, the equations described by $d[G-S_i]/dt$ are dropped. It is assumed that $[S] \gg [G]$, so that the diffusion rate steps are pseudo-first-order. If $[F_i]$ is comparable to $[G]$, then $[F_i]$ varies within the course of the process and must be replaced with $[F_i]_1 - [G-F_i]$, in which $[F_i]_1$ is the initial value of $[F_i]$. All surface concentrations, $[S]$, $[F_i]$, $[G-F_i]$, and $[G-S_i]$ are in the same units as the gas concentrations, $[G]$ and $[F_i]$, and are defined as the number of moles per unit chamber volume. The value chosen for N does not affect the quality of the model fit, but does affect the values for the fitted parameters. Although in theory N is quite large, N is normally set to 2 for speed of calculation.

These differential equations cannot be solved analytically, except for the most trivial cases. The finite difference method for numerical integration has been applied for obtaining solutions. The model can be fitted to the data using standard statistical routines with the modification that the estimated values for the dependent variable be generated from a numeric integration rather than a simple function.

The Marquardt nonlinear least squares approach was used to fit the model versions to the data. The program used (Statistics Volume 4, Tape 1) was run on the Model 4054 Tektronix computer. Although the program was not designed for the user-defined function to be a series of differential equations, the program could perform the fit with a properly written subroutine. The user-written subroutine required an iterative procedure to conduct the numeric integration up to the time for each data point. The step size for the independent variable, time, was normally set at .01 hour.

RESULTS AND DISCUSSION

Figure 2 shows plots of absorbance of hydrazine vapor (normalized to unit absorbance) vs. time in hours for a run in dry air and a run in dry nitrogen. Although in the dry nitrogen run, oxygen did leak back into the system after several hours, the results show that the oxygen in air has little effect on the rate of hydrazine vapor loss in Teflon® film chambers. Since it is unlikely that hydrazine is being depleted that fast by another chemical reaction, the only other explanation for hydrazine vapor loss is by some physical process, such as adsorption or permeation. Figure 3 shows a first-order fit and a model fit to a typical dry atmosphere kinetic run and illustrates hydrazine is not being depleted by just a first-order process.

Only condensed versions of the model are required to fit the data. Two condensed versions of the model have been used to fit single data sets: adsorption and desorption onto nonpermeable surface sites in conjunction with effusion, and permeation. Both versions require three parameters: $k_s[S]$, k_{-s} , and $k_p[S]$ for the permeation version and $k_1[F_1]$, k_{-1} , and k_e for the adsorption/desorption-effusion version. Both model versions fit the data equally well and hence it is difficult to determine which version is more accurate. However, for sequential data set fits (single model fits on two or more consecutive runs), these simple models do not fit. Modification of the adsorption/desorption-effusion version by replacing $[F_1]$ with $[F_1]_1 - [G-F_1]$ creates a version that fits much better. This version allows sites F_1 to become filled, hence showing a conditioning effect which is only slowly reversible.

Figure 4 shows the modified adsorption/desorption-effusion version fit to a sequential data set. The data sets were generated by allowing the chamber to be purged for a month and then performing kinetic runs in a row. The long purge allowed for at least partial "unconditioning" and the sequential runs allowed the effect of conditioning to be seen. The fitted parameters are: $k_1 = .75(.03) \text{ Au}^{-1} \cdot \text{hr}^{-1}$, $[F_1]_1 = .74(.02) \text{ Au}$, $k_{-1} = .0075(.0003) \text{ hr}^{-1}$, and $k_e = .087(.002) \text{ hr}^{-1}$ (Au is absorbance units).

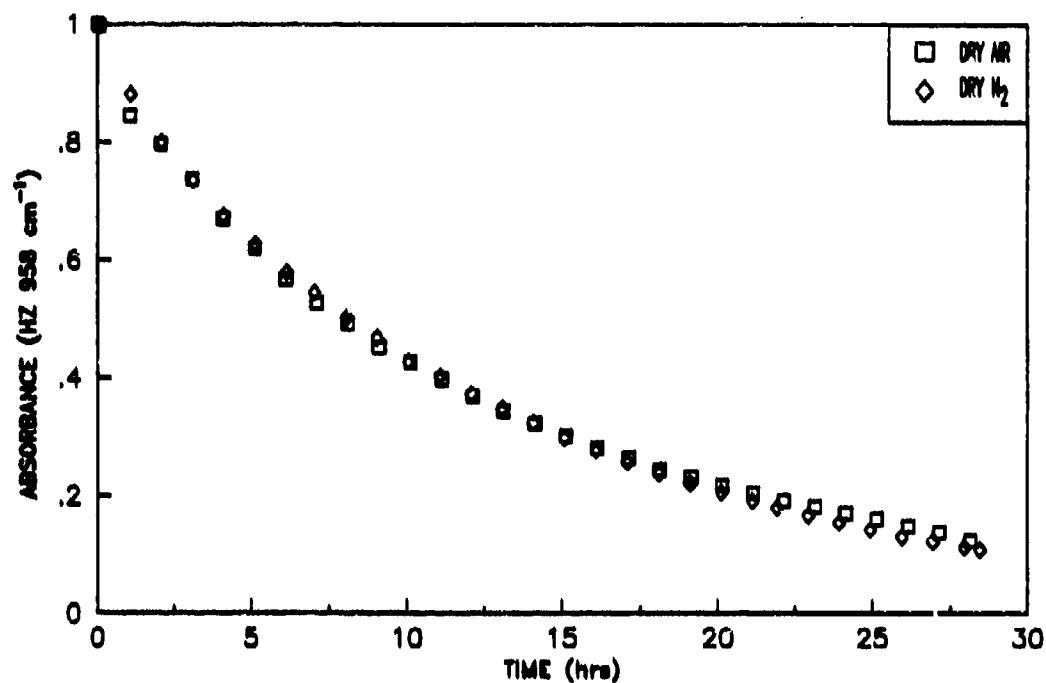


Figure 2. Plots of the normalized absorbance of hydrazine vs. time in hours for kinetic runs in dry air and dry nitrogen.

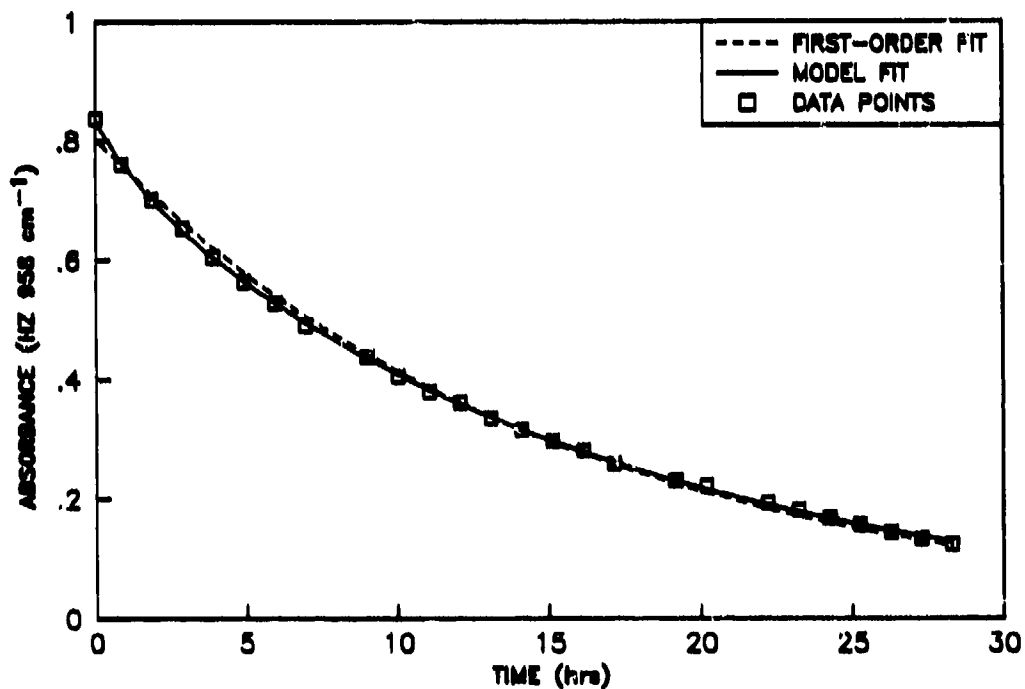


Figure 3. Fits of the permeation model and first-order model for a typical data set taken in dry conditions.

In this case, the first order term, k_g , may not represent effusion, but could represent steady-state permeation, which is also a first-order process. The conditioning effect and the decay rates are more sharply pronounced in humid conditions.

Since Teflon[®] is a polymer and hence shows unusual interactive properties with many gaseous compounds, it is not surprising that hydrazine interacts physically with the Teflon[®] film. In fact, Teflon[®] film chambers can be expected to interact strongly with other fuels and chemicals. Moreover, other polymeric film chambers can be expected to interact with hydrazine and other fuels. Other materials, such as glass¹³ and certain metals^{11,14}, apparently catalyze hydrazine oxidation. At least two hydrazine vapor loss runs must be performed to properly analyze any hydrazine reaction where the rate of the reaction is comparable to or less than the physical loss rate of hydrazine vapor in the chamber. The two data sets must be analyzed with a version of the model that fits the data well and considers the conditioning process. The fitted version of the model can then be used to predict how a third run should behave in the absence of any added reactant. This entire procedure "calibrates" the chamber system. If any reactive gas or surface material is then added to the system, the version used must be modified to account for the additional process. Of course, any reaction significantly faster than the physical loss processes of hydrazine vapor can be studied without resorting to this modeling calibration procedure.

CONCLUSION

The experimental work conducted in our laboratory and the modeling presented in this paper show strong evidence that hydrazine does not react with oxygen in the gas phase at ambient conditions. Past studies with hydrazine vapor in environmental chambers have been plagued by surface interactions which have been mistaken for air oxidation. These surface effects have not always been appreciated, but often account for the major loss processes of hydrazine vapor in chambers. Future hydrazine vapor research must consider that air oxidation is essentially nonexistent at ambient conditions and that surface interactions are important.

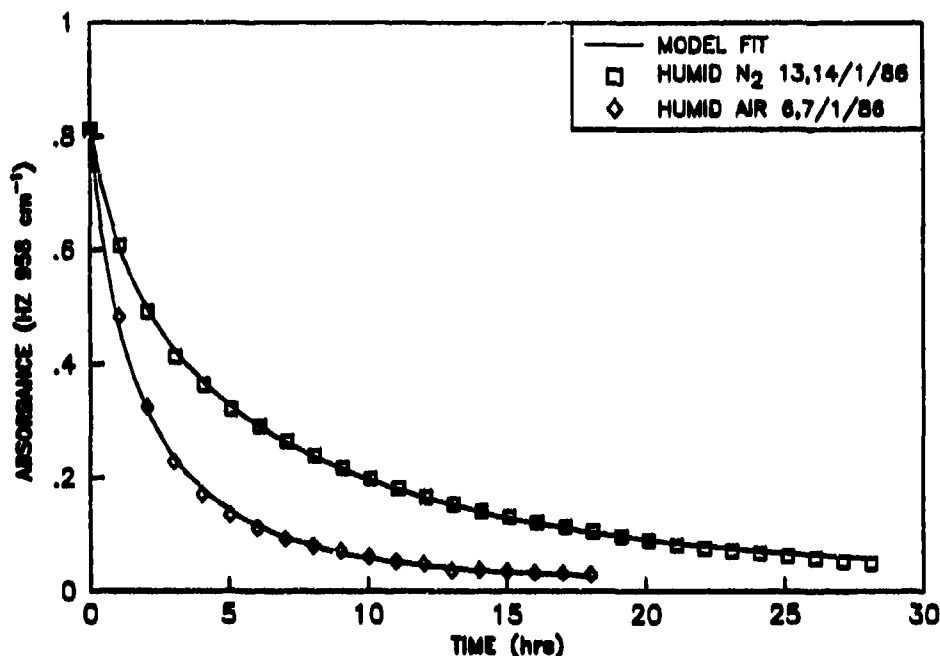


Figure 4. Fit of the modified adsorption/desorption-effusion model to a sequential data set taken in humid conditions. The dates the runs were taken are shown in the legend.

Future studies at the Engineering and Services Laboratory at Tyndall AFB will involve the use of a Teflon[®]-coated steel chamber for hydrazine fuels studies. This chamber will be constructed with heating coils to maintain constant temperature and will be designed for a more controlled environment. The chamber will be constructed to prevent any kind of leakage and will also allow for temperature studies. Model versions will be specifically designed to take into account all physical and chemical processes which may occur in this chamber.

REFERENCES

1. Stone, D.A., Wiseman, F.L., "The Decay of Hydrazine Vapor in a Teflon[®] Film Reaction Chamber," 1987 JANNAF Safety and Environmental Protection Subcommittee, Cleveland, OH; to be published.
2. Wiseman, F.L., Stone, D.A., "Modeling of Hydrazine Vapor Loss Processes in Teflon[®] Film Reaction Chambers," 1987 JANNAF Safety and Environmental Protection Subcommittee, Cleveland, OH; to be published.

3. Tuazon, E.C., W.P. Carter, R.V. Brown, R. Atkinson, A.M. Winer, J.N. Pitts Jr., "Atmospheric Reaction Mechanisms of Amine Fuels," Statewide Air Pollution Research Center, University of California. Final Report, March 1982, ESL-TR-82-17.
4. Pitts, J.N. Jr., E.C. Tuazon, W.P. Carter, A.M. Winer, G.W. Harris, R. Atkinson, R.A. Graham, "Atmospheric Chemistry of Hydrazines: Gas Phase Kinetics and Mechanistic Studies," Statewide Air Pollution Research Center, University of California. Final Report, August 1980, ESL-TR-80-39.
5. Stone, D.A., "The Autoxidation of Hydrazine Vapor," Civil and Environmental Engineering Development Office, January 1978, CEEDO-TR-78-17.
6. Tuazon, E.C., W.P. Carter, A.M. Winer, J.N. Pitts Jr., "Reactions of Hydrazines with Ozone Under Simulated Atmospheric Conditions," Environmental Science Technology, V15, No. 7, July 1981.
7. Dalgood, S.B., M.O. Sanford, "Review of the Hydrazine/Oxygen Reaction Kinetics," Paper No. 15, The International Corrosion Forum Sponsored by the National Association of Corrosion Engineers, April 1981.
8. Bellerby, J.M., "The Autoxidation of Hydrazine and Alkyl Substituted Hydrazine Vapours," PERME MEMO92, Propellants, Explosives, and Rocket Motor Establishments, Westcott, England, May 1980, N80-31520.
9. Winning, W.I.H., "The Thermal Oxidation of Hydrazine Vapour," J. Chem. Soc., 1954, 916 (1954).
10. Bowen, E.J., A.W. Birley, "The Vapour Phase Reaction Between Hydrazine and Oxygen," Trans. Faraday Soc., 47, 580 (1951).
11. Naik, D.V., "Air Oxidation of Hydrazine - A Kinetic Study," Air Force Office of Scientific Research Summer Faculty Program Final Report, August 1984.
12. The model presented in this work is conceptually very similar to one proposed by Vieth and Sladik (Vieth, W.R.; K.J. Sladik, "A Model for Diffusion in a Glassy Polymer," J. Coll. Science, 20, 1014 (1965)). However, the mathematical approach in this work is one of simple kinetic steps, whereas Vieth's and Sladik's work involves the use of diffusion equations.
13. Moody, K.N., "The Vapor Phase Oxidation of Hydrazine," Doctor of Philosophy Dissertation, Department of Chemistry, University of Leeds, Leeds, England, 1985.
14. Stone, D.A., M.V. Henley, D.V. Naik, "The Effects of Surfaces on the Air Oxidation of Hydrazine," 1985 JANNAF Safety and Environmental Protection Subcommittee Meeting, 151, (1985).

TRACE METAL CATALYSIS OF HYDRAZINE DECOMPOSITION: THE ROLE OF CHROMIUM

J. M. Bellerby

Chemical Systems Group
Cranfield Institute of Technology
Royal Military College of Science
Shrivenham, Swindon, Wilts SN6 8LA, UK

D. A. Edwards, D. Thompsett

School of Chemistry
University of Bath
Claverton Down, Bath BA2 7AY, UK

ABSTRACT

A new chromium (II) carbazato- complex, $\text{Cr}(\text{N}_2\text{H}_3\text{CO}_2)\cdot\text{H}_2\text{O}$, prepared by the reaction of aqueous carbazic acid with chromium (II) chloride, is described. The pale lilac solid, which has been fully characterised, is stable in air but undergoes oxidation to a chromium (III) carbazato- species on treatment with excess aqueous hydrazine in the presence of carbon dioxide. Evidence is presented showing that other complexes of chromium (II) are oxidised under similar conditions, leading to the conclusion that the stable oxidation state of chromium in anhydrous hydrazine is +3. Speculations are made regarding the significance of this in relation to the known activity of dissolved chromium as a homogeneous catalyst for the decomposition of propellant hydrazine.

INTRODUCTION

Dissolved carbon dioxide is known to increase the homogeneous decomposition rate of propellant hydrazine in stainless steel systems (Reference 1). This is thought to be due to the corrosive action of carbazic acid in leaching catalytically active trace metals such as chromium (Reference 2) from stainless steel surfaces. In order to understand more fully the role of chromium in the catalytic process the behaviour of the metal in both anhydrous hydrazine and in aqueous hydrazine in the presence of

carbon dioxide has been studied, the intention being to establish the relative stabilities of the +2 and +3 oxidation states in these situations.

Complexes of chromium (II) with hydrazine ligands (e.g. $\text{Cr}(\text{N}_2\text{H}_4)_2\text{Cl}_2$) are among the most stable compounds containing the metal in the +2 oxidation state (Reference 3). It is normally supposed that hydrazine, being a reducing agent, stabilises the lower oxidation state of chromium in preference to the more common +3 state. However the only known chromium species containing the closely-related carbazato- ligand is a stable chromium (III) complex, $\text{Cr}(\text{N}_2\text{H}_3\text{CO}_2)_3 \cdot 2\text{H}_2\text{O}$ (Reference 4), and there are no reports of this compound being reduced by hydrazine. Investigations into the chromium/hydrazine system therefore began with attempts to isolate a chromium (II) carbazato- complex.

RESULTS

PREPARATION, CHARACTERISATION AND REACTIONS OF A CHROMIUM (II) CARBAZATO-COMPLEX

The addition of an aqueous solution of chromium (II) chloride to a solution of carbazic acid in water precipitated a pale lilac solid which was found to be relatively air-stable when dry. A variety of techniques were used to characterise the complex.

Magnetic susceptibility measurements using the Gouy method produced a magnetic moment for the complex of 4.87 BM which is indicative of mononuclear high-spin chromium (II). Further support for this oxidation state came from the reflectance electronic spectrum of a fresh sample of the complex which showed bands at 551 nm, 400 nm and 275 nm. These band positions are similar to those of $\text{Cr}(\text{N}_2\text{H}_4)_2\text{Cl}_2$, which has its major transition at 570 nm (Reference 5), indicating that the new complex is subject to the considerable distortion from regular octahedral symmetry, presumably through the operation of the Jahn-Teller effect. This feature would again be consistent with a chromium (II) species.

Final confirmation of the chromium (II) metal centre came from redox titrimetry in which ~9 equivalents of $\text{Fe}(\text{CN})_6^{3-}$ were consumed on titration with a solution of the complex in 2M NaOH, pointing to a chromium (II) complex containing two hydrazine ligands. Together with micro-analytical data this information was sufficient to establish the lilac solid as the first reported carbazato- complex of chromium (II), $\text{Cr}(\text{N}_2\text{H}_3\text{CO}_2)_2 \cdot \text{H}_2\text{O}$. The supporting data which gave rise to this conclusion are summarised in Table 1.

TABLE 1. PROPERTIES OF $\text{Cr}(\text{N}_2\text{H}_3\text{CO}_2)_2 \cdot \text{H}_2\text{O}$.

Effective magnetic moment, $\mu_{\text{eff}}(\text{BM})$	4.87 (296K)
Reflectance electronic spectrum (nm)	551, 400, 275
Microanalytical data (%)	
Required	C, 10.9; H, 3.7; N, 25.5; Cr, 23.6
Found	C, 11.2; H, 3.1; N, 25.9; Cr, 23.3.
Equivalents of $\text{Fe}(\text{CN})_6^{3-}$ for oxidation	
Required	9
Found	9.3

The new complex was found to be insoluble in all common solvents but dissolved slowly in aqueous hydrazine in the presence of carbon dioxide to produce a bright red solution from which the known chromium (III) carbazato-complex, $\text{Cr}(\text{N}_2\text{H}_3\text{CO}_2)_3 \cdot 2\text{H}_2\text{O}$, could be isolated (Reference 6). The reaction took place even in the absence of air and this led to the conclusion that hydrazine or the hydrazinium ion was oxidising chromium (II) to chromium (III), an observation which has been made previously (Reference 7). Further work showed that any one of a range of chromium (II) complexes (e.g. $\text{Cr}(\text{N}_2\text{H}_4)_2\text{Cl}_2$) could be oxidised to the chromium (III) carbazato- species by treatment with excess aqueous hydrazine and carbon dioxide.

The relative stability of $\text{Cr}(\text{N}_2\text{H}_3\text{CO}_2)_2 \cdot \text{H}_2\text{O}$ in air is in line with the behaviour of other chromium (II) hydrazine complexes. However, it has been demonstrated (see above) that such complexes are readily susceptible to oxidation by hydrazine. The fact that they can be isolated at all in the presence of hydrazine would seem to be due to their extreme insolubility in the reaction medium used for their preparation. This is normally aqueous or alcoholic hydrazine. It is interesting to note that no chromium (II) hydrazine complex has been prepared directly from a chromium (III) source or in an anhydrous hydrazine reaction medium. These observations therefore raise the possibility that chromium (III) may be the more stable oxidation state in anhydrous hydrazine.

THE BEHAVIOUR OF CrCl_2 AND CrCl_3 IN SOLUTION IN ANHYDROUS HYDRAZINE

Anhydrous chromium (II) chloride (CrCl_2) dissolved in anhydrous hydrazine to give a pale violet solution which rapidly turned a bright red colour. The dissolution process was accompanied by a considerable evolution of heat and gas. The corresponding chromium (III) salt, CrCl_3 , also dissolved in anhydrous hydrazine with some vigour and produced a similar red solution. Despite repeated attempts it was not possible to isolate solid complexes from these chromium solutions and therefore investigations were carried-out to establish the identity of the dissolved species in each case. All experiments were conducted under nitrogen using deoxygenated anhydrous hydrazine which had been distilled from calcium hydride.

A close similarity was found between the electronic solution spectra of CrCl_2 and CrCl_3 in anhydrous hydrazine (Table 2) and this suggested that the oxidation state of the metal is the same in the two cases. However the spectra are not typical of octahedral chromium (III) species in hydrazine (e.g. $\text{Cr}(\text{N}_2\text{H}_3\text{CO}_2)_3 \cdot 2\text{H}_2\text{O}$).

Magnetic susceptibility measurements were carried-out on 10^{-3} molar solutions of CrCl_2 and CrCl_3 in anhydrous hydrazine using the Evans nuclear magnetic resonance (NMR) method (Reference 8). Acetonitrile was used as the

frequency shift indicator. Measurements were also made on CoCl_2 solutions for comparison purposes. High-spin octahedral cobalt (II) complexes such as $\text{Co}(\text{N}_2\text{H}_4)_6^{2+} \cdot 2\text{Cl}^-$ (the species assumed to be present in hydrazine solutions of CoCl_2) have magnetic moments of about 5BM at room temperature which is within the range observed for high-spin octahedral chromium (II). Therefore, for species of similar molecular weight the susceptibility values for chromium (II) and cobalt (II) in hydrazine will be similar.

TABLE 2. PROPERTIES OF CHROMIUM SPECIES IN HYDRAZINE

	CrCl_2	CrCl_3	$\text{Cr}(\text{N}_2\text{H}_3\text{CO}_2)_3 \cdot 2\text{H}_2\text{O}$	CoCl_2
Solution electronic spectra (nm)	694,525, 387,364.	698,532, 390,356.	700,522, 402	-
Magnetic susceptibility ($10^{-6} \text{ cm}^3\text{g}^{-1}$ at 296K)	23.7	15.8	19.19 (Gouy method on solid)	57.0
Molar conductance ($\Omega^{-1}\text{m}^{-2}\text{kmol}^{-1}$)	25.7 (2:1)	36.6 (3:1)	-	23.7 (2:1)

Measurements showed (Table 2) that the two chromium solutions had susceptibilities similar to one another but considerably different from that of CoCl_2 in hydrazine. This suggested that the chromium-hydrazine solutions did not contain the metal in the +2 oxidation state. The susceptibility values are more in line with those of chromium (III) complexes such as $\text{Cr}(\text{N}_2\text{H}_3\text{CO}_2)_3 \cdot 2\text{H}_2\text{O}$. Assuming $\text{Cr}(\text{N}_2\text{H}_4)_6^{3+} \cdot 3\text{Cl}^-$ is the dominant species in the CrCl_3 solution, a view supported by conductance measurements (Table 2) which confirmed the presence of a 3:1 electrolyte, then the measured susceptibility would give a magnetic moment of 3.7BM. This is in the region expected for a chromium (III) complex.

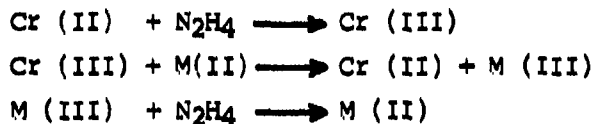
The higher susceptibility of the CrCl_2 solution implies that in this case a chromium (III) species of lower molecular weight than $\text{Cr}(\text{N}_2\text{H}_4)_6^{3+} \cdot 3\text{Cl}^-$ is the principal complex in hydrazine. With conductance measurements showing

the presence of a 2:1 electrolyte (Table 2) a possible species would be $\text{Cr}(\text{N}_2\text{H}_4)_5\text{OH}^{2+} \cdot 2\text{Cl}^-$, the hydroxide ion arising from residual water in the hydrazine.

CONCLUSIONS

Experiments have shown that chromium (II) can be oxidised to chromium (III) in the presence of hydrazine. However it is possible to isolate chromium (II) hydrazine complexes such as $\text{Cr}(\text{N}_2\text{H}_3\text{CO}_2)_2 \cdot \text{H}_2\text{O}$ (reported here for the first time) as a result of their extreme insolubility in all common solvents. In solution in anhydrous hydrazine the stable oxidation state of chromium is +3.

The observation that chromium (II) is converted to chromium (III) in anhydrous hydrazine may be important in relation to the catalysis of propellant hydrazine decomposition by trace metals in which chromium is known to be active (Reference 2). A typical catalytic cycle would be expected to include steps for the oxidation and reduction of hydrazine. Several transition metals in their common oxidation states are capable of oxidising hydrazine (e.g. Fe (III)), but so far only chromium (II), of the first-row transition series, has been confirmed as a reducing agent. A possible catalytic cycle may therefore include the following sequence of reactions (M is a metal ion):



Further work is in hand to explore the role of other active metals.

ACKNOWLEDGEMENTS

We should like to thank the UK Science and Engineering Research Council and Royal Ordnance plc, Westcott, for the award of a CASE studentship to D.T.

REFERENCES

1. Bellerby, J. M., The Chemical Effects of Storing Hydrazine Containing Carbon Dioxide Impurity in Stainless Steel Systems, Journal of Hazardous Materials, vol.7, 1983, pp 187-197.
2. Bellerby, J. M., The Effect of Some Dissolved Metal-Ion Contaminants on the Homogeneous Decomposition Rate of Anhydrous Hydrazine, Journal of Hazardous Materials, vol.13, 1986, pp 57-60.
3. Traube, W. and Pasarge, W., Chromous Oxide Compounds Stable in Air, Berichte, vol.46, 1913, pp 1505-1508.
4. Macek, J., Rahten, A. and Slivnik, J., Proceedings of the European Symposium on Thermal Analysis, 1976, pp 161-163.
5. Earnshaw, A., Larkworthy, L. F. and Patel, K. S., Magnetic and Other Properties of Chromous N_2H_2 Halides, Z. Anorg. Allg. Chem. vol.334, 1964, pp 163-168.
6. Bellerby, J. M., Edwards, D. A. and Thompsett, D., Chromium (II)-Hydrazine Reactions: Polymeric $(Cr_2(O_2CCH_3)_4(\mu-N_2H_4))_n$ and Cleavage of its Metal-Metal Bonds on Reaction with Carbon Dioxide Affording Mononuclear Chromium Carbazates, Inorganica Chimica Acta, vol.117, 1986, pp L31-L32.
7. Wells, C. F. and Salam, M. A., Kinetics of the Reaction of Chromium (II) with Hydrazine, Hydroxylamine and Hydrazoic Acid in Perchlorate Media: the Formation of Halo- and Sulphato- Complexes of Chromium (II) Journal of the Chemical Society (A), 1968, pp 1568-1575.
8. Evans, D.F., Determination of the Paramagnetic Susceptibility of Substances in Solution by Nuclear Magnetic Resonance, Journal of the Chemical Society, 1959, pp 2003-2005.

SECTION IV

SOIL, SURFACE, AND MATRIX ISOLATION STUDIES

INTERACTIONS OF HYDRAZINES WITH COLLOIDAL CONSTITUENTS OF SOILS

M. H. B. Hayes, K. Y. Chia, and T. B. R. Yormah¹
Department of Chemistry, Univ. of Birmingham, Edgbaston,
B15 2TT, England

ABSTRACT

Studies are described of interactions of hydrazine and of monomethyl hydrazine (MMH) with homoionic-exchanged clays, and with humic acid preparations. The hydrazines were shown to degrade in solution in the presence of oxygen. Degradation increased with pH, and was enhanced by the heterogeneous surfaces provided by clays homoionically exchanged with K^+ , Na^+ , Mg^{2+} and Ca^{2+} . Mn^{2+} , Cu^{2+} , and Fe^{3+} -exchanged clays catalysed the degradation because of the abilities of the cations to engage in redox reactions. In the presence of Cu^{2+} -montmorillonite, degradation of hydrazine in solution was rapid and vigorous.

Sorption by the Na^+ -clay decreased as pH increased, but sorption by Al^{3+} and Fe^{3+} -clays, increased as the pH was raised from 4 to 8. This is explained in terms of oxyhydroxide species, and the mechanisms of sorption are discussed.

Sorption by humic acids is governed by the shapes of the macromolecules, and these in turn are influenced by the charge neutralizing cations. Much of the hydrazines sorbed are irreversibly bound.

Sorption in the soil environment will be strongly influenced by the humic substances and to a lesser extent by the clays. Interactions with oxyhydroxides are intermediate between those with clays and with humic substances.

1 INTRODUCTION

The colloidal constituents are the active surfaces in so far as sorption and desorption processes in the soil environment are concerned. These constituents are composed mostly of the soil clays, which are related structurally to the clay minerals, various oxyhydroxides, and especially those of aluminium, iron, and manganese, and the organic humus colloids. Each of these colloidal classes can have an independent existence in the soil, but in every soil there will be an association of clays, oxyhydroxides, and humus substances in what might be considered to be a 'conglomerate soil colloid' structure.

In order to understand the nature of soil colloid-sorbate interactions it is appropriate first to investigate interactions of sorptives with well characterized preparations of clays from deposits, with laboratory synthesized oxyhydroxides, or with homogeneous well-characterized oxyhydroxides from deposits, and with organic colloids isolated from soil organic matter. When interactions with such substances are understood plausible predictions can be made of the interactions with the colloids in soils when the abundance and the compositions of these colloids are known.

Because water is the solvent in the soil environment, reactions with soil colloids of hydrazines in aqueous solutions are most relevant. However, hydrazines have significant vapour pressures at normal soil temperatures, and vapour phase hydrazine-soil colloid interactions are important, particularly when the concentrations of sorptive are high and the amounts of soil water are low.

Dissolved oxygen extensively degrades hydrazines at high pH values (Ellis *et al.*, 1960), and so it is important to be able to distinguish between sorption and degradation under alkaline conditions. This can be done by carrying out the sorption experiments under aerobic and under strictly anaerobic conditions.

¹ Present address Department of Chemistry, Fourah Bay College, Univ. of Sierra Leone, Freetown, Sierra Leone.

Many of the transition metals are known also to catalyse the degradation of the hydrazines (Cosser and Tompkins, 1971), and this catalysis can function in the absence of oxygen when the metals act as one or two electron acceptors (Bottomley, 1970). Experimental work by Lurker (1976) has shown that hydrazine, except in the case of Cu^{2+} is not degraded by the concentrations of transition metals found in natural waters. However, the effective concentrations of such metals at the surfaces of soil colloids are much higher than those in the bulk solution, and work by the authors (Hayes *et al.*, 1984a) has shown that interactions of hydrazine with homoionic metal-exchanged soil colloids gave rise to degradations of hydrazine that were significantly greater than that by equivalent amounts of metals in aqueous solutions.

The work described here used hydrazine hydrate and monomethylhydrazine for studies of the extents and the mechanisms of sorption of these sorptives by homoionic exchanged clays, by oxyhydroxides of iron and aluminium associated with clays, and by humic acids isolated from soil.

2 SOME RELEVANT SURFACE PROPERTIES OF SOIL COLLOIDS

The structures of pure clays from deposits are well understood (see for example, Brown *et al.*, 1978; Brown, 1988), and rapid progress is being made in understanding the various types of interstratified structures characteristic of many soil clays. Much is known also about the composition and the properties of the various oxyhydroxides in soils (Taylor, 1987; Schwertmann, 1988; Dixon *et al.*, 1988). Although less is known about the details of the structures of humic colloids, there is good awareness of functionality, shapes, and sizes of humic and fulvic acids.

Hydrogen bonding prevents interlayer expansion when the siloxane oxygen plane contacts a plane of hydroxyls, such as happens in kaolinite, and when an oxyhydroxide layer intercalates between the layers of 2:1-layer clays, as for chlorite. In the absence of isomorphous substitution (in clays such as kaolinite), the charge arises predominantly at the lateral boundaries or the edges where charge excesses or deficiencies arise from broken bonds. Hydroxyl groups at the edges, for example, may be singly coordinated to Al(III) species in the octahedral sheet, and the aluminol hydroxyl can be protonated at low pH, or it can release the proton at high pH. Thus the charge on edge hydroxyls is pH dependent. Water can also coordinate with Al(III) species, and the water can release a proton at the higher pH values to leave a negatively charged hydroxyl at the surface.

Isomorphous substitution, where it occurs, also contributes to the charge at the edges of 2:1 layer clays, and such substitution is the major contributor to the charge on non-expanding clays, such as the chlorites and the hydrous micas. Isomorphous substitution is the major contributor to the charge at the surfaces of expanding 2:1 layer clays. When the substitution is located in the octahedral sheet the charge on the siloxane surface tends to be smeared uniformly over the surface. When the silicon in the tetrahedral layer is substituted, the surface charge is more localized and located more specifically on the three surface oxygen atoms coordinated to the substituting ion than on the oxygens coordinated to silicon. This more localized charge makes possible inner sphere coordination between the siloxane groups and certain cations, and K^+ ions, for example, fit snugly in the hexagonal holes of adjacent superimposed layers of vermiculite and 'fix' the layers. Hence K^+ -exchanged vermiculites are non-expanding in aqueous media, and serve as models for illites or hydrous micas.

The 2:1 and 1:1 layers of clay minerals can articulate well at their interfaces and can stack in many different ways (Newman and Brown, 1987). Chlorite minerals with hydroxide layers interspersed regularly, provide one example of such interstratification, but there are numerous other irregular sequences of clay layers which give rise to the interstratified clay minerals.

The clay mineralogy of a soil is the result of the interaction of several factors with the parent material of the soil. These factors include the nature of the parent material, the climate, relief, vegetation and the microfauna. Kaolinite is the dominant clay mineral in acid tropical soils, and smectites (especially montmorillonite) often dominate the clay mineralogy of chernozems or vertisols. Allophane, a 'ribbon clay' can dominate the clay mineralogy of soils formed from volcanic ash. The clay mineralogy of most soils is generally not dominated by a single clay mineral species and it is not unusual to find in soils mixtures such as kaolinite, smectite, vermiculite, chlorite and mixed layer minerals inherited from the parent materials (Brown, 1988). The task of identifying the soil clays can be complex, particularly where interstratification is involved. It is important to recognize that clays in soils can have associated with their surfaces oxyhydroxide species, as well as organic matter.

Taylor (1987) has summarized the origins and the nature of the charges at the hydroxylated surfaces. Because the charges on these are pH dependent, the pH of the soil environment will determine the nature and the extent of the charge on the oxyhydroxide surface. There is, of course, the zero point of charge (ZPC) or the pH value at which positive and negative charges balance.

Isomorphous substitution by cations of higher or of lower valence can take place in oxide and oxyhydroxide materials, but the contribution of this process to the surface charge of such minerals is small. Because oxide surfaces hydrate readily, the oxide minerals would be hydrated in the soil environment where the relative humidity is high.

Soil polysaccharides and humic substances are the principal components of the soil organic colloids. It is well known that the polysaccharides play an important role in stabilizing soil aggregates, but there is no evidence to indicate that such polymers are effective binders of organic chemicals. Because of the presence of uronic acids in some soil polysaccharide structures, it is possible that the acid groups could form salts with hydrazines, and it is possible also that the carbaldehyde groups at the reducing ends of the polysaccharides could form schiff base structures with hydrazines. However, because of suspected limited reactivities between polysaccharides and small sorptive molecules, their compositions and properties will not be discussed here.

Humic acids, fulvic acids and humin materials are the components of humic substances, and these are classified on the basis of their solubilities in aqueous acids and bases. *Humic acids* are solubilized in base, but are precipitated when the pH of the medium is adjusted to 1.0. *Fulvic acids* remain in solution when the pH values of alkaline solutions of humic substances are adjusted to 1.0. *Humin* materials are insoluble in aqueous acid and base.

Hayes and Swift (1978), among others, have discussed structures of humic substances, and up to date treatments of data relating to the composition and structures of these substances are contained in Hayes *et al.*, (1988). Hayes and Himes (1986) and Hayes and Isaacson (1988) have dealt with aspects of the structures of humic substances which are important for the binding of organic chemicals.

From our knowledge of reaction mechanisms, and from identifications of digest products when humic substances are degraded, it may be concluded that the 'cores' of humic macromolecules have varying extents of aromaticity, that the aromatic units are predominantly single ring structures, and that these rings carry one or more hydroxyl (phenolic) or methoxyl group substituents, and generally a carboxyl group as well. The linking units would include ether structures (aromatic-O-aromatic, aromatic-O-aliphatic, and aliphatic-O-aliphatic), and aliphatic hydrocarbon structures also link the aromatic units. These hydrocarbons may have a degree of unsaturation and have several carbon atoms, and the aliphatic carbons may variously be substituted by carboxyl, hydroxyl, and carbonyl- including quinone and carbaldehyde groups.

From analysis of titrations data it can be deduced that the cation exchange capacity (CEC) of humic acids is in the range of 4000 to 6000 $\mu\text{eq g}^{-1}$ and the corresponding values for fulvic acids are in the range of 6000 to 12000 $\mu\text{eq g}^{-1}$. In the cases of both macromolecular acids, the carboxyl group is the major contributor to the acidity.

A knowledge of shapes and sizes is important in order to understand the sorption characteristics of humic substances. In their natural environments these substances are highly polydisperse with respect to size and charge. In a classic set of experiments Cameron *et al.*, (1972) carefully fractionated humic acids using gel chromatography and graded porosity membrane procedures, and from sedimentation equilibrium data they calculated molecular weight values ranging from 2.6×10^3 to 1.36×10^6 for the fractions isolated. From plots of frictional ratio versus molecular weight values Cameron *et al.*, concluded that humic substances adopt random coil conformations in solution.

Humic substances are present in soils as solids or as gels, and the shapes of the solid and gel structures can be deduced from our knowledge of the solution conformations of the macromolecules. Precipitation of humic substances from solution, whether by hydrogen bonding of the H^+ -exchanged structures or by bridging through divalent or polyvalent cations, will have the general effect of causing the diffuse spherical boundaries of the random coil structures to shrink. As the molecular strands are pulled together and precipitation takes place, the humic substances will be compacted into spherical-type structures, and the contributions of hydrogen bonding and of the bridging cations to the contraction of the sphere will be enhanced by van der Waals forces, and in particular by those acting between hydrophobic components within and between adjacent macromolecules. It would appear that during shrinking or drying the more polar groups associate with each other (and with cations as appropriate), and orientate towards the interiors of the structures. In this way the more hydrophobic components are orientated towards the exteriors of the structures. Such would explain why humic acids (and

highly organic soils) are difficult to rewet after drying. It is relevant to point out that fulvic acids are not leached from soils because of the associations which they form (by hydrogen bonding and by cation bridging) with the humic acids and with the inorganic soil colloids.

In the 'conglomerate soil colloid' coulombic attraction can hold the negatively charged clays and positively charged oxyhydroxides together at pH values below the ZPC of the oxyhydroxides. The attractive forces between these inorganic colloids are very strong, as exemplified by the interlayer associations of oxyhydroxides in 2:1 layer clays to give chlorites. Humic substances and other negatively charged organic macromolecules can in turn be held by coulombic forces to the oxyhydroxides.

Cation bridging mechanisms are also important for the binding of humic substances to clays, and divalent and polyvalent metal cations are involved in the bridging processes.

The 'conglomerate colloid' will expose surfaces which have a mixture of the properties of clays (because not all of the clay surface need be covered), oxyhydroxides, and humic substances. However, a sorptive species will bind to the first of these components that it contacts, provided it has an affinity for the surface. Because of sorption-desorption equilibrium processes, the sorptive will end up as a sorbate species predominantly on the component of the 'conglomerate' for which it has the greatest affinity.

3 STUDIES OF SORPTION OF HYDRAZINES: MATERIALS AND PROCEDURES

3.1 Materials

Clays. The $< 2 \mu\text{m}$ fractions of a montmorillonite (Camp Berteau, Morocco), a kaolinite (Oneal Pit, Georgia), and a bentonite (Wyoming) were isolated after the clays had been pretreated with NaOCl to remove organic matter. CEC values were determined for each sample using isotope dilution (with ^{22}Na as the tracer ion). In addition to the Na^+ -exchanged forms, Al^{3+} -, Fe^{3+} -, Cu^{2+} -, Mn^{2+} -, Ca^{2+} -, Mg^{2+} -, and K^+ -montmorillonite and kaolinite clays were prepared by dispersing each clay (1g) in 50 cm^3 of the metal chloride solution (1M), equilibrating, centrifuging, washing with H_2O , then with ethanol, and finally with H_2O to remove chloride salts.

Humic substances. Humic and fulvic acids were extracted in 0.5M aqueous NaOH in an atmosphere of dinitrogen gas. After centrifugation the supernatant was adjusted to pH 1.0 with HCl, and the precipitated humic acids were separated by centrifugation. The fulvic acids remained in solution. This solution was dialysed against distilled water and the fulvic retentates were freeze dried. The sedimented humic acids were first washed with distilled water, then dialysed against distilled water to remove salts and low molecular weight organic components, and the non-dialyzable components were freeze dried.

Clay-oxyhydroxide preparations. NaOH (0.105M) solutions were added in 0.2 cm^3 increments to 0.5 per cent w/v or 1.0 per cent w/v suspensions of aluminum- or ferric-montmorillonite and -kaolinite clay preparations. Base was added till pH values of 8.0 and 10.0 were obtained. Suspensions were then left to equilibrate overnight while N_2 gas was bubbled slowly through.

Hydrazine compounds. Hydrazine hydrate ($\text{N}_2\text{H}_4 \cdot \text{H}_2\text{O}$) was supplied, pure, by Koch-Light Laboratories, and monomethylhydrazine (MMH, CH_3NHNH_2 ; 98% purity) was supplied by the Aldrich Chemical Co. Ltd.

3.2 Methods for Studying Sorption

In any study of sorption processes it is important to know whether or not the sorptive species are degraded in the sorption medium. In order to check the stabilities of hydrazine and of MMH in water, solutions of the compounds in distilled water in sealed vials were monitored at regular intervals. Analyses used a modification of the spectrophotometric procedure of Reynolds and Thomas (1965) in which p-dimethylaminobenzaldehyde (DMBA) is used to form a dimeric, coloured azine with the hydrazo group. The modification used a 0.4 per cent DMBA solution instead of the 4 per cent used in the general procedure.

In order to investigate degradations of the hydrazines in the presence of homoionically-exchanged clays, suspensions of Na^+ -, K^+ -, Ca^{2+} -, Mg^{2+} -, Al^{3+} -, Fe^{3+} -, and Cu^{2+} -exchanged clays were dispersed in sealed vials in an ultrasonic bath, and aliquots of hydrazine were injected through the 'sub-a-seal' top.

Concentrations of hydrazine materials were monitored at hourly intervals. To check the influences of the cations in the absence of clays 320 ppm of the appropriate cation chloride solution were treated in the same way and changes with time of the concentrations of hydrazines were monitored.

Batch slurry procedure. This procedure was used for studies of sorption/desorption in clay systems. Fixed aliquots of stock solutions of the sorptives were added to clay suspensions, and after equilibration for 15 minutes (using a vortex shaker) the mixtures were centrifuged and the supernatants were analysed.

For desorption studies successive volumes of supernatant were removed and replaced by deoxygenated distilled water at the pH of the clay suspensions. Desorption was calculated from the concentrations of sorptive in the supernatants. In order to determine the influence of salt on desorption, some experiments used 0.1M NaCl solutions.

The continuous flow stirred cell automated colourimetric analysis technique (CFSC-ACA). The theory behind the CFSC technique has been described in some detail by Ryan and Hanna (1971), Smedley (1987), Hayes (1980), Hartmann (1981), and Isaacson and Hayes (1984) have described the CFSC-ACA procedure relevant to the present study.

A known amount of humic acid was suspended in water and continuously stirred in a reaction cell. Hydrazines of known concentration was passed continuously from a reservoir into the cell, and the concentrations of the hydrazines in the eluates from the cell were monitored by the ACA system. The basis of the ACA procedure is as follows:

- 1, a continuously flowing stream of sample solution from the cell is segmented using a gas bubble (usually air or N₂). This process reduces laminar flow, and prevents interfacial mixing of one segment with the next;
- 2, local mixing of the sample and reagent (DMBA) within each segment is achieved as the 'plugs' pass over each turn of a helical mixing coil with its axis orientated horizontally;
- 3, the reproducibility of the colour development and detection - i.e. the colour of the complex - need not be developed to its maximum as long as the point at which the colour is measured is reproducible.

Chia (1982) and Hayes *et al.*, (1984a) have described in detail the extensive precautions which are needed in order to obtain accurate measurements when employing the CFSC-ACA procedure.

Sorption from the vapour phase. A modified McBain-Baker type of apparatus was used to measure gravimetrically the amount of vapour sorbed, using a helical silica spring.

3.3 Methods for Investigating Sorption Mechanisms

Microcalorimetry studies. An LKB 10700- Batch microcalorimeter was used. To investigate the energetics of interactions with clays and humic acids suspensions were prepared such that concentrations of sorbent in the cells after mixing were the same as those used in sorption studies. Details of procedures are contained in Chia (1982) and Hayes and Isaacson (1984).

X-ray studies. A Phillips PW 1050/70 diffractometer was used employing CuK α radiation ($\lambda = 1.541 \text{ \AA}$). The technique of sedimentation on glass was used for sample preparation.

Infrared analysis. Self supporting clay films were used. The films were first prepared prior to equilibrating with the hydrazine vapours (brought into contact with the clay by standing the film over liquid hydrazine or MMH in dessicators at 28°C. To obtain infrared spectra of H⁺-humic acid-hydrazine complexes, samples of the complexes (1-2 mg) made up in KBr discs (300mg) were used.

Differential thermal analysis. A Stanton Redcroft 780 simultaneous Thermal Analyser was used in this study, and alumina was employed as a reference material and a stream of dry N₂ (flow rate 60 cm³ min⁻¹) was passed into the system to provide an inert atmosphere.

4. RESULTS FROM SORPTION STUDIES

4.1. Solution Degradations of Hydrazines in the Presence or Absence of Montmorillonites

Camp Berteau montmorillonite and Oneal Pit kaolinite were used in these studies. The hydrazines in solution underwent an initial oxidation by the oxygen dissolved in the solution; thereafter the concentrations of the hydrazine and of the MMH remained constant. In the absence of clay, the concentrations of hydrazine and of MMH which persisted in solution were ca. 90 and 85 per cent. respectively, of the starting materials.

On addition of the hydrazines to the clay suspensions some were adsorbed and some were oxidized. Microcalorimetry showed that sorption was rapid. Equation (1) indicates how the extents of degradation were measured, and Table 1 provides the data for the degradation of the hydrazines in the presence of 1% clay suspensions at different pH values, where K is the extent of degradation of hydrazine in 1% clay suspensions, and A is the amount of hydrazine in supernatant after a period of reaction, and B is the amount of hydrazine added at the start, and C is the amount of hydrazine adsorbed.

$$K = A/(B - C) \quad 1$$

Table 1 Extents of degradation and adsorption at different pH values of hydrazines in the presence of 1% (w/v) suspensions of homolonic-exchanged montmorillonite preparations.

Exchangeable cation on clay	pH of suspension		% unadsorbed Hydrazine degraded after		Sorbate held (g ⁻¹ clay)
	Before	After	3h	24h	($\mu\text{eq g}^{-1}$)
Addition of Hydrazine					
K ⁺	6.4	9.6	30-5	40-5	-
Na ⁺	5.6	9.9	"	"	100
Ca ²⁺	7.2	9.2	"	"	90
Mg ²⁺	6.5	9.5	"	"	83
Cu ²⁺	4.9	5.2	>95	>95	243
Mn ²⁺	5.6	9.6	30-5	60-5	113
Al ³⁺	3.6	7.6	"	30-5	738
Fe ³⁺	2.8	7.6	"	50-5	819
Addition of Monomethylhydrazine (MMH)					
Na ⁺	5.6	8.8	30-5	-	81

The data in Table 1 show that, with the exception of the Cu²⁺-clay, about 30% of the hydrazine in solution was degraded after 3h, and further degradations after prolonged interaction was significant only for the Mn²⁺- and Fe³⁺- systems. Sorption of hydrazines was small in the pH range 8.8 to 9.9, but the amounts sorbed by the Fe³⁺- and Al³⁺- exchanged clays (pH 7.6) were high.

Vigorous effervescence was observed after addition of hydrazine to the Cu²⁺-clay suspension. Although the sorbed hydrazine did not degrade further, a negligible amount was left in solution after 1h.

Data in Table 2 give the extents of degradation of hydrazine in the presence of 320 ppm of cations in metal chloride solutions at different pH values. Additions of hydrazine did not raise the pH in the cases of CuCl₂, AlCl₃, and FeCl₃ solutions. Again degradation was most rapid and greatest, (and was accompanied by effervescence and the formation of a grey precipitate), in the CuCl₂ solution, and degradation also increased during the 3-24h interval in MnCl₂ when the medium darkened and a light white gelatinous precipitate

Table 2 Extents of degradation of hydrazine in the presence of metal chloride solutions (320 ppm Mn^{2+}) at different pH values.

Cation of chloride solution	pH of solution		% of added hydrazine degraded after	
	Before	After	3h	24h
Addition of Hydrazine				
K^+	5.4	8.4	<10	<10
Na^+	5.7	8.5	<10	<10
Ca^{2+}	5.5	8.1	<10	20
Mg^{2+}	5.2	8.4	<10	20
Cu^{2+}	4.5	4.3	50	>95
Mn^{2+}	5.8	8.3	<10	75
Al^{3+}	3.6	3.6	< 5	< 5
Fe^{3+}	2.2	2.2	< 5	20

formed. A gelatinous brown precipitate also formed during the 3–24h interval of degradation in the FeCl_3 solution.

4.2 Microcalorimetry Results

The enthalpies of the interactions of hydrazine with preparations of homoionically-exchanged montmorillonite and with metal chloride solutions are given in Table 3.

Interactions with Na^+ -, Mg^{2+} -, Ca^{2+} -, Al^{3+} -, and Fe^{3+} -salts gave a single exothermic peak, and no additional enthalpy peaks were observed on subsequent mixings. Interaction with the CuCl_2 was highly exothermic, and energy of interaction was still measurable after five mixings of the cell contents. The energy evolved when the hydrazine was interacted with the salt solutions was greater than for the interaction with the clay suspension in the cases of the Cu^{2+} -, Mn^{2+} -, and Fe^{3+} - salts. In the cases of the interaction with the homoionic-exchanged clay suspensions, at least three mixings were necessary to complete the reaction, and significant amount of energy were released even after six mixings in the case of the Cu^{2+} -clay.

When 320 ppm of solutions of Mn^{2+} -, Cu^{2+} -, Al^{3+} -, and Fe^{3+} - chlorides were reacted with sodium hydroxide solutions (pH 12) the enthalpies of the reactions, expressed as J meq^{-1} , were 13.00, 33.48, 8.67, and 50.01, respectively, for the cations, and these values were similar to those for interactions with hydrazine in the cases of the Mn^{2+} -, Al^{3+} -, and Fe^{3+} salts.

4.3 Interactions of Hydrazine and MMH with Homoionic-exchanged clays

Degradation of hydrazine in suspensions of Na^+ -, K^+ -, Mg^{2+} -, and Ca^{2+} -exchanged montmorillonites (pH 9.2 to 9.9) was greater than in the corresponding metal chloride solutions (pH 8.1 to 8.5). The higher pH contributed to the degradation, and also losses of hydrazine in the supernatants (30–40%) was considerable in the presence of dissolved oxygen. Montmorillonite, a heterogeneous component in the system catalysed the degradation. Degradation of MMH was enhanced even by Na^+ -montmorillonite, and the effect was not one of pH.

The enthalpy data for the interactions with these four metal-exchanged clays (Table 3), were net heat outputs. The adsorption data, Table 1, show that hydrazine was not adsorbed by the K^+ -clay, and data in Table 3 show that the net energy for the interaction of the sorptives was less for the Ca^{2+} - and Mg^{2+} -clays than for the Na^+ -clay, though the amounts adsorbed were similar. The energy differences can be attributed to the increased energy needed to displace water in the hydration shells of the divalent cations during the sorption process.

Table 3. Enthalpies of the interactions of 10 meq dm⁻³ hydrazine with 1% w/v homoionic-exchanged montmorillonite at 28 ± 0.05 °C and with 320 ppm metal chloride solution at 29 ± 0.05 °C.

Exchangeable Cation	pH of suspension Before interaction	pH of suspension After interaction	Number of mixing	Enthalpy (Jg ⁻¹)	Enthalpy* J meq ⁻¹
K ⁺	5.3	8.5	1	11.90	-
			2	0.85	-
Na ⁺	5.3	9.9	1	12.80	1.42
			2	2.06	-
Mg ²⁺	6.5	9.5	1	3.12	0.40
			2	1.01	-
Ca ²⁺	7.4	9.2	1	4.83	0.58
			2	1.85	-
Cu ²⁺	4.5	5.2	1	86.30	103.00
			2	23.30	16.68
			3	9.71	9.60
			4	5.99	8.96
			5	3.93	5.98
Mn ²⁺	6.1	9.6	6	2.00	-
			1	9.73	13.40
			2	4.23	8.46
Al ³⁺	3.6	6.8	3	3.88	7.54
			1	11.70	10.62
Fe ³⁺	2.8	6.4	1	31.70	69.00
			2	5.20	-
			3	4.33	-

When hydrazine solution, with the pH adjusted to 8, was added to Fe³⁺- and Al³⁺-montmorillonite, the pH of the suspension was 8.0, and 30% of the sorptive degraded in the metal chloride solutions at low pH. Thus the higher pH and the catalytic effect of the clay enhanced degradation.

Degradation in Mn²⁺-montmorillonite was greater than in MnCl₂ solution (30% versus 10%, and pH values were 9.6 and 8.3). Hydrous oxides of Mn formed at the higher pH. On standing for 24h the concentration of hydrazine dropped to 40% of the original indicating that the exchangeable Mn²⁺ enhanced degradation above that for the K⁺-, Na⁺-, Ca²⁺-, and Mg²⁺-exchangeable species. The ability of Mn²⁺ to complex hydrazine, and its ease of hydrolysis (pKa of Mn²⁺ is 10.5) gave rise to greater interaction between the sorptive and Mn²⁺-montmorillonite.

The data in Table 3 show that the interaction of hydrazine with Cu²⁺-montmorillonite and with CuCl₂ solution is highly energetic. The catalytic effect of Cu²⁺ on the decomposition of hydrazine is well established. As mentioned (Section 4.2) the heat of hydrolysis of Cu²⁺ ions was 33.48 J meq⁻¹ when 320ppm CuCl₂ solution was added to NaOH solution at pH 12. Thus the major part of the heat produced in the separate reactions between hydrazine and Cu²⁺-montmorillonite and hydrazine and CuCl₂ solution was attributable to the degradation of hydrazine.

In the CuCl₂ solution, the initial rapid degradation was accompanied by reduction of Cu²⁺ to Cu⁺. Complexation of Cu(I) by hydrazine protects the hydrazine against degradation. In the presence of clay, enhanced degradation of hydrazine could take place because of the increased effective Cu²⁺ concentration at the clay surface compared with that in the CuCl₂ solution. Even after the concentration of sorptive in the supernatant was zero, sorbate was still detectable on the clay. Hydrolysis or reduction of the exchangeable

Cu^{2+} would cause an imbalance in the negative charges on the clay, and this would be balanced by hydrazinium ions. The adsorbed hydrazine was stabilized against rapid decomposition.

Data in Table 4 give the values for the maximum adsorption of hydrazine by homoionically-exchanged montmorillonite and kaolinite clays, and of MMH by an Al^{3+} -montmorillonite.

Table 4 Maximum adsorption of hydrazine (N_2H_4) and MMH (CH_3NHNH_2) by montmorillonite (M) and kaolinite (K) clays exchanged with cations of different valence.

Clay	Initial pH of clay suspension	pH of hydrazines solution	Maximum adsorption ($\mu\text{eq g}^{-1}$) of	
			N_2H_4	CH_3NHNH_2
Na^+M	5.6	4.0	650	-
	5.6	8.0	100	-
Ca^{2+}M	4.0	4.0	70	-
	6.8	10.0	97	-
Al^{3+}M	4.0	4.0	149	-
	4.0	10.0	900	1000
	8.0	8.0	1500	2000
	10.0	10.0	225	-
Fe^{3+}M	2.8	8.0	900	-
	2.8	10.0	1100	-
Na^+K	6.7	4.0	120	-
	6.7	8.0	75	-
Al^{3+}K	4.5	4.0	42	-
	8.0	8.0	220	-

The data show that the pH of the solution with the hydrazine sorptive influenced sorption significantly. Sorption by the Na^+ -exchanged clays decreased as the pH of the sorptive solution increased. Water washing removed $200 \mu\text{eq g}^{-1}$ sorbate from the Na^+ -montmorillonite system (pH 4), and $340 \mu\text{eq g}^{-1}$ was subsequently removed on washing with 0.1M NaCl. When hydrazine in solution at pH 8 was added to Na^+ -montmorillonite, pH 5.6, the medium soon attained pH 8, and maximum adsorption decreased to $100 \mu\text{eq g}^{-1}$. Adsorption by Ca^{2+} -montmorillonite was low even at pH 4. None of the hydrazine sorbed by the montmorillonite at the two pH values was removed with water, but all was with 0.1M NaCl.

Al^{3+} -exchanged clay at pH 8 and above gave rise to hydroxyaluminium (oxyhydroxide) structures. All of the Al^{3+} could be exchanged from Al^{3+} -montmorillonite (pH 4) using 1M NaCl. Some lattice Al was also removed in a 1.0M NaCl and 1.0M HCl solution. No Al^{3+} was removed by washing hydroxyaluminium-montmorillonite (pH 8) in 0.1M NaCl. However, the Al^{3+} was exchangeable in 1M NaCl and 0.1M HCl. When the pH of the medium was 10 all of the Al^{3+} was exchangeable in 1M NaCl. Similar effects were observed for Al^{3+} -kaolinite preparations. The data show that when hydroxyaluminium species were formed, especially at pH 8, these species were fixed on the clay surface.

Sorption of $220 \mu\text{eq g}^{-1}$ of hydrazine by Al^{3+} -kaolinite at pH 8 (Table 4) amounted to twice the CEC of the clay (shown by Na^+ -exchange to be $105 \mu\text{eq g}^{-1}$). Assuming surface coverage to be 23.1 \AA^2 per molecule, the total area covered by the sorbate was $30.5 \text{ m}^2 \text{ g}^{-1}$, which is in the range of the specific surface area ($29 - 44 \text{ m}^2 \text{ g}^{-1}$) for the clay (Yormah, 1981).

Al^{3+} -montmorillonite, pH 4, adsorbed $149 \mu\text{eq g}^{-1}$ hydrazine, but only $90 \mu\text{eq Al}^{3+} \text{ g}^{-1}$ was displaced. NaCl (0.1M) desorbed $56 \mu\text{eq g}^{-1}$ hydrazine and $130 \mu\text{eq g}^{-1} \text{ Al}^{3+}$. Adsorption of hydrazine caused hydrolysis of some exchangeable Al^{3+} , but the amount sorbed was not sufficient to cause fixation of all of the exchangeable Al^{3+} in the interlayer spaces.

No Al^{3+} exchange occurred during the sorption of hydrazine by Al^{3+} - and hydroxyaluminium-montmorillonite, pH 8, and none resulted from washing with labelled 0.1M NaCl solution. Hydrolysis of the cations had rendered them non-exchangeable.

The Na^+ -exchange capacity of this montmorillonite was $1250 \mu\text{eq g}^{-1}$, and the increased CEC was attributable to the contribution of the pH-dependent charges on the oxyhydroxide species. Sorption of hydrazine and of MMH by hydroxyaluminium-montmorillonite (pH 8) was 17% and 37% greater, respectively, than the CEC of the clay (Table 4).

Table 5 Effects of different concentrations of $^{22}\text{NaCl}$ on the desorption of hydrazine and MMH and sorption of Na^+ by hydrazine- and MMH- interacted Al^{3+} - and hydroxyaluminium-montmorillonite complexes.

Clay Preparations	Desorption medium (M NaCl)	Amount of hydrazine desorbed ($\mu\text{eq g}^{-1}$)	Amount Na^+ adsorbed ($\mu\text{eq g}^{-1}$)
(a) Hydrazine interacted complexes.			
Al^{3+} -mont. (pH 4) interacted with hydrazine solution pH 8	0.01	304	375
	0.1	642	572
Hydroxyaluminium-montmorillonite hydrazine complex (pH 8)	0.01	466	472
	0.1	722	911
(b) MMH interacted complexes			
Al^{3+} -mont. (pH 4) interacted with MMH solution (pH 8)	0.01	509	440
	0.1	1000	1520
Hydroxyaluminium montmorillonite - MMH complex (pH 8)	0.01	658	408
	0.1	1130	1490

When the hydrazine-treated hydroxyaluminium-clay (pH 8) was washed with labelled NaCl solutions, $722 \mu\text{eq g}^{-1}$ hydrazine was desorbed and $911 \mu\text{eq g}^{-1}$ of Na^+ was sorbed (Table 5). The corresponding data for MMH were 1130 and $1490 \mu\text{eq g}^{-1}$, respectively. Comparisons of data in Tables 4 and 5 indicate that not all of the hydrazine and MMH was desorbed, and it is clear that more Na^+ was sorbed than hydrazine or MMH desorbed. The data for sorption and desorption by Al^{3+} -montmorillonite, pH 4, indicate that relatively straightforward ion exchange had taken place (Tables 4 and 5).

An Fe^{3+} -montmorillonite suspension (pH 2.8) sorbed only $198 \mu\text{eq g}^{-1}$ hydrazine (pH 4). This sorbate was not removed by water, though 56% was with 0.1M NaCl. When hydrazine solution, pH 8-10, was used sorption was of the order of the CEC of the clay (Table 4), and up to 65% was removed in 0.1M NaCl.

Isotherms for sorption by hydroxyferric-montmorillonites were linear, and a plateau was not reached for the concentrations used. As was observed for the hydroxyaluminium system more hydrazine was sorbed at pH 8 than at pH 10, and desorption occurred when the pH of an adsorbate - adsorptive complex was adjusted from pH 8 to 10. NaCl (0.1M) removed $360 \mu\text{eq g}^{-1}$ hydrazine from $950 \mu\text{eq g}^{-1}$ in the adsorbate - adsorbent complex at pH 8, but none was removed by similar treatment of a complex containing $400 \mu\text{eq g}^{-1}$ at pH 10.

4.4 Vapour Phase Sorption of MMH by Clays

Details of the sorption - desorption process are given by Hayes et al (1984b). Isotherms for sorption of MMH vapour by Na^+ -montmorillonite (Polkville) were of type II, but hysteresis was evident along the entire

sorption - desorption path. The 'loop-shape' described by the isotherms is characteristic for sorption and desorption of polar vapours by montmorillonite, and is attributable to the intercalation of organic molecules between the layers. X-ray diffraction measurements gave an (001) spacing of 1.34 nm after desorption was complete, compared to 0.97 nm prior to adsorption, which indicates that some residual MMH was held in the flat conformations between the layers.

Isotherms (see Hayes *et al.*, 1984b) for sorption by kaolinite (Oreal Plt) were type II, or L-type characteristic of physical sorption onto non-porous or macroporous sorbents with the formation of multilayers of sorbate. The desorption isotherms showed that, although some hysteresis occurred at the high relative pressure values, desorption followed sorption closely over the major portion of the isotherm, and only 0.01 mmol g⁻¹ resisted desorption. No irreversible interaction was indicated by X-ray diffraction data.

The isotherm for sorption of MMH by Fe³⁺-kaolinite was also type II, but hysteresis in the desorption was clearly evident, and 0.4 mmol g⁻¹ was not removed when the sorption process was reversed. The retained sorbate was only 0.04 mmol g⁻¹, however, when the system was subjected to evacuation for 24h.

Table 6 compares data from the BET analysis of isotherms for the sorption of MMH and water vapour by the homoionic-exchanged clays.

Table 6 BET analysis of data obtained from studies of vapour phase sorption of MMH and water by homoionic-exchanged kaolinite and montmorillonite clays.

BET Analysis	MMH			Water Vapour		
	Na ⁺ -K	Fe ³⁺ -K	Na ⁺ -M	Na ⁺ -K	Fe ³⁺ -K	Na ⁺ -M
C-constant	506	33	434	36	245	6.4
Specific surface (m ² g ⁻¹)	50	32	725	29	15	460.2
Monolayer cap. (mmol g ⁻¹)	0.39	0.21	2.5	0.39	0.21	3.1
Heat of sorpn. (kJ mol ⁻¹)	-15.4	-8.6	-15.1	-8.9	-13.4	-4.6
Sorbate:Exchangeable ion	4:1	7:1	3:1	4:1	7:1	4:1

It is recognised that applications of BET and isosteric analysis are not strictly valid where the sorption processes show irreversibility, but the data are, nevertheless, useful for purposes of comparison.

The specific surface area from MMH sorption by Na⁺-montmorillonite (725 m² g⁻¹) is as expected. That measured for water vapour (460 m² g⁻¹) suggests the inclusion of a monolayer of water between the clay layers. Surface area of Na⁺-kaolinite as measured from MMH sorption (50 m² g⁻¹) was greater than that estimated from sorption by water vapour and for Fe³⁺-kaolinite.

A plot of surface coverage versus the isosteric heat of interaction (see Hayes *et al.*, 1984b) gave a linear decrease in the heat of interaction as coverage by MMH increased in the case of the Na⁺-kaolinite system, and the initial binding was almost twice as energetic as that which accompanied sorption as monolayer coverage was approached.

4.5 Sorption of Hydrazine by Humic Acid preparations

H⁺-, Ca²⁺-, and Al³⁺-humic acid preparations were interacted with hydrazine solutions of pH 4 (see Isaacson and Hayes, 1984).

At pH 4 the hydrated hydrazine compounds were more extensively held by H⁺- then by Ca²⁺- and Al³⁺-exchanged humic acid preparations. In all cases the maximum sorption measured was only a fraction (12 - 23%) of the CEC of the sorbent. The steric hindrance to diffusion to binding sites inside the macromolecular structure (see Section 2) provides one reason for the relatively low extents of sorption. Although the interactions were shown by microcalorimetry to be isothermic in every instance, the energies of sorption were different for the three humic acid preparations. Whereas the differential enthalpy decreased as more hydrazine was added to the H⁺- and Al³⁺-exchanged humic acids, that for the Ca²⁺-preparation increased. It is considered that this increase resulted from the availability of new sites (in the interior of the

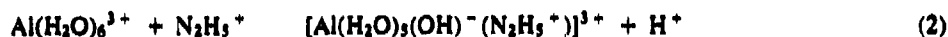
new structure) as the Ca^{2+} ions bridging adjacent humic strands (Section 2) were replaced by the hydrazinium ions.

5. MECHANISMS OF SORPTION

5.1. Adsorption at pH 4

At pH 4 the sorptive species will be the hydrazinium ion (N_2H_5^+ or $\text{CH}_3\text{NHNH}_3^+$). The strength of binding of cations to the clay surfaces decreases in the order $\text{Na}^+ < \text{Ca}^{2+} < \text{Al}^{3+} < \text{Fe}^{3+}$. Thus sorption from solution at pH 4 was greatest for Na^+ -clays because the process involved simple exchange of Na^+ for hydrazinium ions.

The polarizing and coordination powers of the cations decrease in the order $\text{Fe}^{3+} > \text{Al}^{3+} > \text{Ca}^{2+} > \text{Na}^+$. An appropriate mechanism of binding to multivalent cation-exchanged clays would involve coordination to the cation, or the exchange of a hydrazinium ion with a proton from the ionized water coordinated to the cation. The adsorption of hydrazine by Al^{3+} -montmorillonite at pH 4 was of the order of $150 \mu\text{eq g}^{-1}$, which is less than that for the Na^+ -, but greater than that for the Ca^{2+} -clay. This increased sorption by the Al^{3+} -system is attributed to the polarizing power of the cation. Thus an exchange reaction such as that in scheme (2) could take place readily.



In the case of sorption by the humic acid (pH 4), similar mechanisms could take part. The fact that less hydrazine was sorbed by the Al^{3+} - than by the Ca^{2+} -humic acid can be attributed to the fact that it was more difficult to remove by ion exchange the Al^{3+} ions which held the humic strands together, and so penetration of the sorptive to binding sites in the interior of the macromolecule was inhibited. Inevitably, some chemisorption occurred, such as the formation of Schiff base structures between the hydrazine and carbonyl groups on the adsorbent. Substitution could also take place in carbons alpha to the keto structures of quinones (Hayes and Swift, 1978; Isaacson and Hayes, 1984).

5.2. Sorption from Sorptive Solution, pH 8

Sorption by Na^+ -montmorillonite of hydrazine from solution at pH 8 was significantly less than that at pH 4. At this pH the concentrations of hydrazine and hydrazinium ions in solution were essentially the same. Sorption by Ca^{2+} -montmorillonite was similar at pH 8 and 4. Cation exchange did not predominate for this species, and was less important than hydrolysis of and coordination to the cation.

In the cases of Fe^{3+} - and Al^{3+} -montmorillonites, ease of hydrolysis of the cations contributed to the sorption. Because of the extents of dissociation of water coordinated to the polyvalent cations more hydrazinium ions would form close to the clay to give rise to exchange with H^+ as indicated by reaction scheme (2). Sorption by the Fe^{3+} and Al^{3+} -clays was similar to the CEC of the clays, and this suggests the exchangeable cations were hydrolyzed to the neutral species. (The pH of the Al^{3+} -montmorillonite suspension rose more rapidly than that of the Fe^{3+} -clay, indicating the greater acidity conferred by the Fe^{3+} ion). This mechanism is substantiated by the fact that metal ions were not exchanged for hydrazine. The cations were fixed to the clay on hydrolysis, and were not desorbed with 0.1M NaCl (although 70% of the hydrazine sorbate was desorbed and Na^+ was sorbed).

It is probable that at pH 8 and 10 reduction of Fe^{3+} took place. The resultant oxidation of the hydrazine led to degradation, and hence to the detection of less sorptive in solution.

5.3. Sorption by Hydroxymontmorillonites and Hydroxykaolinites

The formation of oxyhydroxide 'islands' on the surfaces of Fe^{3+} - and Al^{3+} -exchanged clays is highly likely when these clays were equilibrated for 24h in dilute NaOH.

Extensive studies with the Al^{3+} -system showed that the cation was neutralized to the hydroxyaluminium species, and this species was non-exchangeable with 1.0M NaCl. The hydroxyl groups in the hydroxyaluminium complexes contributed to the negative charges.

The predominant mechanism of binding of hydrazine and MMH by hydroxyaluminium montmorillonite, pH 8, up to the CEC, was cation exchange of hydrazinium ions for Na^+ ions (from the NaOH used to make the hydroxyaluminium species). Extensive investigations of the reaction mechanisms, as described by Hayes et al (1984a), using isotherm analysis, microcalorimetry, measurements of displaced inorganic cations from the clay, X-ray diffraction, infrared spectroscopy, and differential thermal analysis indicated that cation exchange was the predominant mechanism for the adsorption of hydrazine and of MMH by hydroxyaluminium-montmorillonite, pH 8, up to the CEC of the clay.

Beyond the CEC the experimental data suggested that the predominating mechanisms involved included:

- 1, the interaction of the strongly basic hydrazine with the hydroxide surface to give;

$$-\text{Al}-\text{OH} + \text{N}_2\text{H}_4 \rightleftharpoons \text{AlO}^- + \text{N}_2\text{H}_5^+ \quad (3)$$
- 2, the action of van der Waals forces between the sorbate and the clay surface and between the sorbate molecules on the surface;
- 3, hydrogen bonding between protonated and non-protonated species; and
- 4, the involvement of hydrazine or MMH as monodentate, or as bridging ligands between aluminium sites on the surface.

The fact that less adsorption took place at pH 10 than at pH 8 demonstrates that the hydroxy complexes are stable only within a certain pH range. Maximum adsorption occurred when the pH was such that the formation of neutral species at the clay surface was maximum, and not when the pH was such that negative hydroxy species were generated.

Acknowledgements The work described here is a part of that supported by a grant from the U.S. Air Force. The authors also wish to thank Miss Ingrid Appelqvist and Dr. Jonathan J. Tuck for their help with the phototypesetting process for this manuscript.

REFERENCES

- Bottomly, F.S. 1970. The reactions of hydrazine with transition metal complexes. *Q. Rev. Chem. Soc.* 24, 617-638.
- Brown, G., Newman, A.C.D., Rayner, J.H. and Weir, A.H. 1978. The structures and chemistry of soil clay minerals. In D.J. Greenland and M.H.B. Hayes (eds.), *The Chemistry of Soil Constituents*, Wiley, Chichester, pp. 29-178.
- Brown, G. 1988. Structure, crystal chemistry, and origin of phyllosilicate minerals common in soil clays. In M. DeBoodt, M.H.B. Hayes, A. Herbillon, and J.J. Tuck (eds.), *Soil Colloids and their Association in Soil Aggregates*. Plenum, In press.
- Cameron, R.S., Thornton, B.K., Swift, R.S. and Posner, A.M. 1972. Molecular weight and shape of humic acid from sedimentation and diffusion measurements on fractionated extracts. *J. Soil Sci.* 23, 394-408.
- Chia, K.Y. 1982. The Interactions of Hydrazine and Monomethylhydrazine with Homoiionically Exchanged Montmorillonite and Hydroxy-Aluminium Montmorillonite Preparations. PhD. Thesis, Univ. of Birmingham.
- Cosser, R.C. and Tompkins, F.C. 1971. The heterogenous decomposition of hydrazine on tungsten films. *Trans. Faraday Soc.* 67, 526-544.
- Dixon, J.B., Golden, D.C., Uzochukwu, G.A., and Chen, C.C. 1988. Soil manganese oxides. In M. DeBoodt, M.H.B. Hayes, A. Herbillon and J.J. Tuck (eds.), *Soil Colloids and their Association in Soil Aggregates*. Plenum, In press.
- Ellis, S.R.M., Geffreys, G.V. and Hill, P. 1960. Oxidation of hydrazine in aqueous solution. *J. Appl. Chem.* 10, 347.
- Hartmann, E.H. 1981. Applications of the Continuous-flow Stirred Cell Technique for Studying Adsorption of Organic Chemicals by a Humic Acid Preparation. PhD. Thesis, Univ. of Birmingham.
- Hayes, M.H.B. 1980. The role of natural and synthetic polymers in stabilizing soil aggregates. In R.C.W. Berkely et al (eds.), *Microbial Adhesion to Surfaces*. Ellis Harwood, Chichester, pp 262-296.
- Hayes, M.H.B. and Himes, F.L. 1986. Nature and properties of humus-mineral complexes. In P.M. Huang and M. Schnitzer (eds.), *Interactions of Soil Minerals with Natural Organics and Microbes*. SSSA Special Publication No. 17. Wudison, Wis., pp. 103-158.
- Hayes, M.H.B. and Isaacson, P.J. 1988. Interactions of organic chemicals with soil humic substances. In P. MacCarthy, M.H.B. Hayes, R.L. Malcolm, and R.S. Swift, (eds.), *Humic Substances III. Interactions with Metals, Minerals, and Organic Chemicals*. Wiley, Chichester, In press.

- Hayes, M.H.B., Isaacson, P.J., Chia, K.Y., Lees, A.M. and Yormah, T.B.R. 1984a. Interactions of hydrazine and of hydrazine derivatives with soil constituents and with soils. Final Report. AFOSR-80-0032. European Office of Aerospace Research and Development, London, England.
- Hayes, M.H.B., Isaacson, P.J., Lees, A.M. and Yormah, T.B.R. 1984b. Vapour phase sorption and desorption of monomethylhydrazine by homoionic-exchanged clays. *J. Colloid Interface Sci.* 97, 48
- Hayes, M.H.B., MacCarthy, P., Malcolm, R.L. and Swift, R.S. (eds.). 1988. Humic Substances II. In Search of Structure. Wiley, Chichester. In press.
- Hayes, M.H.B. and Swift, R.S. 1978. Soil Organic colloids. In D.J. Greenland and M.H.B. Hayes (eds.), *The Chemistry of Soil Constituents*. Wiley, Chichester, pp. 179-320.
- Isaacson, P.J. and Hayes, M.H.B. 1984. The interaction of hydrazine hydrate with humic acid preparations at pH 4. *J. Soil Sci.* 35, 79-92.
- Lurker, P.A. 1976. Catalytic deoxygenation of aqueous solutions by hydrazine. Technical Documentary Report No-AMRL-TR-76-23, Aerospace Medical Laboratory, Wright-Patterson Air Force Base, Dayton, Ohio.
- Newman, A.C.D. and Brown, G. 1987. The chemical constitution of clays. In A.C.D. Newman (ed.), *Chemistry of Clays and Clay Minerals*. Mineralogical Soc., London, pp. 1-128.
- Reynolds, B.A. and Thomas, A.A. 1965. A colorimetric method for the determination of hydrazine and monomethylhydrazine in blood. *Am. Ind. Hygiene Assoc. J.* 26, 527-531.
- Ryan, M.T. and Hanna, N.S. 1971. Investigation of equilibrium ultrafiltration as a means of measuring steroid-protein binding parameters. *Anal. Biochem.* 40, 364-376.
- Schwertmann, U. 1988. Some properties of soil and synthetic iron oxides. In M. DeBoodt, M.H.B. Hayes, A. Herbillon and J.J. Tuck (eds.), *Soil Colloids and their Associations in Soil Aggregates*. Plenum, In press.
- Smedley, R.J. 1978. Interactions of Organic Chemicals with Clays and with Synthetic Resins. PhD. Thesis, Univ. of Birmingham.
- Taylor, R.M. 1987. Non-silicate oxides and hydroxides. In A.C.D. Newman (ed.), *Chemistry of Clays and Clay Minerals*. Mineralogical Soc. London, pp. 129-201.
- Yormah, T.B.R. 1981. The Composition and Properties of Selected Samples from a Tropical Soil Profile. PhD. Thesis, Univ. of Birmingham.

HYDRAZINE FATE AND TRANSFORMATIONS IN
NATURAL WATERS AND SOILS

J.J. STREET AND A.M. MOLINER
SOIL SCIENCE DEPARTMENT
UNIVERSITY OF FLORIDA
GAINESVILLE, FLORIDA 32611

INTRODUCTION

Widespread use of hydrazine poses a potential environmental hazard from accidental spills and leakage of underground storage vessels. The inadvertant loss of hydrazine to soils may result in contamination of soils and/or subsurface waters. Although several papers have been published on the fate of hydrazine in the environment, the mechanisms of degradation and interaction of hydrazine with soil components may not be fully understood. The disagreements found among researchers appear to be due to the interaction between hydrazine solution and the reaction vessels used in various studies. The present work deals with the effect of several environmental factors on the fate of hydrazine. The effect of certain laboratory experimental conditions has also been evaluated.

MATERIALS AND METHODS

REAGENTS

Hydrazine monohydrate was purchased from Aldrich Chemical Co. (Milwaukee, WI). All other chemicals were analytical grade or the highest grade available.

CLAYS

Montmorillonite (Saz-1) used in these studies was obtained from the Clay Minerals Repository, Department of Geology, University of Missouri.

NATURAL WATERS

Natural waters were collected in 20 gallons plastic carboys from the Saint Johns River and Santa Fe Lake. The lake samples were taken near Buddy's landing on Lake Santa Fe in Melrose, Florida. River water samples were collected under the East Palatka Bridge located on U.S. 17. After arrival to the laboratory the oxygen concentration and total carbon content were measured. Two liters of each type of water were autoclaved and two other liters were filtered through a 0.2 um membrane to sterilize and eliminate

solids in suspension. They were stored in a refrigerator at 10 C until ready for use.

ANALYTICAL METHODS

Hydrazine concentrations less than 11 mmol l⁻¹ were analyzed by the paradimethylaminobenzaldehyde (PDBA) method (reference 1). Higher concentrations were analyzed by direct iodate titration using carbon tetrachloride to detect the end point (reference 2).

Oxygen was analyzed with a dissolved oxygen microelectrode (Microelectrodes, Inc.). Total metals concentration was analyzed with an atomic adsorption spectrophotometer (Perkin Elmer 460). A specific ion electrode was used to detect ammonia in the degradation studies.

EXPERIMENTAL PROCEDURES

Aqueous Studies

Solutions of hydrazine ranging from 10 to 500 ug l⁻¹ were prepared in 2 liter volumetric flasks. After the desired chemical compositions were obtained, 10 ml aliquots were put into small bottles and incubated in a constant temperature water bath. Three bottles were opened for analysis at various intervals of time. The frequency of analysis depended on the rate of hydrazine degradation. Constant ionic strength was maintained using CaCl₂. Low pH's were obtained with HCl. Neutral pH's were obtained with phosphate buffers at different ionic strengths.

Three different types of bottles were used in the study to investigate the effects of the container material: glass scintillation vials, glass serum vials (with crimped aluminum top with a teflon liner), and polyethylene bottles. Most of the experiments were carried out in serum vials because we assumed them to be impermeable to oxygen. New bottles were opened each time an analysis was needed and the rest of the solution and/or suspension was discarded. However; in a recent experiment we found that oxygen could diffuse very slowly into the bottles. Because of this we incubated vials in an anaerobic incubator under a nitrogen atmosphere whenever we wanted to minimize autoxidation.

One set of experiments was carried out in a 1.5 liters Pyrex cell that had a glass top to which a pH electrode, an oxygen electrode and a redox electrode were attached. The cell also had an entrance for bubbling gases and

a syringe to withdraw samples. The contents of the cell were continuously stirred with a Teflon coated magnetic stirring rod. Different Cu concentration solutions were equilibrated with gases of a known oxygen content ($0.275 \text{ } \mu\text{mol l}^{-1}$ or less). Under ambient air conditions a trap was installed between the air pump and the cell to remove CO_2 . We found later that CO_2 had a slight effect on the pH solution. After the addition of 10.3 mmol l^{-1} of hydrazine the electrode readings were monitored and samples were withdrawn periodically for analysis.

Clay Studies

Clay fractions smaller than $0.5 \text{ } \mu\text{m}$ were selected for the degradation studies. This was accomplished by washing the clay three times with 0.1 N NaCl in order to disperse the particles. Samples were washed with deionized water until a negative test for chlorides. The smaller fractions were separated using an ultraspeed centrifuge. To minimize dissolution of clays samples were stored in 0.1 N NaCl solution until ready for use.

In the Cu-clay studies 1 ml aliquots of different Cu stock solutions were added to serum vials containing 9 ml of a Na-saturated clay suspension. They were equilibrated for three days and Cu concentrations in the supernatant was measured. The technique used to detect Cu concentration was differential pulse stripping voltametry with NH_4^+ -citrate at pH 3.0 as the supporting electrolyte. Hydrazine was added to the vials and hydrazine concentration in the supernatant and in the suspension were measured with time.

RESULTS AND DISCUSSION

DEGRADATION OF HYDRAZINE IN WATER

Natural Waters

Waters obtained from Saint Johns River and Santa Fe Lake differed widely in chemical composition, however degradation rate of hydrazine in those waters was very similar and higher than in the control (Fig. 1). The fact that sterilization had very small effect on the rate of hydrazine disappearance indicates that the mechanism was mainly chemical and not microbiological. This is in agreement with the findings by Ou and Street (reference 3) that concentrations above 5 mmol l^{-1} might be toxic for microbial populations.

Effect of Reaction Vessels

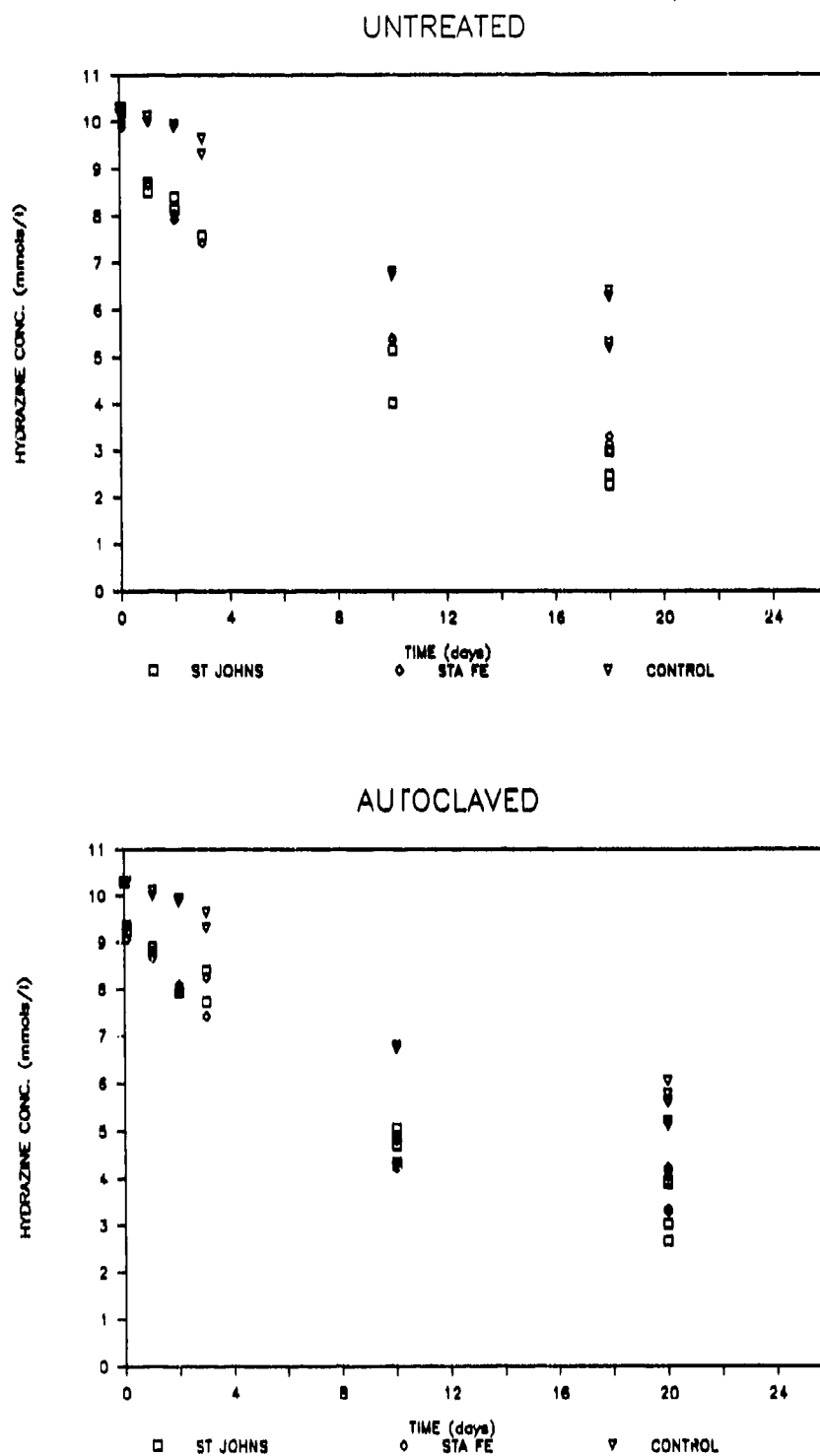


Fig. 1. Degradation of hydrazine in natural waters: Effect of sterilization.

The interaction between hydrazine solutions and the container material of the vessels has been previously reported (reference 4). In our experiment serum vials had the strongest catalyzing effect on hydrazine degradation in distilled water and this effect was even more pronounced when the vials had a head space. Surface catalysis of this type of bottles was also demonstrated when the rate of hydrazine degradation was found to be higher in vials with higher surface:volume ratio and head space volume:solution volume ratio.

On the other hand when Cu was present, degradation of hydrazine was faster in polyethylene bottles. Initially we attributed this to faster leakage of oxygen into the bottle but this may not be conclusive since recent experiments demonstrate a similar rate of oxygen replenishment in both types of bottles after hydrazine has disappeared.

Effect of Copper Concentration

During preparation of the Cu-hydrazine solution we observed the appearance of a greenish precipitate that occurred at concentrations as low as 0.015 mmol l⁻¹ of Cu and 0.2 mmol l⁻¹ of hydrazine. Under these conditions no Cu²⁺ was detected in the solution. For this reason we assumed that a complex had been formed between Cu⁺ and hydrazine. The precipitate turned a brown color when hydrazine concentrations were increased to 10.3 mmol l⁻¹ and was very stable under anaerobic conditions. The fact that the precipitate decomposes in the presence of air, prevented the isolation and evaluation of the complex. The counter anion associated with the Cu had no effect on the appearance of the complex.

The studies with Cu were conducted at different temperatures. The initial rate of hydrazine degradation was strongly affected by Cu concentration. However after the oxygen from the solution and the head space had disappeared the slope of the curves was constant and independent of Cu concentration (Fig.2). The same pattern was evident at 25, 30 and 45 C. In every case NH₃ was monitored during the course of the reaction. We did not detect ammonia in the control, but it was present at all temperatures when Cu was catalyzing the reaction. The ratio of ammonia produced to hydrazine degraded ranged between 1:9 and 1:12. An interesting observation was made for the higher temperatures. Ammonia concentration was linearly correlated with hydrazine disappearance at 25°C, but not at 30° and 45° C. This suggested that hydrazine degradation was going through an intermediate reaction and the rate of formation of the

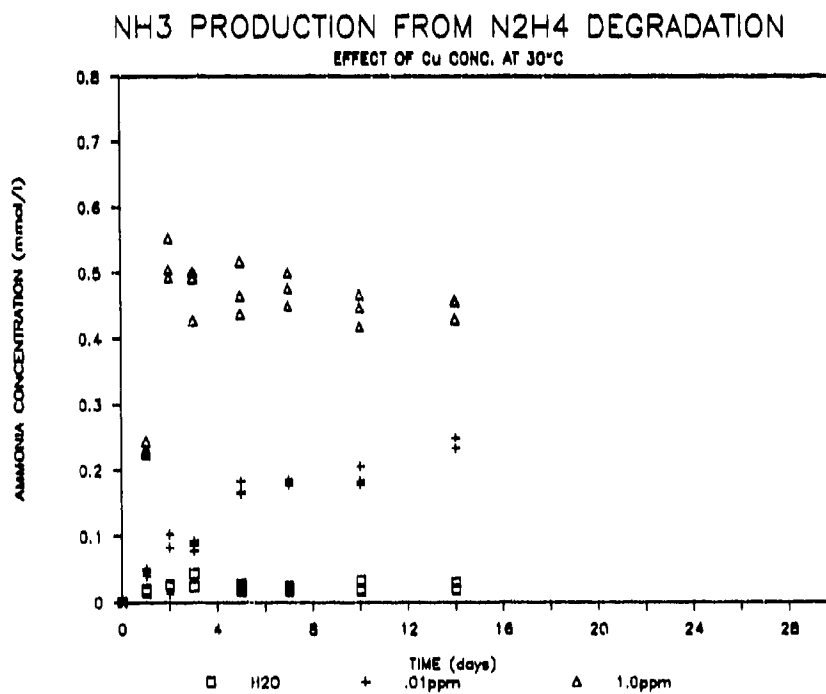
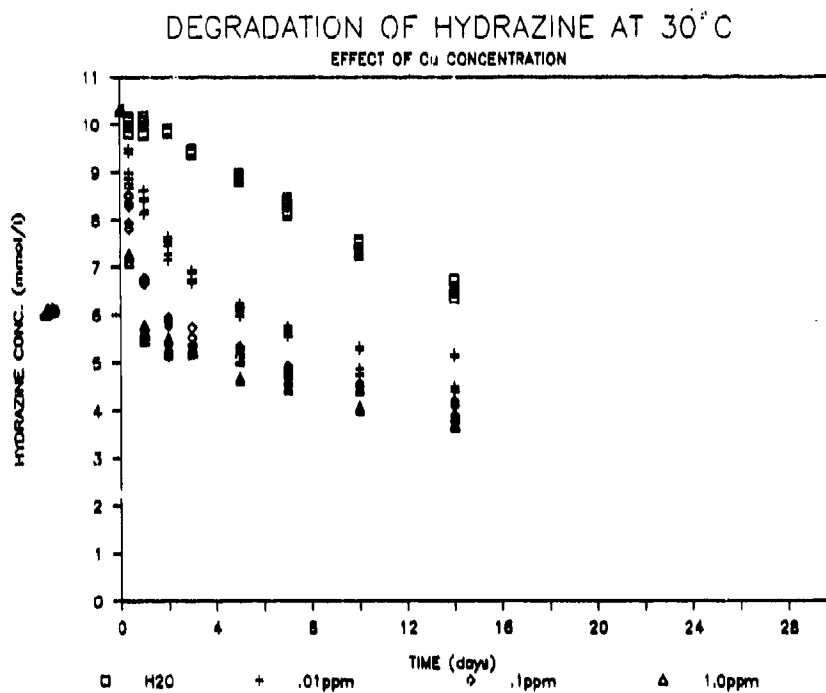


Fig. 2. Effect of Cu concentration on hydrazine degradation at 30°C.

intermediate was faster than the rate of decomposition.

The experiments carried out in a 1.5 l Pyrex cell suggested that solution pH greatly affected the rate of hydrazine degradation (Fig.3). The highest rate of degradation was at a pH close to 10. Oxygen in the range of concentrations found in the environment did not have an appreciable effect on the rate of degradation. However levels of oxygen below 0.1 mmol l^{-1} greatly reduced autoxidation and it was stopped in the absence of oxygen.

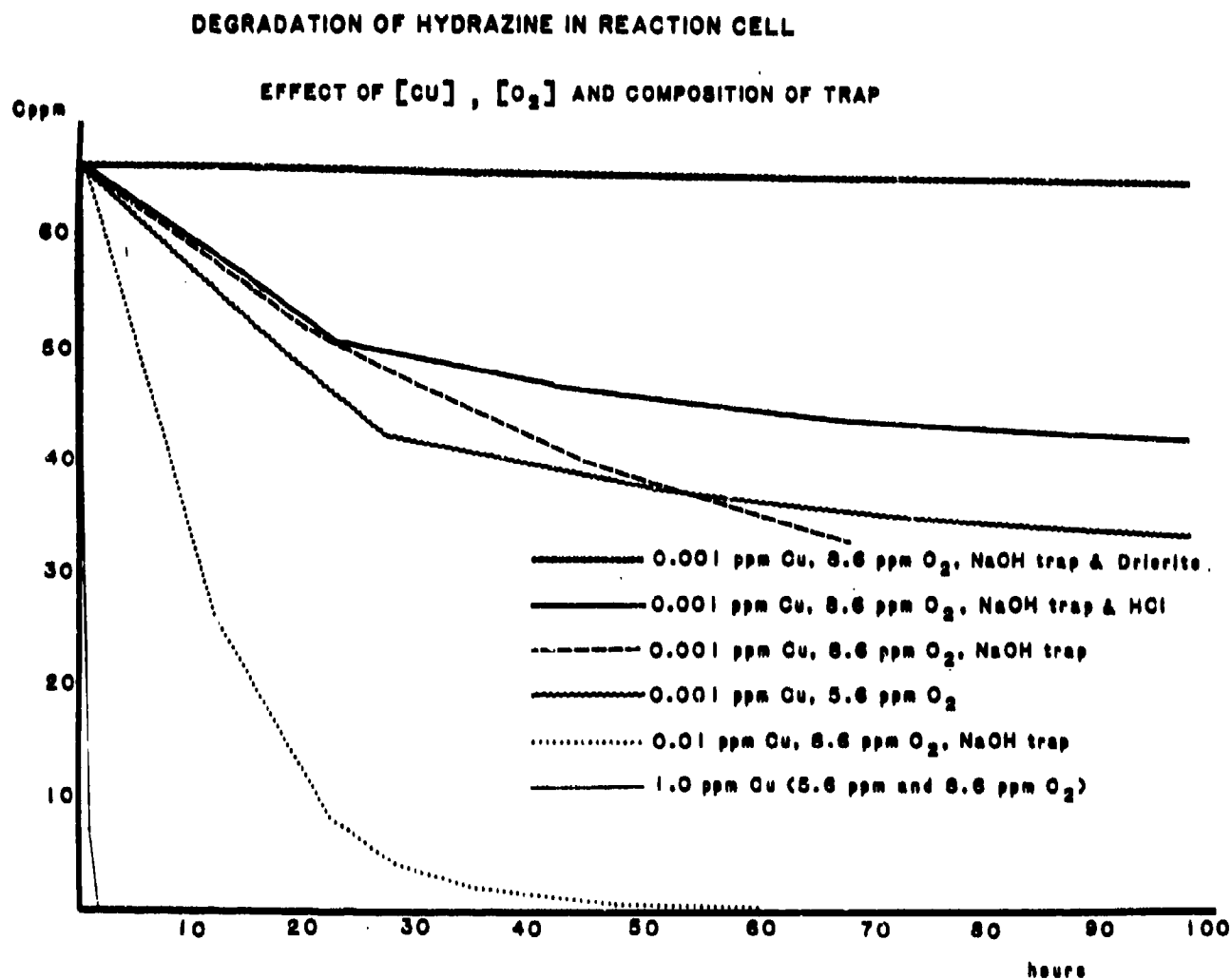
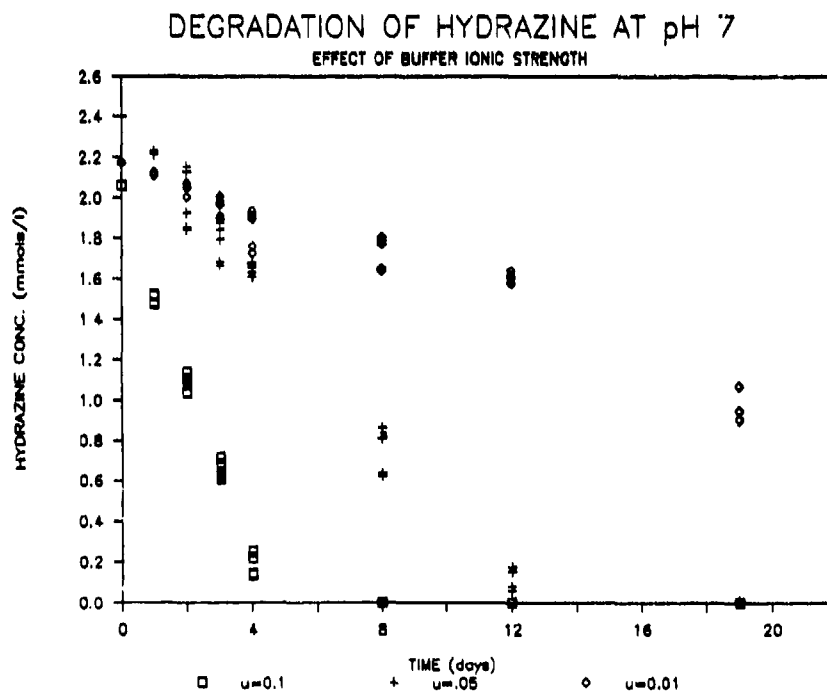
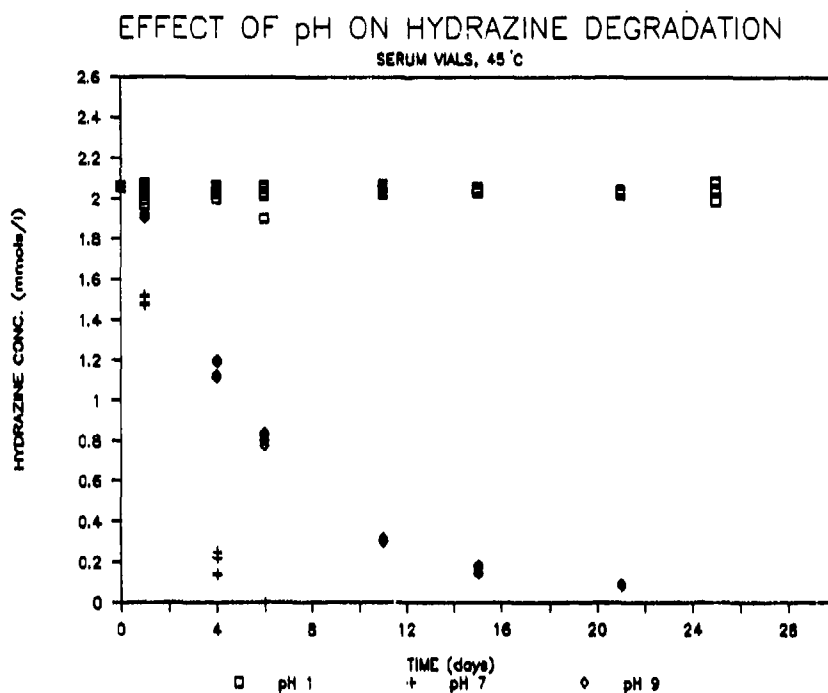


Fig. 3. Hydrazine degradation studies at constant oxygen concentration.



Figs. 4 and 5. Degradation of hydrazine at 45°C: Effect of pH and buffer ionic strength.

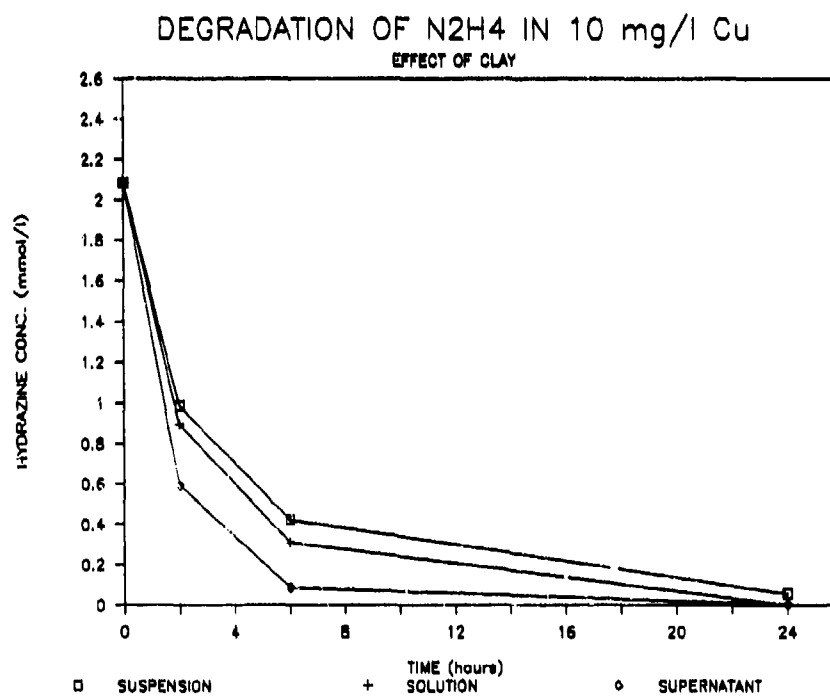
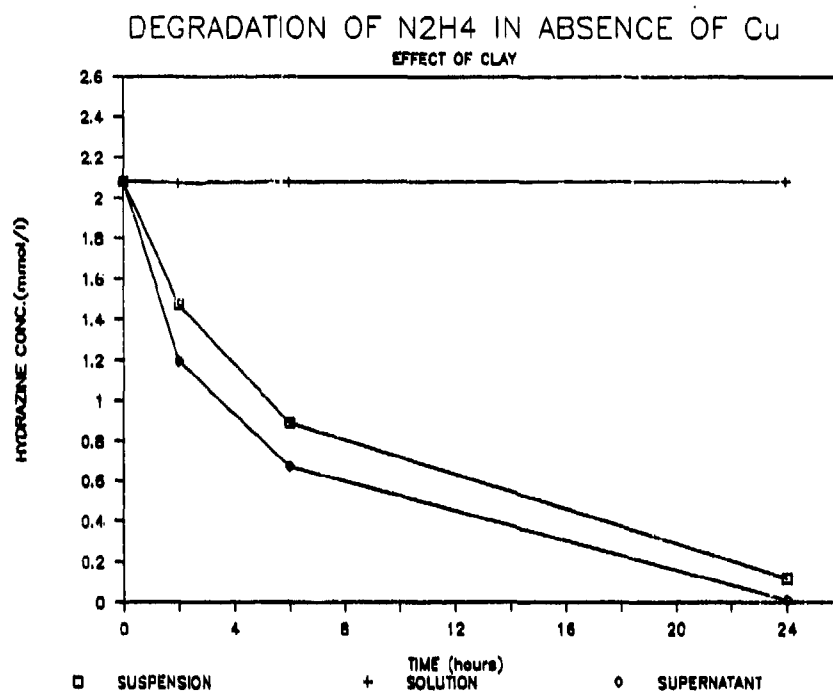


Fig. 6. Effect of clay and Cu concentration on hydrazine degradation.

Effect of pH

In preliminary studies conducted in a wide range of pH's we found the highest rate of hydrazine degradation to be at pH 7 (Fig.4). This contradicted what some authors have reported previously (reference 5). For this reason we set up a study maintaining a pH of 7.0 but reducing the ionic strength of the buffering system. We found that hydrazine degradation rate was approximately first order with respect to buffer concentration (Fig 5). In the presence of $1 \mu\text{g l}^{-1}$ of Cu autoxidation rate greatly increased above pH 9.7 and was almost negligible below pH 4.

CLAY STUDIES

The objective of this part of the study was to evaluate the extent of autoxidation due to Cu in the supernatant or in the vicinity of the clay surface. The results are presented in Figure 6. The amount of Cu reported in the graph represents the total amount of Cu in the suspension. In every case the amount of Cu remaining in the supernatant was between 14% and 20% of that originally added. When Cu was present the effect of clay on hydrazine degradation was less than that for Cu alone. Thus it appears that the clay-Cu complex is less effective in degrading hydrazine than Cu alone. This may be due to reduced activity of Cu in the presence of clay.

REFERENCES

1. Watt, G.W. and J.D. Chrisp, "A Spectrophotometric Method for the Determination of Hydrazine", Analytical Chemistry, 1952, vol. 24, pp. 2006-2008.
2. Penneman, R.A. and L.F. Audrieth, "Quantitative Determination of Hydrazine", Analytical Chemistry, 1948, vol. 20, pp. 1058-1061.
3. Ou, L.T. and J.J. Street, "Hydrazine Degradation and its Effect on Microbial Activity in Soil", Bulletin of Environmental Contamination and Toxicology, 1987, vol. 38, pp 179-183.
4. Gaunt, H. and E.A.M. Wetton, "The Reaction Between Hydrazine and Oxygen in Water" Journal of Applied Chemistry, 1966, vol 16, pp 171-176.
5. MacNaughton, M.G., G.A. Urda and S.E. Bowden, "Oxydation of Hydrazine in Aqueous Solutions", CEEDO-TR-78-11 (1978). AD-A058239. N79-12242.

VIBRATIONAL SPECTROSCOPIC STUDY OF THE KAOLINITE - HYDRAZINE INTERCALATION COMPLEX

C. T. Johnston, Asst. Professor
Department of Soil Science
University of Florida
Gainesville, Florida 32611

D. A. Stone, Tyndall AFB
L. A. Applewhite, University of Florida

ABSTRACT

In-situ vibrational spectroscopic methods have been used to study the interaction of hydrazine with the kaolinite mineral surface. Non-invasive Raman and FT-IR spectra were obtained for the kaolinite-hydrazine (KH) intercalation complex at low temperatures and at reduced pressure values. Strong vibrational perturbations of the guest intercalate, hydrazine, and of the clay mineral kaolinite were observed. Upon expansion of the kaolinite structure by hydrazine, a significant reduction in the intensities of the inner-surface hydroxyl groups was observed which indicated that strong hydrogen bonds were formed between the intercalated hydrazine species and the kaolinite interlamellar surface. In addition, several Raman- and IR-active vibrational modes of hydrazine were influenced by the kaolinite surface.

INTRODUCTION

The attenuation of hydrazine and its methyl derivatives by soil and aquifer constituents is of interest to the United States Air Force because of their use in several Air Force weapon systems and their adverse biological activity to man. Although the macroscopic adsorption behavior of hydrazine by clay minerals has been studied¹, little is known about the chemical mechanism(s) of interaction. Adsorption data are macroscopic data and, therefore, are intrinsically insensitive to molecular phenomena; adsorption data cannot be interpreted to obtain unequivocal, molecular-level information about the adsorbed species². The objective of this paper will be to examine the molecular-level interactions of hydrazine with kaolinite using several non-invasive, in-situ spectroscopic methods.

The vibrational spectrum of kaolinite, a ubiquitous 1:1 clay mineral that is found throughout the world, has been studied more intensively than that of any other clay mineral³. This spectroscopic interest in kaolinite is, in part, a result of its well-resolved hydroxyl stretching bands. In contrast to the broad vibrational linewidths of hydrous metal oxides and 2:1 clay minerals that typically have bandwidths of greater than 50 cm^{-1} , the measured full-width-at-half-maximum (FWHM) values for the hydroxyl stretching bands of kaolinite range⁴ between 5 and 12 cm^{-1} . These comparatively sharp vibrational bands of kaolinite provide surface-sensitive probes of changes in the chemical environment surrounding these hydroxyl groups.

A more complete vibrational analysis of adsorbate-surface complexes can be obtained when perturbed vibrational modes of the adsorbate and of the surface are observed. This study will employ the surface hydroxyl groups of kaolinite as molecular probes of the interaction between kaolinite and hydrazine upon formation of the intercalation complex. Changes in the frequency, intensity, and lineshape of the vibrational modes of the adsorbed species can provide direct information about the structure of the adsorbed species and what chemical functional group(s) of the adsorbate are involved in bonding to the surface. However, these data do not provide unambiguous information about the orientation of the adsorbed species, or about which surface functional groups are involved in bonding to the adsorbate. This information can best be obtained by observing the perturbed vibrational modes of the substrate. The well-resolved IR- and Raman-active bands of kaolinite should allow perturbed vibrational modes of the substrate to be resolved.

EXPERIMENTAL

The sample studied was the KGa-1 kaolinite from Washington county Georgia, obtained from the Source Clays Repository of The Clay Minerals Society. A complete description of the physical properties of this clay sample has been given by van Olphen and Fripiat⁵. In addition, Raman and IR spectra of this clay have been reported by Johnston et. al.^{4,6}. A dilute aqueous suspension of the kaolinite sample was prepared by suspending 0.1 grams of oven-dry kaolinite in 100 ml. of distilled-deionized water. The clay suspension was dispersed by adjusting the pH of the suspension to 9.2 by the addition of small aliquots of 0.01 M NaOH. All of the FT-IR spectra reported here correspond to transmission FT-IR spectra of kaolinite samples deposited upon a 25mm x 2mm ZnSe window.

FT-IR spectra were obtained on a Bomem DA3.10 Fourier transform spectrometer. The DA3.10 spectrometer incorporates a Michelson interferometer with the beamsplitter positioned at a 30 degree angle to the optical axis. A MCT detector was used in this investigation with a measured D^* value of $3.13 \times 10^9 \text{ cm}^2\text{Hz}^{0.5}$ and a cutoff wavenumber of 400 cm^{-1} (25 microns). The nominal resolution used in these studies ranged between 2.0 and 0.5 wavenumbers. A comparison of the several spectra obtained

for different nominal resolution values showed that, for the samples being studied here, the spectra were not instrument limited for nominal resolution values of 0.5 and 1.0 wavenumbers; the 2.0 wavenumber spectrum was, however, instrument limited.

Low temperature FT-IR spectra were obtained on the Bomem DA3.10 spectrometer using an air cooled Air Products CS-202 cryogenic refrigeration system. A 25mm x 2 mm ZnSe window was mounted in the Air Products DMX-1 sample holder using indium gaskets and the vacuum shroud was fitted with 2 49mm x 4 mm ZnSe windows. The temperature of the sample holder was measured using a Chromel/Gold 0.07 Atomic % Iron thermocouple.

Raman spectra were collected on a Spex 1403 3/4 m double monochromator interfaced to a Nicolet 1180E computer. The 488 nm line of an argon ion laser (Spectra Physics 171) was used at an incident power output of 100 mW measured at the sample. The spectral slit width ranged from 2 cm^{-1} to 1 cm^{-1} . X-Ray diffraction patterns were obtained using a Nicolet computer controlled X-Ray diffraction system with a stepping motor accuracy of 0.0025° 2 θ . Samples were scanned at 2° 2 θ /min. using CuK α radiation.

RESULTS

Expansion of the kaolinite lattice upon intercalation by hydrazine is shown by a plot of the X-ray diffraction d001 reflections of kaolinite and of the KH complex versus time. (Figure 1). As hydrazine was adsorbed by kaolinite, the intensity of the non-intercalated d001 reflection at 12.36 ° 2 θ (0.716 nm spacing) decreased, and a corresponding increase in intensity was observed for the "new" KH d001 reflection at 8.60 ° 2 θ (1.03 nm spacing). Assuming that the ratio of the KH reflection against the kaolinite d001 reflection is directly proportional to the fraction of kaolinite intercalated, these data (Figure 1) indicated that after two hours of exposure to hydrazine more than 90 percent of the kaolinite was intercalated by hydrazine. The sharp decrease in intensity with time of the non-intercalated d001 reflection (Figure 1), however, may indicate that the intercalation process reached completion after only 30 minutes. X-ray diffraction (XRD) patterns showing the d001 reflections of kaolinite and of kaolinite-hydrazine (KH) intercalates are presented in Figure 2. Upon expansion of the kaolinite lattice by hydrazine, the interlamellar spacing increased from 0.716 nm to 1.030 nm, an increase of 0.314 nm. This increase indicated that one molecular layer of hydrazine was adsorbed between each structural 1:1 layer of the clay lattice. By comparison to the other d001 reflections, the well-defined, relatively sharp 8.60 ° 2 θ reflection in the XRD pattern of the KH complex obtained at 1 atmosphere of pressure (labeled "K:H air" in Figure 2), indicated that the KH complex was fairly well ordered under these conditions and that very little non-intercalated kaolinite remained after intercalation.

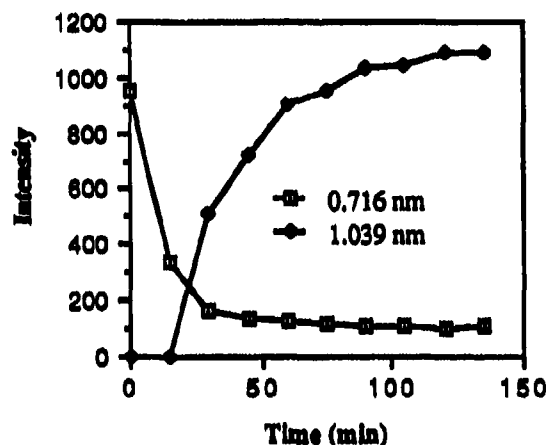


Figure 1. Intensity of the XRD d[001] reflections versus time of kaolinite (0.716 nm) and of the kaolinite-hydrazine complex (1.039).

These XRD results are in good agreement with those of Ledoux and White⁷ who reported a d₀₀₁ spacing of 1.040 nm for the KH complex at 25° C and 1 atm. Space filled drawings of the expanded kaolinite crystal structure (d₀₀₁=1.030 nm) and of hydrazine (Figure 3) illustrate the

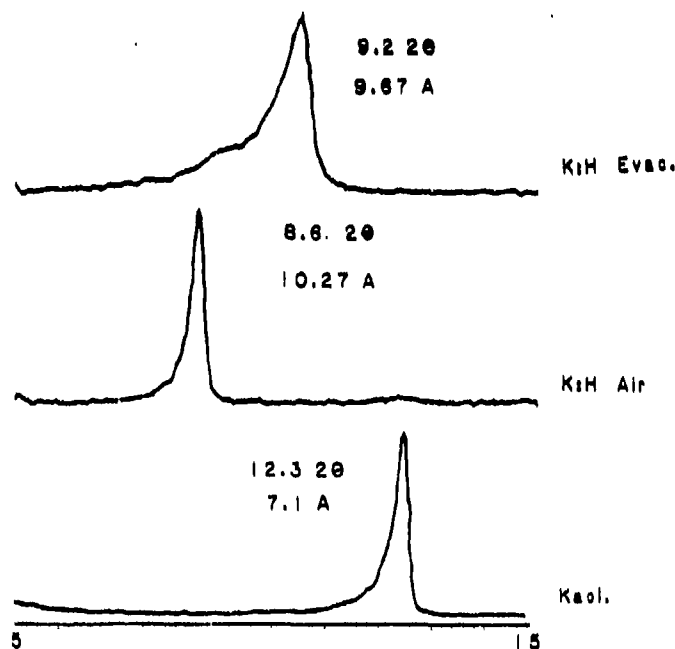


Figure 2 X-ray diffraction patterns of non-intercalated kaolinite (bottom) , KH complex at 760 torr , KH complex under vacuum (A.III).

approximate amount of space available for the intercalate in the interlamellar region and the corresponding dimensions of the hydrazine molecule.

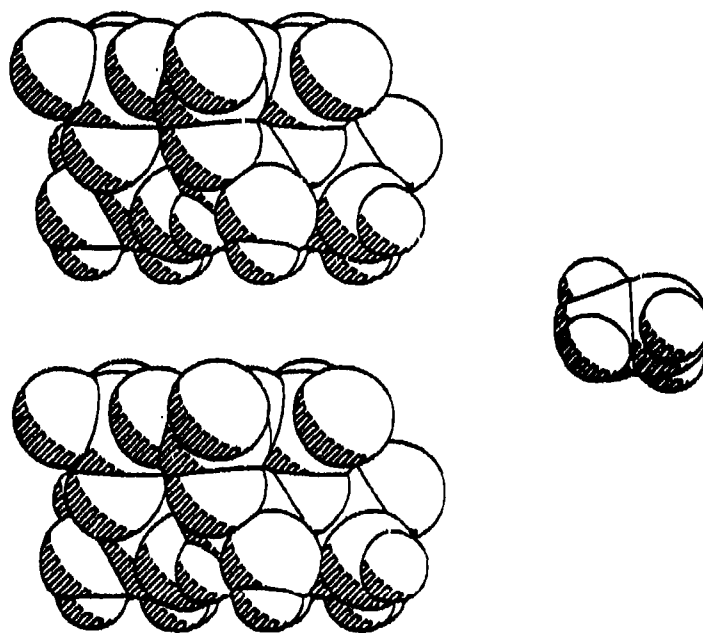


Figure 3. [010] projection of the expanded kaolinite structure after expansion of lattice by hydrazine to a 1.03 nm d001 spacing. A hydrazine molecule drawn to the same scale using van der Waals radii is shown on the right.

Raman spectra in the 3600 to 3725 cm^{-1} region of kaolinite (top), and of a KH complex at 760 torr (bottom), are shown on the left side of Figure 4. The 3620 cm^{-1} band was not perturbed upon intercalation under these conditions. In contrast, the intensities of the hydroxyl stretching bands at 3652 , 3668 , and 3694 cm^{-1} bands were strongly reduced upon formation of the KH complex. A similar result was observed in the FT-IR spectra (right side of Figure 4): the 3652 , 3669 , and 3692 cm^{-1} bands of kaolinite (Figure 4a) were reduced in intensity upon intercalation (Figure 4b-c), and the 3620 cm^{-1} band was not affected. These results are in agreement with a previous IR study of the KH complex⁷.

The molecular structure of kaolinite projected along the [010] face (looking along the y axis with the z-axis pointing up) is shown in Figure 5. The space filled drawing shown on the right was constructed using van der Waals radii for Si, Al, O, and H⁸. The ball and stick drawing shown on the left illustrates the two distinct types of hydroxyl groups that reside within the crystal structure of kaolinite: the inner hydroxyl "sandwiched" between the the Al-octahedral and Si-tetrahedral layers of the clay lattice, and the inner-surface hydroxyl groups located on the basal plane of the Al-

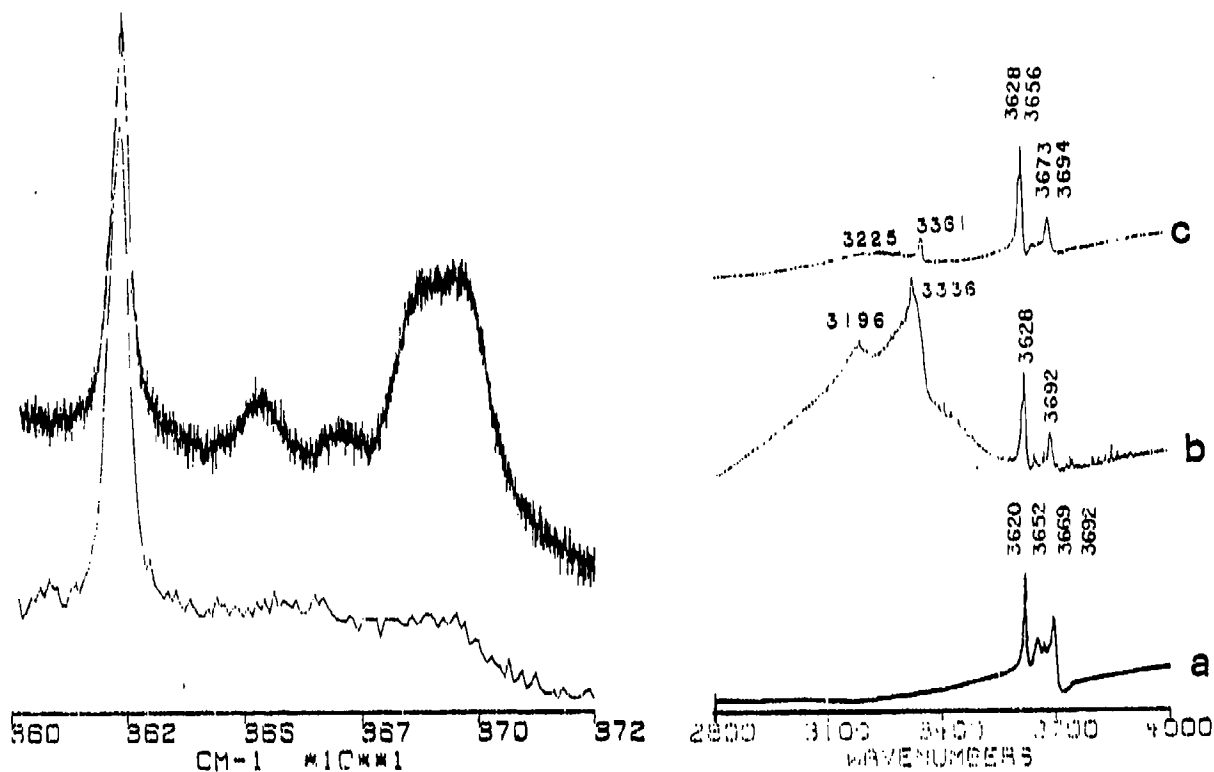


Figure 4. [left side] Raman spectra in the 3600 to 3725 cm^{-1} region of KH complex at 760 torr (bottom), and of a dry non-intercalated Mesa Alta kaolinite sample (top). [Right side] FT-IR absorbance spectra in the 2800 to 4000 cm^{-1} region of kaolinite (a), KH complex at 760 torr (b), and of the KH complex under a vacuum of 0.0001 torr (c).

octahedral layer. Numerous infrared studies of kaolinite^{3,9-16} are in agreement that the 3620 cm^{-1} band is assigned to the inner hydroxyl group (Figure 5), and that this hydroxyl group has a

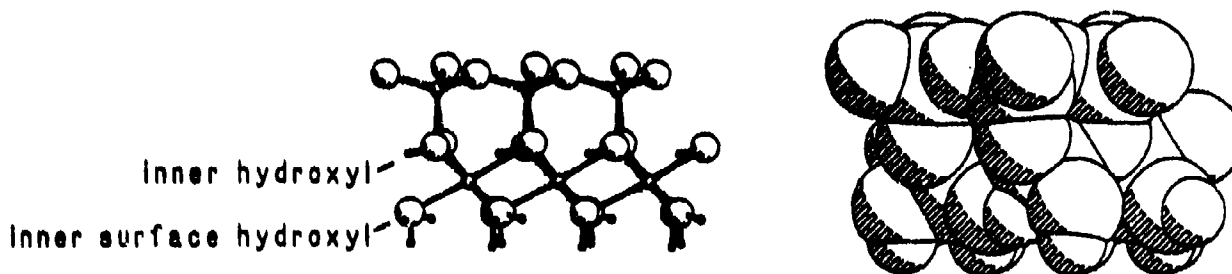


Figure 5. [010] projection of the crystal structure of kaolinite showing the inner hydroxyl and inner-surface hydroxyl groups of kaolinite.

considerably greater resistance to isotopic exchange with deuterium and to dehydroxylation at elevated temperatures in comparison to the labile inner-surface hydroxyl bands at 3652, 3669, and 3690-5 cm^{-1} .

FT-IR spectra of the KH complex in the 3550 to 3750 cm^{-1} region are shown in Figure 7 at 1 atm of pressure and at several reduced pressure values. As the KH complex is exposed to a reduced pressure, a new, higher-frequency band appeared at 3628 cm^{-1} and increased in intensity at the expense of the 3620 cm^{-1} band. Insofar as these authors are aware, a similar shift in frequency of the

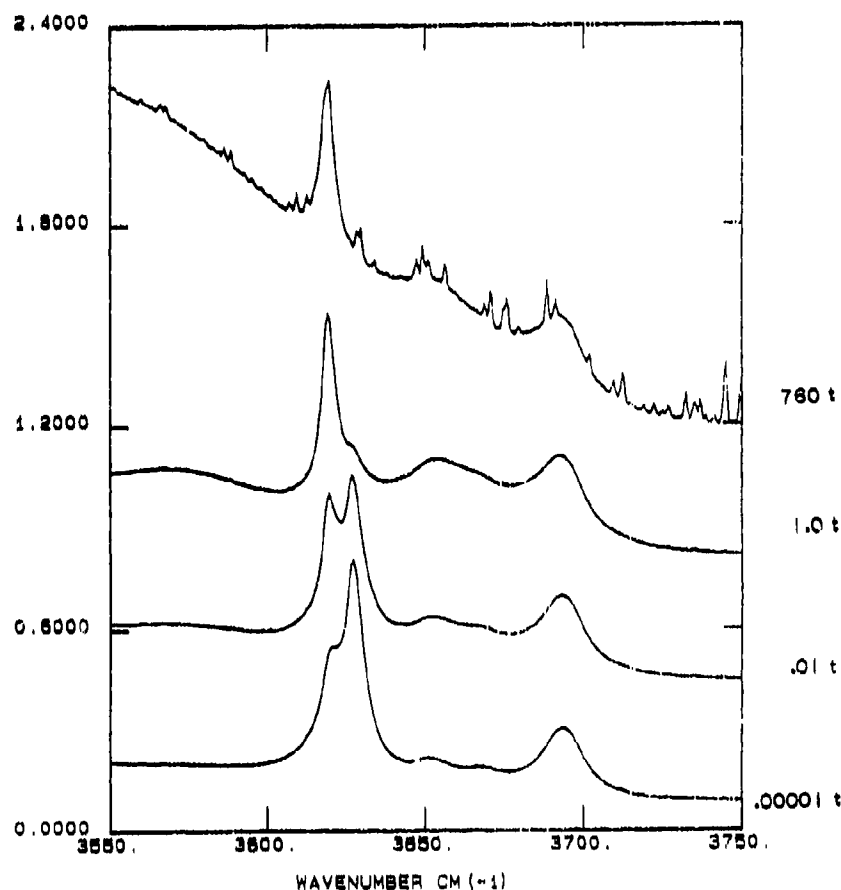


Figure 6 FT-IR absorbance spectra of the KH complex at pressure values of 0.00001 torr, 0.01 torr, 1.0 torr, and 760 torr.

inner-hydroxyl stretching band induced by a guest intercalate has not been reported previously in the literature. There is little doubt regarding the assignment of the 3628 cm^{-1} band to the inner-hydroxyl group because of the strong intensity borrowing between the two bands. The presence of two discrete inner-hydroxyl stretching bands suggests strongly that a different structural conformation of the intercalation complex was induced upon decreasing the pressure. A similar result was not observed in the Raman spectra of the KH complex because the sample was studied at 1 atm of pressure.

To confirm this hypothesis, XRD patterns of the evacuated complex were obtained at reduced pressure values (Figure 7). The d001 reflection of the KH intercalation complex was observed to

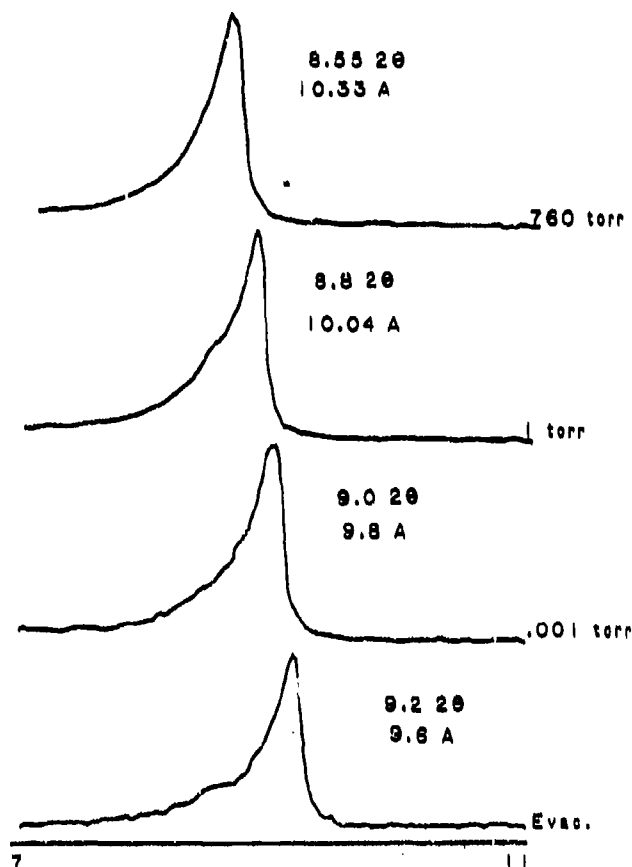


Figure 7. X-ray diffraction patterns showing the d[001] reflection of the kaolinite-hydrazine complex at 760 torr, 1 torr, 0.001 torr, and 0.00001 torr.

increase from its value of $8.60^\circ 2\theta$ at 1 atm to $9.2^\circ 2\theta$, which corresponded to a decrease in the interlamellar spacing from 1.030 nm (760 torr) to 0.960 nm (0.00001 torr). Thus, the interlamellar spacing of the intercalation complex decreased by 0.07 nm upon evacuation, which decreased the available space for the guest species from 0.314 nm to .244 nm. This observed decrease in the interlamellar spacing of the KH complex provided conclusive evidence that a structural change of the KH complex did occur upon evacuation. This change was also reflected by the novel blue-shift of the inner-hydroxyl stretching band from 3620 to 3628 cm^{-1} which indicated that the $-\text{NH}_2$ moiety of the guest hydrazine species was brought into close contact with the inner-hydroxyl group after evacuation.

As the [010] ball and stick projection of kaolinite illustrates (Figure 5), the inner-hydroxyl group resides between the silica tetrahedral and aluminum octahedral layers and is not accessible by most interlamellar species. The fact that hydrazine perturbed the stretching frequency of the inner

hydroxyl group suggested that the -NH_2 moiety keyed into the kaolinite surface resulting in a slight electrostatic repulsion between the -NH_2 and -OH groups responsible for the 8 cm^{-1} blue shift. Considering the molecular structure of kaolinite, the inner-hydroxyl group can only be approached by a guest molecule small enough to penetrate through the siloxane ditrigonal cavity. A space-filled [001] projection of the kaolinite structure showing the siloxane ditrigonal cavity and the molecular structure of hydrazine drawn to the same scale (Figure 8) illustrates qualitatively that the -NH_2 moiety is small enough to "fit" into the cavity.

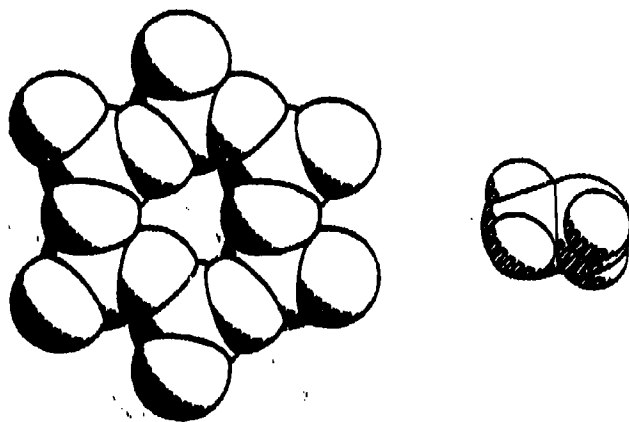


Figure 8 [001] projection of the kaolinite siloxane ditrigonal cavity. A hydrazine molecule drawn to scale using van der Waals radii is shown on the right.

CONCLUSION

In conclusion, the Raman and FT-IR spectra of the KH complex in the hydroxyl stretching region are in agreement in that both methods show a strong reduction in intensity of the inner-surface hydroxyl groups upon intercalation resulting from the formation of hydrogen bonds between the inner-surface hydroxyl groups of kaolinite and the interlamellar hydrazine species. XRD patterns of the KH complex indicated that the interlamellar region increased in size by 0.314 nm at 1 atm of pressure to accommodate the guest intercalate. As the pressure was reduced, however, this value decreased to 0.244 nm and the FT-IR spectra of the reduced pressure KH complexes showed clearly the presence of a new, higher frequency inner-hydroxyl stretching band at 3628 cm^{-1} . These results indicated that a structural change of the KH complex occurred at a reduced pressure, and that the -NH_2 moiety of hydrazine was brought into close contact with the inner-hydroxyl group through the siloxane ditrigonal cavity. In addition, it was shown that the Raman- and IR-active hydroxyl stretching modes of kaolinite were sensitive probes of the interaction between hydrazine molecules and the kaolinite surface.

REFERENCES

1. Hayes, M.H.B.; Isaacson, P.J.; Chia, K.Y.; Lees, A.M.; Yormah, T.B.R. (1984) Interactions of hydrazine and of hydrazine derivatives with soil constituents and with soils. Final Report to AFOSR and EOARD (1984) AFOSR-80-0032.
2. Johnston, C.T.; Sposito, G. (1987) Disorder and early sorrow: Progress in the chemical speciation of soil surfaces. *Soil Sci. Soc. Am. J.* (In press)
3. Farmer, V.C. (1974) Chapter 15 in "The infrared spectra of minerals" Ed. Farmer, V.C. Publ. by the Mineral Society of London.
4. Johnston, C.T.; Sposito, G.; Birge, R.R. (1985) Raman spectroscopic study of kaolinite in aqueous suspension. *Clays and Clay Minerals* 33, 483.
5. van Olphen, H., and Fripiat, J. J. (1979) Data handbook for clay materials and other non-metallic minerals. Pergamon Press, Oxford.
6. Johnston, C.T.; Sposito, G.; Bocian, D.F.; Birge, R.R. (1984) Vibrational spectroscopic study of the interlamellar kaolinite-dimethyl sulfoxide complex. *J. Phys. Chem.* 88, 5959-5964.
7. Ledoux, R.L.; White, J.L. (1966) "Infrared studies of hydrogen bonding interaction between kaolinite surfaces and intercalated potassium acetate, hydrazine, formamide, and urea." *J. Coll. Interface Sci.* 21, 127-152.
8. Sutch, P.R.; Young, R.A. (1983) Atom positions in highly ordered kaolinite. *Clays and Clay Min.* 31, 357-366.
9. Prost, R. (1984) Etude par spectroscopie infrarouge a basse temperature des groupes OH de structure de la kaolinite, de la dickite et de la nacrite. *Agronomie*, 4, 403-406.
10. Ledoux, R.L.; White, J.L. (1964) Infrared study of selective deuteration of kaolinite and halloysite at room temperature. *Science* 145, 47-49.
11. Wada, K. (1967) A study of hydroxyl groups in kaolin minerals utilizing selective deuteration and infrared spectroscopy. *Clay Minerals* 7, 51.
12. Farmer, V.C. (1964) *Science* 145, 1189.
13. Farmer, V.C., Russell, J.D. (1964) The infrared spectra of layer silicates. *Spectrochim. Acta* 20, 1149.
14. Stubican, V.; Roy, R. (1961) A new approach to assignment of infra-red absorption bands in layer-structure silicates. *Zeitschrift fur Kristallographie* 115, 200-214.
15. Rouxhet, P.G.; Samudacheata, N.; Jacobs, H.; Anton, O. (1977) Attribution of the OH stretching bands of kaolinite. *Clay Minerals* 12, 171-178.
16. Fripiat, J.J., Toussaint, F. (1963) Dehydroxylation of kaolinite. II. Conductometric measurements and infrared spectroscopy. *J. Phys. Chem.* 67, 30-36.

SURFACE-CATALYZED AIR OXIDATION REACTIONS OF HYDRAZINES:
TUBULAR REACTOR STUDIES

Jan E. Kilduff, Scientist
Lockheed-EMSCO
White Sands Test Facility
Las Cruces, NM 88004

Dennis D. Davis, Senior Scientist
Lockheed-EMSCO
White Sands Test Facility
Las Cruces, NM 88004

Steven L. Koontz, Project Scientist
NASA
White Sands Test Facility
Las Cruces, NM 88004

ABSTRACT

The surface-catalyzed air oxidation reactions of hydrazine, monomethylhydrazine, unsymmetrical dimethylhydrazine, symmetrical dimethylhydrazine, trimethylhydrazine and tetramethylhydrazine were investigated in a metal-powder packed tubular flow reactor at 55 ± 3 °C. Hydrazine was completely reacted on all surfaces studied. The major products of monomethylhydrazine (MMH) oxidation were methanol, methane and methyldiazene. The di-, tri- and tetra-methyl hydrazines were essentially unreactive under these conditions.

The relative catalytic reactivities toward MMH are:

$\text{Fe} > \text{Al}_2\text{O}_3 > \text{Ti} > \text{Zn} > 316 \text{ SS} > \text{Cr} > \text{Ni} > \text{Al} > 304\text{L SS}$

A kinetic scheme and mechanism involving adsorption, oxidative dehydrogenation and reductive elimination reactions on a metal oxide surface are proposed.

INTRODUCTION

Air oxidation reactions have been considered as a major factor in the environmental fate of hydrazines. Previous studies in environmental chambers (References 1, 2) have provided

convincing evidence that these reactions are strongly surface dependent. A convenient and rapid method for physicochemical, kinetic and product studies of heterogeneous catalytic reactions using a TFE tubular reactor in a gas chromatograph has been developed and applied to the study of the surface-catalyzed air oxidation of hydrazine and its methylated derivatives.

EXPERIMENTAL

MATERIALS

The metal and metal oxide powders were obtained commercially. BET surface area determinations were performed by Micromeritics Instrument Corp., Norcross, GA.

Hydrazine (HZ) and monomethylhydrazine (MMH) were propellant grades (Olin) analyzed according to MIL-P-26536-C and MIL-P-2740413, respectively. Unsymmetrical dimethylhydrazine (UDMH), (Aldrich), and tetramethylhydrazine (TMH), (Fluka), were reagent grade materials and used as received. Methylamine (Airco), dimethylamine (Matheson), and trimethylamine (Matheson) were used as supplied. 1,2-Dimethylhydrazine (SDMH) was prepared from dimethylhydrazine dihydrochloride (Aldrich) by distillation from saturated potassium hydroxide. The crude SDMH was dried over barium oxide overnight and then fractionally distilled from fresh barium oxide (bp 76.5 °C, 660 torr). Trimethylhydrazine (TMH) (bp 53 °C, 660 torr) was prepared using the procedure of Class, Aston, and Oakwood (Reference 3). All other materials were reagent grade used as supplied.

Tubular reactors were constructed from 12.7 cm sections of 0.63 cm o.d. TFE tubing with an i.d. of 0.25 cm. The reactor tubes were capped with Zitex (Chemplast, Inc.) 90-X TFE filter membranes wedged into TFE compression fittings to prevent the loss of powdered material. The outlet of the reactor tubes was connected by TFE tubing to the flame ionization detector of a HP 7620A gas chromatograph. The injector port of the GC was TFE lined.

PROCEDURE

A tubular reactor, filled with 1 to 3.5 grams of powdered metal or oxide, was mounted in the GC oven and allowed to stabilize in a flow of air or nitrogen carrier gas (10 - 12 ml/min) at 55 ± 3 °C for 30 minutes. A series of constant volume injections, usually 0.25 microliters, was made until the area and shape of the eluted peak(s) were constant. The eluents from the reactor tube were trapped in an IR gas cell and the contents analyzed by FTIR. Because of small flame response, eluted hydrazine was trapped on acid-coated firebrick and analyzed by coulometric titration. In control experiments, recoveries of 103 percent and 93 percent for MMH and UDMH, respectively, were attained.

RESULTS

Hydrazine reacted quantitatively with air on 316 SS, 304L SS, Fe, Al, Al_2O_3 , Zn, Cr, Ni, Ti, sand, concrete, and powdered cinder block. Blank experiments using unpacked reactor tubes showed an 89 percent recovery of unreacted hydrazine. When nitrogen was used as the carrier gas, hydrazine eluted quantitatively from powdered TFE and iron but was completely consumed by Fe_2O_3 .

The reaction products of MMH with air and metal and oxide surfaces are methane, methyldiazene (MD), methanol, and in some cases, traces of ammonia. The product distributions are shown in Table 1. MMH is unreactive in nitrogen.

A typical injection sequence for MMH on 316 SS in air is shown in Figure 1. The first injection shows several broad small peaks consisting of MMH and reaction products. The second injection of MMH results in greater amounts of eluents at shorter retention times. Typically, the third and subsequent injections showed constant peak shapes and retention times. Presumably at this time, the surface is in adsorption equilibrium with MMH and its reaction products. Methane is first to elute, followed by methyldiazene, MMH, and methanol.

TABLE 1. TUBULAR REACTOR PRODUCTS: MMH IN AIR AT 55 ± 3 °C

Catalyst	Products (%)					Recovered Carbon (%)
	CH ₃ OH	MD	CH ₄	NH ₃	MMH	
316 SS	2.6	21.3	0.9	-	50.5	75.3
304L SS	7.8	16.5	0.6	3.4	39.5	67.5
Fe	8.5	16.5	17.0	1.1	9.6	53.0
Fe ₂ O ₃	18.9	-	29.0	-	-	48.1
Al	5.7	21.3	-	2.1	19.1	48.0
Al ₂ O ₃	18.1	14.9	29.0	2.6	10.6	75.2
Zn	1.1	16.5	-	-	69.0	86.6
Cr	2.1	19.7	8.2	-	60.4	90.4
Ni	7.4	15.4	14.9	-	7.4	45.1
Ti	4.0	24.2	9.6	-	38.8	76.6
Cu ₂ O	3.2	17.5	18.6	-	41.0	80.3

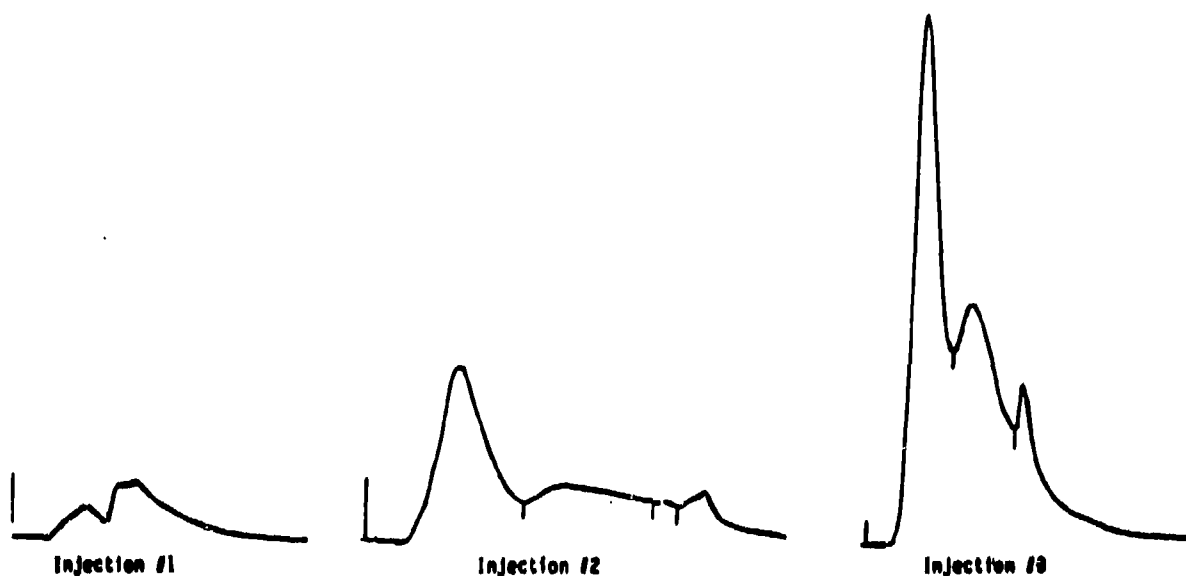


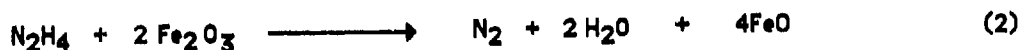
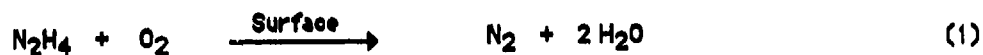
Figure 1. FID Response Curves for Three Sequential Injections of MMH on 316 SS Powder in a Tubular Reactor: Air 10 ml/min, 55 ± 3 °C

The di-, tri-, and tetra-methyl substituted hydrazines are much less reactive than hydrazine or MMH. SDMH showed only a slight reactivity on the most reactive surface, Fe_2O_3 . The product was tentatively identified as dimethyldiazene. Trace amounts of oxidation products from UDMH and TMH were not identified. The fully substituted TTMH and the methylamines are unreactive on all surfaces.

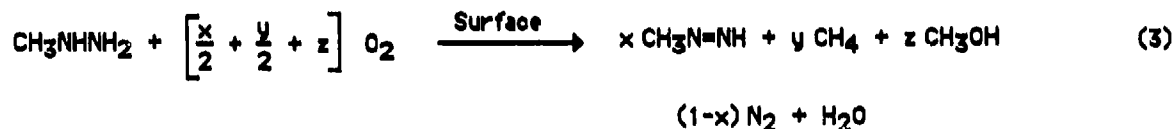
DISCUSSION

The reactivities in air range from hydrazine which is completely reacted by contact with all the surfaces studied to the essentially unreactive tetramethylhydrazine. Surface-promoted thermal decomposition reactions are apparently not involved at the temperature of this study since blank runs in nitrogen showed no evidence of reaction in empty tubes or on TFE powders. However, iron (III) oxide, which can provide its own oxidizing equivalents, completely consumed hydrazine reactant, even in nitrogen.

The following reactions occur:



The balanced equation for MMH air oxidation can be shown as:

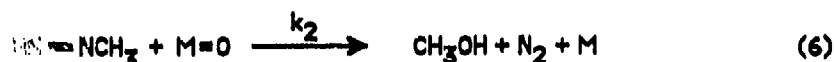


$$\text{Where: } x + y + z = 1$$

The stoichiometry above does not account for the traces of ammonia detected in a few reactions.

Scheme 1 shows a general kinetic system for the surface-catalyzed air oxidation of MMH.

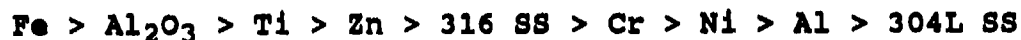
SCHEME 1



$$-\frac{d[\text{MMH}]}{dt} = k_1 [\text{MMH} \cdot \text{O=M}] = k_1 K_{so} [\text{MMH}][\text{M=O}] \quad (9)$$

$$= k_1' K_{so} [\text{MMH}] = k_{obs} [\text{MMH}] \quad (10)$$

The metal surface is represented by M and M=O represents a catalytically active surface-oxide site. Surface re-oxidation as shown in Eq. 8 is assumed to be fast in a flowing air carrier gas. K_{so} is the isosteric adsorption equilibrium constant (Reference 4) which describes the adsorption step. The overall surface reactivity, represented by k_1' , can then be calculated as $k_{obs}/[\text{M=O}]$ where $[\text{M=O}]$ is the catalyst surface area. This assumes that the entire surface area is an oxide coating. The microscopic rate constant k_1 is then k_1'/K_{so} . The K_{so} values for methylamine were determined gas chromatographically (Reference 5) and have been used as estimates of the MMH values, Table 2. The overall reactivity order (k_1') of the catalysts for the air-oxidation of MMH is:



The reactivity in the dehydrogenation step (k_1) is:



TABLE 2. SURFACE REACTIVITIES^a FOR MMH OXIDATION, 55 ± 3 °C

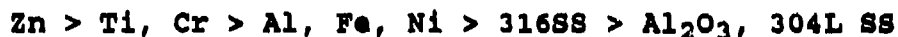
Surface	k_{obs} (sec ⁻¹)	K_{sc}^b (ml/m ²)	k'_1 (sec ⁻¹ m ⁻²)	k_1 (sec ⁻¹ ml)
316 SS	6.80E-02	4.0	2.8E-01	7.0E-02
304L SS	1.53E-02	9.6	2.7E-02	2.9E-03
Fe	2.93E+00	0.18	5.5	3.1E+01
Al	4.55E-02	5.2	7.1E-02	1.4E-02
Al ₂ O ₃	6.31E-01	1.5	1.9	1.3
Zn	1.14E-01	1.4	4.8E-01	3.4E-01
Cr	1.16E-01	1.0	2.0E-01	2.0E-01
Ni	1.88E-01	0.72	8.9E-02	1.2E-01
Ti	1.15E+00	0.06	7.4E-01	12.3

^a Normalized data from Table 1

^b K_{sc} for methyl amine

Scheme 2 provides a set of structural intermediates which depict the adsorption, initial oxidative dehydrogenation of MMH and water formation by reductive elimination from a surface hydroxy-hydride intermediate. Scheme 3 utilizes a similar sequence involving the oxidative dealkylation of methyldiazene. Product selectivity is provided by a partitioning of the alkoxy-hydride between a reductive elimination to methanol or a 1,2-elimination to methane.

Product selectivity, as measured by the methanol/(methanol + methane) ratio should then reflect surface oxide stability. The selectivity ratio for methanol formation increases:

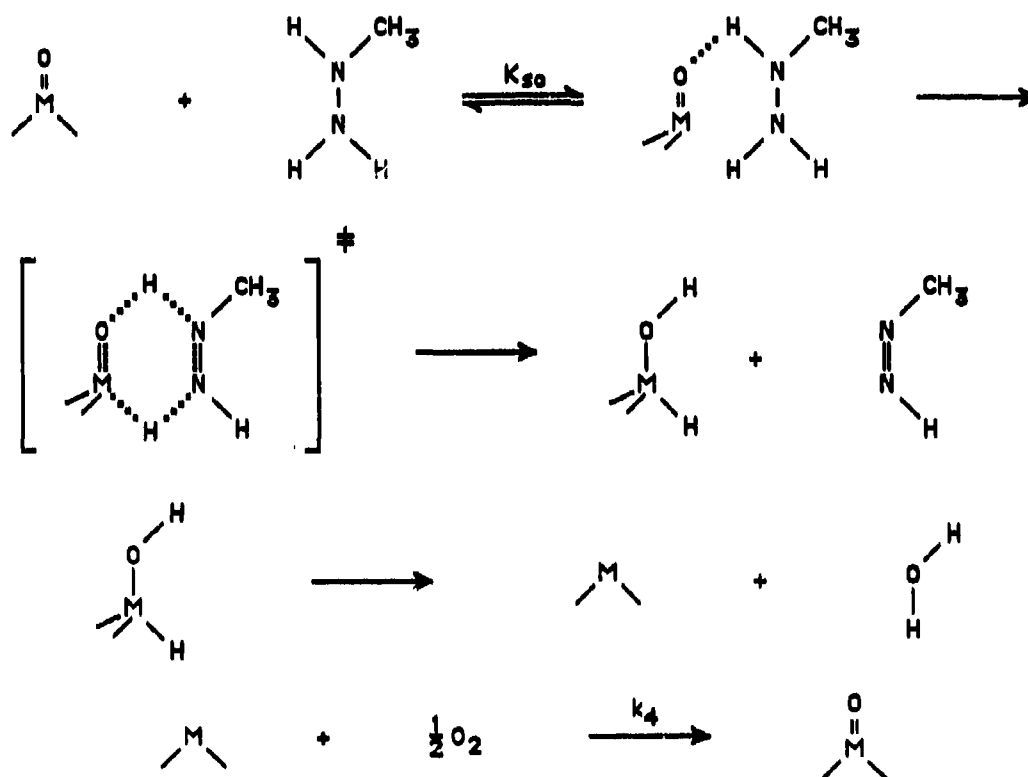


while the M=O stability decreases:

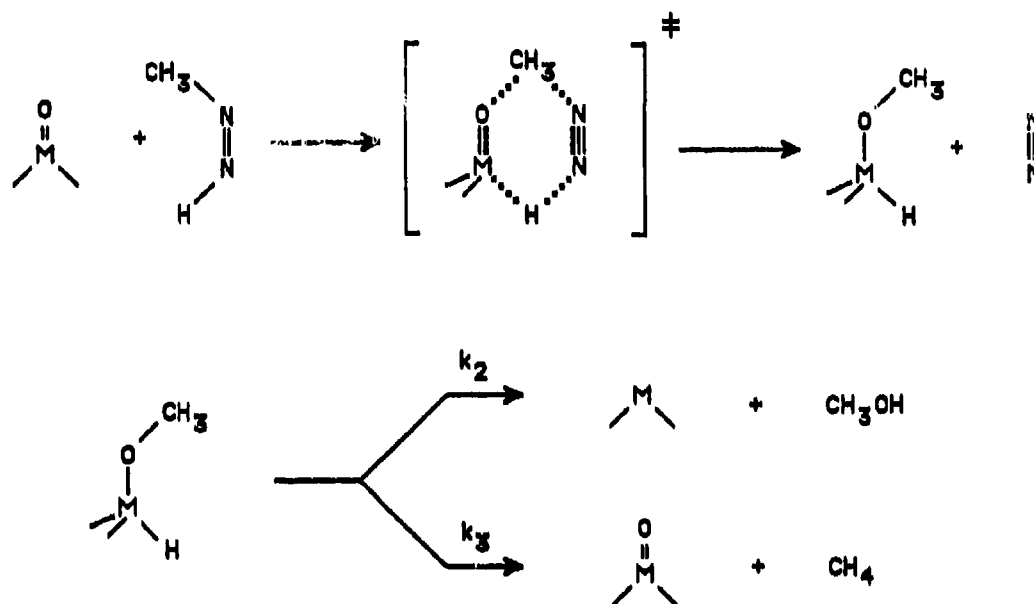


Although Schemes 2 and 3 are representational, they provide a certain economy of structure yet allow some reactivity and selectivity predictions.

SCHEME 2



SCHEME 3



CONCLUSIONS

Physicochemical, kinetic and product information necessary to develop insights into the environmental fates of hydrazines is easily obtained by a tubular reactor/gas chromatographic technique. These studies have proven to be useful in the elucidation of the mechanisms of the heterogeneous air oxidation reactions of hydrazines. Mechanistic studies such as these may allow the prediction of catalytic properties of metals and their oxides.

REFERENCES

1. Stone, D.A., M.V. Heenley, and D.V. Naik, "The Effects of Surfaces on the Air Oxidation of Hydrazine," Chemical Propulsion Agency Publication No. 436, November 1985, pp. 151-159.
2. Tuazon, E.C., W.F.L. Carter, R.A. Brown, A.M. Winer, and J.N. Pitts. Atmospheric Reaction Mechanisms of Amine Fuels. ESL-TR-82-17, March 1982.
3. Class, J.B., J.G. Aston, and T.S. Oakwood. J. Am. Chem. Soc. 1953, 75, 2937.
4. Rocca, F.F., L. de Mourges, and Y. Trambouze. J. Gas Chromatograph 1968, 6, 161. Gruber, H.L. Anal. Chem. 1962, 34, 1828.
5. Habgood, H.W. and J.F. Hanlon. Can. J. Chem. 1959, 37, 843.

A MATRIX-ISOLATION FT-IR STUDY OF HYDRAZINE

T. Tipton, Research Associate
University of Florida
Gainesville, Florida 32611

W. B. Person, K. Kubulat, M. Vala, D. A. Stone

ABSTRACT

FT-IR spectra ($4000\text{--}420\text{ cm}^{-1}$) have been obtained for hydrazine in argon and nitrogen matrices over a concentration range of 1:200 to 1:5000, and a temperature range of 14 K to 30 K. This investigation, in conjunction with a concurrent ab initio calculation, has eliminated much of the uncertainty in the previous matrix and vapor-phase vibrational assignments for hydrazine.

INTRODUCTION

The present study of hydrazine was undertaken as part of an investigation of the interaction of toxic chemicals with environmentally significant surfaces. The study of these substances in the relatively unperturbed environment of matrices should assist similar investigations that are being performed on clays (1). The ultimate goal is to understand the mechanisms by which hazardous chemicals, coordinated with metal ions, interact with soil surfaces. The current matrix isolation study expands upon the single previous matrix study (2) and revises some of the earlier vibrational assignments.

A summary of previous vibrational data for hydrazine has been given by Durig et al (3). Since there is still some uncertainty in the matrix and vapor-phase assignments (2-4), a new ab initio calculation was carried out concurrently with the present matrix isolation experiments. This calculation proved useful in assigning the matrix spectra.

EXPERIMENTAL

The hydrazine sample was obtained from Aldrich at 98% purity. It was then transferred under argon to a distillation apparatus, refluxed over reagent grade NaOH for 4 hours, and distilled. The fraction collected at 387 K comprised the purified sample. The nitrogen and argon samples were research grade (Air Products). Before use, they were passed through a 1.2-m coil of 1/8-in stainless steel tubing immersed in a 178 K acetone bath.

The deposit window was usually a 25- x 2-mm Irtran 2 disk although some runs were made using a 25- x 2-mm CsI disk so that the 700 cm^{-1} to 420 cm^{-1} region could be investigated. This window was cooled by means of a closed-cycle refrigerator (Air Products Displex model CSA-202). KBr windows were used on the evacuated shroud surrounding the cold head. All deposits were made at the minimum attainable temperature of 13 K.

The deposit rate was in the range of 4 to 8 $\mu\text{mol/hr}$ for both argon and nitrogen. The rate was controlled by a metering valve (Granville-Phillips series 203) which was periodically adjusted to maintain a steady flow while the pressure in the gas mixing bulb dropped. The deposit material was flowed continuously for about 2.5 hours. For the nitrogen runs, a second 2.5-hour deposit was made on the opposite side of the window. These large deposits were necessitated by the low intensities of the NH stretching bands. The amount of material that was used in a deposit was determined by the scattering properties of the matrix. Under the conditions described above, the scattering was negligible for the first 2.5 hr of the deposit but increased rapidly thereafter.

Spectra were taken with a Nicolet 6000C FT-IR spectrometer, upgraded to model 1608X capabilities (hardware and software). All runs reported here were made at 0.5 cm^{-1} resolution since higher resolutions did not reveal any additional structure in the observed bands. A liquid-nitrogen-cooled HgCdTe-B (5000-400 cm^{-1}) detector was used.

Both the argon and nitrogen spectra were run at five different hydrazine concentrations: 1:200, 1:500, 1:1000, 1:2000, and 1:5000. Concentrations less than 1:5000 were not used because of poor signal/noise and because of the tendency of hydrazine to be adsorbed on the walls of the deposit tube. The concentration dependence of the observed hydrazine bands, in combination with annealing studies, enabled monomer peaks to be distinguished from aggregate peaks.

RESULTS

Hydrazine has seven bending and five stretching modes in accordance with its C_2 point group symmetry (3). All of these except the torsion mode, ν_7 , are expected to lie in the 4000-420 cm^{-1} region investigated in the present FT-IR study.

Tables 1 and 2 show the frequencies and infrared intensities of the fundamental modes of N_2H_4 obtained from vapor-phase (4), ab initio, and matrix-isolation studies. The ab initio frequencies were obtained by

TABLE 1. FREQUENCIES (WAVENUMBERS) OF HYDRAZINE FUNDAMENTALS.

Vibrational Mode	Ab initio	Argon Matrix	Nitrogen Matrix	Vapor ^a
7 torsion	425	----	----	377
6 s-wag	837	810	834	780
12 a-wag	950	953	983	950
5 NN str.	1082	1086	1091	1098
11 HNH twist	1253	1262	1267	1275
4 HNH twist	1284	1299	1314	----
10 scissor	1617	----	1595	1608
3 scissor	1632	----	1595	1493
9 HNH s-str.	3294	3313	3301	3297
2 HNH s-str.	3302	----	----	----
1 HNH a-str.	3395	3390	3387	3325
8 HNH a-str.	3400	3398	3396	3350

^aReference 4.

TABLE 2. RELATIVE INTENSITIES (KM/MOL) OF HYDRAZINE FUNDAMENTALS.

Vibrational Mode	Ab initio	Argon ^a Matrix	Nitrogen ^a Matrix	Vapor ^{a, b}
7 torsion	50.66	---	---	---
6 s-wag	98.54	86	71	74
12 a-wag	190.46	206	203	142
5 NN str.	5.48	39	38	27
11 HNH twist	7.75	8	5	10
4 HNH twist	5.85	5	5	---
10 scissor	14.31	---	17	37
3 scissor	13.70	---	---	---
9 HNH s-str.	15.01	4	6	30
2 HNH s-str.	0.50	---	---	---
1 HNH a-str.	0.01	2	3	---
8 HNH a-str.	1.84	3	5	33

^a These data are scaled in accordance with the ab initio calculation.^b Reference 4. These data are based on band maxima.

scaling the results of a 6-31G** basis set calculation (scale factor = 0.886). Vibrational assignments for the matrix-isolation spectra were obtained from comparisons of data in these tables.

The purpose of running both argon and nitrogen matrices was to determine whether hydrazine has any tendency to rotate in a matrix environment. Nitrogen has been found to be less conducive to rotation of trapped species than argon (5). Water, for example, has rotational structure in argon but not in nitrogen (6). No evidence of rotational structure was found in the present hydrazine spectra. For the most part, the $\text{N}_2\text{H}_4/\text{Ar}$ vibrational bands had approximately the same number of components and the same relative intensities as the corresponding $\text{N}_2\text{H}_4/\text{N}_2$ bands.

A. BENDING AND NN-STRETCHING MODES

All of the observed modes, except those consisting of NH stretching, lie in the $1900\text{--}700\text{ cm}^{-1}$ region shown in Figure 1. Most of the monomer bands in this figure can be assigned readily by comparing the matrix data with vapor-phase (4) and ab initio data (Tables 1 and 2). The vapor-phase spectrum shown in Figure 1 was reexamined in order to check the assertion of Catalano et al (2) that the previously observed bands (4) in the 6.3 micron region are artifacts. The present vapor spectrum is essentially the same as that given in Reference 4 and does not show any features resulting from hydrazine reacting with the KBr cell windows. Thus the band assigned to ν_{10} (1608 cm^{-1}) in the vapor-phase spectrum appears to be legitimate. The assignment of ν_3 (1493 cm^{-1}), however, is much more doubtful in light of the new matrix and ab initio data (Tables 1 and 2).

The present assignments of ν_3 and ν_{10} to a single band at 1595 cm^{-1} in $\text{N}_2\text{H}_4/\text{N}_2$ are based primarily on the theoretical prediction (Tables 1 and 2) that these bands should be closely spaced and nearly equal in intensity. Additional support for these assignments was obtained from a preliminary run on $\text{N}_2\text{D}_4/\text{N}_2$ which appeared to show two scissor-bending frequencies of roughly equal intensities separated by only 2 cm^{-1} . The 1595 cm^{-1} band of $\text{N}_2\text{H}_4/\text{N}_2$ was not reported in the previous matrix study (2). Evidently, it was obscured by the strong $\text{H}_2\text{O}/\text{N}_2$ impurity band at 1597 cm^{-1} , and was subtracted out of the spectrum along with the water band. The surprising absence of both ν_3 and ν_{10} from the present and previous (2) argon matrix spectra remains unexplained.

B. NH-STRETCHING MODES

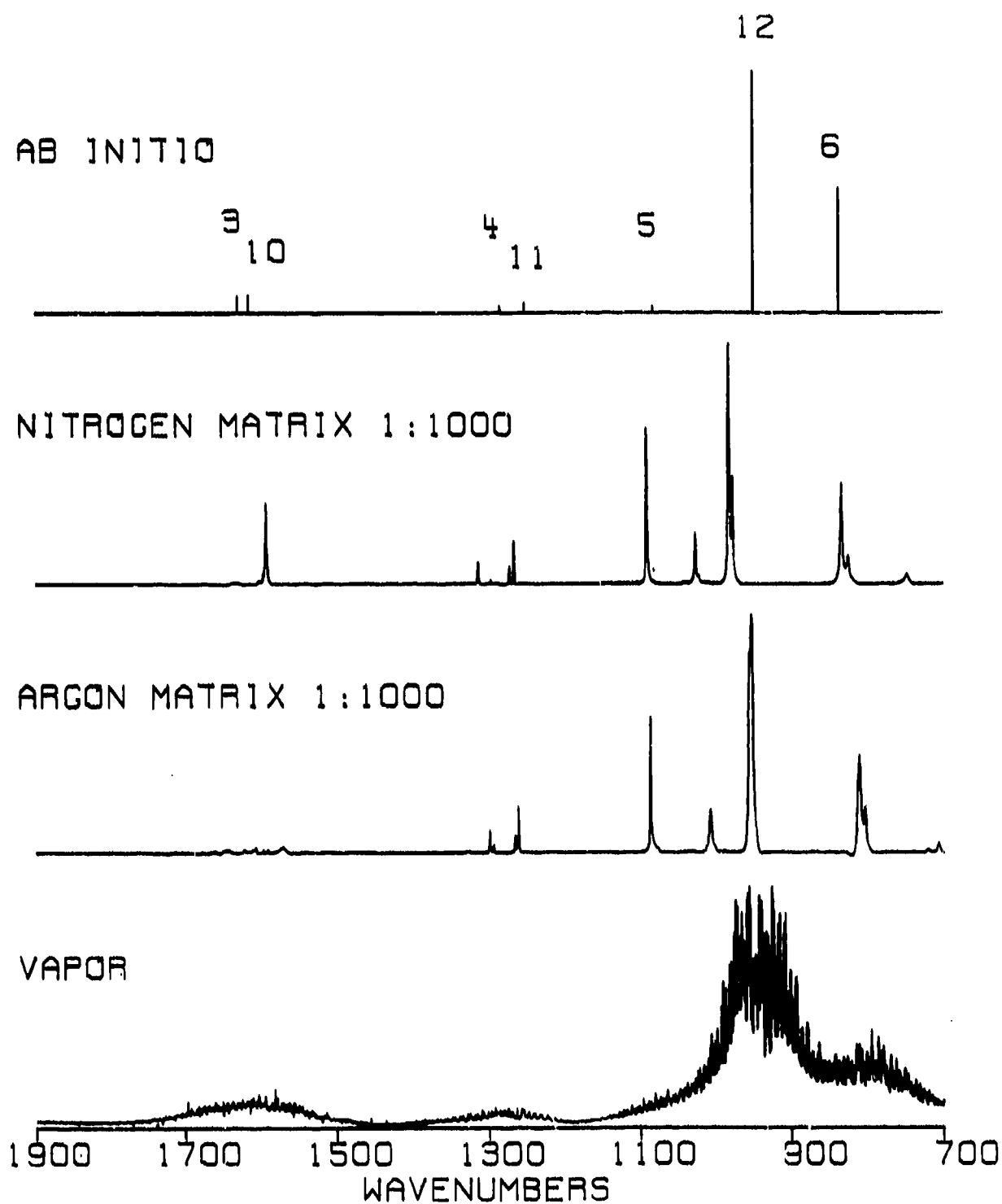


Figure 1. Bending and NN-Stretching Absorptions of Hydrazine.

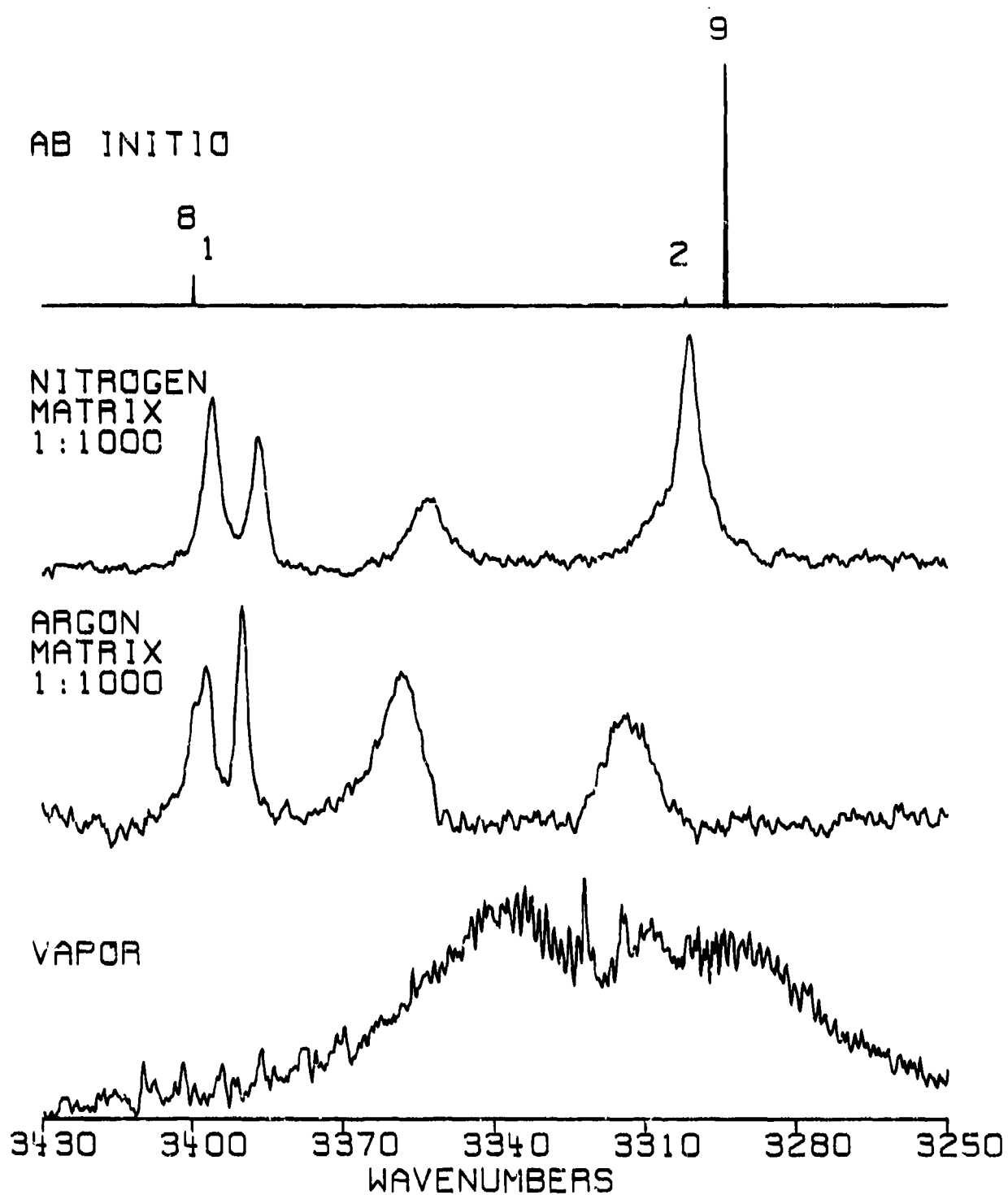


Figure 2. NH-Stretching Absorptions of Hydrazine.

Spectra of the NH-stretching region are shown in Figure 2, and the corresponding mode assignments are given in Table 1. Although there are four NH-stretching modes in hydrazine, only three monomer matrix bands were observed. A fourth band, which occurs near 3350 cm^{-1} in both argon and nitrogen matrices, is due to hydrazine dimer.

The assignments of the monomer bands in Figure 2 were deduced primarily by comparison of matrix-isolation and ab initio frequency data (Table 1). The close resemblance of these two sets of data are sufficient to establish the assignment of ν_9 for both matrix spectra in Figure 2. The broad shoulder that accompanies the ν_9 band of $\text{N}_2\text{H}_4/\text{Ar}$ is due to an aggregate.

The assignment of ν_9 to one of the two matrix bands near 3400 cm^{-1} is also straightforward but it is not clear whether the other band is ν_1 , or a different site of ν_9 . Preference has been given to the ν_1 assignment on the basis of the ab initio frequency and the reported appearance of ν_1 in the vapor phase (4). However, the intensity of this band is much greater in relation to ν_9 than expected. A comparison of the present NH-stretching data to the previously reported data (2) for matrix-isolated hydrazine indicates that the latter were obtained at an excessively high hydrazine concentration. The $\text{N}_2\text{H}_4/\text{N}_2$ bands which are found at 3396 cm^{-1} and 3387 cm^{-1} in Figure 2 were previously blended. Also, the dimer band at 3353 cm^{-1} was previously reported to be ν_9 .

REFERENCES

1. C. T. Johnston, to be published.
2. E. Catalano, R. H. Sanborn, and J. W. Frazer, "On the Infrared Spectrum of Hydrazine Matrix-Isolation Studies of the System $\text{N}_2\text{H}_4:\text{N}_2$," Journal of Chemical Physics, vol. 38, pp. 2265-2272, 1963.
3. J. R. Durig, S. F. Bush, and E. E. Mercer, "Vibrational Spectrum of Hydrazine- d_4 and a Raman Study of Hydrogen Bonding in Hydrazine," Journal of Chemical Physics, vol. 44, pp. 4238-4247, 1966.
4. P. A. Giguere and I. D. Liu, "On the Infrared Spectrum of Hydrazine," Journal of Chemical Physics, vol. 20, pp. 136-140, 1952.
5. H. E. Hallam, Vibrational Spectroscopy of Trapped Species, Chap. 1, p. 6, Wiley, London, 1973.
6. R. M. Bentwood, A. J. Barnes, and W. J. Orville-Thomas, "Studies of Intermolecular Interactions by Matrix Isolation Vibrational Spectroscopy," Journal of Molecular Spectroscopy, vol. 84, pp. 391-404, 1980.

LOW TEMPERATURE SPECTROSCOPY OF HYDRAZINE AND AMMONIA COMPLEXES

WITH THE NEUTRAL TRANSITION METALS, Cu AND Fe

M. Vala, Professor of Chemistry

Department of Chemistry
University of Florida
Gainesville, Florida 32611

M. Szczesniak, J. Szczepanski and W. B. Person

ABSTRACT

Complexes of hydrazine and ammonia with the neutral transition metals, Cu and Fe, have been formed and investigated spectroscopically in solid argon matrices at 12 K. Fourier transform infrared spectra of the complexes have revealed large shifts for the metal . ammonia complexes and substantially smaller shifts for the metal . hydrazine complexes. Recent ab initio calculations have ascribed the bonding in $\text{Cu} \cdot \text{NH}_3$ to an electrostatic interaction between the NH_3 dipole moment and the induced effective dipole of the metal atom. All the present observations may be understood on the basis of this bonding picture.

INTRODUCTION

It is well known that hydrazine complexes strongly with the ions of the transition metals (Reference 1). The interaction of neutral transition metal atoms with hydrazine is however virtually unknown. In this report we present the results of our investigation on the Fourier transform infrared spectra (FTIR) of complexes of hydrazine with neutral copper and iron atoms isolated in argon matrices at 12 K. For the sake of comparison parallel studies on the complexes of ammonia with copper and iron atoms are also presented.

In brief, the major findings of this study are: 1) the $\text{Cu} \cdot \text{NH}_3$ complexes exhibit large frequency shifts in the ν_2 NH bending region; the $\text{Fe} \cdot \text{NH}_3$ shift is larger than the $\text{Cu} \cdot \text{NH}_3$ shift; 2) the $\text{Cu} \cdot \text{N}_2\text{H}_4$ and $\text{Fe} \cdot \text{N}_2\text{H}_4$ complexes show practically identical shifts; these shifts are considerably smaller than the corresponding ones in the ammonia . metal complexes. The present observations are consistent with the recent constrained-space-orbital-variation (CSOV) computations of Bauschlicher (Reference 2) on the $\text{Cu} \cdot \text{NH}_3$ complex (amongst others). The bonding in this complex is ascribed to a favorable electrostatic interaction between the NH_3 dipole moment and an effective metal atom dipole moment.

EXPERIMENTAL

The matrix deposition apparatus has been described previously (Reference 3). Copper and iron metals (Spex Industries) were vaporized from a tantalum Knudsen cell resistively heated in the range 1200–1450°C for Cu and in the range 1500–1700°C for iron. The cell temperature was monitored by an optical pyrometer (Leads and Northrup). The hydrazine/argon and ammonia/argon gas mixtures were prepared in a vacuum line and stored in 7.0l pyrex bulbs. A variety of different ratios of complexing gas to argon were tried: the best results were obtained with a ratio of 200:1 of Ar:NH₃ or Ar:N₂H₄. The ammonia (Matheson, 99.99%) and argon (Matheson, 99.999%) were used as received, whereas the hydrazine (Aldrich) was subjected to vacuum distillation before mixing. However, even after distillation, the liquid hydrazine was found to contain trace amounts of water. This amount was reduced significantly by the following procedure. Since the vapor pressure of hydrazine is much lower than the vapor pressure of water at room temperature, the vapor in the 7.0l bulb above several milliliters of distilled hydrazine liquid was simply evacuated. After allowing sufficient time for equilibration with the liquid, the pump-out procedure was repeated several times, each time reducing the amount of water remaining in the liquid. NH₃ and Ar were run through several freeze (to 77K)-pump-thaw degassing cycles before preparation of the gas mixtures. Deposition rates of 1 mmol/h were used for 4 to 10 h periods. Just prior to deposition the gases (NH₃, Ar) were passed through a coil of stainless steel tubing cooled in a dry-ice/acetone slush bath.

Infrared absorption spectra were obtained on a Nicolet 7199 FTIR spectrometer using 2 cm⁻¹ resolution (cooled HgCdTe detector). The absolute band positions are expected to have an accuracy of better than 1 cm⁻¹.

RESULTS

METAL • AMMONIA COMPLEXES

Ammonia isolated in rare gas matrices is known to undergo nearly free rotation about its three-fold axis. The generally accepted (Reference 4) assignments for the rotational and inversional structure on the vibrational bands of matrix-isolated NH₃ are given in Fig. 1. In addition, NH₃ dimer and H₂O • NH₃ complex bands are also indicated. Upon deposition of NH₃ with Cu several new bands can be seen to grow in to higher energies (cf. Fig. 1). The

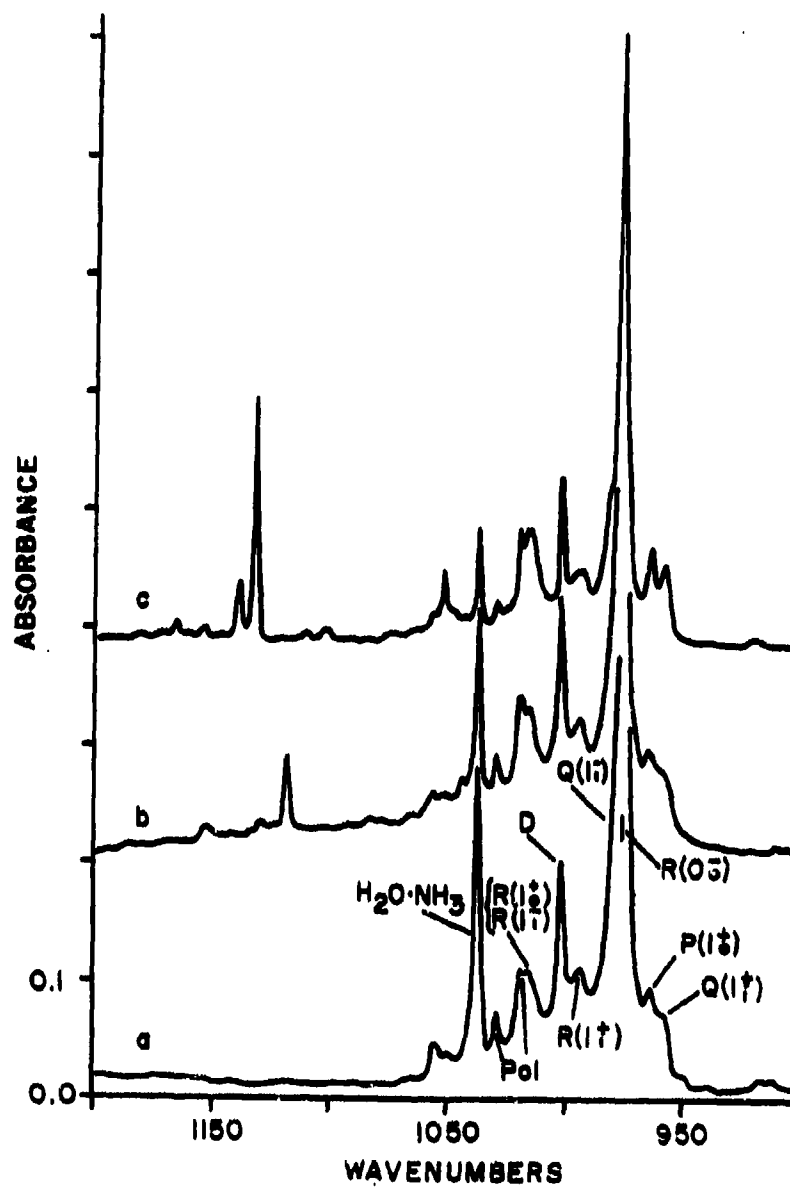


Figure 1. Infrared Spectra of Argon Matrix-Isolated (a) NH₃, (b) Codeposition Mixture of NH₃ and Cu, and (c) Codeposition Mixture of NH₃ and Fe.

most prominent of these (1117 cm^{-1}) is assigned to the perturbed ν_2 bending mode in the 1:1 $\text{Cu} \cdot \text{NH}_3$ complex. This assignment follows from similar observations and conclusions by S  zer and Andrews (SA) (Reference 5) on matrix-isolated NH_3 complexed with the alkali metals. The present results are compared with those of SA in Table 1. Shifts of bands in the NH stretching region upon complex formation have also been observed, but will not be discussed here.

The $\text{Fe} \cdot \text{NH}_3$ complex exhibits similar behavior to $\text{Cu} \cdot \text{NH}_3$ but the magnitudes of the shifts of its ν_2 and ν_3 bands are greater (cf. Table 1). Interestingly, these shifts (for both the Cu and Fe complexes) are in opposite directions. Upon complexation the ν_1 and ν_3 bands shift to lower energies, while the ν_2 bands shift to higher energies. Similar behavior has been observed previously in complexes involving hydrogen bonding (Reference 6).

METAL \cdot HYDRAZINE COMPLEXES

In Table 2 and Fig. 2 we present the results of our metal atom \cdot hydrazine complex formation experiments. In Fig. 2b is shown the spectrum of N_2H_4 in an Ar matrix in the $800\text{--}1300\text{ cm}^{-1}$ region. The assignment of the various N_2H_4 bands (cf. Table 2) are due to Tipton, Stone, Person and Kubulat (Reference 7). Also in Fig. 2 are shown the spectra obtained upon codeposition of N_2H_4 with Fe atoms (Fig. 2d) and upon codeposition of N_2H_4 with Cu atoms (Fig. 2c). Several new bands can be discerned at 838 cm^{-1} and 1038 cm^{-1} (Fig. 2d (Fe)) and at 843 cm^{-1} and 1035 cm^{-1} (Fig. 2c (Cu)). These bands are assigned as perturbed NNH bending vibrations. To accentuate the difference between the $\text{Cu} \cdot \text{N}_2\text{H}_4$ complex and the free N_2H_4 spectra, we have spectrally subtracted Fig. 2b from 2c. The result is shown in Fig. 2a. The new $\text{Cu} \cdot \text{N}_2\text{H}_4$ complex bands (marked with *) stand out clearly. The N_2H_4 dimer band at 1007 cm^{-1} is more intense in Fig. 2c compared to Fig. 2b, and thus appears as a positive peak in Fig. 2a. Its growth is presumably due to the increased diffusion of hydrazine in the matrix under the deposition conditions used for vaporizing the metals (i.e. radiative heating of the matrix from the hot Knudsen cells).

It is noteworthy that the differences between the band positions of the $\text{Cu} \cdot \text{N}_2\text{H}_4$ and $\text{Fe} \cdot \text{N}_2\text{H}_4$ complexes are relatively small. This is particularly evident when the analogous shifts in the metal \cdot ammonia complexes are compared (cf. Table 1). In these complexes the shifts are much larger and the differences between the Cu and Fe complexes greater. These observations are

TABLE 1. COMPARISON OF INFRARED ABSORPTION PEAK POSITIONS AND SHIFTS OF AMMONIA AND HYDRAZINE AND THEIR METAL COMPLEXES.

Species	NH Stretch ^a		NH Bend ^a		NH Stretch ^a	
	ν_1	$\Delta\nu_1$	ν_2	$\Delta\nu_2$	ν_3	$\Delta\nu_3$
NH ₃	3346	--	974	--	3447	--
Cu · NH ₃	3212	-134	1117	143	3392?	-55
Fe · NH ₃	--	--	1130	156	3381	-66
Li · NH ₃ ^b	3277	-69	1133	159	3379	-68
Na · NH ₃ ^b	3294	-52	1079	105	--	--
K · NH ₃ ^b	3292	-54	1064	90	--	--
Cs · NH ₃ ^b	3287	-59	1049	75	--	--
<hr/>						
N ₂ H ₄			804, 811	--		
			954	--		
Cu · N ₂ H ₄			843	39		
			1035	81		
Fe · N ₂ H ₄			838	34		
			1038	84		

^a All entries are in cm⁻¹.

^b Reference 5.

TABLE 2. INFRARED ABSORPTION BANDS AND ASSIGNMENTS OF ARGON MATRIX-ISOLATED HYDRAZINE AND ITS COMPLEXES WITH COPPER AND IRON ATOMS IN THE 800-1300 cm^{-1} REGION.

N_2H_4 (cm^{-1})	$\text{Cu} \cdot \text{N}_2\text{H}_4$ (cm^{-1})	$\text{Fe} \cdot \text{N}_2\text{H}_4$ (cm^{-1})	Assignments, Remarks	Ref.
804	804	804	$\nu_6: \delta\text{NH}_2, \delta\text{NNH}$	7
811	811	811		
	834			
		838	$\nu(\text{N}_2\text{H}_4 \cdot \text{Fe})$	
	843		$\nu(\text{N}_2\text{H}_4 \cdot \text{Cu})$	
954	954	954	$\nu_{12}: \delta\text{NNH}, \delta\text{NH}_2$	7
974	974	974	ammonia	4
988	988	988	$\nu_{\text{N}_2\text{H}_4}(\text{N}_2\text{H}_4 \cdot \text{H}_2\text{O})$	9
994	994	994		
1007	1007	1007	$\nu_{\text{N}_2\text{H}_4}(\text{dimer})$	9
1029	1029	1029	aggregate	
	1035		$\nu(\text{N}_2\text{H}_4 \cdot \text{Cu})$	
		1038	$\nu(\text{N}_2\text{H}_4 \cdot \text{Fe})$	
1086	1086	1086	$\nu_5: \nu\text{NN}$	7
1261	1261	1261	$\nu_{11}: \delta\text{NNH}$	7
1266	1266	1266		
1293	1293	1293	$\nu_4: \delta\text{NNH}$	7
1299	1299	1299		

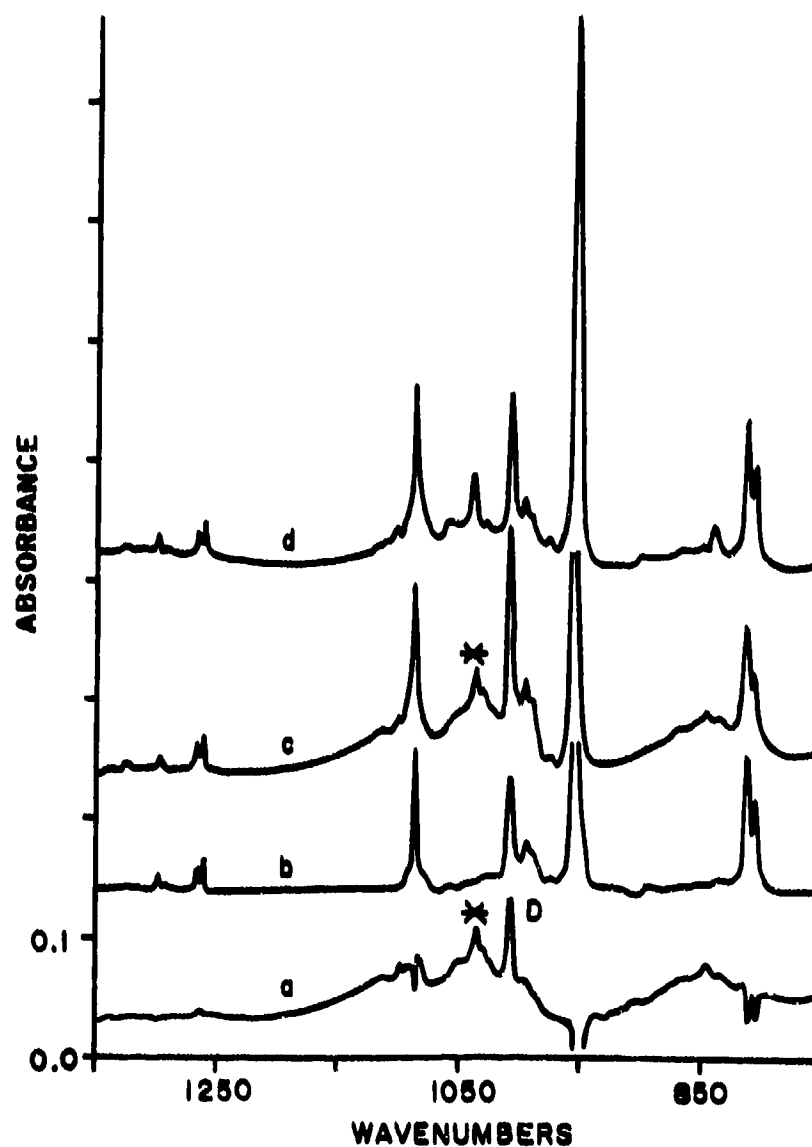


Figure 2. Infrared Spectra of Argon Matrix-Isolated (b) N_2H_4 , (c) Codeposition Mixture of N_2H_4 and Cu, (d) N_2H_4 and Fe, and (a) subtraction of (b) from (c).

crucial to the conclusions drawn in the next section about the bonding mechanisms in the ammonia vs. the hydrazine complexes.

DISCUSSION

Previous matrix isolation studies (References 8, 9) of NH_3 complexed with strong acids such as HF and weak ones like H_2O have demonstrated substantial shifts of the ν_2 bending vibration (61 cm^{-1} for $\text{NH}_3 \cdot \text{H}_2\text{O}$ and 120 cm^{-1} for $\text{NH}_3 \cdot \text{HF}$). Comparing these values and the $\text{NH}_3 \cdot$ alkali metal complex results with the present results (cf. Table 1) it is clear that $\text{Cu} \cdot \text{NH}_3$ and $\text{Fe} \cdot \text{NH}_3$ are strong complexes. The complexes with hydrazine are considerably weaker.

As we shall see, these results are consistent with the recent calculations of Bauschlicher (Reference 2) on $\text{Cu} \cdot \text{NH}_3$ and other complexes (including $\text{Ni} \cdot \text{NH}_3$). Since the Cu ground state electronic configuration is $3d^{10}4s^1$ and the NH_3 ligand contains a lone pair of electrons on N, one expects in simple terms that interaction between these moieties should lead to repulsion and hence no complex formation. Bauschlicher shows however that the interaction is much more complicated. The anticipated repulsion is reduced because the metal polarizes the 4s orbital (promotes electron density into the 4p orbital) such that it now has an effective dipole moment. There is then a favorable electrostatic interaction between the metal dipole and the NH_3 dipole moment; this interaction is in fact larger than expected since the charge clouds of the two overlap. Because of the interpenetration of the NH_3 dipoles' negative end (the dipole moment of the free NH_3 is $0.81\text{ [N}^-\text{H}^+]$) into the metals' charge cloud, the attraction of the metal nucleus for the negative end of the dipole is enhanced. There is also a small σ donation from the NH_3 to the metal. These effects are of the same magnitude for all metal $\cdot \text{NH}_3$ systems.

For systems containing 3d holes, an additional factor arises. Fe has a ground state configuration of $3d^64s^2$ with an excited state (0.88 eV above) of $3d^74s^1$ configuration. Bauschlicher remarks that the latter state may be stabilized by strong interactions with one or more neighbors. For such a system, the 4s and $3d_{\sigma}$ orbitals can mix. Because of the fewer number of electrons along the internuclear axis in these hybrid orbitals the shielding of the metal nucleus from the NH_3 lone pair is reduced and the bonding in the $\text{Fe} \cdot \text{NH}_3$ complex is expected to be stronger. Thus a larger shift in the ν_2 NH bending frequency is expected compared to $\text{Cu} \cdot \text{NH}_3$. This is what is observed (cf. Table 1).

The shifts observed for the hydrazine • metal complexes can also be understood in the above terms. We assume that the N_2H_4 ligand complexes to Cu or Fe in a monodentate fashion via the lone pair on one end of N_2H_4 . By analogy to the bonding with NH_3 it is expected that the dipole moment for the ligand $H_2N(NH_2)$ (so written to emphasize its similarity to NH_3) will be considerably less. This will result in a diminished polarization of the metal 4s orbital and a less favorable electrostatic interaction between the metal effective dipole and the N_2H_4 dipole. Thus a smaller shift is expected for the N_2H_4 • metal complexes. This is as observed. Indeed, the fact that both Cu • N_2H_4 and Fe • N_2H_4 complexes exhibit practically the same shift is evidence that the interpenetration and shielding effects which play a role in the stronger ammonia complexes are virtually absent in the present ones.

REFERENCES

1. Schmidt, Eckart W. Hydrazine and Its Derivatives, p. 371ff, Wiley-Interscience, New York, 1984.
2. Bauschlicher, Jr., C. W., "Transition Metal-ligand Bonding. II", Journal of Chemical Physics, 1986, vol. 84, pp. 260-267.
3. Brittain, R., D. Powell, E. Voigtman, and M. Vala, "The Measurement of Magnetic Circular Dichroism of Matrix-Isolated High Temperature Molecules", Reviews of Scientific Instruments, 1980, vol. 51, pp. 905-910.
4. Abouaf-Marguin, L., M. E. Jacox and D. E. Milligan, "The Rotation and Inversion of Normal and Deuterated Ammonia in Inert Matrices", Journal of Molecular Spectroscopy, 1977, vol. 67, pp. 34-61 and references therein.
5. Suser, S. and L. Andrews, "Infrared Spectra of Alkali Metal Atom-Ammonia Complexes", Journal of the American Chemical Society, 1987, vol. 109, pp. 300-304.
6. Pimentel, G. C., A. L. McClellan, The Hydrogen Bond, W. H. Freeman, San Francisco, 1960.
7. Tipton, T., D. Stone, W. Person and K. Kubulat, work described elsewhere in this volume.
8. Johnson, G. L. and L. Andrews, "Matrix Infrared Spectrum of the H_3N-HF Hydrogen-Bonded Complex", Journal of the American Chemical Society, 1982, vol. 104, pp. 3043-3047.
9. Nelander, B. and L. Nord, "Complex Between Water and Ammonia", Journal of Physical Chemistry, 1982, vol. 86, pp. 4375-4379.

**A DIFFUSE REFLECTANCE INFRARED
FOURIER TRANSFORM SPECTROSCOPIC
STUDY OF ADSORBED HYDRAZINES**

**Dennis D. Davis, Senior Scientist
Lockheed-EMSCO**

**White Sands Test Facility
Las Cruces, NM 88004**

**Jan E. Kilduff, Scientist
Lockheed-EMSCO**

**White Sands Test Facility
Las Cruces, NM 88004**

**Steven L. Koontz, Project Scientist
NASA**

**White Sands Test Facility
Las Cruces, NM 88004**

ABSTRACT

Diffuse reflectance spectroscopy of fuel hydrazines adsorbed on silica, silica-alumina and alumina surfaces indicates that the primary surface-hydrazine interaction is hydrogen bonding. Hydrazine, on adsorption to a deuterated silica surface, undergoes a rapid H/D exchange with deuterated surface silanol (Si-OD) groups. Adsorption equilibria are rapidly established at room temperature. Monomethylhydrazine and unsymmetrical dimethylhydrazine are similarly adsorbed. On adsorption, the C-H stretching and methyl deformation modes of the methylhydrazines are shifted to higher frequencies by 10 - 20 cm^{-1} . These shifts are postulated to be due to changes in the lone-pair electron-density on the adjacent nitrogen atom and an electronegativity effect.

INTRODUCTION

Critical to the study of the environmental fate of fuel hydrazines is the determination of mechanisms for their air-oxidation reactions. Environmental chamber (References 1 - 3) and flow reactor (References 4, 5) studies have clearly indicated

that air-oxidation of hydrazines is primarily a surface-catalyzed reaction in which the first step is surface adsorption. Diffuse reflectance infrared Fourier transform (DRIFT) spectroscopy is a powerful technique for the study of surfaces and adsorbed species. We have applied DRIFT spectroscopic methods to common environmental surfaces such as silica and alumina with adsorbed hydrazines in order to determine the mode of surface interaction and the effects that adsorption has on the structure of the adsorbate.

EXPERIMENTAL

APPARATUS

Diffuse reflectance studies were performed in a Harrick high-vacuum chamber diffuse reflectance apparatus (HVC-DRA) mounted in a Mattson Sirius 100 FTIR spectrometer. The HVC-DRA was fitted with KBr windows, thermocouple sensor, and heaters, and was capable of operating up to 300 °C and under vacuum. Normally, 32 or 64 interferograms were co-added and transformed using triangular apodization. The spectral resolution was 4 cm^{-1} .

Hydrazine and monomethylhydrazine (MMH) were Olin propellant grade materials. Unsymmetrical dimethylhydrazine (UDMH) was used as supplied by Aldrich Chem. Co.. Cab-O-Sil (Cabot), alumina (Woelm W-200), silica-alumina (Grace) and iron (III) oxide (Baker) were commercially available grades. Other materials were reagent grade.

PROCEDURE

The sample cup of the HVC-DRA was filled with finely powdered substrate, the chamber sealed, evacuated and heated to 150 °C for two hours. After cooling to ambient a single beam background spectrum was determined. Using the attached vacuum manifold the adsorbent was exposed to 2 - 50 torr of adsorbate vapor for 10 minutes. The chamber was evacuated to remove excess adsorbate and the sample single beam spectrum determined. In the

deuteration studies the above procedure was repeated three to five times before the background spectrum was determined.

RESULTS

Cab-O-Sil is a finely divided fumed silica whose surface is characterized by the presence of free Si-OH groups (3748 cm^{-1} , sharp), adjacent groups SiO-H...O-HSi (3672 cm^{-1} , broad), and hydrogen-bonded water ($3540 - 3400\text{ cm}^{-1}$, broad). On evacuation and heating the low frequency bands decrease and the free-OH band increases in relative intensity. Repeated exposure to D_2O vapor causes the Cab-O-Sil surface to be predominantly hydrogen-deuterium exchanged. The reflectance spectrum of a vacuum-baked and deuterated Cab-O-Sil sample is shown in Figure 1. The loss of free surface -OH groups is indicated by the sharp negative feature at 3748 cm^{-1} . The corresponding gain of free surface-OD groups is shown by the positive absorbance at 2754 cm^{-1} . The shoulders on the low frequency sides are caused

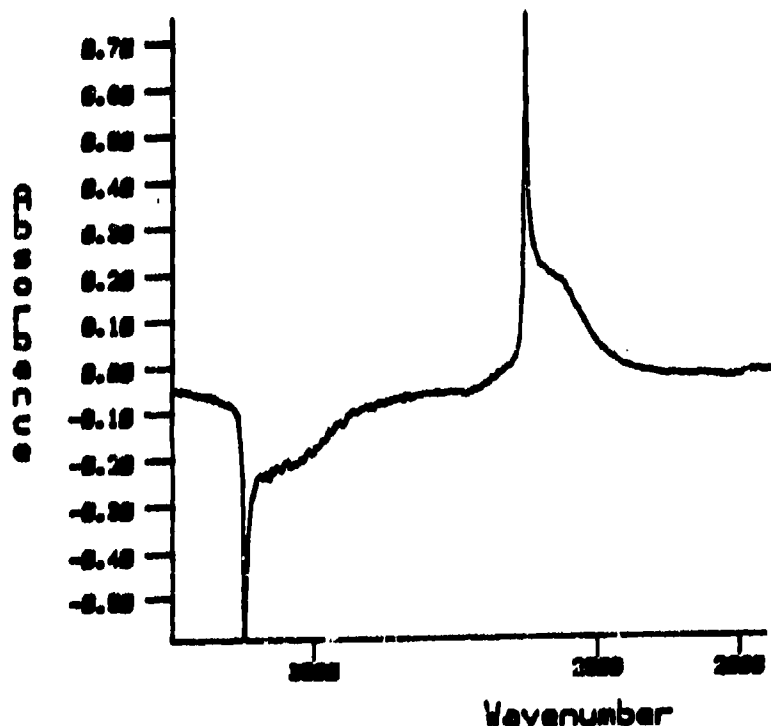


Figure 1. Reflectance Spectrum of Deuterated Cab-O-Sil
(Undeuterated Reference Spectrum)

by adjacent hydrogen bonded Si-OH (or Si-OD) groups. Adjacent H-bonding Si-OD groups appear at $2690 - 2635 \text{ cm}^{-1}$. The -OH region shows a negative absorbance since the same sample, before deuteration, was used to produce the background interferogram. The OH/OD stretching frequency ratio is 1.36, close to the expected 1.41.

After exposure of deuterated Cab-O-Sil to about 2 torr of hydrazine vapor, the spectrum shown in Figure 2 is produced. Both the free and adjacent -OD regions show negative absorbance relative to the deuterated background and the -OH region shows positive absorbance. The free -OH and -OD bands are shifted to 3740 and 2723 cm^{-1} respectively. The broad envelope between 3360 cm^{-1} and 3000 cm^{-1} is assigned to the NH-stretching modes of hydrazine. Liquid hydrazine displays vibrations at 3338 cm^{-1} and 3200 cm^{-1} , and at least four major bands at 3360 , 3294 , 3192 and 2991 cm^{-1} are present in the spectrum of adsorbed hydrazine. Further evidence of -OD/-NH exchange associated with adsorption

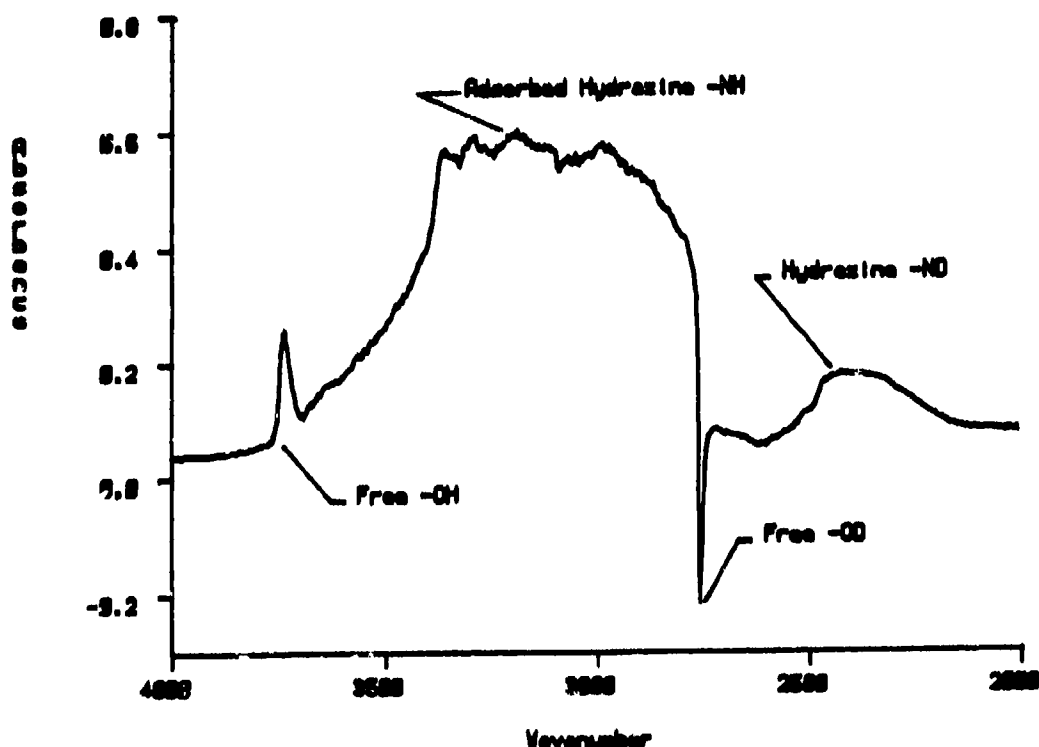


Figure 2. Reflectance Spectrum of Hydrazine Adsorbed onto Deuterated Cab-O-Sil

is the appearance of new bands in the $2450 - 2300 \text{ cm}^{-1}$ region which correspond to -ND stretches. N_2D_4 (liquid) has fundamental stretches at 2415 and 2352 cm^{-1} (Reference 6) and these bands indicate that at least some exchanged hydrazine remains bound to the surface.

Not shown in Figure 2 are two low frequency absorptions at 1613 and 1474 cm^{-1} . Hydrazine vapor has corresponding lines at 1628 cm^{-1} and 1493 cm^{-1} . These bands are tentatively assigned to -NH_2 deformation vibrations of surface hydrogen-bonded hydrazine. The deformation frequency shifts of 15 to 19 cm^{-1} are in the same direction, and of comparable magnitude, to that shown by ammonia when adsorbed to silica surfaces (Reference 7).

The suggestion that H-bonding is the major interaction shown by hydrazines was tested by exposing deuterated Cab-O-Sil to pyridine and observing the in-plane deformations of pyridine in the $1600 - 1400 \text{ cm}^{-1}$ region. Ring modes were observed for adsorbed pyridine at 1445 , 1579 , and 1595 cm^{-1} and are indicative of an hydrogen-bonded pyridine (1445 cm^{-1}) as contrasted to a Lewis-coordinated ($1447 - 1460 \text{ cm}^{-1}$) or Bronsted-protonated (1540 cm^{-1}) species (Reference 8).

Monomethylhydrazine also exchanges and hydrogen bonds to the deuterated Cab-O-Sil surface. Free Si-OH and adjacent Si-OH functions were observed to increase at 3750 , 3710 , 3626 , and 3531 cm^{-1} . The number of -OH stretches may be due to Si-OH groups in different sites, i.e., with -OH or -NH nearest neighbors. Of particular interest are the carbon-hydrogen stretching and methyl group deformation frequencies of MMH. Deuterated Cab-O-Sil as an adsorbent leaves a clear IR window in the -CH stretching region. The -CH regions of adsorbed (Figure 3) and liquid phase MMH (Figure 4) show an overall similarity, but significant shifts can be easily seen. The origin of a sharp, strong band at 2760 cm^{-1} is not definitely assigned but may be due to the -NH_3^+ group (Reference 9). The fundamental bands are shifted to 2990 , 2967 , and 2804 cm^{-1} for adsorbed MMH and occur at higher energy than in the gas-phase, opposite to the small shifts to lower frequencies

which are typically observed in polar molecules when passing from the gas to the liquid phase.

The abnormally low frequency fundamental at 2780 cm^{-1} observed in liquid MMH has been attributed to interaction of a C-H bond with the pair of nonbonding electrons on the adjacent nitrogen (Reference 10). Hydrogen bonding or other Lewis acid interactions with this lone pair should alter or remove this electronic effect and result in a shift to a higher frequency. The methyl-deformation bands in the $1350 - 1450\text{ cm}^{-1}$ region in a wide variety of compounds are known to shift to higher frequencies with increasing electronegativity of the

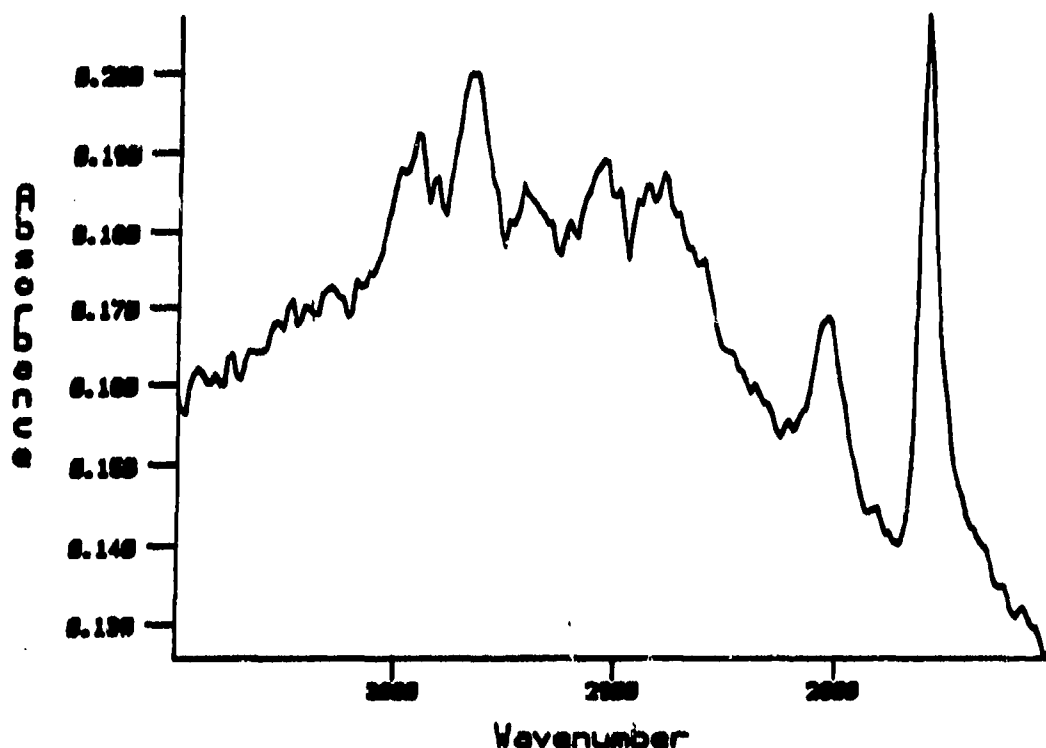


Figure 3. Reflectance Spectrum of Monomethylhydrazine Adsorbed onto Deuterated Cab-O-Sil

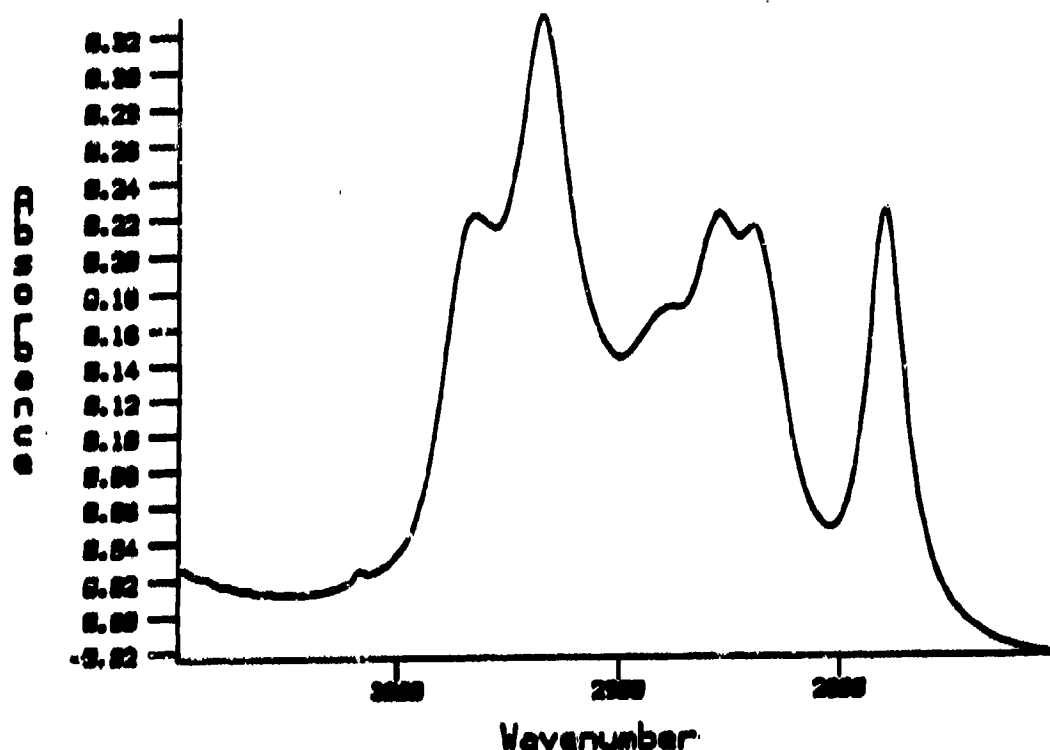


Figure 4. Transmittance Spectrum of Monomethylhydrazine (liquid film)

attached atom (Reference 11). The combination band at 2907 cm^{-1} is the sum of two shifted deformation modes and shows the largest shift, Table 1. The spectral features of UDMH/Cab-O-Sil are shown in Table 2. A summary of MMH, UDMH, methanol and methyl amine frequencies adsorbed on oxide surfaces is shown in Table 3.

DISCUSSION

The use of deuterated Cab-O-Sil as a mechanistic tool for the infrared spectroscopic study of adsorptive interactions with hydrogen-bonding adsorbates, such as the hydrazines, has several distinct advantages. Because the -OH spectral region is cleared by the deuteration and few functional groups have vibrational bands near the -OD group ($2800 - 2400\text{ cm}^{-1}$), both frequency and intensity changes are readily observed. The finely divided form of Cab-O-Sil makes it ideal for diffuse reflectance studies.

TABLE 1. METHYL GROUP FREQUENCIES OF MMH ADSORBED ON CAB-O-SIL^a

Mode	Liquid	Adsorbed	Shift	Gas ^b
			Absorbed-Liquid	
Asym. str.	2966	2990	+24	2969
Asym. str.	2935	2967	+32	2949
Comb. def.	2877	2943	+34	-
Comb. def.	2855	2907	+52	2851
Comb. def.	2840	2879	+39	-
Sym. str.	2780	2804	+24	2875
Def.	1472	1476	+4	1464
Def.	1438	1454	+16	-
Def.	1411	1421	+10	-

a In cm⁻¹

b Reference 12

TABLE 2. METHYL GROUP FREQUENCIES OF UDMH ADSORBED ON CAB-O-SIL^a

Mode	Liquid ^b	Adsorbed	Shift ^c	UDMH · HBr ^d
Asym. str.	2976	2996	+20	3259 (283)
Asym. str.	2947	2967	+20	3143 (196)
Comb. def.	2889	2933	+44	-
Comb. def.	2848	2872	+24	3015
Sym. str.	2811	2836	+25	2970 (159)
Sym. str.	2766	2792	+26	2918 (147)
Def.	1463	1469	+6	-
Def.	1450	1461	+11	-

a In cm⁻¹

b Reference 13

c Shift with respect to liquid phase

d Solid on KBr plate

TABLE 3. CARBON-HYDROGEN STRETCHING FREQUENCY SHIFTS^a
FOR METHYL-ADSORBATES ON OXIDE SURFACES

Adsorbate	Silica	Silica-Alumina	Alumina
MMH	+24	+22	+22
UDMH	+26	+26	+15
MeOH	+26	+12	-11
MeNH ₂	(+7) ^b		

^a For the low-frequency symmetrical C-H stretch, in cm⁻¹ relative to liquid state

^b With respect to gas phase

DRIFT studies of the adsorption of hydrazine, MMH, UDMH and the model compounds, methyl amine and methanol, on the environmentally important silica and alumina surfaces show some striking commonalities. These polar molecules are all rapidly adsorbed/desorbed at room temperature. The adsorption process is accompanied by H/D-exchange on a deuterated silica surface and presumably on others as well. The H/D-exchanged molecules can remain bonded to the surface after exchange. The spectral properties of the surface-bound species are similar to those of the liquid or vapor indicating that the surface interaction is primarily physical. Chemisorption is involved only in the case of methanol and alumina, *vide infra*. Finally, bound N-methyl and O-methyl groups show similar small shifts to higher energies for stretching, combination and deformation modes.

A structure for the H-bonded surface species consistent with the results is shown in Figure 5. The choice of N-1 as the acceptor atom for the unsymmetrical hydrazines is suggested by the similar methyl-group frequency shifts shown by MMH, UDMH and methyl amine. Since N-1 of UDMH cannot act as a N-H donor and is also the more basic nitrogen, the most favorable cyclic structure would involve N-1 as an acceptor and N-2 as a N-H donor. A

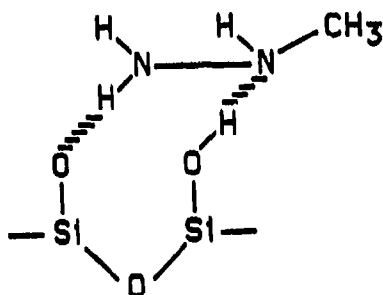


Figure 5. Monomethylhydrazine Adsorbed to Surface
Silanol Groups: A Suggestion

similar structure for water, bound to surface silanol groups, has been proposed (Reference 14).

The unsymmetrical C-H stretching frequency of methanol decreases by 11 cm^{-1} on adsorption onto alumina. Silica, however, causes a shift to higher energy ($+26\text{ cm}^{-1}$) and silica-alumina of intermediate value ($+12\text{ cm}^{-1}$). This is an important observation since Greenler has shown that methanol chemisorbs onto alumina with methoxy formation (Reference 15). The adsorption of methanol onto silica or alumina surfaces occurs with different mechanisms and these mechanisms are effectively probed by the DRIFT technique.

Structure-reactivity relationships have often been developed by using changes in molecular vibrational frequencies as a probes of structure. Bellamy (Reference 11) has reviewed a number of such studies. Electronegativity has been used to rationalize trends in such relationships but the Pauling scale lacks the resolution for satisfactory correlation. Sanderson (Reference 16) has recently developed a precise and internally consistent scale of electronegativities. Correlation of Sanderson electronegativities with the symmetrical methyl deformation frequencies of $\text{CH}_3\text{-X}$ compounds shows a remarkable linearity by Periodic row and monotonic change within Groups, Figure 6.

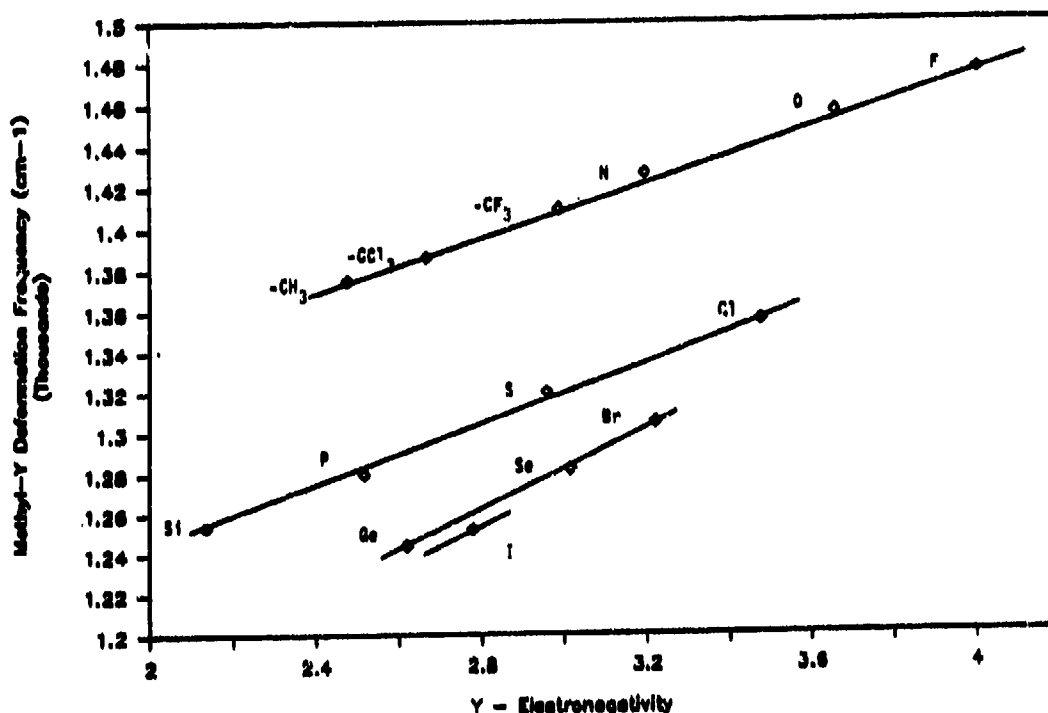


Figure 6. Correlation of Sanderson Electronegativities with Methyl Deformation Frequencies

Using the linear relationship for the First Row elements,

$$E = .015 (v, \text{cm}^{-1}) - 18.122$$

where E is the Sanderson electronegativity and v is the frequency of the symmetrical methyl deformation frequency in wavenumbers of the mono-CH₃-Y compound, the electronegativity of the -NHNH₂ group is estimated to be 3.01 in the liquid state. The 10 cm⁻¹ shift observed on adsorption on Cab-O-Sil corresponds to a change in electronegativity to 3.16. This increase is related to the altered dipole-dipole interactions which occur when the electron density on nitrogen decreases as the lone pair becomes involved in H-bonding. The resultant partial positive charge and the associated 10 cm⁻¹ increase can be compared to the 45 cm⁻¹ shift shown by methyl amine upon protonation. The methyl group deformation frequency in crystalline UDMH hydrobromide could not be confidently assigned, however the symmetrical C-H stretch

showed a shift of 147 cm^{-1} relative to the liquid. Adsorption onto Cab-O-Sil causes a 20 cm^{-1} increase in the UDMH low frequency stretch.

CONCLUSIONS

Adsorption of hydrazine, MMH, and UDMH onto the hydroxylated surfaces of silica, alumina and silica-alumina is the result of reversible physisorption. The primary interaction is through H-bonding and H/D-exchange occurs if the surface is deuterated. The adsorbed structure is similar to that in the liquid as evidenced by similar, but slightly shifted, vibrational frequencies. Analysis of these shifts shows that a 5 percent increase in the apparent Sanderson electronegativity of the hydrazinyl nitrogen occurs on adsorption, consistent with the dipole-dipole interactions of H-bonding. Contrarily, chemisorption of methanol on alumina results in decreases in the methyl group C-H stretching frequencies.

DRIFT spectroscopy then has proven to be a useful probe for the study of small changes in the structure of surface-bound molecules.

REFERENCES

1. Stone, D.A., M.V. Henley and D.V. Naik, "The Effects of Surfaces on the Air Oxidation of Hydrazine," Chemical Propulsion Agency Publication No. 436, November 1985, pp. 151-159.
2. Tuazon, E.C., W.P. Carter, R. Atkinson, A.M. Winer and J.N. Pitts, "Atmospheric Reaction Mechanisms of Amine Fuels," ESL-TR-82-17, March 1982.
3. Kilduff, J.E., D.D. Davis and S.L. Koontz, "Surface-Catalyzed Air Oxidation of Hydrazines: Environmental Chamber Studies," Proceedings of the Third Conference on the Environmental Chemistry of Hydrazine Fuels, Panama City, FL, Sept. 1987, this volume.
4. Kilduff, J.E., D.D. Davis and S.L. Koontz, "Surface-Catalyzed Air Oxidation of Hydrazines: Tubular Reactor Studies," Proceedings of the Third Conference on the Environmental Chemistry of Hydrazine Fuels, Panama City, FL, Sept. 1987, this volume.
5. Winning, W.I.H., J. Chem. Soc., 1954, 926.
6. Durig, J.R., S.F. Bush, and E.E. Mercer, J. Chem. Phys. 1966, 44, 4238.
7. Peri, J.B., J. Phys. Chem. 1966, 70, 2937.
8. Parry, E.P., J. Catal. 1963, 2, 371.
9. Waldron, R.D., J. Chem. Phys. 1953, 21, 734.
10. McKean, D., Chem. Comm. 1971, 1373.
11. Bellamy, L.J. and T. Williams, J. Chem. Soc. 1956, 2753.
12. During, J.R., W.C. Harris and D.W. Wertz, J. Chem. Phys. 1969, 50, 1449.
13. Durig, J.R., and W.C. Harris, J. Chem. Phys. 1969, 51, 4457.
14. Hair, M.L., "Infrared Spectroscopy in Surface Chemistry," Marcel Dekker, New York, 1967.
15. Greenler, R.G., J. Chem. Phys. 1962, 37, 2094.
16. Sanderson, R.L., J. Am. Chem. Soc. 1983, 105, 2259.

THE SOIL MICROBIOLOGY OF HYDRAZINES

L.-T. OU AND J.J. STREET

SOIL SCIENCE DEPARTMENT
UNIVERSITY OF FLORIDA
GAINESVILLE, FLORIDA 32611

INTRODUCTION

Hydrazine fuels are toxic to many forms of life and their persistence in soils is not known. Therefore, we initiated this study to obtain information on the effects of hydrazine (HZ) and monomethylhydrazine (MMH) on soil microbial activity, microbial degradation of the chemicals, and their persistence in soils. Several aspects of the work on hydrazine have been published.^{1,2,3}

MATERIALS AND METHODS

CHEMICALS

Hydrazine monohydrate and hydrazine sulfate were purchased from Aldrich Chemical Co. (Milwaukee, WI) and MMH was provided by Dr. D.A. Stone, AFESC. ¹⁵N-hydrazine sulfate was obtained from Icon (Summit, NJ), and ¹⁴C-MMH was purchased from Amersham (Arlington Heights, IL). All other chemicals were either analytical grade, scintillation grade, or the highest grade commercially available.

SOIL TREATMENT

One hundred g or two hundred g of Arredondo fine sand in 250 mL Erlenmeyer flasks or in 500 mL glass containers with plastic screw caps were treated with HZ or MMH at concentrations ranging from 10 to 500 µg/g. After mixing, water was added to give a soil-water content of 8 mL H₂O/g soil.

SOIL EXTRACTION

For extraction of HZ residue from soil samples, samples suspended in 0.1M NaCl were mechanically shaken for 10 min and centrifuged. This procedure was repeated two more times. 0.1M HCl was used for extraction of MMH residue from soil.

MEASUREMENT OF SOIL RESPIRATION

Carbon dioxide evolved from the samples in closed glass bottles was trapped in KOH and determined by titration⁴. ¹⁴C trapped in the KOH was determined by scintillation counting.

MEASUREMENT OF BACTERIAL AND FUNGAL POPULATIONS

Bacterial and fungal populations in soil were determined using dilution plate-count methods⁵.

MEASUREMENT OF HZ AND MMH

HZ was determined by the colorimetric method of Watt and Chrisp,⁶ and the colorimetric method of Pinkerton et al.⁷ was used for determination of MMH.

MEASUREMENT OF MICROBIAL GROWTH

Growth of bacterial cultures was determined turbidimetrically at 550 nm with a spectronic 20 spectrophotometer.

RESULTS AND DISCUSSION

HYDRAZINE

At low concentrations (100 µg/g and lower), HZ disappeared rapidly from Arredondo soil. Even at 500 µg/g, the chemical disappeared completely in 8 days (Table 1). By comparing the HZ loss from unsterile and sterile samples, autooxidation appeared to be the principal factor contributing to the disappearance of the chemical from soil. Biological oxidation was a relatively minor factor, responsible for perhaps 20% of the disappearance.

Soil respiration (total CO₂ evolution) in hydrazine-treated soil samples was initially inhibited, with the degree of inhibition progressively increasing as HZ concentration increased (Table 2). However, such inhibition was temporary. In fact, not only had all samples recovered from the inhibition within 2 days, but CO₂ production in the HZ-treated samples was actually higher than in the controls. Total cumulative CO₂ production in all treatments was not significantly different after 21 days.

Bacterial populations in hydrazine-treated samples were reduced initially, but fungal populations were not affected (Table 3). Therefore, the

TABLE 1

HZ Remaining in Unsterile and Sterile Arredondo Soil.

Days	HZ (%)			
	100 µg/g		500 µg/g	
	Sterile	Unsterile	Sterile	Unsterile
0.05	83	62	97	93
1	8	0	71	62
2	0	0	52	39
3	0	0	39	25
6	0	0	13	3
8	0	0	8	0

TABLE 2

Effect on HZ on Soil Respiration in Arredondo Soil.

Days	Rate of CO ₂ Production (mg CO ₂ -C/100 g Soil/day)			
	HZ (µg/g)			
	0	2.5	25	125
1	2.73	2.41	1.99	1.64
3	1.55	1.66	1.76	1.68
7	0.70	0.82	0.80	0.86
14	0.54	0.50	0.49	0.69
21	0.50	0.40	0.44	0.52
Total	16.71	16.38	15.74	17.43

reduction of bacterial populations appeared to be the principal cause of initial reduction of CO₂ production for hydrazine-treated samples. For the 100 µg/g treatment, bacterial populations quickly recovered. This reflected the fact that, at this concentration, HZ disappeared completely within one day. In fact, bacterial populations were enhanced in 7 days and remained larger than the control treatment thereafter. Bacterial populations for the 500 µg/g treatment, however, were at least 10 times smaller than for the control treatment throughout the 21 days of incubation. After 7 days, fungal populations for the 100 and 500 µg/g treatments were significantly higher than for the control treatment.

TABLE 3

Effect of HZ on Bacterial and Fungal Populations in Arredondo Soil.

HZ (µg/g)	Days			
	1	7	14	21
	<u>Bacteria (cfu/g x 10⁻⁶)</u>			
0	13.92	15.45	9.83	7.63
100	1.35	24.90	42.60	25.80
500	0.82	0.68	0.91	0.64
	<u>Fungi (cfu/g x 10⁻⁴)</u>			
0	1.05	2.26	2.70	2.22
100	0.87	6.71	9.36	9.59
500	1.00	3.85	11.44	9.49

An Achromobacter sp. was isolated from Arredondo soil. This bacterium degraded HZ rapidly in both growing and resting cell cultures (Figure 1, Table 4). Autoclaved cells lost their capacity to degrade HZ. Thus, the degradation was microbial. The Achromobacter sp. degraded both nonsalt and salt forms of HZ. Using ¹⁵N-HZ, ¹⁵N₂ gas was detected from ¹⁵N-HZ-treated resting cell suspensions. Therefore, it appeared that the Achromobacter sp. oxidized HZ to N₂ gas.

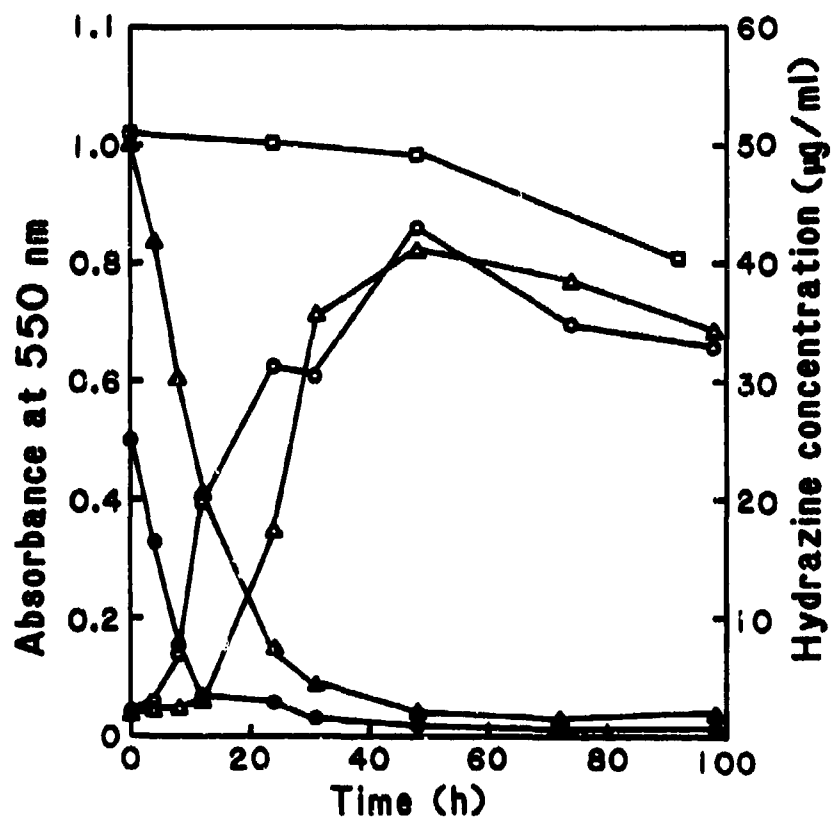


FIGURE 1

HZ Degradation and Growth of the *Achromobacter* sp.

Designations: ○ and △, Absorbance of Culture Fluids with Initial HZ Concentrations of 25 and 51 μg/g, Respectively; ●, and ▲, HZ Concentration in Culture Fluid; and □, HZ Concentration in Culture-Free Glucose-Amended Medium.

TABLE 4

HZ in Cell Suspensions of the Achromobacter sp. after Two Hours of Incubation.

Cell Suspension	Initial HZ ($\mu\text{g/g}$)	% Reduction
Live	25	96
Live	50	95
Live	90	94
Live	104	84
Live	120	56
Live	162	52
Autoclaved	50	0

The Achromobacter sp. also enhanced HZ degradation in waters. When 18-hour-cells of the Achromobacter sp. were added to six waters which contained 50 $\mu\text{g/mL}$ of HZ, 96 to 22% of the HZ was degraded in 2 hours (Table 5). When bacterial cells were not added, HZ was not degraded in these waters during the 2 hours of incubation.

MONOMETHYLHYDRAZINE

Similar to HZ, MMH in Arredondo soil also disappeared rapidly. At concentrations of 100 and 500 $\mu\text{g/g}$, MMH completely disappeared in 48 hours (Table 6). By using ^{14}C -MMH, 32 and 15% of applied ^{14}C -activity in Arredondo soil treated with 100 and 500 $\mu\text{g/g}$ of the chemical was volatilized and trapped in KOH traps, respectively (Table 7). After acidification of the KOH with concentrated HCl to a pH level below 1, only 6 and 4% of ^{14}C -activity remaining in the acidified KOH, respectively. This indicated that the majority of the trapped ^{14}C was in the form of $^{14}\text{CO}_2$. Therefore, ^{14}C -MMH in soil was degraded to $^{14}\text{CO}_2$. Such degradation is microbial.

At concentrations of 10 and 100 $\mu\text{g/g}$, MMH did not have any toxic effect on soil respiration, and on soil bacterial and fungal populations (Tables 8 and 9). In fact, soil respiration in the 10 and 100 $\mu\text{g/g}$ treatment remained

TABLE 5

HZ Degradation in Waters Suspended with the Achromobacter sp.

Water	HZ ($\mu\text{g/g}$)	Water	HZ ($\mu\text{g/g}$)
Santa Fe River	96	Prairie Creek	28
Lake Alice	78	Tap Water	52
Newmans Lake	30	Distilled Water	22

TABLE 6

MMH in Arredondo Soil.

Hours	% of Applied MMH	
	100 $\mu\text{g/g}$	500 $\mu\text{g/g}$
0.05	42	79
4	8	23
24	2	2
48	0	0

TABLE 7

¹⁴C-Activity Trapped in KOH after 48 Hours of Incubation.

MMH ($\mu\text{g/g}$)	% of Applied ¹⁴ C	
	¹⁴ C Trapped in KOH	¹⁴ C Remaining in Acidified KOH
100	32	6
500	15	4

TABLE 8

Soil Respiration in Arredondo Soil Treated with MMH.

Days	Rate of CO ₂ Production (mg CO ₂ -C/g Soil/Day)		
	HZ ($\mu\text{g/g}$)		
	0	10	100
1	4.61	5.00	5.56
3	2.96	3.22	3.42
7	1.47	1.57	1.65
14	1.05	1.21	1.20
21	0.78	0.92	0.93
28	0.64	0.72	0.71
Total	37.91	41.67	43.53

TABLE 9

Bacterial and Fungal Populations in Arredondo Soil Treated with MMH.

MMH ($\mu\text{g/g}$)	Days		
	7	14	21
<u>Bacteria (cfu $\times 10^{-5}$)</u>			
0	201	151	126
10	192	172	185
100	271	175	166
<u>Fungi (cfu $\times 10^{-3}$)</u>			
0	76	87	79
10	81	86	77
100	83	104	100

higher than in the control treatment throughout the entire 28 days of incubation. This was in part due to the degradation of MMH-C to CO_2 , and in part due to the fact that the normal soil respiration process was not inhibited by the chemical.

The Achromobacter sp. which had a high capacity to degrade HZ also had a high capacity to degrade MMH. In addition, A Pseudomonas sp., which was also isolated from Arredondo soil, also degraded MMH.

ACKNOWLEDGEMENTS

I thank Kevin Carter and Bill Harb for their technical assistance.

REFERENCES

1. Ou, L.T. and J.J. Street, "Hydrazine Degradation and Its Effect on Microbial Activity in Soil," Bulletin of Environmental Contamination and Toxicology, 1987, vol. 38, pp. 179-183.
2. Ou, L.T., "Microbial Degradation of Hydrazine," Bulletin of Environmental Contamination and Toxicology, 1987, vol. 39, pp. 78-85.

3. Ou, L.T. and J.J. Street, "Microbial Enhancement of Hydrazine Degradation in Soil and Water," Bulletin of Environmental Contamination and Toxicology, 1987, vol. 39., in press.
4. Ou, L.T., D.F. Rothwell, W.B. Wheeler, and J.M. Davidson, "The Effect of High 2,4-D Concentrations on Degradation and Carbon Dioxide Evolution in Soils," Journal of Environmental Quality, 1978, vol. 7, pp. 241-246.
5. Ou, L.T., J.M. Davidson, and D.F. Rothwell, "Response of Soil Microflora to High 2,4-D Applications." Soil Biology & Biochemistry, 1978, vol. 10, pp. 443-445.
6. Watt, G.W. and J.D. Chrisp, "A Spectrophometric Method for the Determination of Hydrazine," Analytical Chemistry, 1952, vol. 24, pp. 2006-2008.
7. Reynolds, B.A. and A.A. Thomas, "A Colorimetric Method for the Determination of Hydrazine and Monomethylhydrazine in Blood," American Industrial Hygiene Association Journal, 1965, vol. 26, pp. 527-531.

NUMERICAL SIMULATION OF HYDRAZINE TRANSPORT IN A SANDY SOIL

R.S. Mansell, Professor

Soil Science Department, University of Florida

Gainesville, FL 32611

S.A. Bloom and W.C. Downs

ABSTRACT

Aqueous solutions of hydrazinium were miscibly displaced through columns of water saturated Arredondo fine sand in order to measure breakthrough curves (BTC) for concentration in column effluent. Solutions containing approximately $200 \mu\text{g ml}^{-1}$ hydrazinium were applied as a wide pulse and as a continuous application. Two Darcy liquid velocities of 0.5 and 5.0 cm h^{-1} were used to evaluate the importance of kinetics for physical sorption upon mobility of hydrazinium in the soil columns. A finite difference numerical transport model for hydrazinium was evaluated by comparing simulated and experimental breakthrough curves. Kinetic linear physical sorption and irreversible first order chemisorption components of the transport model were observed to be critical in providing adequate simulation of hydrazinium BTC. Initial breakthrough of hydrazinium in the effluent, general shape of BTC, tailing of BTC, and maximum hydrazinium concentrations in the effluent were particularly sensitive to the magnitudes of rate coefficients for sorption and degradation. Ion exchange appeared to be of minimal importance to the transport of hydrazinium under the conditions for the column experiments. Hydrazinium mobility in this soil is clearly dependent upon pore water velocity, and other work indicates that it is also highly dependent upon concentration of hydrazinium in the soil solution.

INTRODUCTION

Hydrazine is a highly reactive and carcinogenic diamine ($\text{NH}_2\text{-NH}_2$) which has multiple uses (6), that range from chemical applications such as deoxygenation of water in boiler systems to aerospace and military application as a component of rocket fuel. Due to the wide spread use and toxicity to humans, the potential exists that accidental spillage or leakage from storage tanks onto soils could result in environmental contamination of underlying groundwater. Interactions of hydrazine between gaseous, liquid and solids phases of soil are very complex (7) and include transfer of hydrazine from soil solution to colloids by irreversible chemisorption and reversible physical sorption, hydrolysis of hydrazine (N_2H_4^0) to hydrazinium (N_2H_5^+) at low pH,

and reversible cation exchange. Hydrazine in a water-saturated soil environment is also subject to chemical (autooxidation) and microbiological (soil bacteria) degradation. Much of the published information concerning interactions between soils and hydrazine actually involves investigations with a single reactive soil component such as crystalline clay minerals, amorphous minerals and organic matter. A need exists to investigate the fate and transport of hydrazine in whole soils which contain all of these components in a known proportion as exists in nature. Of particular importance are sandy soils which have high proportions of inert quartz sand and small proportions of reactive components. Accidental spillage of hydrazine fuels upon such soils could result in convective-transport of hydrazine in the mobile solution phase of the soil profile and possibly contaminate groundwater.

In this work, dilute aqueous hydrazine solutions were applied with steady flux to water saturated columns of a sandy soil, and breakthrough curves of hydrazine and/or hydrazinium (concentrations versus pore volumes of effluent) were used to evaluate a one-dimensional convective-dispersive transport model for describing the transport of hydrazine and/or hydrazinium through soil. Transport equations for the model include sink terms to account mathematically for a number of interactions known to occur between hydrazine and soil.

THEORY

A numerical model was developed to simultaneously describe the fate and transport of three solute species - hydrazine ($N_2H_4^0$), hydrazinium ($N_2H_5^+$), and a soil cation species such as Ca^{2+} - during steady liquid flow through water saturated soil. The model is applicable to the situation where aqueous solutions of hydrazine and/or hydrazinium are applied at constant flux to soil with cation exchange sites initially saturated with a single ion species such as Ca^{2+} . Hydrazine and hydrazinium molecules present in the soil solution are conceptually assumed in the model to be irreversibly transferred to the solids phase by chemisorption, reversibly transferred to the solids phase by physical sorption, and completely removed by separate microbial and chemical degradation mechanisms. For solution pH values less than 7.8 a portion of the hydrazine is assumed to be converted to hydrazinium by hydrolysis. Hydrazinium molecules are also assumed to undergo ion exchange with the cation species (Ca^{2+}) initially present in the exchange phase of the soil.

Mathematical equations for the fate and transport of hydrazine (solute species #1), hydrazinium (solute species #2), and soil cation (solute species #3), respectively, are given by

$$\frac{\partial C_1}{\partial t} = D \frac{\partial^2 C_1}{\partial z^2} - v \frac{\partial C_1}{\partial z} - \sum_1^3 \phi_{1i} ; \quad [1]$$

$$\frac{\partial C_2}{\partial t} = D \frac{\partial^2 C_2}{\partial z^2} - v \frac{\partial C_2}{\partial z} - \sum_1^4 \phi_{2i} ; \quad [2]$$

$$\text{and} \quad \frac{\partial C_3}{\partial t} = D \frac{\partial^2 C_3}{\partial z^2} - v \frac{\partial C_3}{\partial z} - \phi_{31} \quad [3]$$

where C_1 , C_2 and C_3 are concentrations ($\mu\text{g ml}^{-1}$) of hydrazine, hydrazinium and soil cation, respectively. The dispersion coefficient ($\text{cm}^2 \text{h}^{-1}$) is represented as D , $v = q/\theta$ is the pore water velocity (cm h^{-1}), q is the Darcy velocity (cm h^{-1}), θ is the volumetric water content ($\text{cm}^3 \text{cm}^{-3}$), z is distance (cm) through the soil and t is time (h). Reactions for hydrazine, hydrazinium, and soil cation are represented by ϕ_{11} , ϕ_{21} , and ϕ_{31} sink terms, respectively. Eight sink terms in equations [1, 2 and 3] are given for specific reactions. Kinetic reversible physical sorption for hydrazine is represented (3) as

$$\phi_{11} = k_f C_1^n - (\rho/\theta) k_b \bar{C}_1 \quad [4]$$

where k_f and k_b are forward and backward rate coefficients (h^{-1}), respectively, ρ is soil bulk density (g cm^{-3}), \bar{C}_1 is the concentration ($\mu\text{g g}^{-1}$) of hydrazine in the solids phase, and n is the dimensionless exponent associated (3) with the Freundlich sorption isotherm for equilibrium conditions. Under flow conditions suitable for local equilibrium, equation [4] becomes

$$\phi_{11} = n (\rho/\theta) K C_1^{n-1} \frac{\partial C_1}{\partial t} = n (\rho/\theta) \frac{k_f}{k_b} C_1^{n-1} \frac{\partial C_1}{\partial t} \quad [5]$$

where K is the Freundlich distribution coefficient ($\text{cm}^3 \text{g}^{-1}$). Chemisorption, microbial degradation, and chemical degradation for hydrazine are assumed to be apparent first order irreversible reactions as

$$\phi_{12} = k_1 C_1 \quad [6]$$

where k_1 is the sum of the rate coefficients (h^{-1}) for the respective

mechanisms. Hydrolysis of hydrazine is given as

$$\phi_{13} = 10^{\text{pH} - 7.8} \frac{\partial C_2}{\partial t} \quad [7]$$

Reaction terms for hydrazinium include one for cation exchange with soil cations

$$\phi_{21} = (\rho/\theta) \frac{\partial \bar{C}_2}{\partial t} \quad [8]$$

where \bar{C}_2 is the concentration (meq ml⁻¹) of hydrazinium ionic species in the soil exchange phase. A more detailed presentation of the form of equation [8] is given in (4) and (8). Cation exchange capacity (meq g⁻¹) and exchange selectivity coefficients for the soil used are required input parameters for equations [8]. Hydrazinium degradation is expressed as

$$\phi_{22} = k_2 C_2 \quad [9]$$

where k_2 is a summed rate coefficient (h⁻¹). Physical sorption is given as

$$\phi_{23} = k_a C_2^m - (\rho/\theta) k_d \bar{C}_2 \quad [10]$$

where \bar{C}_2 is the concentration (μg g⁻¹) of hydrazinium in the sorbed phase, m is the Freundlich exponent, and k_a and k_d are forward and backward rate coefficients (h⁻¹). A separate equation is also needed for the rate of sorption:

$$\frac{\partial \bar{C}_2}{\partial t} = (\theta/\rho) k_a C_2^m - k_d \bar{C}_2 \quad [11]$$

Hydrolysis is given as

$$\phi_{24} = 10^{7.8 - \text{pH}} \frac{\partial C_1}{\partial t}, \text{ and} \quad [12]$$

cation exchange for Ca⁺⁺ is given as

$$\phi_{31} = (\rho/\theta) \frac{\partial \bar{C}_3}{\partial t} \quad [13]$$

where \bar{C}_3 is the concentration (meq ml⁻¹) of the soil cation species initially

present in the exchange phase (4).

In this paper, acid soil conditions were assumed such that hydrolysis was not considered and the effect of ion exchange was assumed minimal. Thus the transport of hydrazine and soil cation species were not considered in model simulations. Thus, hydrazinium transport equation [2] and reaction terms given as [8], [9], and [10] were used in a simplified version of the model. Initially, C_2 and \bar{C}_2 concentrations were zero within the solution and solids phases of columns of water saturated soil. Steady liquid flow ($v = \text{constant}$) was maintained at all times and dilute aqueous solutions with concentration C_0 was applied both as a step function and as a wide pulse to the soil surface using a flux boundary condition

$$v C_0 = v C_2 - D \frac{\partial C_2}{\partial z} \quad \text{for } t > 0 \quad [14]$$

At the bottom of the columns of length L (cm), the boundary condition was

$$\frac{\partial C_2}{\partial z} = 0 \quad \text{for } t > 0. \quad [15]$$

A Crank-Nicholson finite differencing technique (9) was used to numerically solve equations [2], [8], [9], [10], and [11] subject to conditions [14] and [15]. Values for time steps Δt and space steps Δz used in the numerical solution were adjusted to insure minimal cumulative mass balance errors in the solutions.

METHODS

Samples of the E_2 horizon of Arredondo fine sand were obtained from a site in NW Alachua County, Florida. The samples were air dried and sieved to pass a 2 mm screen before use. Only data from the E_2 horizon is included in this report.

Soil was packed to a bulk density of 1.6 g cm^{-3} , deaerated with helium, and saturated with 0.01 N CaCl_2 [See (1) for details]. A peristaltic pump was used to apply flow rates of 0.5 and 5.0 cm hr^{-1} to the soil columns. An automatic fraction collector was used to collect effluent samples. Alternate test tubes of effluent were treated with 1.0 ml or 0.1 N HCl in order to stabilize the hydrazinium prior to colorimetric analysis in a spectrophotometer. Test tubes without HCl were analyzed for pH and for calcium concentration by atomic absorption spectroscopy.

The soil pH in 0.01 N CaCl_2 was determined as 4.45 and hydrazine input

solutions were prepared in the CaCl_2 solution and adjusted to the soil pH. Information about the physics of flow was determined by using tritiated water as a tracer and observing the breakthrough of tritium in the column effluent at the two flow rates using standard methods. Breakthrough curves were prepared and analyzed for Peclet number and dispersion coefficient.

RESULTS AND DISCUSSION

Steady displacement of aqueous solutions containing approximately $200 \text{ } \mu\text{g ml}^{-1}$ hydrazinium either as a wide pulse or as a continuous application through water-saturated columns of subsurface Arredondo fine sand was performed to investigate the fate and transport of hydrazine. Descriptive parameters for 2 columns with a Darcy liquid flux of 0.5 cm h^{-1} and for 2 columns with a Darcy flux of 5 cm h^{-1} are presented in Table 1. Downs (1) previously showed that even a solute as reactive as hydrazinium can be transported through this sandy soil. Experimental BTC's for hydrazinium from these four soil columns are used in this paper to provide preliminary sensitivity analyses for pertinent input parameter of a numerical transport model presented here and to evaluate the model for comparison of simulated and experimental BTC's. Nineteen model simulations are presented in this paper (Table 2). Initial attempts to provide descriptions of hydrazinium BTC's for the Arredondo soil quickly revealed that ion exchange gave only a minor contribution to hydrazinium mobility in this soil which has a very small cation exchange capacity. Reversible kinetic physical sorption and irreversible chemisorption, however were observed to critically control hydrazinium mobility. Simulations presented in Figure 1 reveal the sensitivity of the model to the magnitudes and ratios of forward k_a and backward k_d physical sorption rate coefficients as well as the magnitude of the first order chemisorption rate coefficient k_2 . Each of these simulations was performed for soil columns #2 where the Darcy water velocity was 5.0 cm h^{-1} and hydrazine solution was applied continuously. Under equilibrium conditions using a stirred soil suspension technique, the sorption isotherm was effectively linear in this concentration range (1). Thus linear physical sorption was used here in the model.

In simulations for Fig. 1A kinetic sorption was included in the model but chemisorption was ignored. Increasing the ratio k_a/k_d while maintaining k_d constant effectively increased the magnitude of k_a . The overriding change in simulations was to translate the BTC to greater numbers of pore volumes of

Table 1: Parameters for columns of subsurface Arredondo fine sand used to investigate hydrazinium mobility during steady liquid flow.

Soil Column Number	Bulk Density ρ	Volumetric Water Content θ	Pore Volume V_o	Darcy Flux q	Pore Water Velocity v	Dispersion Coefficient D	Volume of Applied Hydrazinium Solution	Hydrazinium Concentration in Applied Solution C_o
1	1.65	0.24	149	5.0	20.8	0.97	1.90	233
2	1.63	0.25	151	5.0	20.0	0.97	11.00	216
3	1.65	0.23	137	0.5	2.2	0.56	2.04	207
4	1.61	0.26	160	0.5	1.9	0.56	7.90	235

Table 2. Parameter used in model simulations of hydrazinium breakthrough curves obtained for selected soil columns. Linear physical sorption is assumed in all cases.

Soil Column Number	Simulation Number	Ratio k_a/k_d	Rate Coefficient k_a	Rate Coefficient k_d	Physical Sorption Mode	Rate Coefficient k_4
2	1	1.00	0.00100	0.00100	kinetic	0
	2	1.25	0.00125	0.00100	"	0
	3	1.50	0.00150	0.00100	"	0
	4	1.75	0.00175	0.00100	"	0
	5	2.00	0.00200	0.00100	"	0
	6	1.50	0.00150	0.00100	"	0
	7	1.50	0.00300	0.00200	"	0
	8	1.50	0.00750	0.00500	"	0
	9	1.50	0.00750	0.0050	"	0.000010
	10	1.50	0.00750	0.0050	"	0.000025
	11	1.50	0.00750	0.0050	"	0.000040
1	12	1.50	0.00750	0.0050	kinetic	0.000025
1	13	1.50	0.00750	0.0050	equilibrium	0.000025
2	14	1.50	0.00750	0.0050	kinetic	0.000025
2	15	1.50	0.00750	0.0050	equilibrium	0.0000025
3	16	1.50	0.00750	0.0050	kinetic	0.0000025
3	17	1.50	0.00750	0.0050	equilibrium	0.0000025
4	18	1.50	0.00750	0.0050	kinetic	0.0000025
4	19	1.50	0.00750	0.0050	equilibrium	0.0000025

effluent, thus providing increased retardation and decreased mobility of the hydrazinium.

Absolute magnitudes of the forward k_a and backward k_d sorption rate coefficients were varied while maintaining a constant ratio k_a/k_d for simulations presented in Fig. 1B. Chemisorption was ignored for these simulations. Increasing the absolute magnitudes of k_a and k_d while imposing a constant ratio k_a/k_d tended to rotate the simulated BTC so as to result in steeper curves. Large magnitudes of k_a and k_d in a kinetic sorption submodel for solute transport tend to give BTC's similar to those obtained by an equilibrium sorption submodel. The effect of the magnitudes of k_a and k_d on BTC's for reactive solutes has been shown to be only marginal for small ratios of k_a/k_d , but for increasing ratios of k_a/k_d the magnitudes of the coefficients become very significant (5).

Using constant values for k_a , k_d , and k_a/k_d , the rate coefficient for chemisorption k_2 was varied for simulations presented in Fig. 1C. Increasing k_2 tended to decrease maximum concentrations of hydrazinium in the column effluent and gave BTC's that approached a plateau. Similar effects have been observed for simulations of phosphate transport in columns of sandy soil (2).

Using best visual fit values for k_a , k_d , k_a/k_d and k_2 in the transport model, simulations (Fig. 2A) were performed for soil column #2 using assumptions of kinetic versus equilibrium physical adsorption. The simulation using kinetic sorption described the experimental data while the simulation based upon equilibrium sorption gave an overestimation of retardation of hydrazinium movement through the soil and a BTC that was excessively steep. Similar effects have been observed (10, 5, 2) for simulations for phosphate transport in soil.

Best values for k_a , k_a/k_d , and k_d for column #2 (Fig. 2A) were then used to simulate hydrazinium BTC using assumptions of kinetic versus equilibrium sorption for column #1 with $q = 5.0 \text{ cm h}^{-1}$ that received a pulse application of hydrazinium solution (Fig. 2B), for column #4 with $q = 0.5 \text{ cm h}^{-1}$ that received a pulse application of hydrazinium solution (Fig. 2D), and column #3 with $q = 0.5 \text{ cm h}^{-1}$ that received continuous application of hydrazinium solution (Fig. 2C). Based on analyses of degradation in observed continuous hydrazinium BTC's, there is evidence that chemisorption approaches a limit at long contact times. The value of k_2 was reduced by an order of magnitude in the last two simulations to parallel the reduction in flow rate so as to compensate for this

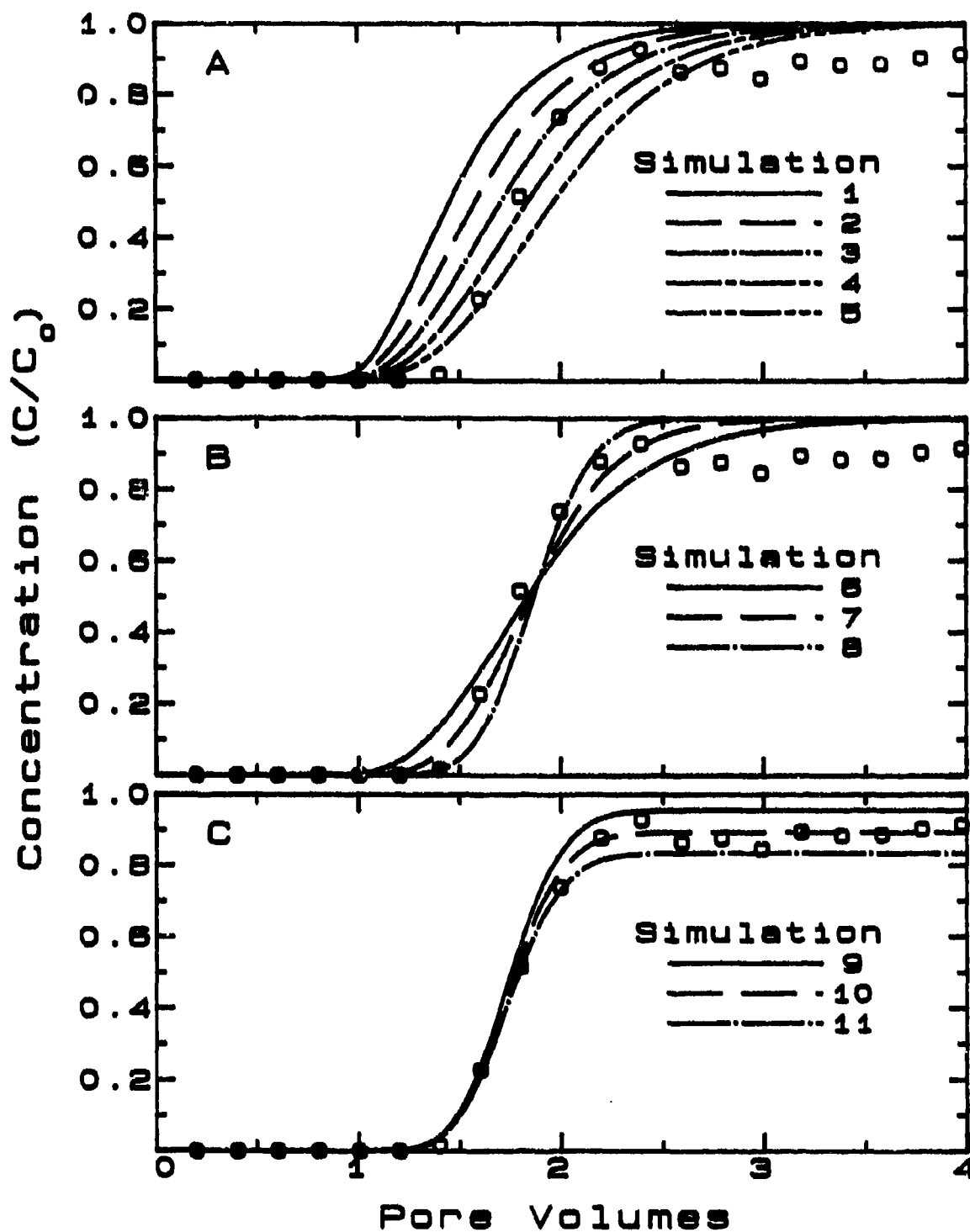


Figure 1. Kinetic BTC's for soil column #2 showing effects of increasing: (A) ratio of k_a/k_d with a constant k_d ; (B) magnitude of k_a & k_d for a constant ratio of k_a/k_d ; and (C) magnitude of k_2 (degradation). See Table 2 for simulation parameters.

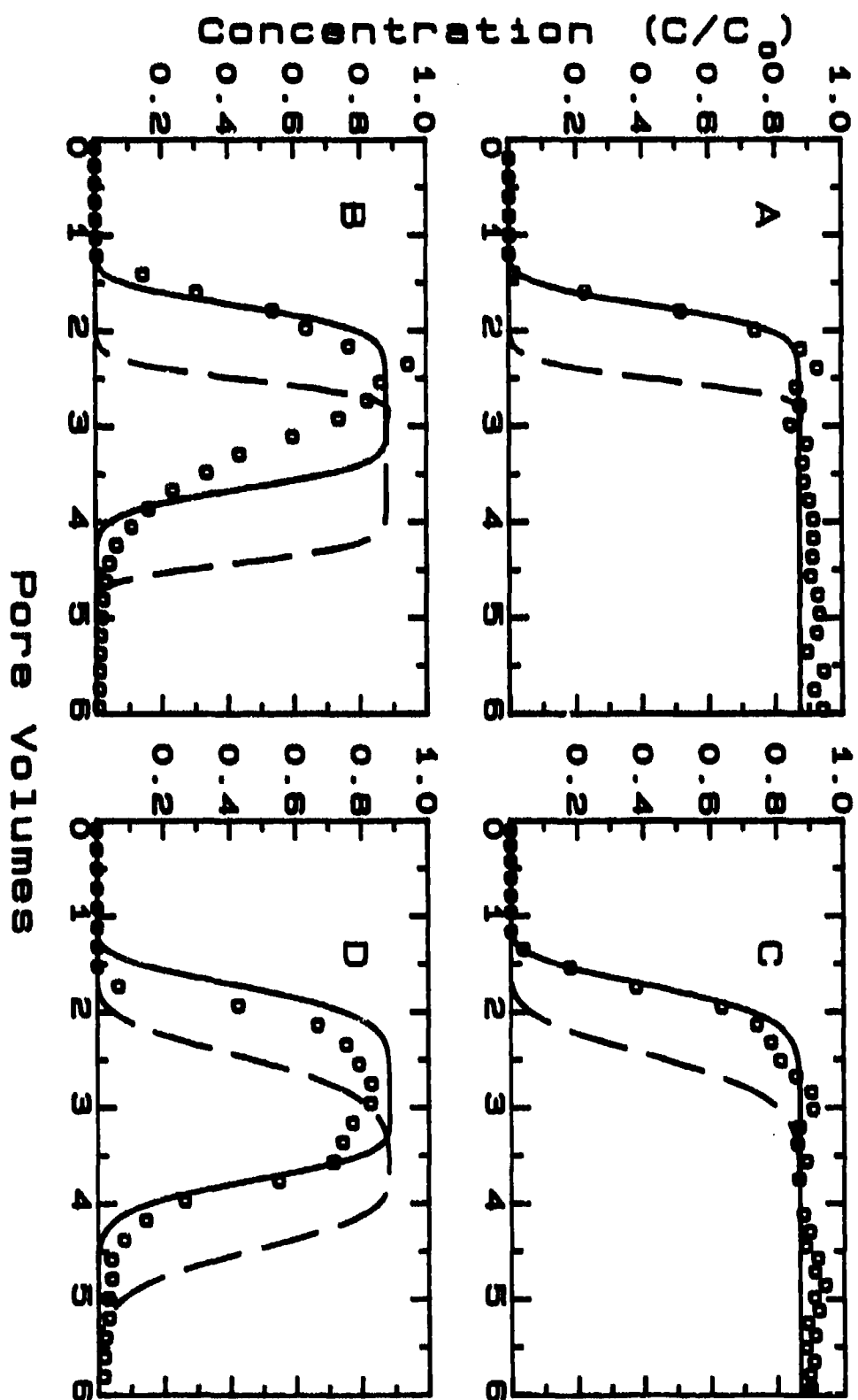


Figure 2: Simulated hydrazinium kinetic (solid) and equilibrium (broken) BTC's for: (A) Soil Column #2; (B) Soil Column #1; (C) Soil Column #3; and (D) Soil Column #4. See Table 2 for simulation parameters.

phenomenon. As in Fig. 2A simulations based upon kinetic sorption provided closer agreement to experimental BTC's than did simulation based upon equilibrium sorption. Although simulations based on kinetic sorption generally described the BTC for $q = 0.5 \text{ cm h}^{-1}$ conditions, the description was not as close to experimental data as was for column #2 where the Darcy flux was ten-fold greater. Large values of pore water velocity tend to have smaller residence times for solute transport than under conditions of slower flow. Kinetic sorption thus tends to become increasingly important as the water pore velocity increases. A similar effect when pesticide BTC's were predicted for high and low values of water flux (9) was observed.

LITERATURE CITED

1. Downs, W.C., R.S. Mansell, J.J. Street, S.A. Bloom, and D.C.M. Augustyn. 1987. Hydrazine transport in columns of sandy soil. Proceeding of International Conference on Impact of Physico-Chemistry On the Study, Design and Optimization of Processes in Natural Porous Media Convened in Nancy, France during June 10-12, 1987. pages 285-291.
2. Mansell, R.S., H.M. Selim, P. Kanchanasut, J.M. Davidson and J.G.A. Fiskell. 1977. Experimental and simulated transport of phosphorus through sandy soils. Water Resour. Res. 13:189-194.
3. Mansell, R.S. and H.M. Selim. 1981. Mathematical models for predicting reactions and transport of phosphorus applied to soil. Chapter 21 in "Modeling Wastewater Renovation Land Application" John Wiley, I.K. Iskandar (ed.). Pages 600-646.
4. Mansell, R.S., S.A. Bloom, H.M. Selim, and R.D. Rhue. 1986. Multispecies cation leaching during continuous displacement of electrolyte solutions through soil columns. Geoderma 38:61-76.
5. Murali, V. and L.A.G. Aylmore. 1981. A convective-dispersive-adsorptive flow model for solute transport in soil. I. Model description and some simulation. Aust. J. Soil Res. 19:23-39.
6. Schiessl, H.W. 1980. Hydrazine - Rocket Fuel to Synthetic Tool. Aldrichimica Acta 13:33-40.
7. Schmidt, E.W. 1984. Hydrazine and its Derivatives. Pages 595-601. John Wiley and Sons, New York.
8. Schulin, R., H. Föhler, R.S. Mansell, and H.M. Selim. 1986. Miscible displacement of ions in aggregated soil. Geoderma 38:311-322.

9. Selim, H.M., J.M. Davidson and R.S. Mansell. 1976. Evaluation of a two-site adsorption-desorption model for describing solute transport in soils. Pages 444-448. Proceedings of 1976 Summer Computer Simulation Conference in Washington, D.C. during July 12-14, 1976.
10. Selim, H.M. 1987. Prediction of phosphate behavior during transport in soils. Proceedings of International Conference on Impact of Physico-Chemistry on the Study, Design and Optimization of Process in Natural Porous Media convened in Nancy, France during June 10-12, 1987. Pages 293-301.

SECTION V
HYDRAZINE DISPOSAL STUDIES

THE CHEMISTRY OF THE HYPOCHLORITE NEUTRALIZATION OF HYDRAZINE FUELS

Kenneth L. Brubaker

Energy and Environmental Systems Division

Argonne National Laboratory

9700 South Cass Avenue

Argonne, Illinois 60439

ABSTRACT

Neutralization of hydrazine fuels with hypochlorite is a recommended procedure for the treatment of fuel spills prior to disposal. Various research workers have shown, however, that incomplete reaction of hypochlorite with the methylated hydrazine fuels monomethylhydrazine and unsymmetrical dimethylhydrazine leads to a wide variety of byproducts, including N-nitrosoalkylamines. The known reaction products and mechanisms are reviewed and summarized.

INTRODUCTION

The U.S. Air Force uses hydrazine (N_2H_4), monomethylhydrazine (MMH), 1,1-dimethylhydrazine (unsymmetrical dimethylhydrazine, or UDMH), and Aerozine-50 (AE-50, a 50-50 mixture by weight of hydrazine and UDMH) in a number of applications, including auxiliary power units, small thrusters, and space vehicles (1). The routine handling of these fuels occasionally results in the accidental spillage of small quantities, and their toxic nature (1,2) dictates that they must be treated and disposed of in an environmentally acceptable manner.

One possible approach to treatment and disposal is to oxidize the collected fuel prior to disposal. The oxidation of hydrazine has been studied for over eighty years (1 and references therein), and more recently the oxidation of methylated hydrazines has also been studied (1,3-11). If chemical neutralization is to be carried out by base personnel however, the oxidizing agent should be cheap, easy to obtain, and easy to use. Ordinary household or commercial hypochlorite bleach fulfills these requirements.

The use of hypochlorite bleach for the neutralization of hydrazine has been recommended by Stauffer and Eyl (12) and Marsh and Knox (13), and for hydrazine fuels in general by Hannum (2). However, previous studies of the oxidation of methylated hydrazine fuels have shown that a wide variety of

partial oxidation products are usually formed. There is therefore reason for concern regarding the use of chemical neutralization procedures for these fuels.

Relatively few studies using hypochlorite have been reported. Castegnaro et al. (3) have evaluated four oxidative methods, including hypochlorite, for the chemical neutralization of hydrazine and several methylated hydrazines. Mach and Baumgartner (7) have examined the products of the reaction between calcium hypochlorite and UDMH. Rianda et al. (9,10) studied the chlorinolysis of MMH and UDMH at several pHs, including alkaline values.

Recently, an investigation was undertaken at Argonne National Laboratory (ANL) to examine the byproducts of the hypochlorite neutralization of methylated hydrazine fuels under a variety of conditions. The reaction was found, as expected, to yield a considerable number of organic byproducts, including N-nitrosoalkylamines. This paper summarizes the known chemistry of the hypochlorite oxidation of these methylated hydrazine fuels.

REACTION PRODUCTS

Product analyses for the hypochlorite oxidation of one or more methylated hydrazine fuels have been reported in several studies (3,7,9,10,14,15).

UDMH. Mach and Baumgartner (7) found the following products from the oxidation of UDMH with $\text{Ca}(\text{ClO})_2$ (HTH®): formaldehyde methylhydrazone (FMH), formaldehyde dimethylhydrazone (FDH), acetaldehyde dimethylhydrazone (ADH), dimethylformamide (DMF) and tetramethyltetrazene (TMT). Based upon the observed changes in the product distribution as the amount of $\text{Ca}(\text{ClO})_2$ used was varied, they suggested that the initial product formed is primarily FDH and that other oxidation products are the result of the further oxidation of FDH. Mach and Baumgartner looked for but did not find any N-nitrosodimethylamine (NDMA) in the product mixture. They did not carry out similar experiments for MMH or AE-50.

Brubaker et al. (14) reported that GC/MS and GC/FTIR analysis of the reaction mixture following oxidation of UDMH with aqueous NaClO revealed 90-100 compounds, with FDH being the major product. Other confirmed products were NDMA, N,N-dimethylcyanogen (DMC), DMF, and chloroform. In addition, ADH and formaldehyde methylethylhydrazone were tentatively identified from their mass spectra. The observed product distribution was substantially different,

however, when solid bleach (HTH®) was used. FDH was no longer present, but the main byproduct found was instead tentatively identified as sym-tetrahydro-1,2,3,5-tetramethyltetrazine, the cyclic dimer of FDH. The other reaction products found in the liquid bleach experiment were also found in the solid bleach run, and in addition, a substance tentatively identified as FMH was also seen.

In the NaClO/UDMH experiments carried out by Brubaker et al. (14), the mole ratio of evolved gas to initial fuel ranged from zero to 0.17, and increased to 0.30 when solid bleach was used. No analysis of the evolved gas was carried out, but most of the reaction products clearly remained in solution in this case.

In a continuation of this work, similar experiments were conducted using NaClO at higher hypochlorite/fuel ratios. Significantly fewer substances were found, and FDH was present at substantially reduced levels. A higher number of chlorinated compounds were also seen. These observations are consistent with the initial formation of FDH, followed by further oxidation. In one experiment, in which a UDMH solution was added to bleach rather than the other way around, N-nitrosoethylmethylaniline (NEMA) was identified in addition to NDMA in the product mixture.

In a study of the utility of different methods for the degradation of chemical carcinogens, Castagnaro et al. (3) examined the use of NaClO and $\text{Ca}(\text{ClO})_2$ as well as KMnO_4 and KIO_3 for the neutralization of several hydrazine fuels. No attempt was made to completely characterize the products from their experiments, but both NDMA and NEMA were produced from UDMH by both NaClO and $\text{Ca}(\text{ClO})_2$. The percent yields found using NaClO were 0.014% and 0.14% for NDMA and NEMA, respectively, and the corresponding yields using $\text{Ca}(\text{ClO})_2$ were 0.05% and 0.014%.

Rianda et al. (9,10) studied the chlorinolysis of aqueous solutions of several hydrazine fuels at a variety of pHs, including alkaline values for which the chlorine in aqueous solution would exist primarily as hypochlorite ion. Their results also indicate that the first step in the oxidation of UDMH is the production of FDH and TMT, followed by further oxidation. Additional products reported include CH_3Cl , CH_2Cl_2 , CHCl_3 , CCl_4 , $(\text{CH}_3)_2\text{NN}=\text{CCl}_2$, $\text{CH}_3\text{N}=\text{NCCl}_3$, CH_3NCl_2 , $\text{Cl}_2\text{C}=\text{CCl}_2$, and $\text{Cl}_3\text{C}-\text{CHCl}_2$, but no nitrosoamines were reported. Finally, Rianda et al. (10) report that the amount of N_2 evolved

was found to be close to the stoichiometric amount, in contrast to the observations of Brubaker et al. (14).

MMH. Brubaker et al. (14) reported finding a very complex reaction mixture following the oxidation of MMH with aqueous NaClO , with over 100 peaks being seen in the total-ion chromatogram from their GC/MS analysis. Unfortunately, very few could be identified. Chloroform was a significant product, but the largest peak was found to be NEMA, and another large peak was identified as N-nitrosodiethylamine (NDEA). The use of solid bleach gave rise to a much less complicated mixture, with approximately 30 peaks in the total-ion chromatogram. Although most still could not be identified, chloroform, NEMA, and NDEA were found to be present. NDMA was never found to be a product of the hypochlorite oxidation of MMH.

Measurement of the evolved gas in the MMH experiments gave a mole ratio of gas/fuel of 0.72 ± 0.05 when liquid bleach was used, and approximately 0.92 using solid bleach. For as yet unknown reasons, in the second phase of their study, Brubaker and coworkers found that the measured gas/fuel ratio jumped to 1.3-1.4. The only apparent difference in experimental procedure was the use of a smaller quantity of fuel (30 mL of approximately 2% solution instead of 300 mL) and a smaller reaction vessel (a 250 mL flask instead of a 2000 mL flask) in the second phase of the study. The consistency of the results within each phase and the observation that the gas yield in phase two was almost exactly twice what it was in phase one suggests that the difference is due to a real difference in reaction mechanism, resulting perhaps from differences in the level of some catalyst.

Castegnaro et al. (3) found that both NDMA and NEMA are produced from the oxidation of MMH with either aqueous NaClO or solid $\text{Ca}(\text{ClO})_2$. Their reported percent yields for MMH are 0.005% for NDMA and 0.11% for NEMA using NaClO , and 0.0005% for NDMA and 0.014% for NEMA using $\text{Ca}(\text{ClO})_2$. No attempt was made to characterize other reaction products.

Rianda et al. (10) found CH_3OH , CH_3Cl and N_2 to be the main products of the chlorinolysis of MMH at pHs from 6 to 10, with the N_2 accounting for 100% of the nitrogen originally present in the fuel. These carbon-containing compounds account for over 70% of the carbon initially in the MMH. No mention is made of the presence or absence of any minor byproducts except CO_2 .

AE-50. The only study currently available on the neutralization of AE-50 with hypochlorite is the work of Brubaker and coworkers (14,15). The product mixture was considerably less complex than was the case with UDMH, and the overall byproduct concentration was substantially less as well. When NaClO was used, no FDH was seen at all but the substance tentatively identified as its cyclic dimer was a significant product. Also detected were chloroform, DMC, DMF, NDMA, and NEMA. Many byproducts could not be identified. Relatively little change was seen in the reaction products when solid bleach was used. The generally lower byproduct concentration is consistent with the lower UDMH concentration, the mole fraction of UDMH in AE-50 being approximately 0.35, and as expected many of the same byproducts are found as in the UDMH case. The absence of FDH and the presence of NEMA in the AE-50 product mixture indicate that the presence of hydrazine does affect the course of at least some of the reactions involved.

Nitrosoamine Formation. The formation of N-nitrosoalkylamines from the hypochlorite oxidation of methylated hydrazine fuels was observed by Castegnaro et al. (3) and by Brubaker and coworkers (14,15), but not by Mach and Baumgartner (7). The conditions employed by the first two groups were reasonably similar, but differed substantially from those used by Mach and Baumgartner. The overall yields of nitrosoamines found by Castegnaro et al. and by Brubaker et al. were of comparable orders of magnitude, 0.1 to 0.01%, but differences in the relative amounts of various nitrosoamines are apparent. For the system NaClO/MMH, Castegnaro et al. (3) found twenty times as much NEMA as NDMA, whereas Brubaker et al. (26) found no NDMA at all, but instead found comparable amounts of both NEMA and NDEA. Similarly, for the system NaClO/UDMH, Castegnaro et al. (3) found ten times as much NEMA as NDMA, but Brubaker et al. (15) found only NDMA present under normal circumstances. In the system NaClO/AE-50, Brubaker et al. (15) found NDMA as expected, but also somewhat smaller amounts of NEMA. Both groups found that nitrosoamine levels from the oxidation of methylated hydrazines were increased by the presence of methanol.

Brubaker et al. (15) found that nitrosoamine formation could be completely suppressed by acidifying the dilute hydrazine solution to a pH of 2 prior to the addition of hypochlorite. They also found that nitrosoamine formation is an increasing function of temperature over a range from -10°C to

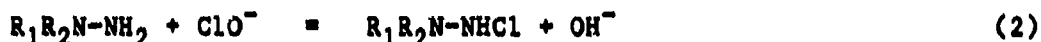
44°C. Finally, in one experiment dilute UDMH solution was added to aqueous NaClO, the opposite of the procedure used in their other experiments. A slightly larger amount of NDMA was found than normal, and NEMA was also found at a level about half that of the NDMA. This was the only UDMH experiment in which NEMA was unambiguously found.

DISCUSSION

The exact mode of the initial attack of hypochlorite on hydrazine or any of its methylated analogs has not been experimentally determined. It is known, however, that the reaction of hypochlorite with primary or secondary amines results in the substitution of a proton by chlorine (16). The most fundamental example is the formation of chloramine from ammonia and hypochlorite:



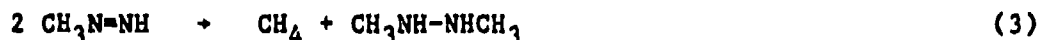
It seems reasonable to suppose, therefore, that the initial attack results in the formation of a chlorohydrazine:



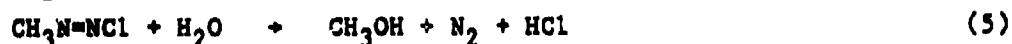
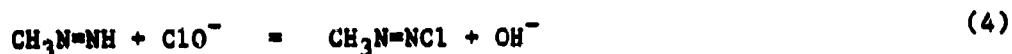
where R_1 and R_2 denote H or CH_3 . The subsequent chemical evolution of the system depends on the fate of the chlorohydrazine formed in reaction (2). Other investigators have proposed similar initial steps in related systems. Overberger and Marks (17) suggested the formation of a 1,1-disubstituted-2-chlorohydrazine as the initial step in the oxidation of 1,1-disubstituted hydrazines with tert-butylhypochlorite, and Cram and Bradshaw (18) proposed the initial formation of RNH-NHBr from RNH-NH_2 in alkaline bromine solution.

Monomethylhydrazine. The most likely fate of the proposed chlorohydrazine intermediate $\text{CH}_3\text{NH-NHCl}$ is loss of HCl and formation of methyldiazene ($\text{CH}_3\text{N=NH}$). Monosubstituted alkyl diazenes of this type have been detected and studied experimentally (19 and references therein, 20,21).

Methyldiazene may react further in at least two distinct ways. Kosower and colleagues (19) observed the bimolecular decay of monosubstituted diazenes and found that the main products are a hydrocarbon and a 1,2-disubstituted hydrazine:

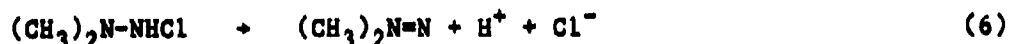


although other unidentified products are also formed. The detailed mechanism for reaction (3) is not known, but may involve free radicals. In addition, the substituted diazene may be oxidized further by hypochlorite. The following sequence seems reasonable:

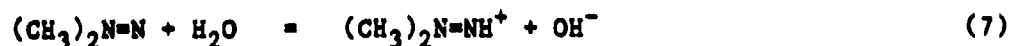


Methanol was found in 65% yield from the chlorinolysis of MMH by Rianda et al. (9,10), in support of the above hypothesis, but the large number of other byproducts observed by Brubaker et al. (14) suggests that reaction (5) is not the only possible fate for 1-methyl-2-chlorodiazene. Complex products would also result from the oxidation of $\text{CH}_3\text{NH}-\text{NHCH}_3$ (symmetric dimethylhydrazine, or SDMH) produced in reaction (3). The NEMA and NDEA found by Brubaker et al. (15) in the MMH reaction products may arise in this way. The presence of chloroform and other chlorinated products suggests also that one or more reaction paths involve the presence of free radicals.

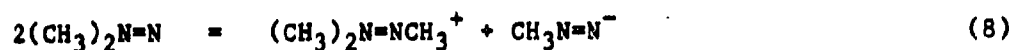
Unsymmetrical Dimethylhydrazine. The 1,1-dimethyl-2-chlorohydrazine formed in reaction (2) is also believed to lose HCl to form a reactive diazene intermediate, but with a somewhat different structure than with MMH:



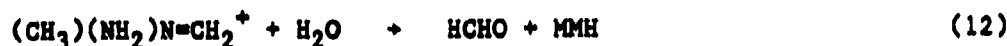
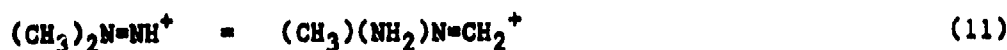
1,1-diazenes of the type shown in reaction (6) were originally proposed by McBride and Kruse (4), and their chemistry has been reviewed by Lemal (22). In aqueous solution, the following equilibrium is also present (22):



Because of the structural difference between 1,1-disubstituted diazenes and monosubstituted diazenes, their respective chemistries are significantly different. A common oxidation product of UDMH is TMT, $(\text{CH}_3)_2\text{NN}=\text{NN}(\text{CH}_3)_2$ (4,7,22). TMT is formed by the direct, bimolecular dimerization of 1,1-dimethyldiazene, and is a major product when the diazene is produced in significant concentrations. At lower concentrations, other reaction pathways are favored over dimerization, with FDH, $(\text{CH}_3)_2\text{N}-\text{N}=\text{CH}_2$, often observed as a major product. At least two possible mechanisms have been proposed in the literature whereby FDH may be produced by the oxidation of UDMH. Mathur and Sisler (8) suggested the following reaction sequence:



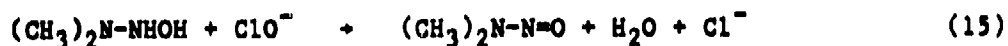
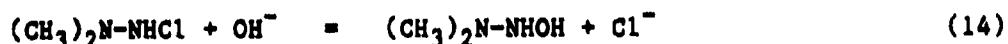
In aqueous systems, instead of reaction (10), the species $\text{CH}_3\text{N}=\text{N}^-$ might hydrolyze to give methyldiazene and a hydroxyl ion. An alternative explanation is that suggested by Banerjee et al. (11):



Tautomers of the type formed in reaction (11) are believed to play a significant role in the chemistry of 1,1-diazenes (22). The formation of a hydrazone from an aldehyde and a hydrazine is well-known (16).

The chemistry that determines the ultimate mix of reaction products is quite complex and poorly understood. As in the MMH case, the presence of chlorinated products may indicate that a free radical mechanism is involved, and may also indicate the involvement of Cl_2 , at least at the part-per-million level.

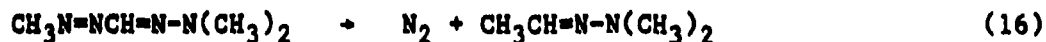
Nitrosoamine Formation. The formation of nitrosoamines at the part-per-million level from MMH, UDMH and AE-50 under a variety of conditions is an extremely important feature of the chemistry of hypochlorite neutralization of hydrazine fuels. The formation of NDMA from UDMH may involve the nucleophilic substitution of the chlorine in 1,1-dimethyl-2-chlorohydrazine by a hydroxyl group, followed by subsequent oxidation of the hydroxyhydrazine by hypochlorite:



Reaction (14) is analogous to the first step in the hydrolysis of chloramine (23), and reaction (15) seems a logical next step in the presence of hypochlorite. This mechanism also explains the observed suppression of NDMA formation in acidic media.

The formation of NEMA and NDEA is not so easy to explain, since it requires the formation of carbon-carbon bonds. One possibility is that N_2 is

split out from, for example, 1,5,5-trimethylformazan to form acetaldehyde dimethylhydrazone, which may undergo further oxidation to give a variety of products:



The formazan has been found in other studies as a product of UDMH oxidation in aqueous systems (3,11) and acetaldehyde hydrazone has also tentatively identified as a reaction product. At present, the mechanism of NEMA and NDEA formation remains unknown, and the formation of NDEA from MMH but not from UDMH or AE-50 and the formation of NEMA from AE-50 but not UDMH as observed by Brubaker et al. (15) remain unexplained.

ACKNOWLEDGMENT

Work performed for Air Force Engineering and Services Center through an agreement with the U.S. Department of Energy, under Interagency Agreement No. N85-14 (MIPR).

REFERENCES

1. Schmidt, E.W., Hydrazine and Its Derivatives, John Wiley and Sons, New York, 1984.
2. Hannum, J.A.E. (ed), Hazards of Chemical Rockets and Propellants. Vol. III. Liquid Propellants., CPIA pub. no. 394, Chemical Propulsion Information Agency, The Johns Hopkins University, Applied Physics Laboratory, Laurel, Maryland, September 1984.
3. Castegnaro, M., I. Brouet, J. Michelon, G. Lunn and E.B. Sansone, "Oxidative Destruction of Hydrazines Produces N-Nitrosamines and Other Mutagenic Species," Am. Ind. Hyg. Assoc. J. 47, 360-364 (1986).
4. McBride, W.R. and H.W. Kruse, "Alkylhydrazines. I. Formation of a New Diazo-like Species by the Oxidation of 1,1-Dialkylhydrazines in Solution," J. Am. Chem. Soc. 79, 572-576 (1957).
5. Boehm, J.R., A.L. Balch, K.F. Bizot and J.H. Enemark, "Oxidation of 1,1-Dimethylhydrazine by Cupric Ions. The Isolation of a Complex of 1,1-Dimethylhydrazine and a Salt Containing the 1,1,5,5 Tetramethylformazanion Ion," J. Am. Chem. Soc. 97, 501-508 (1975).
6. Knoblowitz, M., L. Miller, J.O. Morrow, S. Rich and T. Scheinbart, "Oxidation of Methylhydrazine by Cerium (IV) in Acid Media," Inorg. Chem. 15, 2847-2849 (1976).
7. Mach, M. and A.M. Baumgartner, "Oxidation of Aqueous Unsymmetrical Dimethylhydrazine by Calcium Hypochlorite or Hydrogen Peroxide/Copper Sulfate," Anal. Lett. 12(A9), 1063-1074 (1979).
8. Mathur, M.A. and H.H. Sisler, "Oxidation of 1,1-Dimethylhydrazine by Oxygen," Inorg. Chem. 20, 426-429 (1981).

9. Rianda, R. and M. Easton, "Products of Chlorinolysis of Hydrazine Fuel Waste Waters," Proceedings 1981 JANNAF Safety and Environmental Protection Subcommittee Meeting, 1981.
10. Rianda, R., M.P. Easton, and S.R. Stearn, "Products of Chlorinolysis of Hydrazine Fuels Waste Waters - Part II," Proceedings 1982 JANNAF Safety and Environment Protection Subcommittee Meeting, 1982.
11. Banerjee, S., E.J. Pack, Jr., H. Sikka, and C.M. Kelly, "Kinetics of Oxidation of Methylhydrazines in Water. Factors Controlling the Formation of 1,1-Dimethylnitrosamine," *Chemosphere* 13, 549-559 (1984).
12. Stauffer, T.B. and A.W. Eyl, "Studies on Evaporation of Hydrazine and Procedures for Cleanup of Small Spills," Report No. CEEDO-TR-78-12, Civil and Environmental Engineering and Development Office, Tyndall AFB, Florida 32403 (Aug. 1978).
13. Marsh, W., and B.P. Knox, "USAF Propellant Handbooks - Hydrazine Fuels, Vol. I," Report No. AFRPL-TR-69-149, Air Force Rocket Propulsion Laboratory, AFSC, Edwards AFB, California (March 1970).
14. Brubaker, K.L., J.R. Stetter, J.C. Demirgian, A. Boparai and J.F. Schneider, "Products of the Neutralization of Hydrazine Fuels with Hypochlorite," Proc. 1985 JANNAF Safety and Environmental Protection Subcommittee Meeting, Naval Postgraduate School, Monterey, CA (Nov. 4-6, 1985).
15. Brubaker, K.L., J. Bonilla, V.C. Stamoudis, A.S. Boparai and C.T. Snyder, "Products of the Neutralization of Hydrazine Fuels with Hypochlorite. II," Proc. 1987 JANNAF Safety and Environmental Protection Subcommittee Meeting, NASA/Lewis Research Center, Cleveland, OH (May 5-7, 1987).
16. March, J. Advanced Organic Chemistry, 3rd Ed., John Wiley and Sons, New York, 1985.
17. Overberger, C.G. and B.S. Marks, "Azo Compounds. Oxidation Studies of 1,1-Disubstituted Hydrazines," *J. Am. Chem. Soc.* 77, 4104-4107 (1955).
18. Cram, D.J. and J.S. Bradshaw, "Electrophilic Substitution at Saturated Carbon. XIX. Nitrogen as Leaving Group from an Alkyl Diimide," *J. Am. Chem. Soc.* 85, 1108-1118 (1963).
19. Kosower, E.M., "Monosubstituted Diazenes (Diimides)," *Accts. Chem. Research* 4, 193-198 (1971).
20. Tsuji, T. and E.M. Kosower, "Diazenes. VI.," *J. Am. Chem. Soc.* 93, 1992-1999 (1971).
21. Ackermann, M.N., J.L. Ellenson and D.H. Robinson, "A New Synthesis of Diazenes. The Preparation and Properties of trans-Methyldiazene," *J. Am. Chem. Soc.* 90, 7173-7174 (1968).
22. Lemal, D., "Aminonitrenes (1,1-Diazenes)," pp. 345-403 in Nitrenes, W. Lwowski (ed), Interscience Pub., New York (1970).
23. Anbar, M. and G. Yagil, "The Hydrolysis of Chloramine in Alkaline Solution," *J. Am. Chem. Soc.* 84, 1790-1796 (1962).

OZONATION OF HYDRAZINES AND THEIR ASSOCIATED IMPURITIES

B. J. Jody

P. Kosenka

IIT Research Institute

10 West 35th Street

Chicago, Illinois 60616-3799

S. Lewis

H. Takimoto

H. Judeikis

Aerospace Corp.

Captain J. Betschard

USAF Space Division

ABSTRACT

IIT Research Institute (IITRI) conducted a series of experiments on the ozonation of wastewater containing hydrazine fuels (hydrazine, HZ; monomethyl hydrazine, MMH; and unsymmetrical dimethyl hydrazine, UDMH). Experiments were performed on wastewater containing two different concentrations of hydrazine fuels (3 wt% and 300 ppm) and using various pH levels, ozone flow rates, ultraviolet (UV) radiation levels, and metal catalysts.

Ozone/UV treatment of wastewater containing hydrazine fuels was shown to be capable of destroying the three hydrazine fuels, their associated impurities, and oxidation products including dimethylnitrosamine (DMNA) to environmentally acceptable levels. The DMNA concentration was reduced to below 20 ppt, yielding a "clean solution" free of appreciable concentrations of any harmful species.

EXPERIMENTAL APPARATUS

The experimental apparatus is shown in Figure 1. Pure oxygen from a liquid oxygen Dewar was fed to a Welshbach C-4 ozonator to produce about 3 wt% ozone in oxygen. The ozone/oxygen stream was then bubbled through the reactor containing the simulated wastewater (hydrazine fuels in deionized water). The circulation pump took liquid from the bottom of the reactor and returned it at the top, thoroughly mixing the fuel in the water. A sample taken after the pump ran for several minutes was analyzed to determine the starting concentration of hydrazine fuels in the wastewater. The ozone generator was then turned on and ozone/ oxygen was supplied to the reactor. The circulation pump was kept on during the entire treatment process. The pH of the wastewater was monitored continuously and automatically adjusted by feeding caustic solution or nitric acid solution to the wastewater.

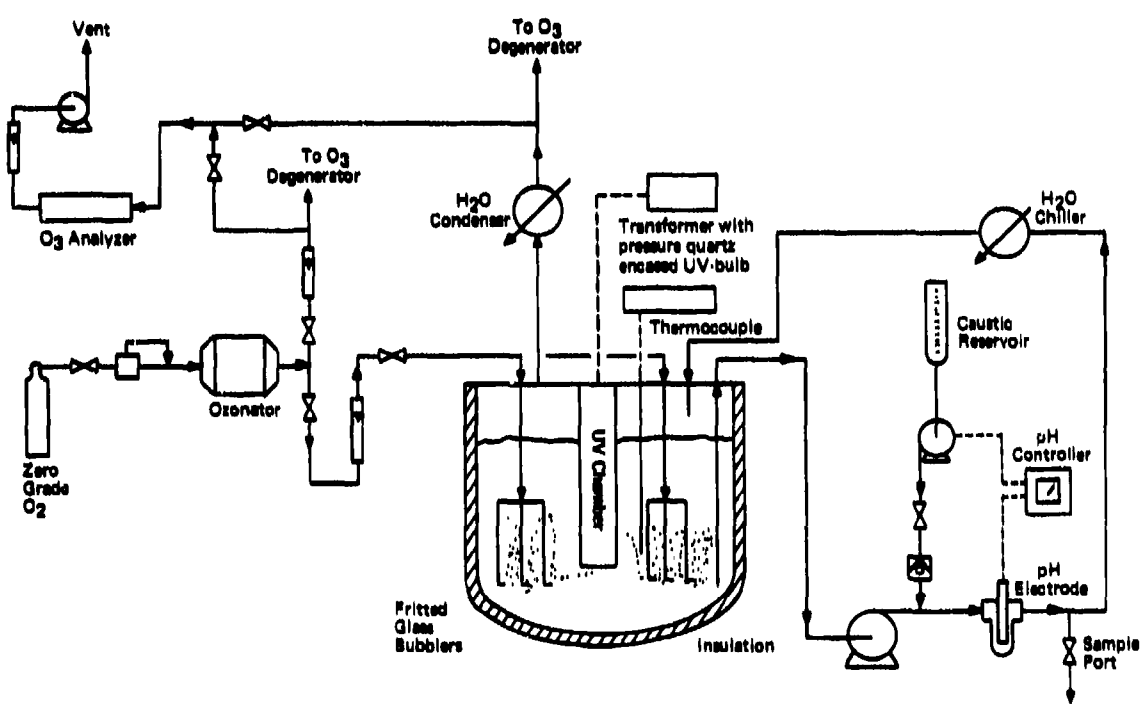


Figure 1. Schematic diagram of pilot test apparatus.

The effluent gas flowed out of the reactor into an ice water-cooled condenser to condense moisture and return it back to the reactor. The cooled gas stream was then passed through a heated alumina catalytic reactor to decompose the ozone before final release to the atmosphere. Split streams from the cooled and dried gas and from the ozonator output were sent to a Dasibi ozone analyzer, Model 1003-HC, where the gases were analyzed to establish the rate of ozone consumption and decomposition in the reactor.

The UV source was also activated when needed. The UV lamp was installed in the reactor in some runs as shown in Figure 1. In other runs it was installed in a separate reactor and water was circulated between the two reactors.

EXPERIMENTAL PROCEDURE

EXPERIMENTS CONDUCTED WITH HIGH CONCENTRATIONS OF HYDRAZINE FUELS

Five pilot-scale (20-L) experiments were conducted at various operating conditions (Table 1) to investigate the feasibility of the ozone/UV process when the hydrazine fuels concentration was about 3 wt%.

TABLE 1. CONDITIONS OF PILOT RUNS.

Run No.	UV Use	Nominal Fuel Conc., wt%		
		HZ	MMN	UDMH
P-1	None	1	1	1
P-2	None	1	1	1
P-3	LPUV ^a	1	1	1
P-4	None	-	3	0
P-5	None	1	3	0

^aLow pressure UV lamp; electrical input = 13.9 W, UV output = 1.9 W, 86% of UV output at 2573 Å, and 10% at 1890 Å.

The following conditions were also common to all the pilot-scale runs: O_3/O_2 flow rate: 14.7 L/min; O_3/O_2 concentration: 3 wt%; pH: 9.5 ± 0.1 ; liquid volume: 20 L; and reactor volume: 28 L. All runs involving UV had air in the annulus surrounding the UV.

EXPERIMENTS CONDUCTED AT LOW pH

Five more bench-scale experiments (Table 2) were conducted at a pH of ~2.5 to investigate whether the reaction mechanisms that take place at low pH result in a more favorable overall destruction of DMNA. One bench-scale run (B-5) was performed at similar conditions but at high pH for comparison purposes. Run B-8 was conducted at mixed pH conditions.

TABLE 2. EXPERIMENTAL CONDITIONS FOR THE FIVE RUNS CONDUCTED AT LOW pH.^a

Run No.	UV Used	pH	HZ Conc., wt%	MMH Conc., wt%	UDMH Conc., wt%
B-5	LPUV ^b	9.5	1	3	-
B-6	LPUV	2.5	1	3	
B-7	None	2.5	1	3	
B-8	None	^c	1	3	-
B-9	LPUV	2.5	1	3	
B-10	LPUV	2.5	2	-	2
B-11	LPUV	2.5	1	1	1

^aIn all the experiments, wastewater volume = 1.25 L, O_3/O_2 flow rate = 3 L/min, O_3 concentration = 3 wt%.

^bLP = Low pressure UV lamp; electrical input = 13.9 W, UV output = 1.9 W, 86% of UV output at 2573 Å, and 10% at 1890 Å.

^cA pH of about 2.5 was maintained for the first 1200 min; it was then increased to 9.5 and maintained at this value for the remainder of the time.

EXPERIMENTS CONDUCTED WITH LOW CONCENTRATIONS OF HYDRAZINE FUEL

Another series of five experiments (B-24 through B-27) was conducted at low hydrazine fuel concentrations (Table 3).

TABLE 3. EXPERIMENTAL CONDITIONS FOR THE FIVE RUNS PERFORMED AT LOW HYDRAZINE FUEL CONCENTRATIONS.

Run No.	Waste-water Vol., L	pH	HZ Conc., ppm	MMH Conc., ppm	UDMH Conc., ppm	O ₃ /O ₂ Flow Rate, ^a L/min	LPUV Lamp, W at 254 nm	Circ. Rates to UV Reactor, L/min
B-24	6	9.5	1700	5000	-	14.3	5.3	0.9
B-25	6	b	100	100	100	0.25	-	-
B-26	6	b	100	100	100	0.25	5.3	0.9
B-27	6	b	-	300	-	0.25	-	-
B-28	6	b	-	300	-	0.25	1.9	0.9

^aOzone concentration is 3 wt% unless stated otherwise.

^bVariable.

DISCUSSION

EXPERIMENTS CONDUCTED WITH HIGH CONCENTRATIONS OF HYDRAZINE FUELS

All five pilot-scale runs (P-1 through P-5) showed the same pattern of destroying hydrazine fuels. Hydrazine fuel destruction in Run P-1 is shown in Figure 2; the formation and destruction of DMNA is shown in Figures 3 and 4. Ozonation alone or with UV radiation at high pH destroyed all three hydrazine fuels tested, their associated impurities, and oxidation by-products including DMNA. Low levels of UV radiation did not improve process performance. The design- and operation-limiting parameter was the destruction of DMNA, not the hydrazine fuels. When we conducted experiments on a synthetic solution containing pure DMNA, the rate of DMNA destruction was faster than when the

DMNA was produced from ozonating the hydrazine fuels. Clearly, other intermediates in the product mixture participate in the DMNA production and destruction mechanisms.

Ozonation of wastewater containing only MMH and HZ (Runs 4 and 5) resulted in significant quantities of DMNA, but an order of magnitude less than when UDMH was present at about one-third the concentration (Runs 1, 2, and 3). The concentration of ozone in the reactor effluent stream was nearly zero while the hydrazine fuels were present, but increased when the hydrazines disappeared and the DMNA concentration was reduced.

Demand for NaOH to maintain a pH of ~9.5 was initially high but gradually tapered off. On the average, about 50 mL of 25% NaOH was needed per liter of wastewater containing about 1% of each of the three hydrazines.

EXPERIMENTS CONDUCTED AT LOW pH

Ozonation at low pH destroyed all three hydrazine fuels and their oxidation products including DMNA. The rate at which the hydrazine fuels were destroyed was about six times slower at a pH of ~2.5 than at 9.5. However, the concentration of DMNA in the wastewater at the time the hydrazines were destroyed was an order of magnitude less than that during treatment at high pH. The final product was very clean. Chromatograms of the final sample of wastewater contained virtually no nitrogen-bearing compounds (detection limit ~30 ppt). Ozonating the hydrazine fuels at low pH (2.5) and then shifting to a high pH (9.5) did not improve the overall performance of the process.

Because the hydrazines are basic and their oxidation products are acidic, HNO_3 and NaOH were added to maintain a pH of 2.5 during the entire treatment time. This increased the volume of the wastewater about 19%.

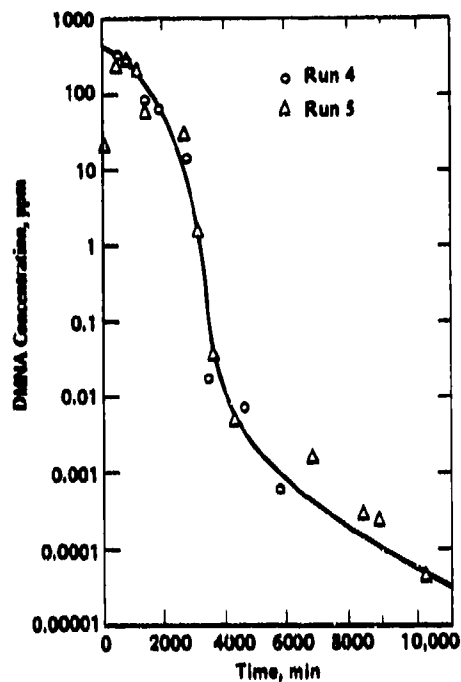


Figure 4. Destruction of DMNA in Runs 4 and 5.

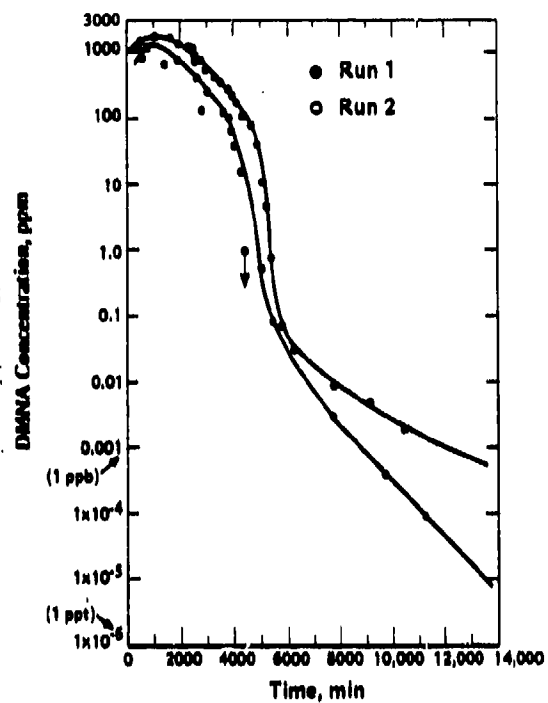


Figure 3. Destruction of DMNA in Runs 1 and 2.

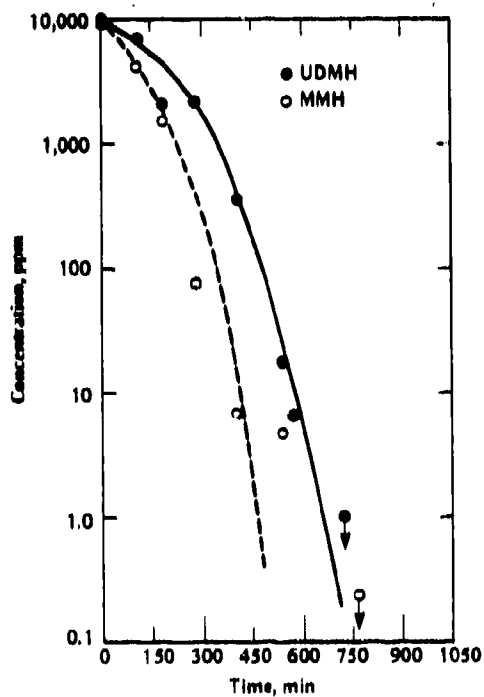


Figure 2. Destruction of UDMH and MMH in Run 1.

Low levels of UV radiation enhanced the rate of DMNA destruction slightly, but had no significant impact on the oxidation rate of the hydrazine fuels. UV, however, resulted in a much cleaner final product.

EXPERIMENTS CONDUCTED AT LOW HYDRAZINE FUEL CONCENTRATIONS

Run B-24. The objective of Run B-24 was to explore the trend of DMNA production and destruction at reduced hydrazine fuel concentrations. A sample analysed 80 min after the start of the experiment (the estimated time for the destruction of the hydrazine fuels) had 28 ppm of DMNA. In previous experiments at the same pH but a high fuel concentration, about 1% of MMH converted to DMNA. Run B-24 showed only a 0.56% conversion, suggesting that the apparent net percent conversion of MMH to DMNA may depend on the initial MMH concentration, among other variables.

Run B-25. The objective of Run B-25 was to generate data on wastewater containing lower concentrations typical of most wastewater expected in the field and using an ozone/oxygen flow rate typical of what a compact mobile ozonation system can attain. This run was conducted without any pH control and UV to serve as a baseline for future experiments.

Initially, the conversion of fuel to DMNA was higher in the low concentration experiments than in experiments at high pH with 10,000 ppm of each fuel. The high concentration experiments produced about 2000 ppm of DMNA from 30,000 ppm of starting hydrazines (Runs 1 and 2, Table 1), a ratio of 0.0667. In Run B-25, the ratio was 50/300 or 0.167, or about 2.5 times more, possibly due to second order side reactions of the UDMH that were not producing DMNA. These reactions would be favored at the high fuel concentrations, but would

not be as important at the lower concentrations. Thus, the $O_3 + UDMH \rightarrow DMNA$ reaction is more dominant.

The decay curve of DMNA followed the same path as observed in the high concentration experiments: an initial fast decay followed by a slower rate of destruction.

The pH dropped to 3 without addition of acid. Our previous experiments had shown that less ozone is needed to keep the solution dosed with ozone at low pH. For treating large volumes of wastewater, this eliminates the need to add substantial quantities of acid or base to change or maintain the pH at a selected level, and also significantly reduces the salt content of the treated water.

A large pH change occurred as the hydrazines were depleted. At 140 min, the total hydrazine concentration was 85 ppm, and the pH of the solution was 8.5. At 247 min, a time when the hydrazines were significantly depleted, the pH of the solution was 3.5, a change 5 pH units in 100 min. This large a change over a short period of time could provide a simple means of monitoring hydrazine decay.

Without UV, the reaction produced low concentrations of DMNA. However, the chromatogram of the final sample showed other peaks larger than the DMNA. This experiment was therefore repeated with UV in Run B-26 to determine its effect with lower starting concentrations of fuel.

Run B-26. A 5.3 watt low pressure UV lamp was used in a side arm reactor. The wastewater circulated through the reactor showed a substantial improvement in the overall destruction rate of the hydrazine fuels. The total time required to destroy the hydrazine fuels to below ~5 ppm was about 60% of

that obtained in Run B-25 without UV. In addition, DMNA fell below 1 ppt in 700 min as compared to 1400 min in Run B-25. These results strongly suggest that UV had a major impact on the destruction rates of the hydrazine fuels and on DMNA.

Run B-27. The objective of Run B-27 was to investigate the production and destruction of DMNA resulting from ozonating wastewater that contains MMH but no UDMH in order to determine the desirability of separately storing and treating wastewater that contains UDMH.

Run B-27 was conducted under the same conditions as B-26, except that the wastewater initially contained only about 300 ppm MMH. The MMH fuel was oxidized to below detectable limits within about 150 min. During ozonation of such low MMH concentrations in the absence of UDMH, there was no net production of DMNA from that initially present in the starting solution. The treatment process can be completed in a few hours depending upon the rate at which ozone was supplied to the reactor. Therefore, when storage facilities are available, wastewater containing low concentrations of MMH and no UDMH should be stored and treated separately.

CONCLUSIONS

The ozone/UV treatment of wastewater containing hydrazine fuels is capable of destroying the three hydrazine fuels, their associated impurities, and oxidation products including DMNA to environmentally safe levels. The process can treat the DMNA to below 20 ppt, yielding a "in solution" free of appreciable concentrations of any harmful species. The ozone/UV process is expected to meet more stringent future regulations without requiring secondary treatment or major modifications. The key operational parameters of the

ozone/UV treatment process are dependence on pH, the presence of metal ions in solution, the ozone supply rate to the reactor, and the UV radiation level.

DEPENDENCE ON pH

The data on pH effects on ozonolysis were obtained primarily using wastewater containing high concentrations (~30,000 ppm) of hydrazines. The oxidation of the fuels is faster under basic than acid conditions (optimum pH = 9.5). However, substantial amounts of DMNA are produced from UDMH at high pH and a lesser amount from MMH. Although DMNA is destroyed with ozone, its rate of destruction decreases when its concentration reaches the sub-ppm range. The final treated solution containing 100 ppt of DMNA or less also contains several other compounds having similar or even higher concentrations. Because of its instability at high pH, higher concentrations and flow rates of ozone are required to maintain the desired concentration in the liquid wastewater. Therefore, the ozone requirements of the treatment process are high at high pH.

Treatment of the hydrazine fuels under acidic conditions (pH = 2.5) proceeded at a slower rate with less net production of DMNA. No net production of DMNA was observed during treatment of wastewater containing about 300 ppm MMH and no UDMH. The total time required to treat the fuels, the DMNA, and other oxidation products was about the same at both pH levels. When UV was added, the process produced a much cleaner treated solution relatively free of other constituents.

Maintaining a selected pH required the addition of NaOH or HNO_3 , increasing the wastewater volume and the concentration of soluble salts. Our experiments, using low concentrations of hydrazine fuels, showed that the same

process performance can be achieved by allowing the pH to drop under the influence of the oxidation products. The pH of fuels containing wastewater is about 9-11. Oxidation of the fuels produces organic acids which, together with the reduction in fuel concentration, lower the pH. Without pH adjustments, the pH could rapidly fall to below 3. The performance of such a process was very similar to what was observed when the pH was initially reduced to 2.5. Therefore when treating wastewater containing a few hundred ppm of fuels, no pH adjustment is required.

DEPENDENCE ON THE PRESENCE OF METAL IONS IN SOLUTION

Metal ions in solution catalyze the oxidation of the fuels. In addition, DMNA and metal ions form complex compounds. As DMNA concentration in solution drops during treatment, additional DMNA is released into solution, resulting in a slower "apparent" destruction rate. The presence of metal ions in solution may also catalyze DMNA, producing side reactions. However, it is impractical and almost impossible in the field to preclude trace amounts of metal ions, especially iron, in wastewaters. The low pH that results from the oxidation of the hydrazine fuels causes some corrosion of even 316 stainless steel. The wastewater generated by cleaning spills and washing empty fuel tanks also contains some metal ions.

Therefore, design and operation parameters should be developed, taking into consideration that metal ions, especially iron, will be present. The use of expensive glass- or Teflon-lined reactors is not economical and will not solve the problem completely.

DEPENDENCE ON THE OZONE SUPPLY RATE TO THE REACTOR

The oxidation rate of the hydrazine fuels is dependent on the rate at which ozone is supplied to the reactor. The time it takes to destroy the fuels can thus be shortened if the supply rate of ozone is increased. As the fuels disappear and the concentration of the oxidation products is reduced to the ppm level, however, the demand for ozone decreases, especially when operating at low pH. At a given ozone concentration in the stream supplying the reactor, the concentration in the reactor effluent stream is governed primarily by the ozone decomposition rate as it goes through the reactor. (The rate at which ozone is consumed in the reaction at the later stages of the treatment process is negligible.) The ozone decomposition rate is enhanced by UV radiation.

The concentration of ozone in the effluent stream determines the ozone concentration in the liquid since the two quantities are related by Henry's Law, and its concentration in solution is what influences the reaction rate. Ideally, the flow rate should be high enough to give near saturation of the water with ozone corresponding to the inlet ozone concentration.

Practically, the ozone production facility must be carefully designed, taking into consideration not only the reaction rates but also the economics of procuring and operating the ozonator system, as well as total ozone decomposition. Size constraints and quantities of waste to be treated must also be factored into the final decision.

DEPENDENCE ON THE UV RADIATION LEVEL

Irradiating wastewater containing high concentrations of hydrazines with low levels of UV did not improve the decay rates of the hydrazine fuels or the DMNA. However, the UV did reduce the concentration of other compounds present in the final product and so helped generate a cleaner final product. UV radiation also noticeably reduced the time required to destroy the hydrazine fuels when their initial concentration was low (~300 ppm), and reduced the net production of DMNA. The UV was thus beneficial in reducing the total treatment time, resulting in less ozone consumption and more effective use of the treatment hardware. Increasing the radiation level further improved the performance of the treatment process. Turning off the UV source during portions of the treatment time increased the concentration of some compounds in the final product.

The treatment system should therefore include a UV reactor that is energized continuously during the entire treatment time. The UV radiation level should be determined based on its effect on the process performance, capital and operating cost, and physical size requirements.

MODELING THE OZONOLYSIS OF HYDRAZINES WASTEWATER

H. S. Judeikis
The Aerospace Corporation
P. O. Box 92957
Los Angeles, CA 90009

ABSTRACT

Modeling of the ozonolysis of wastewaters containing hydrazine propellants is described. Destruction of the hydrazines is rapid and leads to the production of intermediates, some of which help to destroy the hydrazines themselves. The rate limiting process in the overall ozonolysis treatment is, however, the destruction of dimethyl nitrosamine (DMNA), a potent animal carcinogen produced during the ozonolysis of the hydrazines. The data indicate that, especially at low (≤ 1 ppm) DMNA concentrations, this process involves the slow conversion of another intermediate to DMNA which is then rapidly destroyed by ozone.

INTRODUCTION

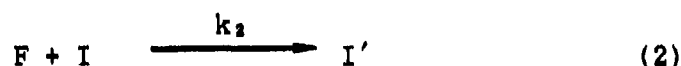
Numerous schemes have been proposed for the chemical treatment of wastewaters containing hydrazine propellants (see for example Reference 1). These treatments which include aeration, oxygenation, chlorination and hydrogen peroxide treatments, among others, have been successful to varying degrees. Most studies however, have focused only on the destruction of the hydrazine propellants, and have paid little heed to intermediates or side products formed during the treatment. The consequences of such neglect can be significant. In the case of the copper catalyzed hydrogen peroxide treatment of unsymmetrical dimethylhydrazine (UDMH), it has been shown that copious quantities of dimethyl nitrosamine (DMNA), a known animal carcinogen, are formed (Reference 2).

Ozonolysis of hydrazine fuels wastewater have been shown to be an effective treatment by the Illinois Institute of Technology Research Institute (IITRI, Reference 3). Although intermediates, including DMNA, are formed during the treatment, these are destroyed by continued ozonolysis. Here the ozonolysis of hydrazines wastewater is discussed, particularly with regard to the IITRI data, with an eye to modeling the waste treatment.

OZONOLYSIS OF HYDRAZINES

The IITRI data led to the following observations regarding ozonolysis of hydrazines fuels wastewater in alkaline solution: 1) Fuel destruction rates were limited by the rate of ozone input, 2) while destruction was rapid, observed "rate constants" were five to six orders of magnitude lower than the true kinetic rate constants (10^7 - 10^8 l/mole min) as measured using stopped-flow techniques in our laboratory, and 3) initial mole ratios of fuel to ozone consumption were about 2-5, this ratio decreasing to less than unity and approaching zero as the ozonolysis proceeded. Acidic ozonolysis led to similar observations except that initial destruction rates were slightly lower and the initial fuel to ozone consumption molar ratio did not exceed unity.

These observations suggest the following generalized reaction scheme for ozonolysis of the hydrazines fuels:



where F is hydrazine (HZ), monomethyl hydrazine (MMH) and/or UDMH and I and I' are unspecified intermediates. Here the value(s) of k_1 are not true kinetic rate constants(s) but include mass transport considerations involving ozone diffusion out of an O_3 - O_2 gas bubble (3% O_3 in O_2 is typically bubbled through the fuels solutions) and

reaction in the aqueous phase (reaction may also occur in the gas phase). It can be shown that for a limiting reagent (O_3) being bubbled through a high concentration solution (hydrazines), that virtually all of the O_3 will be consumed until the fuel(s) concentration(s) drops to certain low values, the latter dependent on the bubble size and residence time in the reactor, after which the ozone concentration in the effluent gas bubble will rapidly increase.

The model described above, assuming total O_3 consumption until experimental breakthrough (O_3 in effluent gas from the reactor) is observed, described alkaline ozonolysis of the hydrazines quite well. An example is shown in Figure 1 for ozonolysis of an alkaline solution containing 3% MMH and 1% HZ. Here (k s are in units of $l/mole.min$) $k_1 = 500(MMH)$, $k_1 = 200(HZ)$ and $k_2 = 0.02$, $k_3 = 7$ and $n = 3.6$ (for both MMH and HZ). It will be noted that the model describes the hydrazines destruction quite well over more than four orders of magnitude in concentration and mimics the ozone profile in the effluent gas stream as well.

Similar results were obtained for other alkaline ozonolysis data. Application of the model to acidic ozonolysis was moderately successful, but did not fit the data as well as in the former case. Better fits of acidic ozonolysis would probably require consideration of the facts that the hydrazines are protonated in acidic solution and direct attack of ozone on the protonated species occurs at considerably slower rates than the ozone attack on the unprotonated hydrazines.

At about this point in time it was realized that ozonolysis of DMNA, produced as an intermediate during ozonolysis of MMH and UDMH was really the rate limiting step in the overall treatment. Consequently, efforts were directed toward the ozonolysis of DMNA.

OZONOLYSIS OF DMNA

Ozonolysis of aqueous solutions containing MMH and/or UDMH led to rapid production of DMNA (Reference 3). As the fuels concentrations approached zero, the DMNA concentration peaked and then rapidly decreased to $\sim 1ppm$ or less, after which the DMNA destruction

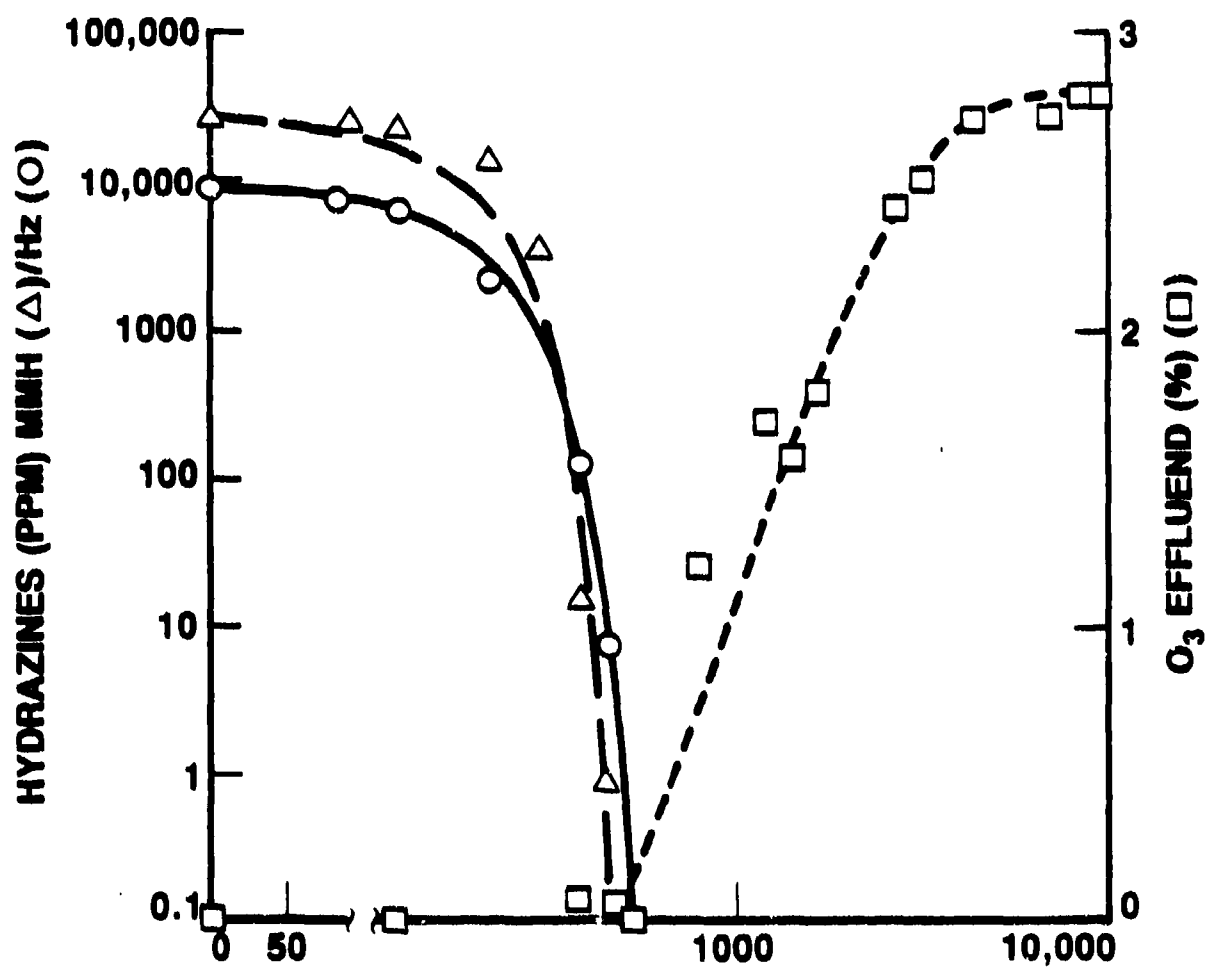


Figure 1. Ozonolysis of a 3% MMH + 1% hydrazine solution. Experimental data are: MMH (Δ); HZ (\circ); O₃ (\square). Solid and dashed curves are model calculations.

continued at a slower rate. Additional experiments with ozonolysis of aqueous solutions of pure DMNA led to rapid destruction without the slowdown at ≤ 1 ppm. In the latter experiments the rate constant for DMNA destruction was ~ 300 l/mole min, which compared favorably to the value observed for gas phase ozonolysis of DMNA of ≤ 200 l/mole min (Reference 4). These observations suggest the scheme for production and destruction of DMNA as:



followed by (once the hydrazine fuels, F are destroyed)



where N is the DMNA concentration and X an unspecified intermediate. Reactions (4) and (5) may actually involve several steps each. Reactions (6) and (7) are the dominant reactions involving DMNA, once the hydrazine fuels are destroyed.

Reaction (6) is simply the ozonolysis of DMNA which should occur at the same rate as ozonolysis of pure DMNA. In fact, the rate of destruction of DMNA observed during the fast portion of decay after the hydrazines are destroyed is approximately 3-5 times slower. This is most likely due to competition for the ozone between DMNA and other ozone consuming intermediates which have been shown by IITRI to be present in the reaction mixture.

Reaction (7), the slow production of DMNA from ozonolysis of X (the latter DMNA then destroyed via reaction 6) could then result in the observed slowdown of DMNA destruction at ≤ 1 ppm.

Kinetically we may write, for reactions (6) and (7)

$$\frac{dN}{dt} = k_7(X)(O_3) - k_6(N)(O_3) \quad (8)$$

Assuming a constant ozone concentration, which is approximately true a short time after the hydrazine fuels have been destroyed, this equation may be integrated to yield

$$N + A \cdot \exp(-k'_7 t) + B \cdot \exp(-k'_6 t) \quad (9)$$

where $k'_6 = k_6(O_3)$, $k'_7 = k_7(O_3)$, $A_0 = k'_7 X_0 / (k'_7 - k'_6)$, $B_0 = N_0 - A_0$ and N_0 and A_0 are the concentrations of DMNA and X extrapolated to $t=0$.

This simple model fit all of the data, whether from alkaline or acidic ozonolysis experiments, exceedingly well. An example is shown in Figure 2 for an alkaline ozonolysis experiment where time axis has been shifted ($t=0$ here is actually ~ 3600 min after the start of ozonolysis of a 1% HZ plus 1% MMH solution) to take $t=0$ as the time the ozone concentration approaches a constant value. Note the good agreement between the experimental data points (circles) in the figure and the model fit (solid curve fitting equation 9 to the data using non-polynomial least squares fitting techniques) over some seven orders of magnitude in DMNA concentration.

The key provision of this model is that reaction (7), the slow oxidation of an intermediate to DMNA, is the step that makes the overall destruction of DMNA the rate limiting process in the ozonolysis of the hydrazine fuels. It also suggests there should be an intermediate in the reaction mixture that decays at the same rate as DMNA during the slow portion of the DMNA destruction.

Indeed, examination of the IITRI gas chromatographic data from these experiments indicated that just such an intermediate does exist, having a retention time of 24 ± 1 min on the columns they used. An example is shown in Figure 3. The circled points in that figure are the DMNA data, the solid curve the model fit, the triangular points the intermediate at 24 ± 1 min and the dashed line a least squares exponential fit of the triangular points. The least squares slope for the slow portion of the DMNA decay in Figure 3 (k'_7 in equation 9) is $7.7 \times 10^{-4} \text{ min}^{-1}$, while the least squares slope for the intermediate is $8.6 \times 10^{-4} \text{ min}^{-1}$. Similar agreement was observed in the only other experiment for which detailed data were available, $12.4 \times 10^{-4} \text{ min}^{-1}$ versus $10.7 \times 10^{-4} \text{ min}^{-1}$, respectively. As yet, the 24 ± 1 min intermediate has not been identified.

CONCLUSION

Simple models have been derived that describe the ozonolysis of aqueous solutions of hydrazines fuels, and especially the ozonolysis

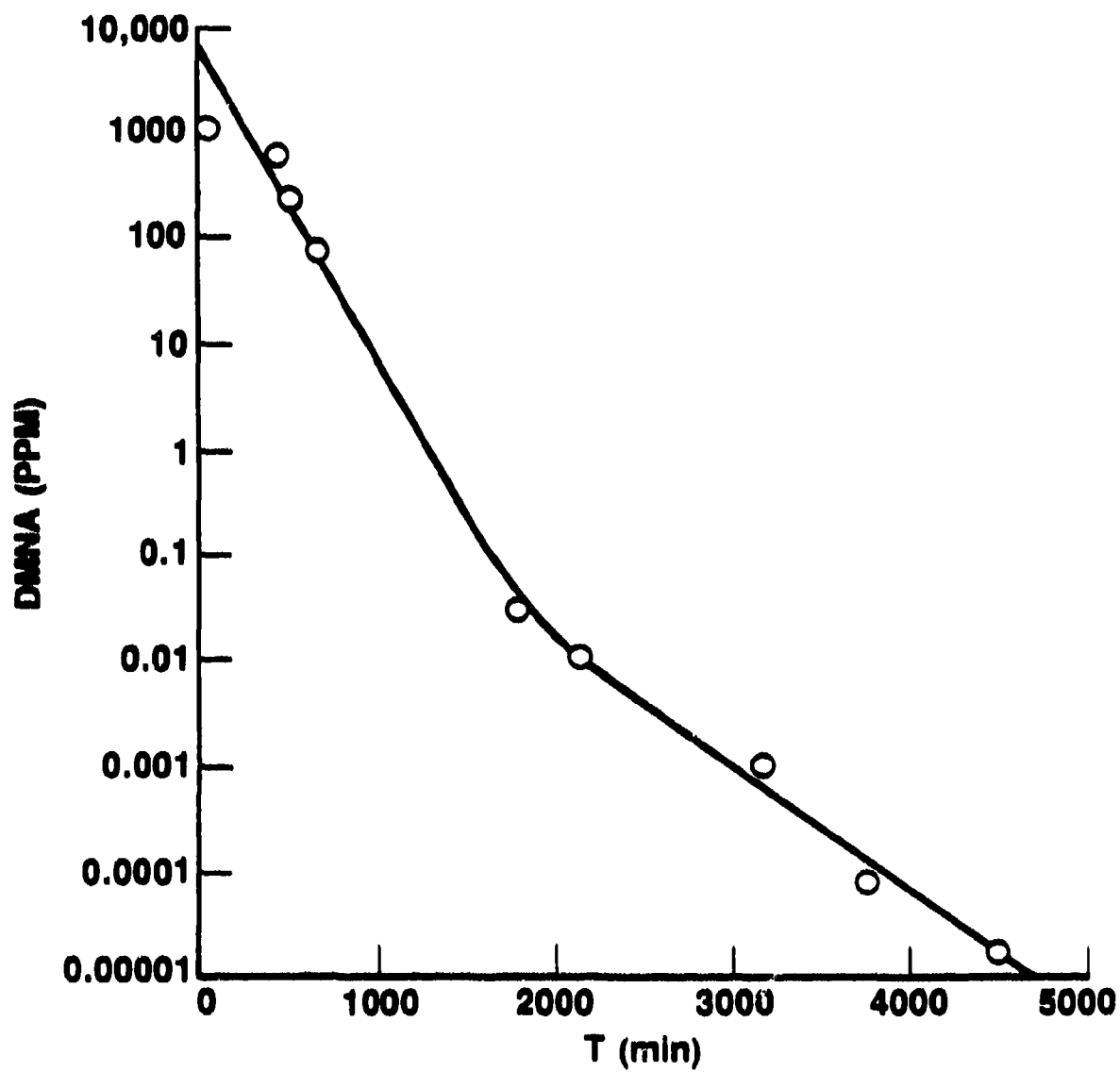


Figure 2. Destruction of DMNA during ozonolysis of a 1% MMH + 1% hydrazine solution. Open circles are experimental data; solid curve is a model fit.

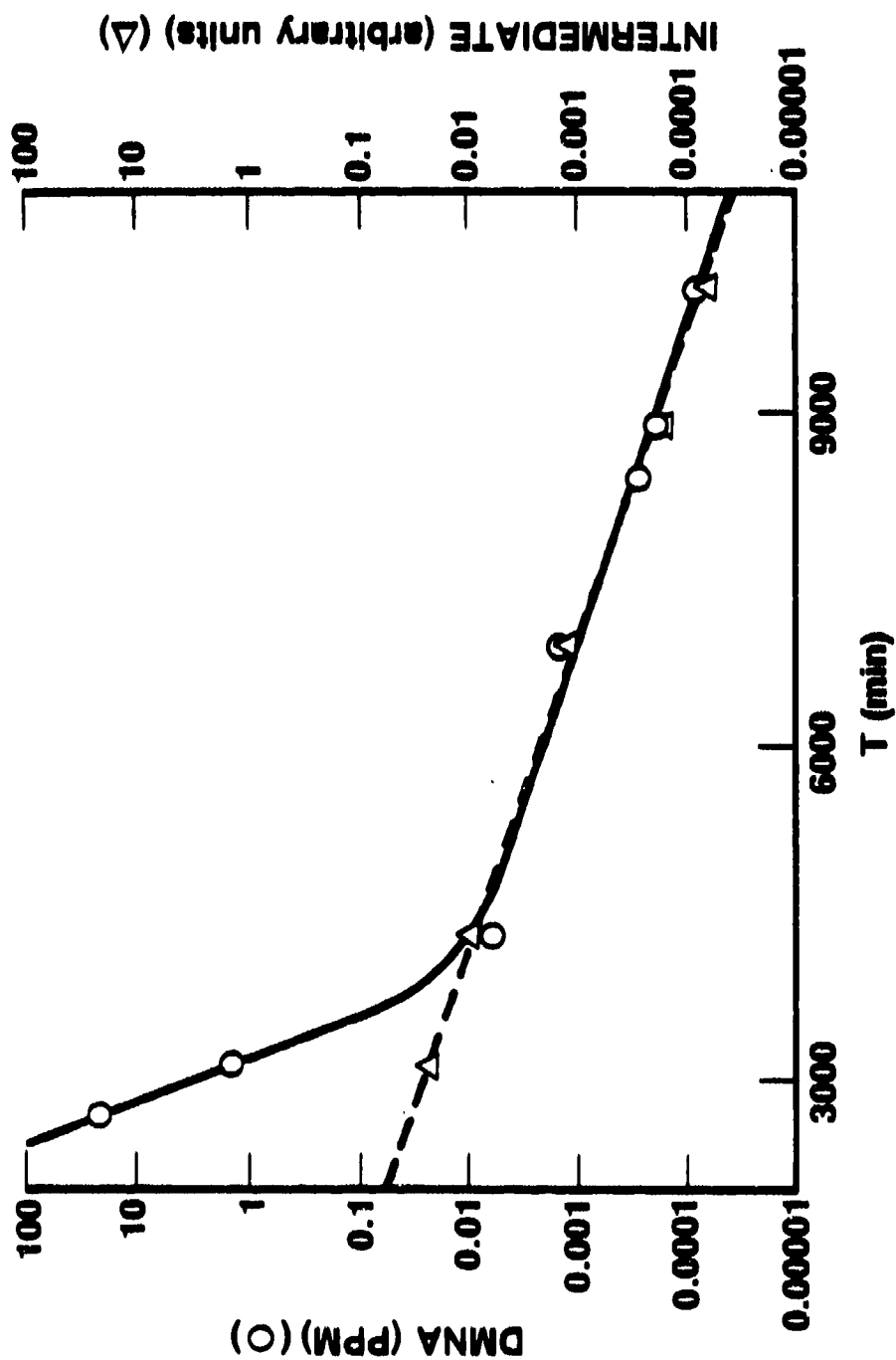


Figure 3. Destruction of DMNA and unidentified intermediate during ozonolysis of 3% MPH + 1% hydrazine solution. Circles and solid curve are experimental data and model fit of DMNA destruction. Triangles and dashed line are experimental data and least squares fit of data for destruction of the unidentified intermediate.

of DMNA, produced as an intermediate in the treatment process, quite well over many orders of magnitude in concentration. The models indicate that the overall rate limiting step in the treatment process occurs after all of the fuels have been destroyed and the DMNA concentration reduced to \leq 1ppm. This step involves the slow conversion of an as yet unidentified intermediate to DMNA.

ACKNOWLEDGEMENTS

The author gratefully acknowledges Sherwin Lewis and Dr. Hideo Takimoto of The Aerospace Corporation for their support of this work, and Dr. Bassam Jody of IITRI and Dr. Erik Neuman, formerly of IITRI for supplying and discussions of the data discussed herein.

REFERENCES

1. T. E. Bowman, et al, Disposal of Hypergolic Propellants, Final Report, NASA-CR-147903, Florida Institute of Technology, November 1974.
2. M. H. Mach and A. M. Baumgartner, Analytical Letters 12 (A9), 1063(1979).
3. B. J. Jody, Illinois Institute of Technology Research Institute, paper presented at this Conference.
4. E. C. Tuazon, et al, Environ. Sci. Technol. 18, 49(1984).

FUEL NEUTRALIZATION BY OZONE OXIDATION

A. B. Swartz, Test Operations Engineer
Lockheed Engineering and Management Services Co.
NASA-JSC White Sands Test Facility
Las Cruces, NM 88004
R. E. Agthe, I. D. Smith, and J. P. Mulholland

ABSTRACT

The viability of a hazardous waste disposal system based on ozone oxidation of hydrazine fuels at low aqueous concentrations in the presence of ultraviolet light (UV @ 2.537×10^{-7} m or 8.324×10^{-7} ft) excitation has been investigated. Important parameters investigated include temperature, solution pH, and ultraviolet light power. Statistically relevant experimentation was done to estimate main factor effects on performance. The best available chemical analysis technology was used to evaluate the performance of the system.

INTRODUCTION

BACKGROUND

White Sands Test Facility (WSTF) currently uses chlorine oxidation as the disposal method for dilute concentrations of waste hydrazine fuels. This process, however, is not a totally effective method because it creates partially oxidized compounds and chlorinated and cyclic hydrocarbons, which in some cases are more hazardous than the waste hydrazine fuels. In addition, this process is unsatisfactory because of the fact that the process is carried out in open tank reactors, allowing volatile hydrocarbons to escape to the open air. Because of the concern over this inadequate disposal method, the "Monomethylhydrazine (MMH) Fuel Neutralization" project was initiated. The project was initially funded by the Directors' Discretionary Fund (DDF). The DDF is implemented with center funding when a vital project is unable to receive outside financing. Subsequent funding was obtained from sources devoted to solving environmental problems. Monomethylhydrazine was selected as the test hydrazine, for the matrix optimization experimentation, since the large

majority of WSTF hazardous waste contains this fuel as a constituent because of the Space Shuttle engine testing programs. This project was created to study the problem in two phases. Phase 1 was implemented by the WSTF chemical laboratory to evaluate viable methods of hydrazine(s) disposal. The NASA test report, TR-382-001, "Oxidation of Aqueous Solutions of Hydrazine, Monomethylhydrazine, and Unsymmetrical Dimethylhydrazine (UDMH) by Ozone and Peroxydisulfate" indicated the ozone/ultraviolet (UV) photo-oxidation (Reference 11) process was the preferable disposal method. Phase 2, the design, construction, and evaluation of a pilot scale reactor based on the ozone/UV process, has been completed. This report is designed to give a concise overview of the findings of the phase two experimentation. A NASA test report, TR-469-001, "Pilot Plant Study of MMH Neutralization by Ozonation" (in print), will cover the experimentation in greater detail.

PURPOSE

The focus of this experimentation was to create an Environmental Protection Agency non-regulated hazardous waste (Reference 3) disposal process for hydrazine propellant(s) as the hazardous constituent, and to prove the effluent from the reactor meets all EPA and state regulations using the best available analytical chemistry methods, prior to discharging it to grade.

SYSTEM DESCRIPTION

The ozone/UV pilot plant is made up of several subsystems, Fig. 1. The first subsystem consists of a Welsbach Ozone Systems T-408 ozonator which is guaranteed to produce at least eight grams of ozone per hour at a concentration of no less than two percent by weight (wt%) when using MIL-0-27210E grade bottled oxygen flowing at $5.664 \times 10^{-5} \text{ M}^3/\text{s}$ ($0.1125 \text{ ft}^3/\text{min}$). A Brinkmann constant temperature bath is used to lower the operating temperature of the T-408 ozonator to approximately 287.15 K (491.67°R), to increase the ozone production to approximately 2.75 wt% at an oxygen flowrate of $6.666 \times 10^{-5} \text{ M}^3/\text{s}$ ($0.1413 \text{ ft}^3/\text{min}$). An in-line drier is installed between the ozonator and the oxygen source to prevent moisture contamination. The second subsystem consists of the reactor and related hardware. The reactor is a modified spray tower using six (6) spray nozzles capable of flowing $6.308 \times 10^{-5} \text{ M}^3/\text{s}$ (0.1337

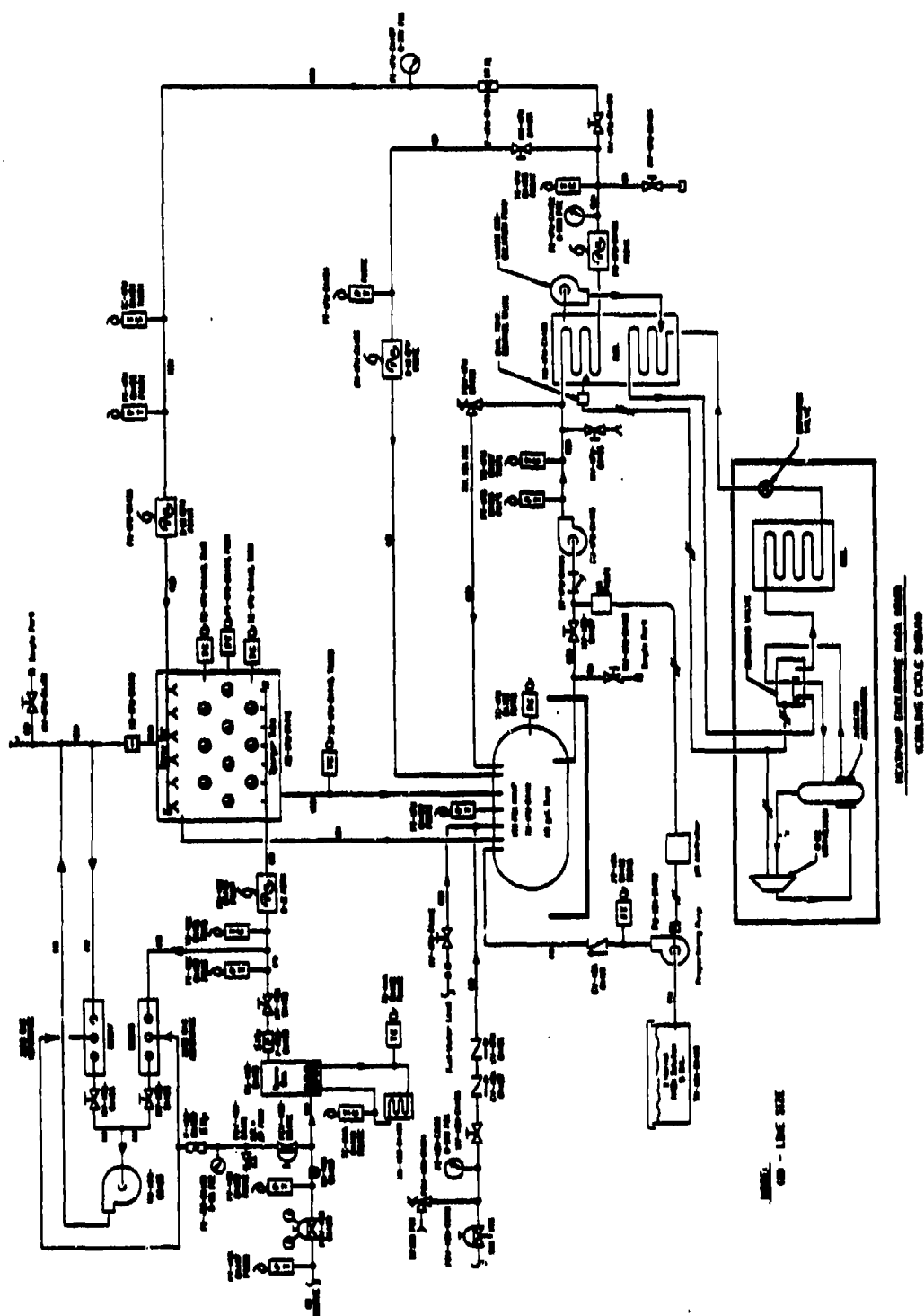


Figure 6. Ozone/UV Photo-Oxidation Three Variable System Trends

ft³/min) at 790828.9 N/M² (114.696 psia), Fig. 2. The liquid is introduced into the reactor as a finely divided spray with a residence time of approximately 14-seconds. The ozone is injected through sparging tubes at the bottom of the reactor countercurrent to the incoming liquid spray. Twenty-three (23) General Electric Germicidal Lamps, model G30T8, rated at an average output of 6.6 Watts of UV light at a wavelength of 2.537×10^{-7} m (8.324×10^{-7} ft), are mounted horizontally inside the reactor chamber for a total of 151.8 W (517.9 BTU/H), Fig. 2. The UV lights are mounted through the sides of the reaction chamber using a 50 derometer UV and ozone stabilized EPDM rubber grommet with an overcoat of GE RTV #108 clear silicone rubber. All other exposed surfaces inside the reactor/spray chamber are 316S stainless steel to

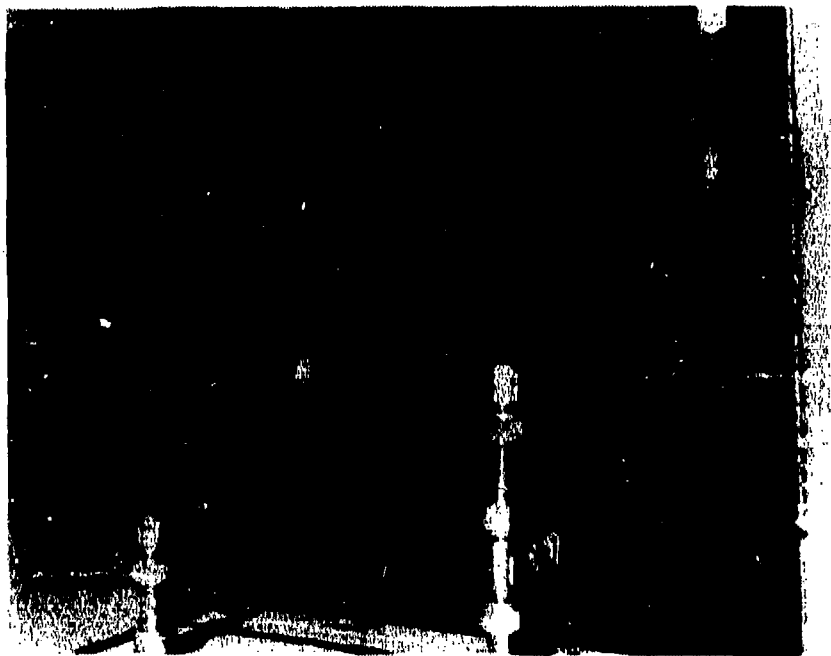


Figure 2. Ozone/UV Reactor Interior

reduce oxidation. Underneath the reactor is a sump tank which holds the bulk of the fluid. A 12.2 m (40 ft) vent stack with a mist eliminator extends above the reactor. The process fluid is circulated from the sump tank by a pump, through a heat exchanger, to the spray nozzles, through the reactor and over

the UV lights, and back to the sump tank, Fig. 3. The sump tank also has a fuel and water inlet line to allow for initial charging of the system. For each trial the tank is filled with approximately $1.325 \times 10^{-1} \text{ M}^3$ (4.68 ft^3) of

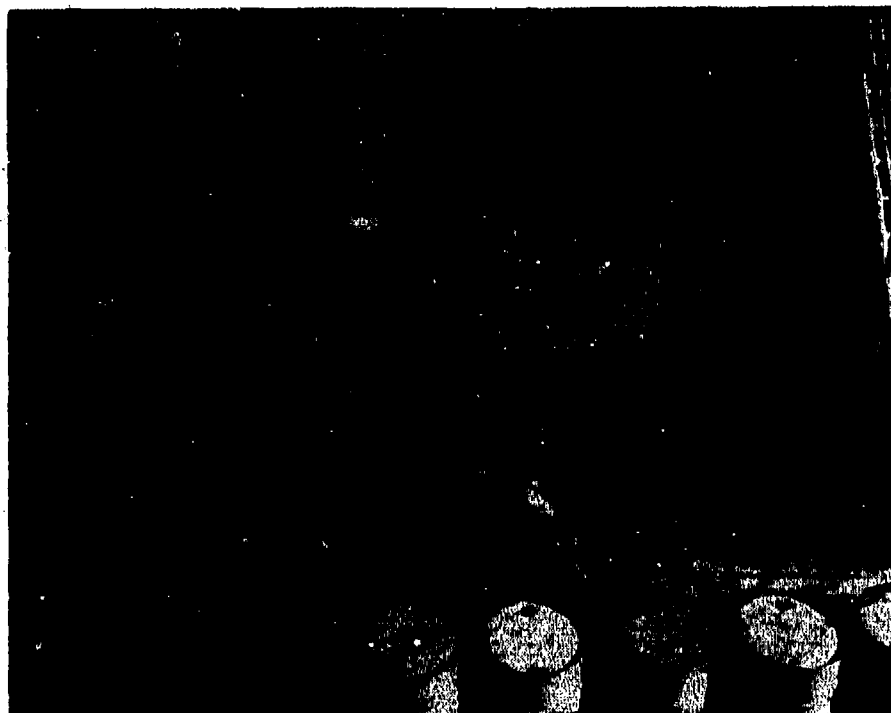


Figure 3. Ozone/UV Pilot Plant Reactor

deionized water, JSC-SPEC-C-20C. A Signet microprocessor pH meter and controller maintains the pH of the basic hydrazine solution, to ± 0.5 pH, by injecting a two normal caustic solution of sodium hydroxide, 2N NaOH. Beneath the whole assembly is a secondary containment system, an aluminum catch basin, to retain liquid in case a spill occurs or a leak develops. The third subsystem consists of the electrical hardware. The systems' control console, Fig. 4, features the UV light control panel and indicator assembly, the PCI Ozone Corporation in-line ozone monitors, model HC-1, the caustic and circulation pump controls, PCI Ozone Corporation ambient ozone personnel safety monitor, model LC-1 (the TLV of ozone is $1.0 \times 10^{-4} \text{ Kg/M}^3$ or $6.245 \times 10^{-6} \text{ lbm/ft}^3$), and the system alarms. The pilot plants' instrumentation is routed from the testing area through the Data Acquisition and Control System to a video display in the control center allowing remote monitoring of the system. Digitized data storage is available at a rate up to 1000 samples per second.

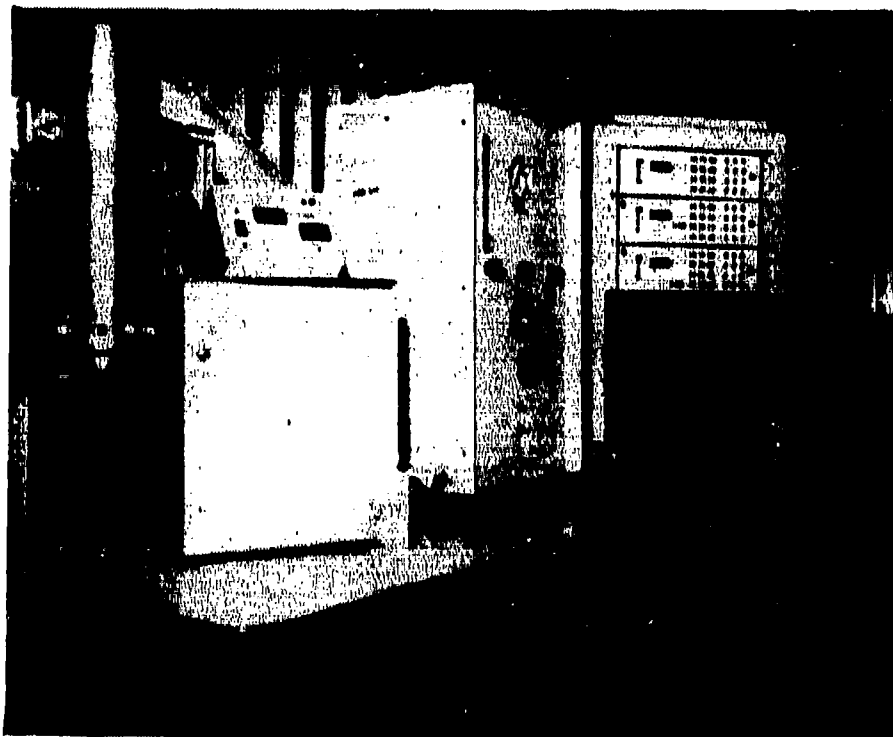


Figure 4. Ozone/UV Pilot Plant Mini-Heat Exchanger, Ozonator, and Control Console

TESTING

EXPERIMENT MATRIX DESIGN

The testing of the ozone/UV photo-oxidation pilot plant was designed from the outset as a statistical optimization experiment. The statistical optimization was done using the Hadamard Matrix Design (Reference 4) Advanced Programming Language (APL) program which reduces the number of repetitions required for statistical significance while retaining the confidence factors selected by the experimenter. The variables initially chosen for investigation were ozone concentration, reaction temperature, UV power, and solution pH. During the course of the testing it was decided that a variable must be eliminated and the number of trials reduced because of funding limitations. The ozone concentration variable was eliminated from consideration and was fixed at its high level, 2.75 wt% in oxygen. The revised test matrix, Matrix IB, was

TRIAL	I	pH	[O ₃] _g	UV
1	+	+	+	+
2	-	+	+	+
3	+	-	+	+
4	-	-	+	-
5	+	+	+	-
6	-	+	+	-
SETTING	T (K/°R)	pH	[O ₃] _g (wt%)	UV (W)/(BTU/H)
(+)HIGH	313.06/585.17	11	4.8	181.8/44.49
(-)LOW	288.89/514.07	9	---	79.2/23.21

Figure 5. Hamard Matrix IB

designed as an 6 x 3 Resolution IV Hadamard Matrix, Fig. 5, using a confidence level of 85% for both alpha (α) and beta (β) type errors. The matrix design was prepared assuming the intrinsic variance (γ) of the system from trial to trial was

equal yet unknown. The Resolution IV Matrix Design estimated all main factor contributions, but not two-factor interactions since they were confounded with other two-factor interactions; the system variance must be known to separate the two-factor interaction effects.

ENVIRONMENTAL PROTECTION AGENCY VALIDATION TESTS

After the statistical optimization experiments were completed a series of five EPA validation tests were conducted. The validation tests were performed at the optimum settings as determined from the Resolution IV Matrix Design analysis APL program. The tests included a water blank, a hydrazine test, two monomethylhydrazine tests, and a test with unsymmetrical dimethylhydrazine. The tests were conducted to evaluate the system as a prospective EPA non-regulated hazardous waste disposal facility. All tests started with an initial fuel concentration of $5.0 \times 10^{-1} \text{ Kg/M}^3$ ($3.123 \times 10^{-2} \text{ lbm/ft}^3$).

CHEMICAL ANALYSIS METHODS

MATRIX TRIALS

The White Sands Test Facility Chemistry Laboratory supported the operation of the ozone/UV photo-oxidation pilot plant reactor statistical optimization Hadamard Matrix Design for the destruction of monomethylhydrazine with three types of aqueous chemical analysis techniques. The first method was constant current coulometry for the determination of the mass of MMH in water. This method entailed the electrochemical generation of chlorine from sodium

chloride. The chlorine produced then oxidized the monomethylhydrazine through a two electron transfer process (Kg-mole per Kg-mole or lb-mole per lb-mole) and when the MMH solution was exhausted the endpoint was detected. The concentration of chlorine-oxidizable material was then determined. This method was not specific for MMH and did not detect certain organic compounds, like methanol. The detection limit of the instrument was approximately 5.0×10^{-10} Kg (1.1023×10^{-9} lbm) for hydrazine when using 5.0×10^{-5} M³ (1.77×10^{-3} ft³) of sample. The second method was the spectrophotometric determination of formaldehyde through reaction with chromotropic acid. Chromotropic acid and formaldehyde react to form a light purple colored solution which absorbs visible light, and the concentration was determined using Beer's Law; the concentration was directly proportional to the absorbance. The detection limit of the analysis was 1.25×10^{-9} Kg (2.757×10^{-9} lbm) of formaldehyde when using 2.5×10^{-5} M³ (8.829×10^{-4} ft³) of sample. This test was not specific for formaldehyde, and did have some type of interferant which sometimes altered the color. The third method was gas chromatographic/thermionic ionization detection for the determination of nitrosodimethylamine (NDMA) in water. The NDMA was separated on the chromatographic column with reproducible retention time and quantified versus a NDMA standard solution. The detection limit of NDMA by this method was 1.0×10^{-14} Kg (2.205×10^{-14} lbm) when using 1.0×10^{-9} M³ (3.53×10^{-8} ft³) of sample.

In addition to the aqueous chemical analysis, the reactor's vent gas was analyzed for vapors of MMH which might off-gas during the circulation of fluid through the reaction spray-chamber. To determine the concentration of MMH in humidified oxygen and ozone a sulfuric acid coated firebrick was used to trap the MMH. The amount of MMH was then determined as chlorine-oxidizable substance with constant current coulometry. The concentration in the sample gas was then calculated from the known volume of gas sampled and the mass of MMH detected.

ENVIRONMENTAL VALIDATION TESTS

Two levels of testing were conducted for the EPA validation testing. Level one used two chemical analysis techniques to monitor the reaction's progress toward completion. The first method was constant current coulometry for the deter-

mination of the mass of hydrazine fuel in water, as described above. The second chemical analysis method used was the EPA approved method for determination of total organic carbon (TOC) (Reference 5). In brief the instrument converts all carbon to carbon dioxide and then uses an infrared spectrophotometer to detect the carbon dioxide. The detection limit for the instrument was approximately 1.0×10^{-9} Kg (2.2046×10^{-9} lbm) for carbon as carbon dioxide when using 1.0×10^{-6} M³ (3.53×10^{-5} ft³) of sample. The instrument was not specific for organic hydrazine(s) or their reaction products, as any carbon bearing compound would be oxidized to carbon dioxide and give a reading.

Each of constant current coulometry and total organic carbon analyzes were done using statistical quality control methods (Reference 2). Known spiked samples were submitted during the chemical analyses, and control charts were used to provide a routine audit procedure for the chemical analysis.

Level two was used for the determination of trace quantities of material that could be listed as a hazardous waste constituent (Reference 3). Extraction/concentration procedures were done following EPA method 3510 (SW-846) (Reference 6), except that a 2.0×10^{-4} M³ (7.063×10^{-3} ft³) sample volume was used instead of a 1.0×10^{-3} M³ (3.531×10^{-2} ft³) sample volume. The extracts were then analyzed using GC/NPD, GC/FID, and GC/MS. Spiked samples were submitted during the chemical analysis as a check method. The GC/NPD used to analyze the samples had the following approximate detection limits, when using 1.0×10^{-9} M³ (3.53×10^{-8} ft³) of sample: hydrazine 7.273×10^{-16} Kg (1.603×10^{-15} lbm), MMH 1.0×10^{-14} Kg (2.224×10^{-14} lbm), UDMH 4.128×10^{-16} Kg (9.10×10^{-16} lbm), NDMA 1.618×10^{-16} Kg (3.567×10^{-16} lbm). Variation in the detection limits was due to changes in the recovery efficiency of the standard samples over the duration of the testing. The GC/FID was used to detect trace quantities of compounds at a nominal detection limit of approximately 1.618×10^{-16} Kg (3.567×10^{-16} lbm), when using 1.0×10^{-9} M³ (3.53×10^{-8} ft³) of sample. The GC/MS was used to detect trace quantities of compounds at a nominal detection limit of approximately 1.618×10^{-16} Kg (3.567×10^{-16} lbm), when using 1.0×10^{-9} M³ (3.53×10^{-8} ft³) of sample. Both the GC/FID and GC/MS were used as qualitative detection instruments rather than quantitative instruments because of the time and funding limitations of the project.

SAMPLING AND DATA REPORTING

MATRIX TRIALS

The sampling of the liquid during the trials was accomplished by using a mixture of deionized water and concentrated sulfuric acid, H_2SO_4 , to trap the MMH in solution. The samples were taken on a regular schedule over the duration of the multi-day-trial. The trials were conducted on an eight (8) hour work schedule to simulate the future work environment that the system might see. Gas samples were taken at the start-up of each trial in sets of three for statistical analysis. Data were reported as concentrations calculated from the volume of the sample used in the analysis. On site, data are reported using the units of part per million ($1.0 \text{ ppm} = 1.0 \times 10^{-3} \text{ Kg/M}^3$), or part per billion ($1.0 \text{ ppb} = 1.0 \times 10^{-6} \text{ Kg/M}^3$).

EPA VALIDATION TESTS

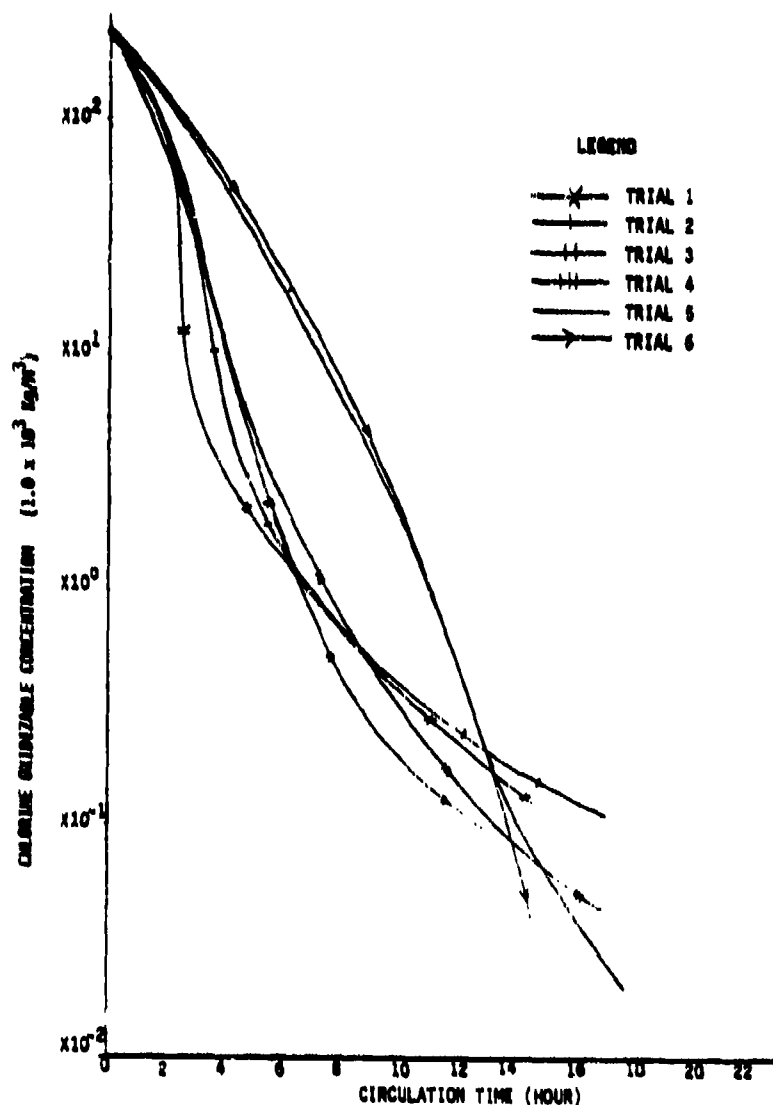
The sampling of the liquid during the tests was done on a regular schedule over the duration of the multi-day tests using the approved EPA sampling method (Reference 7). The tests were conducted on a 24-hour basis. Variable measurement data was archived for submission to the EPA if required. Data were reported as concentrations calculated from the volume of the sample used in the analysis.

ENVIRONMENTAL CONSIDERATIONS

Future plans call for implementation of an on site Environmental Protection Agency non-regulated hazardous waste disposal process for hydrazine propellants using the ozone/UV process. Analyzing the effluent coulometrically would indicate the presence of any chlorine oxidizable substances, e.g., hydrazines. Residual carbon containing compounds, e.g., methanol, can probably best be determined using the TOC (Reference 5) instrument, with the proper reactor design. When these tests indicate concentrations below the detection limits of the instrument a complete chemical analysis would be conducted to certify the effluent as "Regulatory Clean Effluent" (Reference 3) prior to discharging it to grade. These additional tests would be thermionic ionization detection

operating in a nitrogen-phosphorus mode for NDMA and hydrazine fuels, flame ionization detection for all organic constituents, and mass spectrometry detection for identification of all extracted components. These analyses would be used with preconcentration techniques to prove the effluent clean. These analyses are accepted procedures in the trace analytical field and are the "Best Available Technology" (Reference 3) for determination of trace constituents in the ozone/UV reactor effluent which contains mostly water.

CONCLUSIONS



DATA ANALYSIS

The exposure time for each trial was calculated from the circulation rate, the initial volume of deionized water used, the residence time in the reactor, and any volume changes due to sampling or deionized water additions. Error bands were included in the calculated data. Plots of species concentrations versus both circulation and exposure times were then made for each trial. Curves were then fitted to the data and the error bands. All trials were then combined on a "normalized" graph of chlorine-oxidizable concentration versus circulation time Fig. 6.

Figure 6. Ozone/UV Photo-Oxidation Three Variable System Trends

MATRIX ANALYSIS

Analysis of the data in Fig. 6 using the Hadamard Matrix Factorial Design Analysis Software (Reference 4) for a 6 x 3 matrix, Matrix IB, gave information on the relative effect of each of the three main variables on the overall disappearance of the chlorine-oxidizable substances.

The effect of temperature is the most dramatic and the most interesting. At the high setting, 313.98 K (565.16°R), the reaction proceeded much faster than at the low setting, 285.59 K (514.06°R), until the concentration of the chlorine-oxidizable specie(s) reached approximately $2.5 \times 10^{-3} \text{ Kg/M}^3$ ($1.561 \times 10^{-4} \text{ lbm/ft}^3$). After that concentration was reached, the ozone/UV photo-oxidation reaction favored the low temperature setting. In fact, although the high temperature trials were initially faster, the low temperature trials, after a period of time, overtook them and continued to oxidize the concentration of the chlorine-oxidizable species at an apparently faster rate than the high temperature setting. This effect is thought to be due to the increased solubility of ozone in the liquid at lower temperatures which at lower concentrations of chlorine-oxidizable species offsets the kinetic advantage gained by the increase in temperature. The absolute temperature difference was 28.39 K (51.1°R).

The pH dependance of the ozone/UV photo-oxidation reaction was also discontinuous. At high chlorine-oxidizable concentrations the overall reaction rate favored the highly basic setting, 11 pH. However, at lower concentrations the reaction favored the lower setting, 9 pH. It would also seem that the pH determines the lower limit of oxidization by ozone. High pH trials tended to level off much earlier than the low pH trials. The reasons behind this are probably related to the overall reaction mechanism(s) and the formation of free radicals (References 1, 8, 9, 10) but the processes are not well understood.

The reaction dependance on ultraviolet radiation was continuous over the range of the oxidation process. The reaction at all times favored the high level of radiation, 151.8 W (44.493 BTU/H), versus the low level, 79.2 W (23.214 BTU/H). This statistical analysis shows conclusive evidence of the increased overall reaction rate when using ultraviolet light in concert with ozone oxidation. It

has been calculated that the emissions spectra in the UV at 2.537×10^{-7} m (8.324×10^{-7} ft) causes electronic excitation of ozone to an antibonding state which can only be deactivated by fluorescence, phosphorescence emissions, radiationless deactivation processes, or chemical reaction (Reference 12). It has been proposed that ultraviolet radiation can actually be included in the overall kinetic rate expression by using the second law of photochemistry (Reference 11). If this is true, and it appears so, then the more radiation the better since no adverse side-effects of the addition of radiation have been detected in this series of experimentation. Table 1 summarizes the optimal setting of the ozone/UV photo-oxidation reactor.

SETTING	I	PH	[O ₃]	UV
Initial (high concentration)	+	+	+	+
Final (low concentration)	-	-	+	+
SETTING	T (R/OR)	PH	[O ₃] (wt%)	UV (W)/(STU/H)
(+)HIGH	313.98/866.17	11	4.5	181.8/44.49
(-)LOW	285.89/814.07	9	---	79.2/23.21

NOTE: High/low concentration boundary is approximately 2.5×10^{-3} kg/m³ (1.561×10^{-4} lbm/ft³)

Table 1. Optimized Setting of Ozone/UV Reactor

NDMA intermediates. It is also possible that this is the effect of variable interactions which have not yet been analyzed. In any case, it was found that the ozonization process was capable of reducing the NDMA concentration to below the detection limit of the analytical instrumentation.

OTHER TRENDS

The highest concentration of NDMA detected was found to be statistically related to the initial concentration of MMH, Table 2. Trial four produced approximately five (5) times less NDMA than expected. This could be due to the fact that the initial oxidation rate of the MMH was rapid enough to preclude the formation of the

TRIAL	INITIAL [MMH]	HIGHEST [NDMA]	CALCULATED [NDMA]
1	303	.022	.067
2	736	.438	.468
3	287	<.010	.014
4	473	.040	.219
5	497	.283	.241
6	466	.262	.231

NOTE: All concentration have units of 1.0×10^{-3} kg/m³
(Conversion factor: 1.0×10^{-3} kg/m³ $\times 6.246 \times 10^{-2} = 1b/ft^3$)

Table 2. NDMA Production

The oxidation of MMH proceeds in several steps through the intermediate species, methanol, formaldehyde, and formic acid to produce carbon dioxide. It

was determined that the slow step in the oxidation process was the conversion of methanol to formaldehyde. However, the ozonization process was found to reduce the levels of all the intermediate species to below the respective detection limit of the analytical instrumentation used in these trials.

Furthermore, it was found that ozone remained in the test solution overnight. The ozone was not destroyed when it passed through the pump or the spray nozzles as had previously been expected. This, in combination with the eight (8) hour work schedule, led to discontinuities in the data. The chlorine-oxidizable species concentration could either increase or decrease overnight in, as yet, no apparent pattern. The trend could be due to the type of intermediate formed either chlorine-oxidizable, e.g., formaldehyde, or non-chlorine-oxidizable, e.g. methanol. The concentration of NDMA only increased. This suggests that the oxidation of MMH with ozone alone may produce more NDMA than when combined with ultraviolet light photo-activation.

Finally, the vent gas analysis showed only one occasion of escaping chlorine-oxidizable material with a concentration of approximately 5.0×10^{-5} Kg/M³ (3.123×10^{-6} lbm/ft³). It should be noted that the reactor is not pressurized and operates at ambient pressure.

EPA VALIDATION RESULTS

There was no NDMA detected in any of the validation tests including the UDMH test. This could be due to the fact that the tests were run as a 24-hour operation and that the oxidation of the hydrazine fuels produces no NDMA when ozone is combined with ultraviolet light photo-activation, and/or that the initial oxidation rate of the hydrazine fuel was rapid enough to preclude the formation of the NDMA intermediates. It is also possible that this is the effect of variable interactions which have not yet been analyzed. In any case, it was found that when the reactor was operated at the optimum parameter settings the ozonization process was capable of reducing the NDMA concentration to below the detection limit of the analytical instrumentation or precluded the formation of the NDMA species altogether.

For each test the solutions were analyzed for all trace constituents. Methanol was found in every case including the water blank test, at less than 5.2×10^{-7} Kg (1.14639×10^{-6} lbm) when using a 1.0×10^{-9} M³ (1.14639×10^{-6} ft³) sample, and is thought to be a decomposition product of either the UV lights' EPDM rubber grommets or the GE silicone RTV used as a water seal. In fact the GE silicone RTV was actually reported, in a matrix trial, as octamethylcyclotetrasiloxane. In each case the amount of methanol present was small, and its formation could be prevented with proper reactor design. A small amount of unreacted unsymmetrical dimethylhydrazine was reported at the end of the UDMH EPA validation test, approximately 1.2×10^{-9} Kg (2.64552×10^{-9} lbm). The presence of trace amounts of unreacted UDMH was thought to be attributable to the presence of larger quantities of methanol and other organic material within the system which the ozone would preferentially oxidize.

In all hydrazine fuel tests, the water was found to have less than a detectable amount of chlorine oxidizable species by the morning of the second day, 24 hours later. The determination of the total organic carbon remaining was found to be unreliable because it would decrease and then suddenly increase in no apparent order and for no apparent reason. The water blank tests showed only an increase in the amount of TOC. Because of this, ~~the increases were thought~~ to be due to the deterioration of the RTV or the EPDM rubber organic sealing material(s).

In the first MMH test three peaks were evident in the samples. The three peaks could not be identified. The mass spectra did not correspond with anything in the computer library of 43,000 spectra, nor did the spectra correspond to any of the previously identified oxidation products from MMH or UDMH. These compounds did not appear in the second MMH EPA validation test. It is felt that the unidentified compounds are possibly the reaction products from the MMH intermediate decomposition products interacting with system contamination during the test, possibly silicone bearing organics. In any event, the test was repeated and the unidentified compounds did not appear in it or in any of the subsequent tests. For the UDMH test an intermediate sample was analyzed and only acetaldehyde, formamide, and n-methylformamide were identified.

RECOMMENDATIONS

From the statistical optimization experimentation, it is evident that the new reactor design should incorporate some changes. First, the operating conditions should be more tightly controlled. Second, an investigation into the exact demand of ozone by the system should be conducted to size the future system correctly. Third, steps should be taken to eliminate all organic materials used in the reactor and associated piping. Fourth, the reactor should be operated on a 24-hour schedule to reduce the possibility of forming any NDMA. Finally, steps should be taken to approach the EPA on a unified front to convince them to publish updates to the discharge regulations so that an effective disposal system for EPA non-regulated hazardous waste containing hydrazine(s) as a hazardous constituent can treat dilute aqueous solutions of EPA regulated hazardous waste containing hydrazine(s) as well.

REFERENCES

1. Alder, M., Hill, G., "The Kinetics and Mechanism of Hydroxide Ion Catalyzed Ozone Decomposition in Aqueous Solution", Journal of the American Chemical Society, vol. 72, pp. 1884, 1950.
2. AT&T Technologies, "Statistical Quality Control Handbook", Delmark Printing Co., Charlotte, NC, 1985.
3. Code of Federal Regulations, Title 40, Protection of the Environment, Parts 190 to 399, Office of the Federal Register National Archives and Records Administration, 1986.
4. Diamond, William J., Practical Experiment Designs for Engineers and Scientists, Zan-Nostrand-Reinhold, NY, NY, 1981.
5. "Methods for Chemical Analysis of Water and Wastes", EPA-600, 4-79-020, Method 415.1 (Combustion or Oxidation), "Organic Carbon, Total, pp. 415.1-1, Environmental Monitoring and Support Laboratory Office of Research and Development U.S. Environmental Protection Agency, Cincinnati, OH, 1983.
6. "Test Methods for Evaluating Solid Waste", Volume IB: Laboratory Manual Physical/Chemical Methods", Third Edition, SW-846, Method 3510 Separatory Funnel Liquid-Liquid Extraction, U. S. Environmental Protection Agency, Office of Solids Waste and Emergency Response, Washington, DC, 1986.
7. Ford, P., Turina, P. Seely, D., "Characterization of Hazardous Waste Sites -- A Methods Manual, Volume II, Available Sampling Methods, Second Edition", Appendix A, Revision 0, pp 19 of 52, EPA 600/4-84-076, Environmental Monitoring Systems Laboratory Office of Research and Development U.S. Environmental Protection Agency, Las Vegas, NV, 1984.
8. Hoigne, J. and Baker, H., "The Role of Hydroxyl Radical Reactions in Ozonation Processes in Aqueous Solutions", Waste Research, 10, pp. 377-386, 1976.

9. Hoigne, J. and Baker, H., "Ozonation of Water: Kinetics of Oxidation of Ammonia by Ozone and Hydroxyl Radicals", Environmental Science and Technology, vol. 12, number 1, January 1978.
10. Peleg, M., "The Chemistry of Ozone in the Treatment of Water", Water Research, 10, pp. 361-365, 1976.
11. Prengle, H. William Jr., "Experimental Rate Constants and Reactor Considerations for the Destruction of Micropollutants and Trihalomethane Precursors by Ozone with Ultraviolet Radiation", Environmental Science Technology, 17, pp. 743-747, 1983.
12. Suppan, P., "Principles of Photochemistry", The Chemical Society, Burlington House, London, 1973.

SECTION VI
DETECTION AND MONITORING

MICROSENSOR AND PATTERN RECOGNITION TECHNIQUES IN HYDRAZINE DETECTION

S. L. Rose-Pehrsson, Research Chemist

Naval Research Laboratory
Chemistry Division, Codes 6110
Washington, D. C. 20375-5000

J.W. Grate, Research Chemist
Code 6170

ABSTRACT

A new sensor technology combined with pattern recognition methods is being investigated for hydrazine vapor detection. The sensors, chemiresistors, use vapor-sensitive coatings on a set of interdigital electrodes. All of the coatings tested have a rapid response to hydrazine, but are slow to recover. Heating the sensors improves the response and the recovery times. A coating has been tested that is sensitive to part-per-billion (ppb) concentrations of hydrazine. The coating lacks the necessary selectivity, but when used with other coating will provide a fingerprint pattern for hydrazine. Pattern recognition methods combined with sensor arrays have been used to improve the selectivity of the new sensors.

INTRODUCTION

Large quantities of hydrazine, monomethylhydrazine (MMH), and unsymmetrical dimethylhydrazine (UDMH) are used by NASA and the Air Force as fuels. The toxicity and the possible carcinogenicity of the vapors require air monitoring for personnel safety. Fixed-point monitors, portable instruments and dosimeters are needed. No commercially-available instruments can detect 30, 50, and 60 ppb of hydrazine, MMH, and UDMH respectively, which are the threshold limit values (TLV) recommended by the National Institute of Occupational Safety and Health.(1)

The research goals are to determine the feasibility of the chemiresistor technology for hydrazine detection. The sensors have good sensitivity, but lack the necessary selectivity. To overcome the selectivity problems, sensors arrays and pattern recognition methods are being examined. In addition, the sensors are being characterized so that potential problems can be addressed.

Chemiresistors are based on vapor-sensitive organic semiconductors. They act as resistors, where the conductance is changed in the presence or absence of chemical vapors. The sensors have a substrate of interdigital gold electrodes coated with a vapor-sensitive film. Different coatings generate different vapor responses. The use of several small electrodes provides improved ohmic contact and facilitates the

measurement of very low conductances. In addition, the electrode design reduces the power requirement, therefore the coatings have a longer lifetime.(2)

Chemiresistors with phthalocyanine coatings responded to ammonia, therefore the sensors with these coatings were investigated for hydrazine detection.

Phthalocyanines are heteroatom macrocycles that complex a metal atom; the central metal atom effects the selectivity. An array of the phthalocyanine coatings with different metal centers were tested with hydrazine and several other potential interferent vapors including some containing nitrogen. The coatings were deposited using a Langmuir-Blodgett film transfer technique after being derivatized to tetracumylphenoxy phthalocyanine. Stearyl alcohol was added to improve the transfer. The response to hydrazine was fast, but the sensors were very slow to recover.(3)

The data from an array of sensors are difficult to interpret. A vapor is defined by the sensor responses, but a data set of more than three sensors is impossible to visualize. Similar vapors should have similar sensor responses and will cluster in a coordinate space defined by the sensors. Pattern recognition methods give an investigator the ability to examine the high dimensional space defined by the array of sensors.

Pattern recognition methods applied to the array of coatings were able to distinguish hydrazine from the interferences and several other chemically similar compounds. Mixtures of the vapors were more difficult to identify using only phthalocyanine coatings. The pattern recognition results are described in detail in a JANNAF proceeding.(3)

A new coating has been found and is being tested that is very sensitive to hydrazine. Also, the effects of heating the substrate are being investigated.

EXPERIMENTAL

Hydrazine is very difficult to transport due to absorption and reactivity. Therefore, it was important to minimize the interaction of the vapor with walls and hot surfaces prior to the sensors. An aluminum sample holder was machined consisting of two compartments. On one side a glass manifold was positioned to deliver the hydrazine vapor in a parallel manner directly to the top of the sensors. In the second compartment, a platform with small holes was suspended midway in the box. The sensors were placed on the platform. A heating tape could be placed under the sensors. Electrical connections from box to the sensors were made through the platform. A hole was drilled in the side of the compartment under the platform to allow the gas stream to escape. Triaxial cables carried the power to and the signal from the aluminum box to a Keithley 617 programable electrometer. Five sensors could

be tested at once in the sample holder and a Keithley 705 scanner was used to switch the signal from each sensor to the electrometer.

The hydrazine gas stream was generated as described in reference 1.

RESULTS

A new coating, an n-type organic semiconductor, was deposited onto the substrate using the Langmuir-Blodgett method. Different thicknesses of 1, 5, 11, 21, and 33 layers were tested. A typical response to hydrazine is shown in figure 1. The initial response is a very rapid increase in conductance, followed by a more gradual increase. The recovery demonstrates the same type of behavior. The recovery time is also dependent on the film thickness; the thicker the film the slower the recovery time. The magnitude of the response increases linearly with increasing concentration. The sensitivity to hydrazine is shown in Table 1.

TABLE 1. MAGNITUDE OF RESPONSE

<u>VAPOR</u>	<u>CONCENTRATION</u>	<u>CHANGE IN RESPONSE</u>
N ₂ H ₄	500 ppb	100-1000
MMH	500 ppb	10-20
UDMH	500 ppb	2
NH ₃	30 ppm	3
NO ₂	10 ppm	10
Water	60% RH	10

The sensor does response to water as demonstrated in figure 2. Although when hydrazine and water are combined, the hydrazine response is easily observed above the water background. The sensor also responds with an increase in conductance to nitrogen dioxide (NO₂) and is reversible as seen in figure 3. The phthalocyanine response to NO₂ is also an increase in conductance, whereas the response to hydrazine as shown in figure 4 is a decrease in conductance. The combination of these two sensors will allow one to distinguish between NO₂ and the hydrazines.

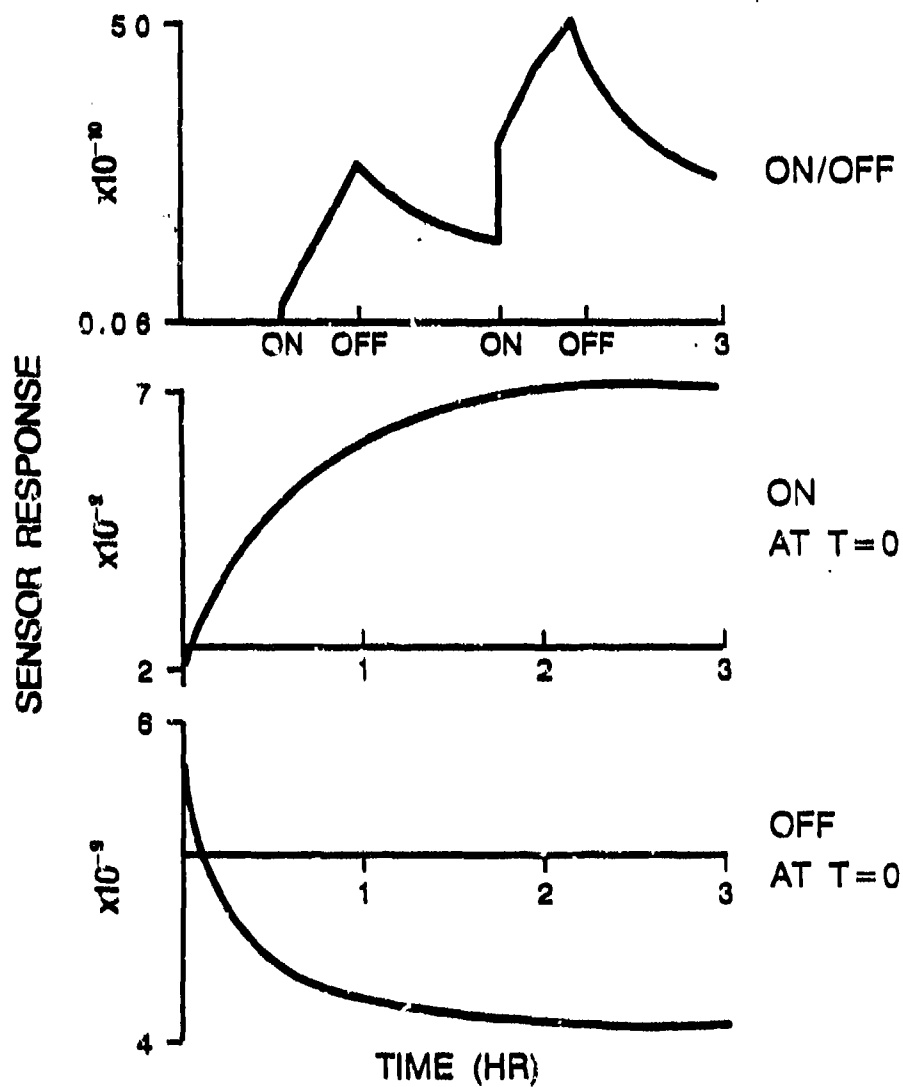


FIGURE 1. The sensor's response to 500 ppb of hydrazine. The sensor had 33 layers of the new coating. Slow responses are shown in 3 examples: (a) response and recovery times, (b) continuous exposure for three hours, and (c) continuous recovery for three hours.

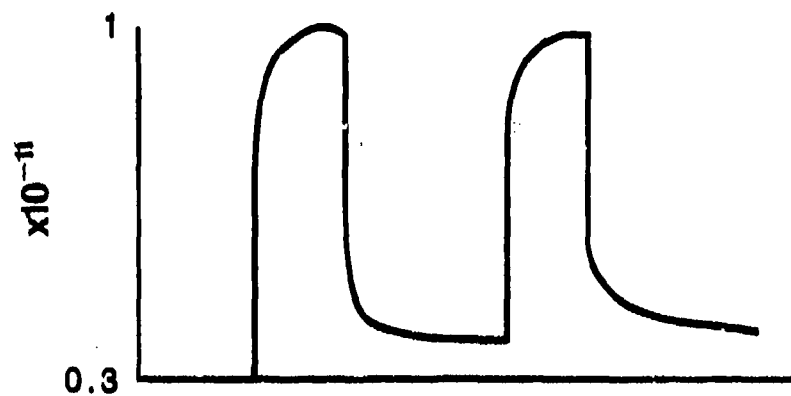


Figure 2. The sensor response to 60% relative humidity.

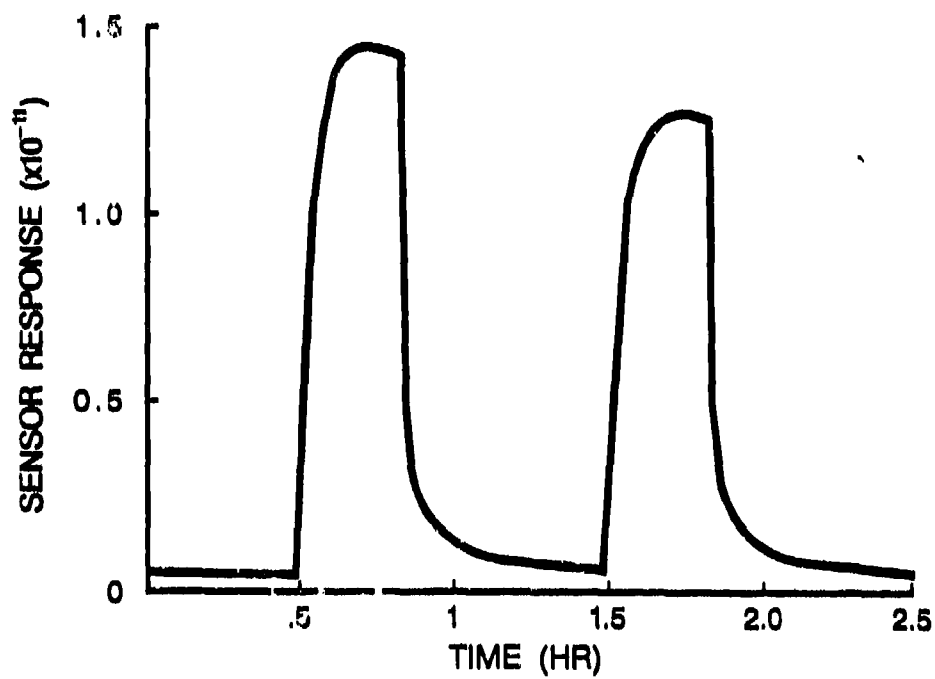


Figure 3. The new coating response to 10 ppm of NO_2 .

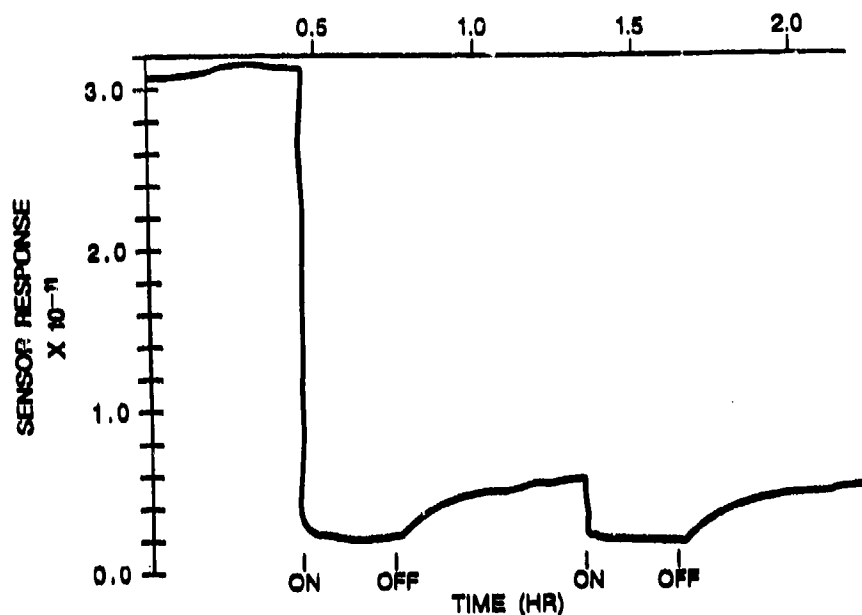


Figure 4: An example of the response of the Phthalocyanine spray-coated chemiresistor with platinum metal center to 1 ppm MMH. The sensor was heated to 140°C.

Figure 5 shows the improvement of the response and the recovery times when the substrate is heated to 45°C. The films deposited using the Langmuir-Blodgett technique cannot be heated above 50°C because stearyl alcohol, used as the transfer agent, melts. Other transfer agents are being investigated.

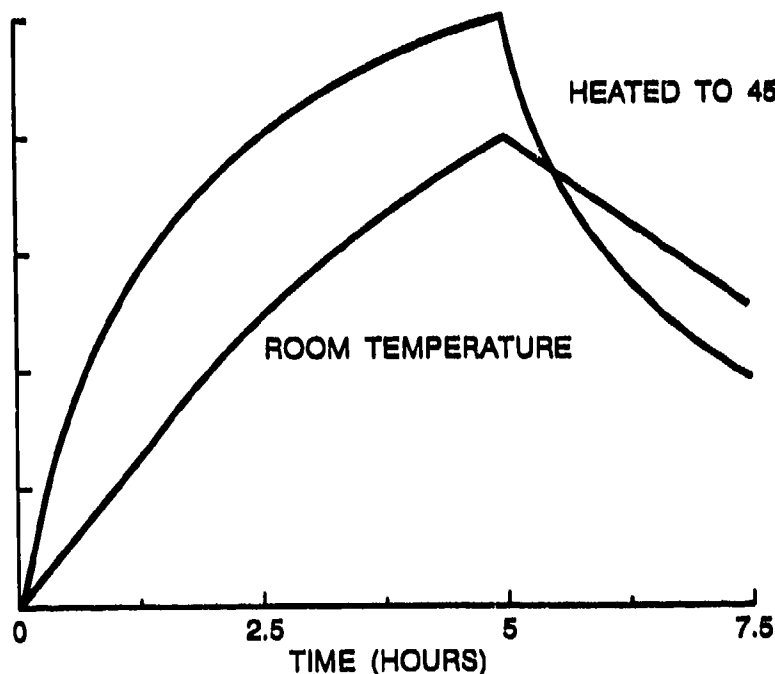


Figure 5. The new coating's response to 100 ppb MMH at room temperature and 45°C.

Two other coating methods are being investigated that can be heated. Sublimed phthalocyanine films have been tested on a different substrate design. The response and recovery times improve with increasing temperature, but the films are so thick that temperatures above 195°C are required. The high temperature degrades the coating at a measurable rate as shown in figure 6.

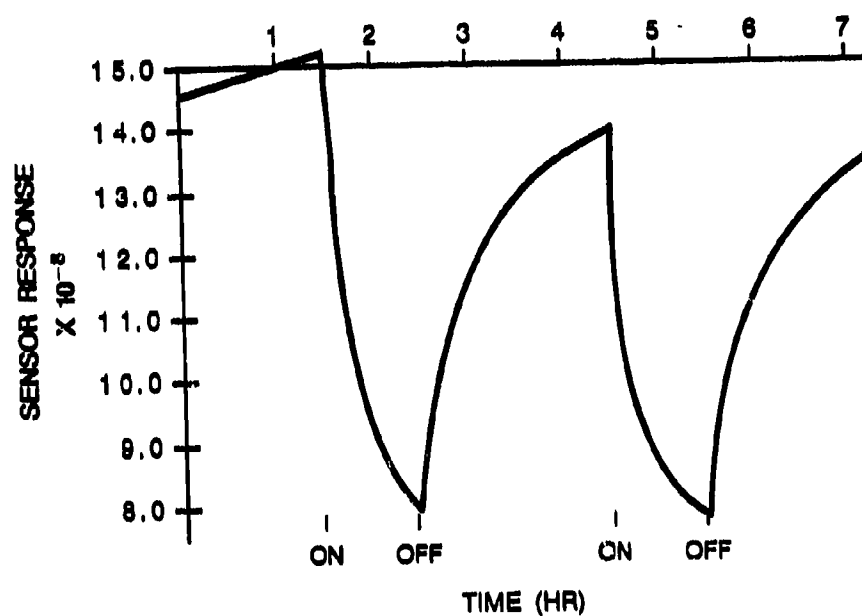


Figure 6. The response of a sublimed film of lead phthalocyanine to 1 ppm of hydrazine when heated to 195°C.

Film coatings that have been sprayed onto the substrate are also being tested. The thickness of the coatings are similar to the Langmuir-Blodgett transferred phthalocyanine films tested earlier. Figure 4 shows the response is rapid, but the recovery is still too slow even when heated to 140°C. This suggests that the way a film is deposited is as important as the thickness.

CONCLUSIONS

Chemiresistors show much promise as hydrazine vapor detectors. Without improving the recovery time, the response time is satisfactory for use as alarm devices. Pattern recognition methods make the use of array sensors feasible, therefore the variety of coatings improve the selectivity. New coatings and transfer methods that allow the film to be heated will improve recovery times, which would allow the technology to be used for all air monitoring applications.

REFERENCES

1. Rose, S.L.; J.R. Holtzclaw, "A Critical Comparison of Commercially Available Hydrazine Detectors," NRL Report 8848, 1985.
2. Wohltjen, H.; W.R. Barger, A.W. Snow, N.L. Jarvis, "A Vapor-Sensitive Chemiresistor Fabricated with Planar Microelectrodes and a Langmuir-Blodgett Organic Semiconductor Film," IEEE Transactions on Electron Devices, 1985, ED-32(7), 1170-1174.
3. Rose, S.L.; W.R. Barger, A. Snow and H. Wohltjen, "Hydrazine Detection Using Chemical Microsensors and Pattern Recognition Techniques," CPIA Publication 436, November 1985, p. 423-433.

HYDRAZINE DOSIMETRY

P. A. Taffe, Scientist
GEO-CENTERS, INC.
10903 Indian Head Highway
Fort Washington, MD 20744
J. H. Callahan
K. P. Crossman
S.L. Rose-Pehrsson

ABSTRACT

Passive dosimetry methods applicable to personnel and area monitoring are being developed for hydrazine detection in ambient air at the part-per-billion (ppb) level. A new badge design, molded from polyethylene, consisting of a diffusion barrier and an organic acid collection medium provides quantitation of exposure when analyzed by the NIOSH colorimetric method or a coulometric titration procedure. The diffusion barrier containing 144 one millimeter diameter holes establishes a collection rate of approximately 30 ml/min. The accuracy of data collected with this badge is within 25% of actual values. The dosimeter has demonstrated accuracy for up to 65 hours of sampling monomethylhydrazine (MMH) at the threshold limit value (TLV) concentration (200 ppb) with minimal interference effects from ammonia, freons, and isopropyl alcohol. A new colorimetric dosimeter has given qualitative hydrazine measurements in 15 minutes for TLV levels of MMH in relative humidities (RH) of 0 to 55 percent. It has also shown no interference from ammonia and none is expected from freons and alcohols. The potential use of the color badge in combination with the quantitative dosimeter will be discussed.

INTRODUCTION

Hydrazine (HZ), monomethylhydrazine (MMH), and unsymmetrical dimethylhydrazine (UDMH) continue to play an important role as hypergolic fuels. The potential carcinogenicity of these compounds has caused concern for the health and safety of the workers that may come in contact with them. Monitoring of the employees and their work places should be conducted to ensure their exposure remains below the defined levels.

A lightweight, inexpensive, personal dosimeter has been developed by Naval Research Laboratory (NRL) personnel and can be used to quantitatively monitor TLV exposures. It consists of three basic parts: the collection disk, the diffusor, and the badge housing. The collection disk is made of a thin piece of polyester coated with a citric acid solution. This organic acid was selected for its properties as an antioxidant. It serves as a trap for the hydrazines allowing analysis by colorimetric or coulometric procedures.

The collection characteristics of the coated disk were examined independent of the badge housing. A direct relationship between the amount of MMH collected and the face velocity was observed. To eliminate this problem several styles of diffusion caps were tested, and theoretical modeling employed. A design having 140 one millimeter diameter holes was selected for its ability to minimize face velocity effects without severely increasing the detection limit (Reference 1).

Machined badge housings deviated from linearity especially at low concentrations. Adsorption of the hydrazines into the "sintered" teflon stock and the tool marks from machining were thought to be responsible. A molded badge housing with drilled holes exhibited improved response results, therefore it was tested extensively. It demonstrated a detection limit of 15 minutes at the TLV, linearity up to 91 hours, and stability for up to 8 days. Deviations were still observed at short exposure times and low concentrations presumably due to adsorption on the irregular holes (Reference 1).

A new badge was molded in the same design from polyethylene. Teflon and polypropylene materials were preferred, but were too difficult to manufacture. The resulting badge is inexpensive, and could be disposable.

The quantitative dosimeter must be returned to a laboratory for analysis. This is acceptable to document exposures, but an immediate warning device would provide better protection for workers. Therefore, a scheme for a new colorimetric dosimeter that will provide real-time indication of exposure has been discovered and is being tested. It is based on the reaction of gaseous hydrazines at the TLV level with an indicator coated on a substrate.

This report contains laboratory testing of the molded badge and the initial investigation results of the colorimetric dosimeter.

EXPERIMENTAL

QUANTITATIVE BADGE

The badges are molded polyethylene following the design specifications discussed in an earlier paper (Reference 1). They consist of a collection disk and four molded pieces which include a base, spacer, diffuser, and cap. The cap may be snapped on the back of the base during badge exposure and snapped over the diffuser for storage following exposure.

The diffuser has a one inch diameter pattern of 144 one millimeter diameter holes which establishes a sampling rate of approximately 30 ml/min. It is designed to snap on the base and to accommodate the cap or a second diffuser. Multiple diffusion caps

would provide a decreased sampling rate and reduce possible face velocity effects.

A collection disk made of polyester matted drafting film is coated with an organic acid solution and held in place with the spacer. The acid selected is citric acid monohydrate. When dissolved in methanol to form a 30% solution and aged for one week at room temperature, it provides an excellent medium for collection of hydrazines; see Figure 1.

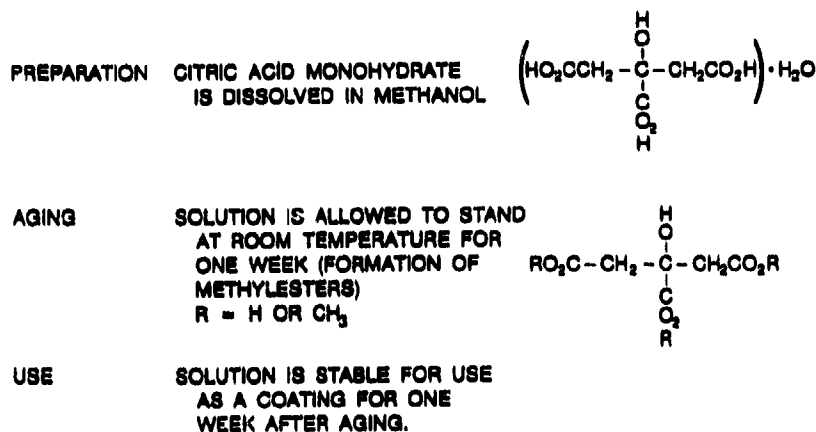


Figure 1. Citric Acid Collection Layer.

QUALITATIVE DOSIMETER

This dosimeter is in the early experimental stages and currently consists of a hydrazine vapor-sensitive coating on a substrate. A number of indicators and substrates have been investigated, but no final decision has been made. Selection of the coating compounds has been based on their ability to give a visual indication upon reaction with hydrazines in air. The chemistry involved is the reduction of aldehydes or ketones containing chromophores. In some cases, the addition of a catalyst is necessary. Substrates which have been examined for this passive system are silica gel coated on glass and plastic, Whatman filter paper, and Teslin (a micro porous polymeric membrane produced by PPG Industries, Inc.)

TEST APPARATUS AND ANALYSIS

The generation of the MMH dynamic test atmosphere was achieved using the set-up described in Reference 2. The exposure of the badges was accomplished with the same glass test chambers used in Reference 1 for the initial dosimetry investigations. The face velocity, linearity, relative humidity, and stability experiments also followed the same procedures outlined in that study.

Analysis of the badges was performed by removing the coating from the collection disk with a solvent designated by the selected technique. Two accepted wet chemical methods are applicable to this procedure: coulometric titration (Reference 3, a NRL/White Sands modification miniaturized to achieve the desired sensitivity), and a

colorimetric method (Phosphomolybdic acid, NIOSH approved method #S149).

MASS SPECTROMETRY

To investigate the composition of the collection solution, fast-atom bombardment (FAB) mass spectra were obtained on a Finnigan TSQ-70 triple quadrupole mass spectrometer. The samples were prepared by placing a drop of the methanolic citric acid solutions on a copper probe tip, allowing the methanol to evaporate, and placing a drop of glycerol on the probe tip. The spectra were obtained by sputtering the glycerol solution with an 8 KV xenon fast-atom beam from an Ion Tech saddle-field fast atom gun.

RESULTS

QUANTITATIVE BADGE

Face velocity testing was performed on badges using machined diffusors of three different hole sizes for the purpose of selecting the optimum design. The number of holes varied to allow each design the same sampling area. The diffuser design selected for production had a one inch diameter pattern of 140 one millimeter diameter holes. This minimized the face velocity effects without severely increasing the detection limit. Designs with fewer but larger diameter holes exhibited pronounced face velocity effects by increasing the collection rate with increasing face velocities.

The diffuser selected was tested with a MMH gas stream at face velocities of 2, 4, 8, 11, and 22 feet per minute. The test atmosphere was dry air contaminated with approximately 200 ppb MMH. The badges were exposed for five hours. The average calculated collection rate was 38.3 ml/min, with a minimum of 31.4 ml/min, and a maximum of 44.9 ml/min. All of the data points are within the designated +25% as shown in Figure 2.

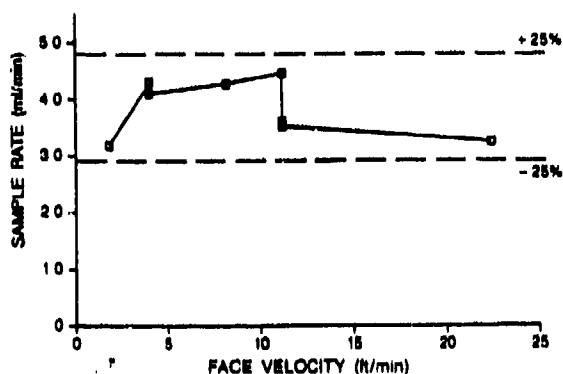


Figure 2. The Effect of Face Velocity on the Sampling Rate of the Prototype Diffuser.

The sampling rate of the molded diffusor was found to approximately 30 ml/min, which is less than that of the drilled prototype. It was calculated from a series of exposures to TLV MMH atmospheres ranging in time from .25 to 64.75 hours as shown in Figure 3. The variation in the data for exposures of one hour or less is believed to be partially caused by the disruption of the test atmosphere upon insertion of the badges. Samples obtained from exposures of 4 to 8 hours consistently collect at a rate of 30 ml/min.

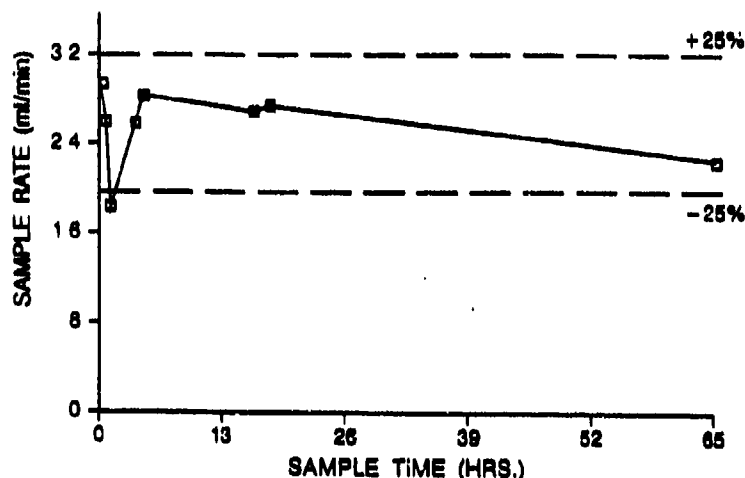


Figure 3. Sampling Rate of the Molded Badge.

The linearity of the badge collection was tested by varying the exposure times between .25 and 64.75 hours. The test atmosphere contained an average MMH concentration of 200 ppb in air with 45% RH, delivered at 2 ft/min. All of the data except a one hour exposure and a .25 hour exposure, fell within the acceptable region as shown in Figure 4. Fluctuations again at the .25 hour exposures may be partially due to disruption of the test atmosphere when the badges were placed in the chamber. Also adsorption on the badge housing could be a factor.

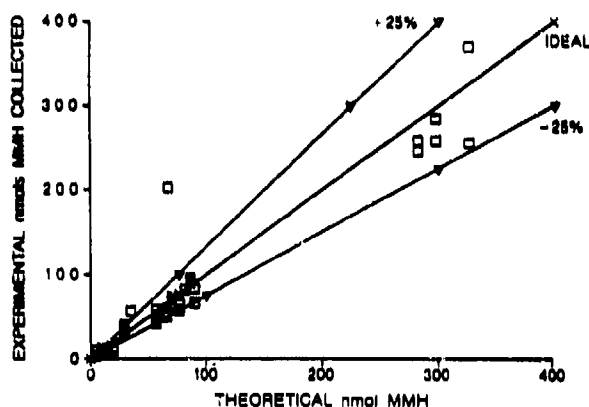


Figure 4. Linearity of the Results Obtained Using the Molded Badge, (assuming a collection rate of 30 ml/min).

Badges exposed to TLV atmospheres of MMH at various relative humidities and exposure times were stored capped for periods up to 62 hours. They all showed a significant loss of analyte as seen in Figure 5. A decrease of 30% to 75% of the original value was observed after storage of 24 hours.

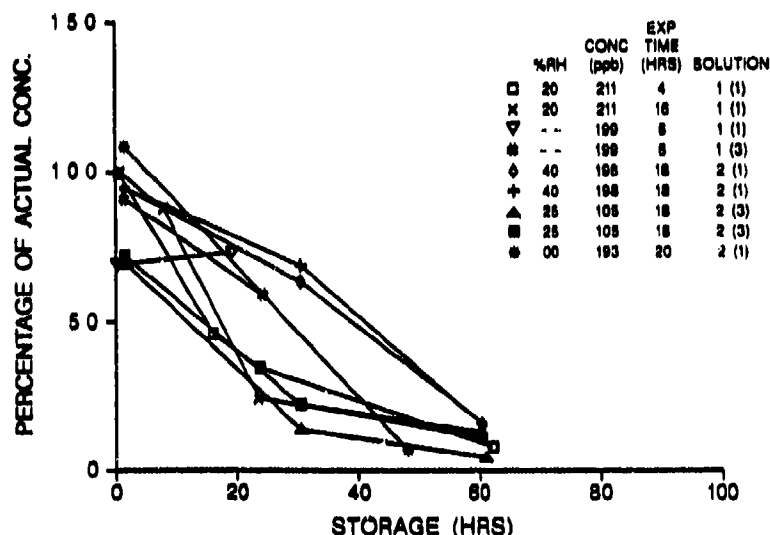


Figure 5. Storage Stability of Exposed Badges.

During the initial experiments with the citric acid coating, it was observed that the desired tacky film could only be obtained when the solution had been aged at room temperature for one week. This solution was then only stable for a period of one week. It would be of interest to define the composition of the solutions at different points in the aging process and to determine the unique characteristic(s) of the properly aged solution. Samples of solutions representing the stages of aging were investigated by mass spectrometry. The mass spectra indicated methylation of the carboxylic acid groups of the citric acid. The freshly prepared solution appeared to have only citric acid, Figure 6. The properly aged collection solution consisted of citric acid along with mono-, di-, and trimethylated esters; see Figure 7. As shown in Figure 8, the mass spectrum of a solution that had aged too long indicated the presence of the same esters but at different ratios, and a significantly reduced amount of the original acid. Quantitation of the ratios has not yet been accomplished.

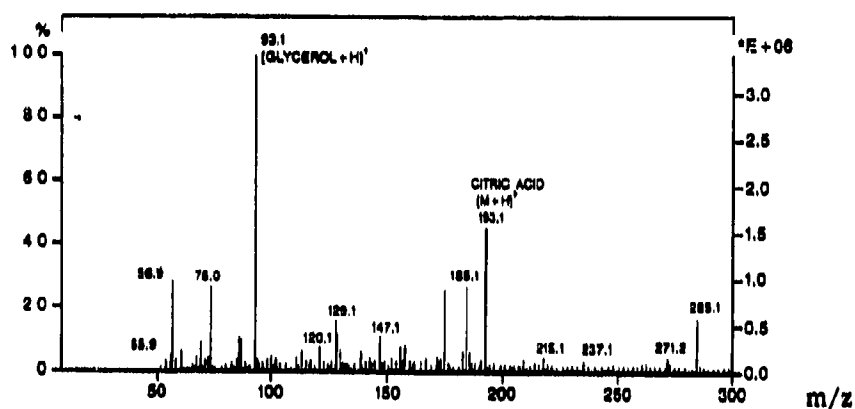


Figure 6. FAB-MS of Newly Prepared Citric Acid Solution Using a Glycerol Matrix.

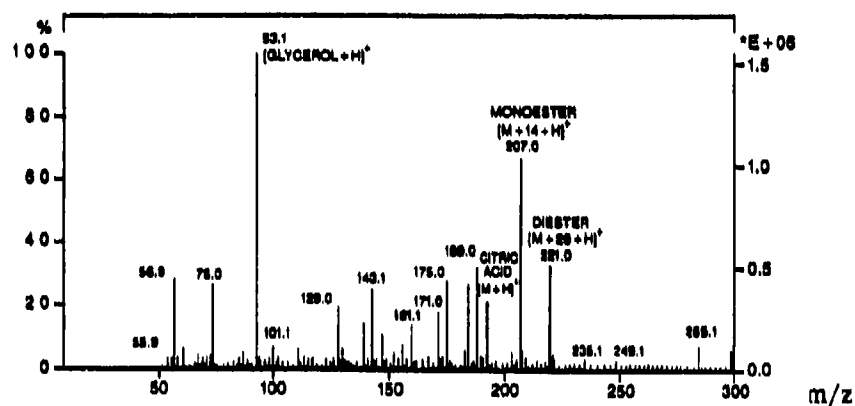


Figure 7. FAB-MS of Properly Aged Citric Acid Solution.

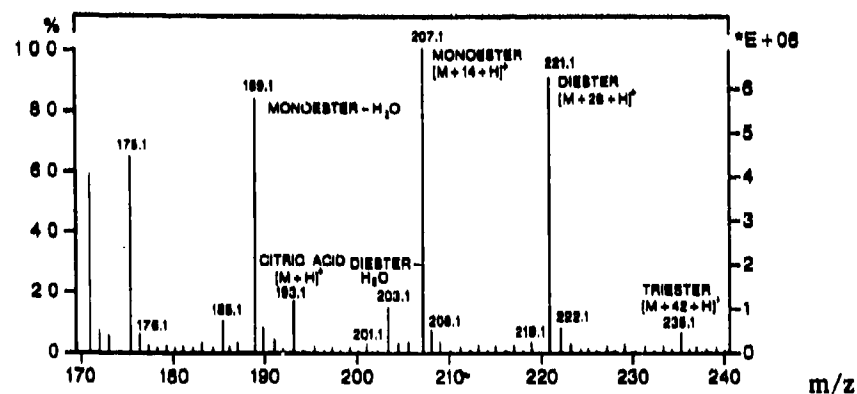


Figure 8. FAB-MS of an Old Citric Acid Solution which did not Perform Adequately as a Collection Coating.

QUALITATIVE DOSIMETER

Three of the chemicals examined for use as indicators were selected for continued testing. They were vanillin, anisaldehyde, and para-dimethylaminobenzaldehyde (PDAB). Each reacts with TLV atmospheres of MMH to form a bright color: vanillin produces a lemon yellow; anisaldehyde produces a greenish yellow; PDAB produces an orange.

Vanillin was the first compound investigated and has been tested more extensively than the others. The detection limit for TLV level exposures is 10 to 15 minutes. At that time the first indication of color is observed; with continued exposure the color intensifies. The upper limit of detection has not yet been established. The relative humidity of the test atmosphere appeared to have little effect on the color development. Dry air and air with 45% RH gave similar results. Limited interference testing has been done with ammonia, carbon dioxide and carbon monoxide. There appear to be no effects. Unexposed vanillin dosimeters have been stored in a desiccator for up to four months. Some discoloration was noted, but they still produced a yellow color in 10 to 15 minutes of exposure to TLV levels of MMH.

The anisaldehyde and PDAB do not appear to require desiccated storage. Coated samples have performed well after four months of storage in zip lock plastic bags. The anisaldehyde does however have a slightly slower response after extended storage.

CONCLUSION

The molded polyethylene badge provides an excellent housing for the collection disk. The diffusor serves its function to minimize face velocity effects while retaining a TLV detection limit of 10 minutes. The assembling of the badge is simplified by its ability to be securely snapped together. The resulting badge is durable, inexpensive, and lightweight, which are desirable qualities of a disposable personal dosimeter.

The limiting factor in the performance of the dosimeter is the collection solution. It was established during initial investigations that the coating solution of methanolic citric acid monohydrate can not be used for a period of one week after preparation. If used, the coating crystallizes which, based on mass spectrometry data, we now believe to be composed of mostly citric acid. This coating will not effectively collect the hydrazines. A different type of crystal growth develops when the solution is more than two weeks old. At this point the mass spectrometry data indicates the majority of citric acid has been converted to the methyl esters. In a properly aged solution, a coating, which is a tacky film is comprised of a mixture of citric acid and the mono-, di-, and trimethylated esters. The results obtained with this coating are consistently within the specified 25% of actual. There were no interference effects from ammonia, freons, and

isopropyl alcohol. In addition, relative humidity appears to have a minimal effect on the collection rate.

Further investigation is being performed on the cured citric acid solution to determine the ratios of the methyl esters. It is believed that the storage stability problems encountered are caused by the collection solution and may be due to improper aging.

Another approach is to avoid the stability problem by immediate analysis of the collection disk. With a colorimetric dosimeter used as a qualitative indicator in combination with the citric acid badge, the latter could be removed and turned in for quantitative analysis upon indication of exposure. When analyzed immediately the badge has shown reproducible and accurate results.

The chemicals vanillin, anisaldehyde, and PDAB have shown excellent potential as colorimetric indicators. The coated substrates have exhibited a reasonable shelflife for each of the compounds. There appear to be no effects from humidity or interferants (carbon dioxide, carbon monoxide, and ammonia) on the performance of vanillin.

REFERENCES

1. Hawkins, C.M., S.L. Rose, J.R. Wyatt, "A Passive Dosimetry Method for Determining Hydrazine in Air," CP1A 436, Proceedings of the 1985 IANNAF Safety and Environmental Protection Subcommittee Meeting, (Monterey, CA, 4-8 November 1985) Naval Postgraduate School, November 1985.
2. Rose, S.L., J.R. Holtzclaw, A Critical comparison of Commercially Available Hydrazine Detectors, NRL Report 8848, Naval Research Laboratory, Washington, DC, March 19, 1985.
3. Olson, E.C. "The Coulometric Determination of Hydrazine and Substituted Hydrazine," Analytical Chemistry, Vol. 32, No. 12, November 1960, pp. 1545-1547.

DESCRIPTION OF A CHEMILUMINESCENCE DETECTOR SYSTEM
SPECIFICALLY DESIGNED FOR MONITORING AIRBORNE
HYDRAZINE AND OXIDIZER PROPELLANT VAPORS*

F. Fraim, D. Rounbehler, D. Fine, J. Buckley and P. Nama
Thermedics Inc.
Woburn, Massachusetts

ABSTRACT

A new ambient air monitoring instrument designed specifically for detection of airborne levels of the three hydrazine propellants, hydrazine, monomethylhydrazine, and unsymmetrical dimethylhydrazine, has been developed under U.S. Air Force sponsorship. The objective of this work is a fast-response, wide-response range, sub-PPM detector for these propellants, with high specificity, insuring interference-free monitoring at very low vapor levels. The detection method relies on the unique chemistry that occurs between the hydrazine fuel vapors and acetaldehyde. A two-channel fuel vapor detection system based on this chemistry and NO chemiluminescence has been demonstrated to meet many practical detection needs. This technology has now been applied to a multiple-channel system, which monitors for both fuel and oxidizer vapors, and is capable of fully automatic operation.

INTRODUCTION

The hydrazine propellants, hydrazine (HZ), monomethylhydrazine (MMH), and 1,1 dimethylhydrazine, (unsymmetrical dimethylhydrazine) (UDMH), are used in large quantities by the military and NASA.¹ These propellants are being used both individually and as mixtures for primary rocket propellants, small spacecraft and satellite thrusters, and in emergency electrical systems in some military aircraft. Because of their wide use and the known toxicity of these propellants, there has been an ongoing need for reliable detection of the vapors of these propellants. A historic survey of the ACGIH permissible exposure levels for these compounds also shows that as more has been learned of their toxicity, the lower the permissible levels have become. This lowering, in turn, has put pressure on the performance of existing vapor detectors, and has led to the development of several new types of vapor detectors.

Thermedics became involved in the development of hydrazine vapor detectors as a result of a need for an improved system for the Titan II silo.² The requirement called for measuring both Aerozine 50 and nitrogen tetroxide vapors. Existing NO chemiluminescence technology, the preferred measurement method used for many years for ambient oxides of nitrogen monitoring, was the obvious choice for oxidizer vapors. To use the same technology for Aerozine 50 vapors, Thermedics developed a method to convert fuel vapors to NO, allowing these vapors to be detected with the same system. This approach was developed under an Air Force contract in 1982, and a system was successfully field tested both in a Titan II silo, and for two years at the Titan III facility at Vandenberg Air Force Base.

*This work was supported by the U.S. Air Force (USAF/AFSC) under Contract No. F04701-83-C-0069.

The original Titan II requirement was unique in that detection of the Aerozine 50 vapor is essentially the detection of UDMH vapor. Any Aerozine spill creates mostly UDMH vapor, with only approximately 10 percent of the vapor being HZ. Most other hydrazine detection problems, however, require the detector to respond to one or both of the other two hydrazines, HZ itself, or MMH. An additional requirement that has become important for any new detection approach is specificity. The need to accurately monitor every lower level has increased the problem of interferences. An excessive number of false alarms in a system caused by responses to nonhydrazine vapors renders the system useless. Therefore, as new approaches are developed, one of the main requirements, besides accurate low-level measurement, is the need to be highly specific.

Because the original Titan II system developed by Thermedics is not appropriate for measuring the other hydrazines, the Air Force has sponsored the development of a more general detection method based on the same chemiluminescence approach. In undertaking this development, the overall objective was not only to measure the three hydrazines, but to achieve as many of the features considered important for new systems as possible. The result should have a wide dynamic range, but still provide accurate results at sub-TLV levels. It should have a fast response to be able to immediately indicate vapors from a fuel or oxidizer leak. And finally, it should be highly specific to fuel and oxidizer vapor to minimize false readings. The results of this development work are the subject of this paper.

DETECTION OF PROPELLANT VAPORS WITH CHEMILUMINESCENCE

The chemiluminescence of nitric oxide (NO) with ozone has been the method of choice for many years for measuring the ambient levels of the oxides of nitrogen in the environment. The basic chemistry of this detection method is shown in Equations 1-3.



Nitric oxide combines with ozone to form NO_2 in an excited energy state. The NO_2 loses this energy, either through a collision with another molecule or by giving off light in the near infrared. This light can be easily detected at extremely low levels. Figure 1 indicates a typical detection system. In this case, the detector is a cooled photomultiplier tube. The sample is mixed with ozone in front of the tube at low pressure. The low pressure minimizes the chances that the NO_2^* will lose energy through a collision. A bandpass filter in front of the detector allows light to pass through to the detector only in the wavelength range of interest.

Other oxides of nitrogen, such as NO_2 and molecules containing nitrogen in their structure, can be detected using NO chemiluminescence by first converting the nitrogen in the molecule to NO. This is usually accomplished by heating the sample in the presence of air and a catalyst.

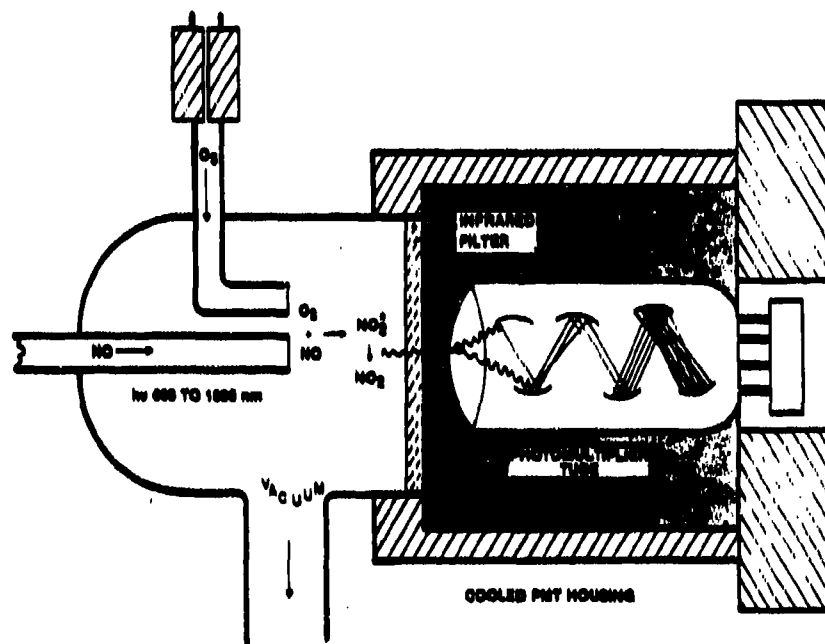
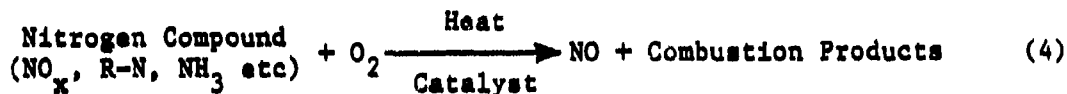
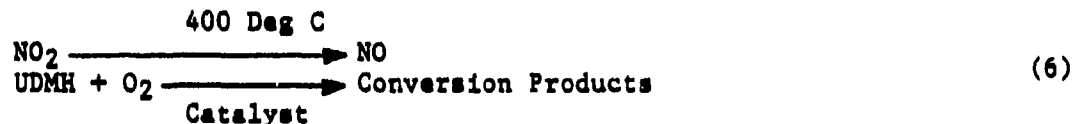


Figure 1. Reaction Chamber Design for a Chemiluminescence Nitric Oxide Detector

This is the technique used to measure UDMH and NO₂ in the original Titan II vapor detector application. In order to measure both fuel and oxidizer vapor levels independently, two detection channels are required, as shown in Figure 2. The two channels are identical except for the conversion conditions. A high-temperature pyrolyzer is used to convert UDMH to NO. At the conditions of this converter, both UDMH and NO₂ are converted to NO.



The second channel utilizes a converter designed to selectively convert NO₂. At these conversion conditions, UDMH does not produce NO.



The fuel and oxidizer levels in a sample are obtained by manipulating the signal outputs from the two chemiluminescence chambers shown in Figure 2. The difference in the two signals is proportional to the level of fuel in the

sample because no fuel signal is obtained from the oxidizer channel. Since there is no fuel response in the latter, the oxidizer channel output is proportional to the oxidizer level.

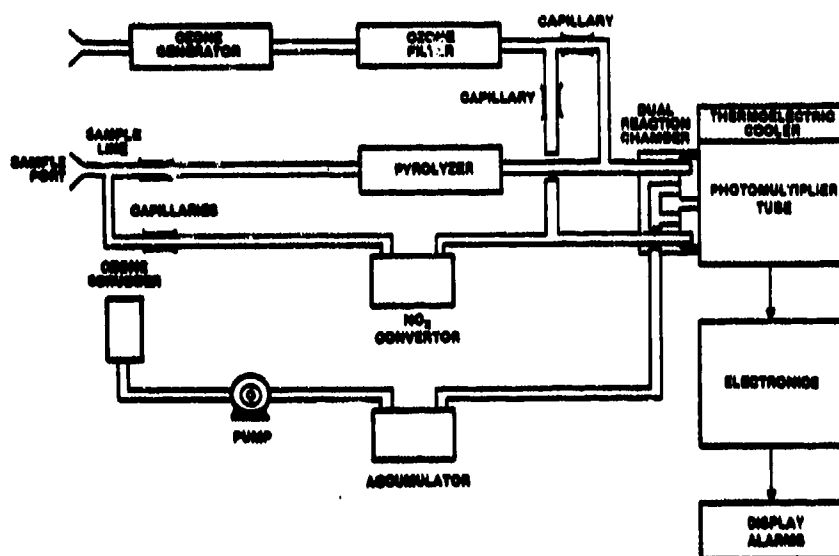


Figure 2. Chemiluminescence Analyzer for UDMH and NO₂ Detection

The detector design shown in Figure 2 is the design used for the Titan II system. Two chemiluminescence chambers are used with sample flowing continuously through both. A single photomultiplier tube detector, combined with a shutter to select one or the other chamber is used as a light detector. The continuous flow, combined with the inherently fast ozone chemiluminescent reaction, results in a nearly instantaneous measurement of the vapor levels. Continuously measuring the light output of each chamber for short intervals and calculating the resultant vapor levels provides real-time tracking of the vapor levels.

One important aspect of the NO chemiluminescence approach is its inherent wide dynamic range. The NO-ozone-light output reaction is linear up to NO levels that exhaust the supply of ozone. For the PFVDS design, this upper limitation is approximately 300-500 ppm of fuel or oxidizer. Since a PMT detector is a wide range linear detector, it produces a linear output over the entire range. The low detection limit is determined by the noise level of the PMT. For the PFVDS this is at approximately 0.010 ppm of fuel or oxidizer.

The NO chemiluminescence approach achieves another important goal, that of selectivity. Table I indicates the measured output for fuel and oxidizer of the two-channel system of Figure 2 for a variety of interferent compounds. Because NO chemiluminescence has few interferents from hydrocarbons, the system rejects most of these interferents with a high rejection ratio. Only ammonia, which is a nitrogen-containing compound, indicated a substantial signal. For the Titan II silo application, this ammonia response was not considered a problem.

TABLE I. TITAN II SYSTEM INTERFERENCE RESPONSES

FUEL INPUT: 1.5 PPM
OXIDIZER INPUT: 1.7 PPM

INTERFERENT	CONCENTRATION (PPM)	REJECTION RATIO	
		FUEL CHANNEL	OXIDIZER CHANNEL
TOLUENE	110	+1100:1	-11000:1
ETHYLACETATE	110	-2200:1	∞
HEXANE	110	+ 733:1	∞
METHANOL	100	-3333:1	- 2000:1
ACETONE	100	+1428:1	∞
PENTANE	110	+1571:1	-11000:1
FREON -113	100	+2000:1	-10000:1
DICHLOROMETHANE	95	- 950:1	- 4750:1
AMMONIA	125	+ 2:1	+ 250:1
HYDROGEN SULFIDE	100	-1000:1	∞
SULFUR DIOXIDE	100	∞	- 4000:1
HYDRAZINE, MMH	100	+ 20:1	+ 400:1
NO	100	+ 150:1	--
NO ₂	20	+ 105:1	--
UDMH	100	--	+ 200:1
WATER VAPOR	70% R.H.	>-50000:1	∞

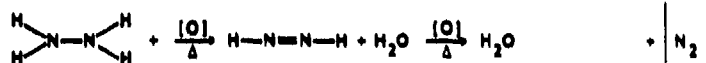
Although the system has a substantial response for ammonia, Table I indicates that its response to HZ and MMH is very low, 5 percent or less of the actual level. This occurs because the thermal and catalytic conditions that convert UDMH to NO tend to convert these two hydrazines to mostly nitrogen gas. Thus, the system designed for the Titan II application cannot be effectively used for the other two hydrazines.

DERIVATIVE DETECTION OF HYDRAZINES

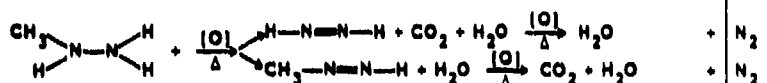
Although the original system filled the need for the Titan II silo monitoring system, its lack of response for HZ and MMH means that it cannot be used for more general propellant vapor detection. In addition, detection of propellants in the Space Shuttle system brings up the need to have good rejection for ammonia vapor. These two shortcomings of the original detection approach established the goals for an improved detection approach. Two years of development work resulted in a modification of the chemiluminescent approach which retains the basic performance characteristic of the original system, but allows all three hydrazines to be detected with increased rejection of nonhydrazine vapors.

The starting point for developing a new approach was a thorough investigation of the oxidation of the three hydrazines. The results of both theoretical and experimental investigations is summarized in Figure 3. HZ and MMH tend to oxidize to nitrogen gas, while the oxidation of UDMH produces both NO and nitrogen gas. No conditions have been found that produce nearly equal amounts of NO from all three hydrazine vapors.

HYDRAZINE



MMH



UDMH

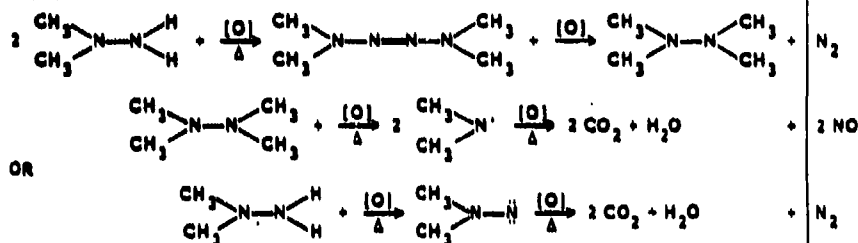


Figure 3. Oxidation of Hydrazine Propellants

Because direct oxidation of the hydrazines cannot be made to work, a variety of other approaches were considered. From this work, the idea of derivatization of the hydrazines developed. Basically, the idea is to convert the vapors of the hydrazines into compounds which can be oxidized to NO. Several problems arise with this approach. First, all three hydrazines have to be converted in such a way that the NO formed from each are nearly equal, in order to provide equal responses. Second, the derivatization has to occur rapidly in the gas phase, immediately eliminating many possible reactions. Third, the reaction has to be linear over a wide range of hydrazine vapor levels. Finally, the derivatizing material has to be easy to store and be practical to inject into the gas stream. Both liquid and solid materials were investigated. After many tests, it was found that the hydrazone-azine derivatives formed by using acetaldehyde produced the desired results. Figure 4 indicates the reactions that occur. Acetaldehyde vapor is mixed with the vapor of the hydrazines. In all three cases, a derivative is formed, a hydrazone or azine. When these are heated in the presence of a catalyst in air they form NO, as shown in Figure 5. Experimental results indicate that HZ and MMH produce approximately one mole of NO for each mole of hydrazine, while UDMH produces more than one mole per mole.

Figure 6 indicates a fuel vapor detection system based on the derivative approach. The detector consists of two identical channels operating at the same temperature and using the same catalyst. Acetaldehyde is introduced into one channel. The delivery system consists of a volume of liquid aldehyde in a tank pressurized with nitrogen. A flow restrictor controls the flow of nitrogen-aldehyde into the sample stream. The NO signal is measured in both channels, and the difference is the amount of hydrazines in the sample. The derivative channel is called the fuel channel, and the second channel the reference channel. The reference channel is identical with the fuel channel of the original Titan II design.

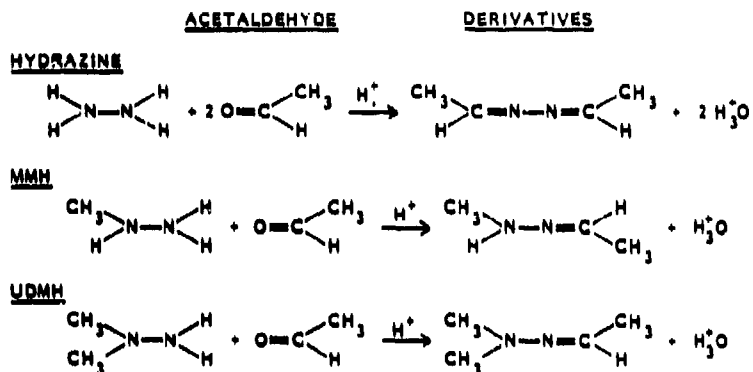


Figure 4. Acetaldehyde-Hydrazine Propellant Reaction Products

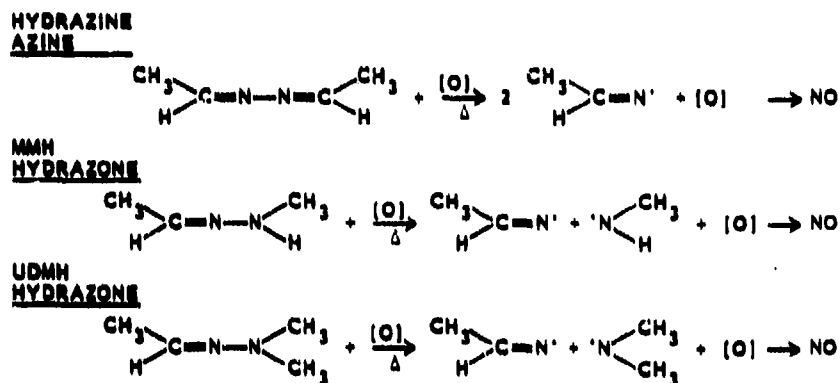


Figure 5. Oxidation Reactions of the Hydrazine Propellant Aldehyde Derivatives

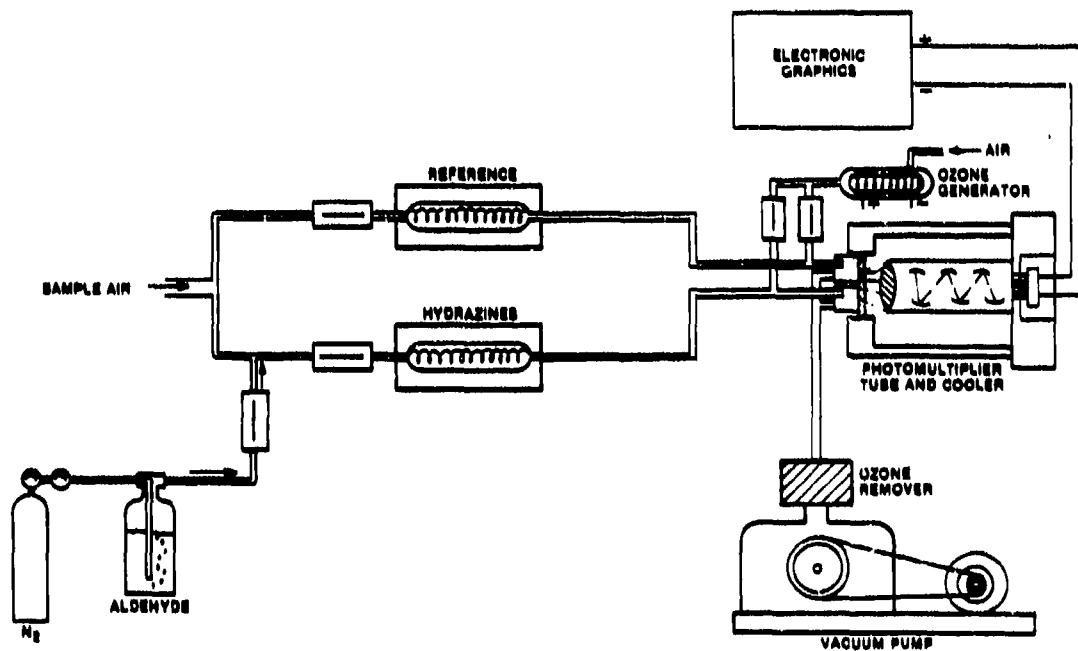


Figure 6. Hydrazines Detector System

The ideal output of this system is shown in Table II. Because the two channels are identical, any material that does not react with the acetaldehyde produces an identical output in each channel; therefore, the difference signal is 0. For the three hydrazines, the output of the fuel channel is increased because of the derivative oxidation. For HZ and MMH, the output of the fuel channel is one NO per molecule of fuel, while for UDMH it is two. However, the higher UDMH signal is balanced by the higher output for UDMH in the reference channel. When the operating conditions are properly adjusted, all three hydrazines will produce nearly equal difference signals with this system.

TABLE II. NITRIC OXIDE FORMATION FROM AIRBORNE PRECURSORS IN THE HYDRAZINES DETECTOR PYROLYZERS

COMPOUND SPECIES	OXIDATION PRODUCT		
	REFERENCE CHANNEL	ALDEHYDE CHANNEL	FUEL
$\text{NO} + \text{O}_2 \rightarrow$	NO	NO	-
$\text{NO}_2 + \text{O}_2 \rightarrow$	NO	NO	-
$\text{N}_2\text{O} + \text{O}_2 \rightarrow$	N_2	N_2	-
$\text{N}_2 + \text{O}_2 \rightarrow$	N_2	N_2	-
$\text{NH}_3 + \text{O}_2 \rightarrow$	NO	NO	-
AMINES + $\text{O}_2 \rightarrow$	NO	NO	-
NITRO COMPOUNDS + $\text{O}_2 \rightarrow$	NO	NO	-
CYANO COMPOUNDS + $\text{O}_2 \rightarrow$	NO	NO	-
HYDRAZINE + $\text{O}_2 \rightarrow$	N_2	2 NO	2 NO
MMH + $\text{O}_2 \rightarrow$	N_2	2 NO	2 NO
UDMH + $\text{O}_2 \rightarrow$	NO	2 NO	NO

The actual performance of the derivative system is close to the theoretical prediction of Table II. Tests performed with all three hydrazines with a system of the design of Figure 6 gave the results below:

FUEL & LEVEL	FUEL CHNL	OUTPUTS REFERENCE CHNL	DIFFERENCE
HZ 5.0 ppm	4.1	0.20	3.9 (78%)
MMH 5.0 ppm	4.7	0.30	4.4 (88%)
UDMH 5.0 ppm	6.0	1.20	4.8 (96%)

These readings differ from the theoretical, and the UDMH readings for the reference channel differ from the original Titan II system performance readings because the pyrolyzer operating conditions have been tuned to achieve as close a match as possible between the difference signals for the three fuels.

The amount of acetaldehyde in the sample stream determines the completeness of the aldehyde-hydrazine reaction and the linearity of the detector at high fuel vapor concentrations. Experiments have determined that levels between 1500 and 2500 ppm of aldehyde are sufficient to achieve almost complete conversion of any hydrazine in the sample, and will provide a linear response for vapor levels up to at least 100 ppm.

The specificity of the derivative approach has been demonstrated by its response to ammonia. Ammonia is representative of a variety of nitrogen-containing compounds that might be in an air sample. In addition, it is of particular interest to shuttle operations because ammonia is used on the shuttle. Several tests have been run with ammonia levels in the 1.0 to 9.0 ppm range, and the results have shown that the difference signal is less than 1 percent of the ammonia level being applied.³ These results indicate that the system should have a similar rejection ratio for other compounds of the same type. This is one of the strongest points of the derivative technique. It has a very high specificity for the hydrazines.

In order for a detection system based on the derivative approach to be responsive to both fuel and oxidizer vapor, another detection channel has to be added, one that responds to the oxidizer only. The same design that was used in the original Titan II system can be used. (See Figure 2.) The result is the three-channel design shown in Figure 7. The two fuel channels produce the fuel reading using their difference signal. The oxidizer channel has no response to the hydrazines or other nitrogen compounds, such as ammonia; therefore, its output is the oxidizer vapor level in the sample.

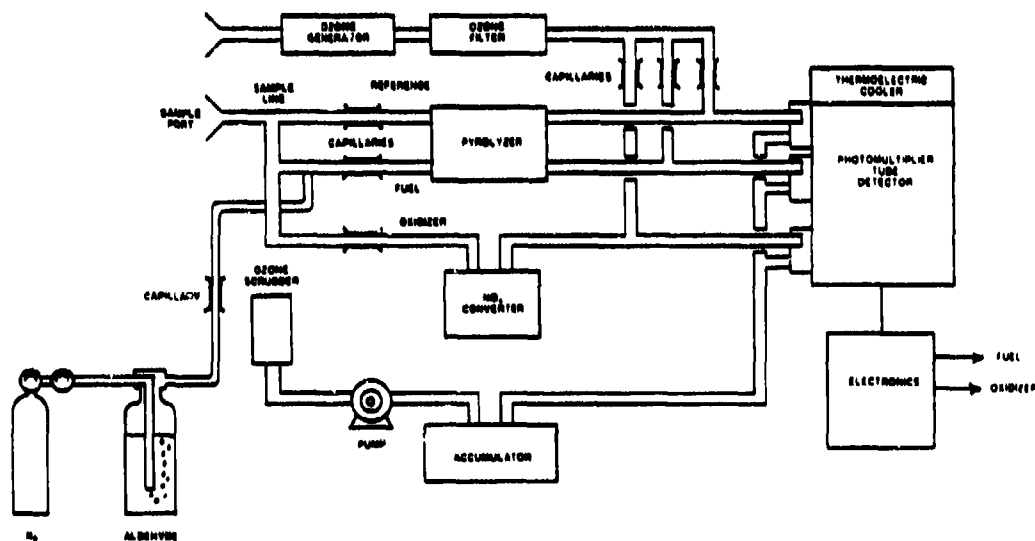


Figure 7. Design of a Hydrazines and Oxidizer Detection System

With the three-channel design, additional information can be obtained from the three signals generated. Once the fuel and oxidizer levels have been determined, these levels can be subtracted from either the fuel or reference

channel signal level. What remains is an indication of the level of ammonia or other nitrogen-containing vapor in the sample. As a result, this configuration can provide not only fuel and oxidizer levels, but also the levels of ammonia and other materials of this type in the sample. The relationships for all of these outputs are shown in Equations 7, 8 and 9.

$$(\text{ppm})_{\text{fuel}} = C_f \cdot (\text{ppm}_f - \text{ppm}_r) \quad (7)$$

$$(\text{ppm})_{\text{ox}} = C_o \cdot (\text{ppm}_o) \quad (8)$$

$$(\text{ppm})_{\text{nit}} = C_n \cdot [\text{ppm}_r - C_1 \cdot (\text{ppm})_{\text{fuel}} - C_2 \cdot (\text{ppm})_{\text{ox}}] \quad (9)$$

$\text{ppm}_f, \text{ppm}_r, \text{ppm}_o$ - NO outputs for fuel, reference and oxidizer channels

$(\text{ppm})_{\text{fuel}}, (\text{ppm})_{\text{ox}}, (\text{ppm})_{\text{nit}}$ - ppm levels readout for fuel, oxidizer, and nitrogen compounds

The parameters C_f, C_o , and C_n are calibration constants that convert the ppm NO outputs of the chemiluminescent detection chambers into levels of fuel, oxidizer, and nitrogen compounds. C_1 and C_2 are the conversion factors for fuel and oxidizer in the reference channel. C_1 is an average for the three kinds of hydrazines.

MULTIPLE-CHANNEL FUEL-OXIDIZER DETECTION SYSTEM

Part of the original development program for the Titan II application was the construction of a multiple-sample, fully automatic vapor analyzer system called the Propellant Fixed Vapor Detection System (PFVDS). This system was intended, at that time, to be a replacement for the existing fixed system in the Titan silos. Following the deactivation of the Titan II system, the PFVDS was field tested at the Titan III facility at Vandenberg AFB. After the successful demonstration of the derivative method for general hydrazine detection, the PFVDS was redesigned to incorporate this new technology. It utilizes the three-channel detection approach shown in Figure 7. The overall design of the system is shown in block diagram form in Figure 8. The system has nine individual sample inlet lines which consist of 3/8-in.-o.d. FEP Teflon tubing. All the lines can be individually controlled. The sample inlet consists of a Teflon filter and flame arrestor. Up to 500 feet of sample line can be used; however, very long sample lines slow the response of the system. Valving inside the main system enclosure selects which sample to analyze. The three-channel analyzer then measures the vapor levels in the selected sample. All of the operation of the system is controlled by a microprocessor-based controller. Because the main console should be close to the sampling points, the system is equipped with a remote readout and control console, the Vapor Detector Annunciator Panel (VDAP). This unit controls the system and provides a remote readout of the vapor levels. It can be located up to 5000 feet from the main console. In addition (particularly for NASA shuttle use), the system is equipped with a computer interface to the Launch Processing System (LPS) to allow control and readout of the system through a central computer.

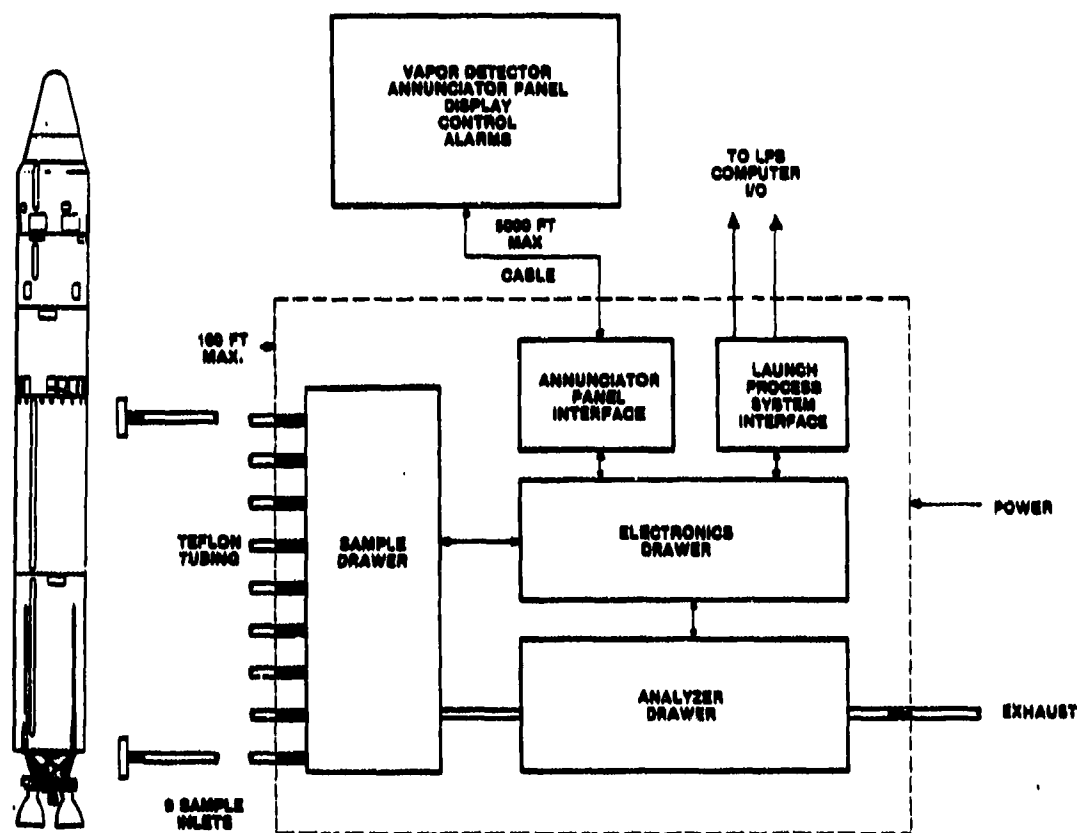


Figure 8. Block Diagram of the Principal Modules of the PFVDS

The main console of the PFVDS (see Figure 9) contains all of the components for the analyzer and sample system, and can be a stand-alone unit. The control panel of the console provides complete operational control of the system. However, when remote manual operation is required, the system is operated from the VDAP (Figure 10). Computer control of the system occurs through the LPS interface, a module in the upper half of the main console. This interface, which consists of a combination of digital and analog signals (68 in all) provides information to a central controller and receives operational commands from it.

A variety of operating modes are available with the PFVDS. One sample line can be sampled continuously, or all the active samples can be sampled in order. The number of sample lines that are active can be programmed, as well as how long each one is to be sampled. In addition to the fixed or scan modes, there is a mode that continuously samples all of the active samples. If a vapor level is detected in this combined sample, the system will scan the active samples to find the location of the vapor level. The system reports the levels of fuel, oxidizer, and "amines" in each sample. The amines reading is the ammonia and other nitrogen compounds channel. The system can be programmed to indicate two levels of alarms for each channel and for each of these readings. All of these levels are adjustable. For system maintenance, two forms of calibration can be performed, either manual or fully automatic,



Figure 9. PFVDS System Console

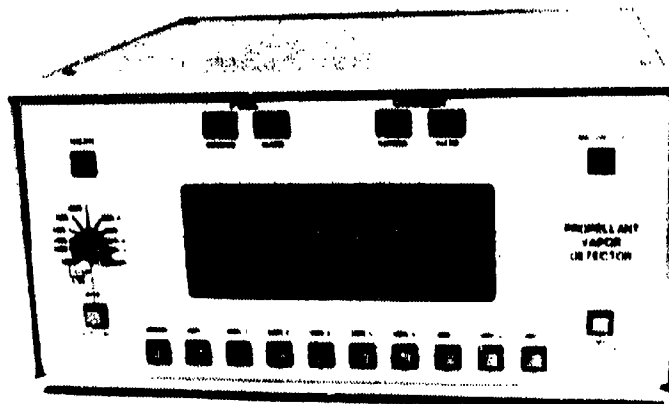


Figure 10. VDAP Display-Controller Module

the latter either on command or every 24 hours. To ensure that any malfunction is not overlooked, the system incorporates an automatic diagnostics system which continuously checks on critical parameters and flags any incorrect readings with a combination of malfunction indicators and messages on the system displays.

The updated PFVDS has been designed to meet the general range of needs for propellant vapor detection in Space Shuttle type applications. For this use, measurement of hydrazine, and MMH are the primary concern. The PFVDS is designed to have a linear measurement range for hydrazine, MMH, and oxidizer of 0 to 100 ppm. The designed low measurement limit of the system is

0.01 ppm, allowing accurate readings to be made to below present and anticipated TLV levels. The amine channel also allows the system to monitor ammonia levels, an important feature for shuttle applications. Because one analyzer is shared between the nine samples, the speed of recovery of the analyzer is important. Significant design effort went into the system to minimize this time.

Recent performance testing of the updated system demonstrates how well the PFVDS has met these design goals. Figure 11 indicates the response for hydrazine, MMH, and NO_2 . The response is basically linear over the target 0 to 100 ppm range, with only a slight nonlinearity in the hydrazine response. The difference in response to hydrazine and MMH is similar to that seen in the original derivative testing, and is caused by differences in the conversion efficiencies of the fuel and reference channels for the two vapors.

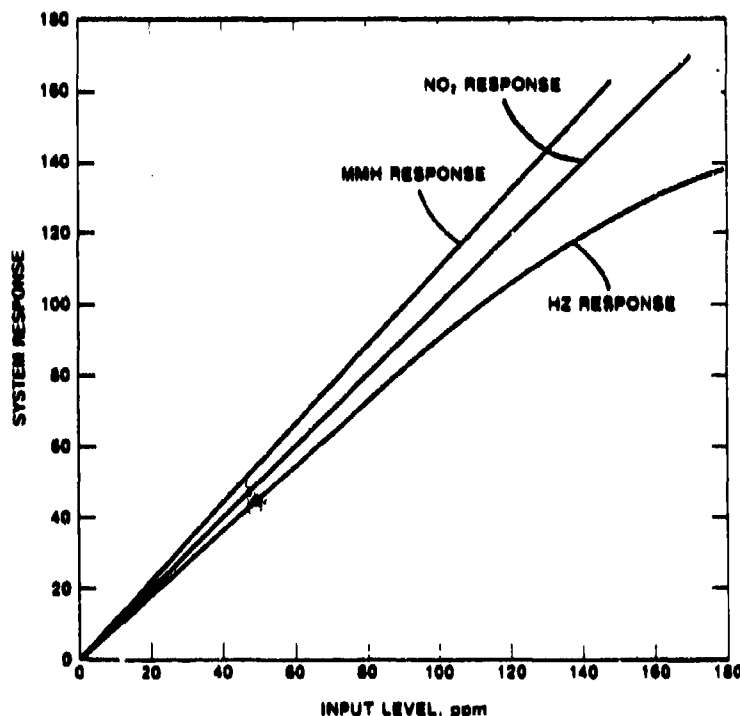


Figure 11. System Response for Fuels and Oxidizers

The measured noise level of the system is between 0.01 ppm for the oxidizer channel, and 0.02 ppm for the fuel channel, based on standard deviation measurements.

The response of the updated PFVDS to typical interferent materials is shown in Table III. As would be expected from the derivative technique, the results for fuel and ammonia responses are significantly improved from the original. The derivative approach enables the system to respond to hydrazine and MMH, but to discriminate against ammonia and other nitrogen-containing compounds.

TABLE III. SYSTEM INTERFERENCE RESPONSES

INTERFERENT	CONCENTRATION (ppm)	INTERFERENT RESPONSE, ppm		
		FUEL CHANNEL	AMINE CHANNEL	OXIDIZER CHANNEL
ACETONE	133	+0.00083	0	+0.00038
CYCLOHEXANE	114	+0.00080	0	+0.00035
TOLUENE	108	+0.00055	0	+0.00065
MEK	132	+0.00015	0	+0.00136
METHANOL	159	0	0	+0.00084
ISOPROPYL ALCOHOL	108	-0.00037	0	+0.00037
PENTANE	165	+0.00061	0	0
PERON-113	127	+0.00080	0	+0.00024
DICHLOROMETHANE	172	+0.00028	0	-0.00011
AMMONIA	111	-0.015	-	-0.0022
HYDROGEN SULFIDE	121	+0.00050	0	-0.0025
SULFUR DIOXIDE	117	+0.0018	0	-0.0030
HYDROZINE	1.1	0.927	0	0
MMH	0.96	1.115	0.05	0
NO ₂	6.16	0	0	1.06
WATER VAPOR	50% R.H.	-0.00002	-0.00002	0

- NOTE: 1. The above data are the ppm of fuel, amine or oxidizer obtained from 1 ppm of interferent.
2. The second column shows the actual level of interferent concentration used during the tests.

Because many vapor measurement situations involve measurements outdoors, the response of the system with varying humidity is important. Table IV indicates the measured performance of the PFVDS. Except at extreme conditions humidity has only a small influence on the sensitivity for fuel vapors, and almost no influence on oxidizer measurements.

TABLE IV. PFVDS RESPONSE TO DIFFERENT HUMIDITY LEVELS

		HUMIDITY LEVEL (RH)			
		0%	20%	50%	90%
MMH	INPUT LEVEL, ppm	0.95	1.02	0.96	0.91
	SYSTEM READING, ppm	0.86	1.19	1.07	0.65
H ₂	INPUT LEVEL, ppm	1.20	1.20	1.10	1.08
	SYSTEM READING, ppm	0.62	0.80	1.02	1.45
NO ₂	INPUT LEVEL, ppm	2.12	2.12	--	2.12
	SYSTEM READING, ppm	2.39	2.28	--	2.10

The response time for fuel and oxidizer vapor measurements is shown in Table V. In all cases the system indicates a first response within 20 seconds of applying a vapor level. As would be expected the response time to 75 percent of the final level for hydrazine and MMH is significantly slower than for NO₂. However, except for extremely fast scan rates, the system will always detect a level in a sample line, and will have little carryover to a subsequent sample, except in the case of a very high sample level in one line, and no sample in the subsequent line.

TABLE V. RESPONSE TIMES OF PFVDS

		HZ		MMH		NO ₂	
		FIRST DETECTION	75% OF SIGNAL	FIRST DETECTION	75% OF SIGNAL	FIRST DETECTION	75% OF SIGNAL
20% RH	GOING UP	22 sec	92 sec	20 sec	105 sec	18 sec	25 sec
	GOING DOWN	--	108 sec	--	57 sec	--	18 sec

NOTE: Going up meaning the signal rise and going down meaning the signal fall.

These performance data for the updated PFVDS system demonstrate the capabilities of the chemiluminescent-derivative approach for propellant detection. The current status of this system is that it has been completed, and will soon be delivered to the Naval Research Laboratories for further laboratory testing, after which it is scheduled to be field tested at NASA shuttle facilities in Florida.

REFERENCES

1. Rogers, P.M., "Remote Detection of Hazardous Materials (Propellants and Related Items)," Chemical Propulsion Information Agency, Laurel, MD, CPIA Publication 365 (1982).
2. Fraim, F.W. and Carroll, A.L., "Description of a New Rocket Propellant Vapor Detector for Titan II Missile Silos," CPIA Pub. No. 373, pp. 281-290 (1983).
3. Rounbehler, D.P., Fraim, F., Michalson, G., and Fine, D.H., "Description of a Chemiluminescent Detector System Specifically Designed for Monitoring Airborne Hydrazine Propellants: Hydrazine, Monomethylhydrazine, Unsymmetrical Dimethylhydrazine and Nitrogen Tetroxide Oxidizer," CPIA Pub. No. 436, pp. 389-400 (1985).

MEASUREMENT OF HYDRAZINE CONTAMINATION IN SOILS

C.S. Leasure, Senior Scientist

Lockheed-EMSCO

White Sands Test Facility

Las Cruces, NM 88004

E.L. Miller, Principal Scientist

Lockheed-EMSCO

White Sands Test Facility

Las Cruces, NM 88004

ABSTRACT

A dilute acidic extraction method was developed to quantitatively extract three hydrazines (hydrazine, HZ; monomethylhydrazine, MMH; and unsymmetrical-dimethylhydrazine, UDMH) from soil. The soil used in the extraction is representative of local soil, and the calculated efficiency of extraction takes oxidation of the hydrazines by the soil into account. Derivatization of the hydrazines in the resulting aqueous extracts was unsuccessful with acetone and several other agents, but successful with 2,4-pentanedione. All three hydrazines were derivatized, including UDMH which formed 2-dimethylhydrazone-4-pentanone. The derivatized hydrazines were analyzed by gas chromatograph (GC) equipped with a thermionic ionization detector operating at nitrogen-sensitive conditions. The concentration of 2,4-pentanedione in the extract was found to affect the derivatization efficiency of the three hydrazines, especially UDMH. Detection limits of the hydrazines in the soil, without preconcentration, are 0.1 ppm for HZ, 0.2 ppm for MMH, and 0.5 ppm for UDMH. This method is also applicable to the determination of hydrazines in water.

INTRODUCTION

BACKGROUND

Hydrazine fuels, used in aerospace applications, are suspected carcinogens and considered hazardous substances by the US Environmental Protection Agency (Reference 1). Soil

contamination by these chemicals is therefore subject to regulation, and the identity and quantity of hydrazines in soil must be determined. Adequate analytical methods have been developed for the determination of trace levels of hydrazines in air and water. Many of these methods derivatize hydrazines before analysis by gas chromatography (GC). Aqueous extraction of hydrazines from soil, however, may produce matrices that interfere with agents used in the subsequent derivatization.

Since the hydrazines are thermally labile compounds and not amenable to gas chromatography, they are usually derivatized by reaction with a carbonyl-containing organic compound. More than six different derivatizing agents have been reported for hydrazines, including pentafluorobenzaldehyde, p-chlorobenzaldehyde, salicylaldehyde, furfuraldehyde, acetone, and 2,4-pentanedione (References 2 - 6). Acetone has been found to be the most satisfactory derivatizing agent for the determination of hydrazines from air or water (References 4 and 5). However, the reaction between acetone and hydrazines to form hydrazones is reversible and may not be appropriate for soil extracts.

Soil matrices and the interaction of these matrices with hydrazines in soils are complex. These interactions can include complexation, adsorption, chemisorption, autooxidation, and catalytic decomposition. Therefore, an effective soil extraction method must extract all the available hydrazines from the soil.

APPROACH

An extraction method is required to quantitatively extract all hydrazines from soils, less those which have been oxidized or decomposed, into a solution that can be analyzed. Such an extraction method, however, may also extract substances that interfere in either the derivatization or rate of derivatization of these hydrazines when analyzed. Therefore, a derivatization reaction that produces stable reaction products and is not matrix dependent is needed.

EXPERIMENTAL

EXTRACTION

To obtain percent recovery of the hydrazines from soil using the extraction procedure, hydrazines were first added to the soil. The soil was then rolled in a ball mill for 15 minutes before the hydrazines were extracted using the following procedure.

To a mass of 100 grams of soil, 200 mL of deionized water and then 10 mL of reagent-grade concentrated sulfuric acid were added. The soil and acid were mixed and boiled for five minutes. The mixture was filtered, and the residue was rinsed with two 25-mL volumes of deionized water, the rinse liquid being combined with the filtrate. The filtrate was then passed through a membrane filter, and the residue was rinsed with 10 mL of deionized water, the rinse liquid again being combined with the filtrate. The resulting filtrate was then ready to be analyzed for extracted hydrazines.

DERIVATIZATION AND ANALYSIS

The extracted hydrazines were derivatized immediately after extraction from soil by adding 5 mL of 2,4-pentanedione to the filtrate, adjusting the pH to 9 using a 50 percent NaOH solution, and diluting the solution to 500 mL with deionized water. The hydrazine derivatives in aqueous solution were analyzed using a Hewlett Packard model 5890A gas chromatograph (GC) equipped with a thermionic ionization detector (TID). Analysis was performed under conditions which were both sensitive and selective to nitrogen-containing compounds. The conditions for analysis were as follows:

- Column: 0.25 mm id, 20 m, 0.25 m, Carbowax 20M capillary column
- Detector: thermionic ionization detector
- Detector temperature: 230°C
- Injector temperature: 250°C
- Split flow: 70 cm³/min

- Splitless time: 1 min
- Oven Initial Temperature: 70°C
- Oven Initial Time: 0 min
- Program Rate: 10 °C/min
- Oven Final Temperature: 190 °C
- Carrier Flow (Helium): 1 cm³/min
- Makeup Flow (Helium): 24 cm³/min
- Hydrogen Flow: 3 cm³/min
- Air Flow: 100 cm³/min

Three derivatives were formed upon extraction with 2,4-pentanedione: 3,5-dimethyl pyrazole (DMP) from HZ; 1,3,5-trimethyl pyrazole (TMP) from MMH; and 2-dimethylhydrazone-4-pentanone (DMHP) from UDMH. Each of these derivatized compounds was prepared at concentrations near 250 ppm. In addition, DMP and TMP were obtained as 95 - 99 percent pure reagents (from Aldrich Chemical Co., Milwaukee WI, and K & K Laboratories, Plainview, NY). The third derivative, DMHP, could not be obtained. Therefore, DMHP was prepared by mixing a known amount of 99 percent UDMH (from Olin Chemicals, Stamford, CT) with a large excess of 2,4-pentanedione.

Each of these derivatives was identified by gas chromatography/mass spectrometry (GC/MS) and fourier transform infrared spectroscopy (FTIR). Calibration curves were collected for DMP, TMP, and DMHP at the same detector sensitivity.

RESULTS

EXTRACTION

Standard solutions of HZ, MMH, and UDMH were prepared by mixing known volumes of the 98 - 99 percent pure liquids in sufficient dilute sulfuric acid to make 1.00 liter of each solution. The concentration of each solution was certified by coulometric titration of a known volume of the solution (Reference 7). Known masses of each hydrazine were treated according to the extraction procedure described previously (no soil was used), and the recovery was determined in each case by coulometric titration. The extraction of each mass of hydrazine

was tested in triplicate, and the percent recoveries are indicated in table 1.

Soil believed to be free of hydrazines was treated according to the extraction procedure previously described. Oxidants in the extract were quantitatively determined by adding potassium iodide to the extract and titrating the liberated triiodide with an arsenic(III) oxide solution prepared from primary-standard As_2O_3 . The test was performed in triplicate. The soil from the area was found to contain sufficient oxidants to consume 1.7 mmol of arsenic(III) oxide per kg. (This is equivalent to 54 mg of hydrazine, or 78 mg of monomethylhydrazine, or 203 mg of unsymmetrical dimethylhydrazine, per kg of soil.)

Soil was artificially contaminated with hydrazines and extracted. The hydrazine content of each extract was determined by coulometric titration and, in the cases of HZ and MMH, by spectrophotometer with para-dimethylaminobenzaldehyde (PDAB). The extraction of each mass of hydrazine from soil was tested in duplicate and gave the yields and recoveries (after allowance for oxidation by the soil) indicated in table 2.

TABLE 1. RECOVERY OF HYDRAZINES FROM KNOWN SOLUTIONS

Compound	Mass (mg)	Recovery (%)
HZ	0.025	99
	0.248	102
	2.48	98
MMH	0.037	105
	0.368	100
	3.680	101
UDMH	0.046	97
	0.459	101
	4.590	100

TABLE 2. YIELD AND RECOVERY OF HYDRAZINES FROM CONTAMINATED SOIL

Compound	Mass (mg)	Yield (mg)	Recovery ^a (%)
HZ	1	<0.01	---
	5	<0.01	---
	10	4.5	98
	25	19.6	100
MMH	5	<0.01	---
	10	2.2	100
	25	17.4	101
UDMH	10	<0.01	---
	25	4.4	94
	100	80.1	101

^a The average unrecoverable amount lost to the soil is equivalent to 5.4 mg HZ, 7.8 mg MMH, and 19.9 mg UDMH. Therefore, when 17.4 mg of MMH is recovered from soil spiked with 25 mg of MMH, the percent recovery is $17.4 \text{ mg recovered} / 17.2 \text{ mg theoretical recovery} = 101 \text{ percent recovery}$.

DERIVATIZATION AND ANALYSIS

Six derivatizing agents were considered for the hydrazines in the aqueous extracts. The initial choice was acetone, since acetone was reported to be successful for all three hydrazines in question (Reference 4) and worked well at White Sands Test Facility with samples of deionized water spiked with hydrazines. However, when acetone was used as the derivatizing agent in actual spiked soil extracts, no derivatized hydrazines were obtained. Several of the other potential derivatizing agents were discarded after experimentation showed that they would not derivatize all three of the hydrazines. Finally, 2,4-pentanedione was tried, which was reported in Reference 6 to derivatize HZ and MMH but not UDMH (Reference 6). Relatively

high concentrations of 2,4-pentanedione (approximately 1 percent) did derivatize UDMH, and the derivative was identified by GC/MS as DMHP.

The retention times, mass spectra, and infrared spectra for the purchased DMP and TMP are identical to those substances extracted using the appropriate hydrazine and 2,4-pentanedione. No source of pure DMHP was found. The mass spectrum and infrared spectrum for DMHP are shown in figures 1 and 2.

The average derivatization efficiencies for hydrazine and MMH were determined and found to be 127 percent and 101 percent, respectively. The derivatization efficiency for DMHP was probably near-quantitative under the identical conditions but could not be measured since a primary standard was not available. The DMHP response factor of 32,326 area counts/ppm was near that for DMP (19,224 area counts/ppm). The response factor for TMP was 21,342 area counts/ppm. The response of the detector was

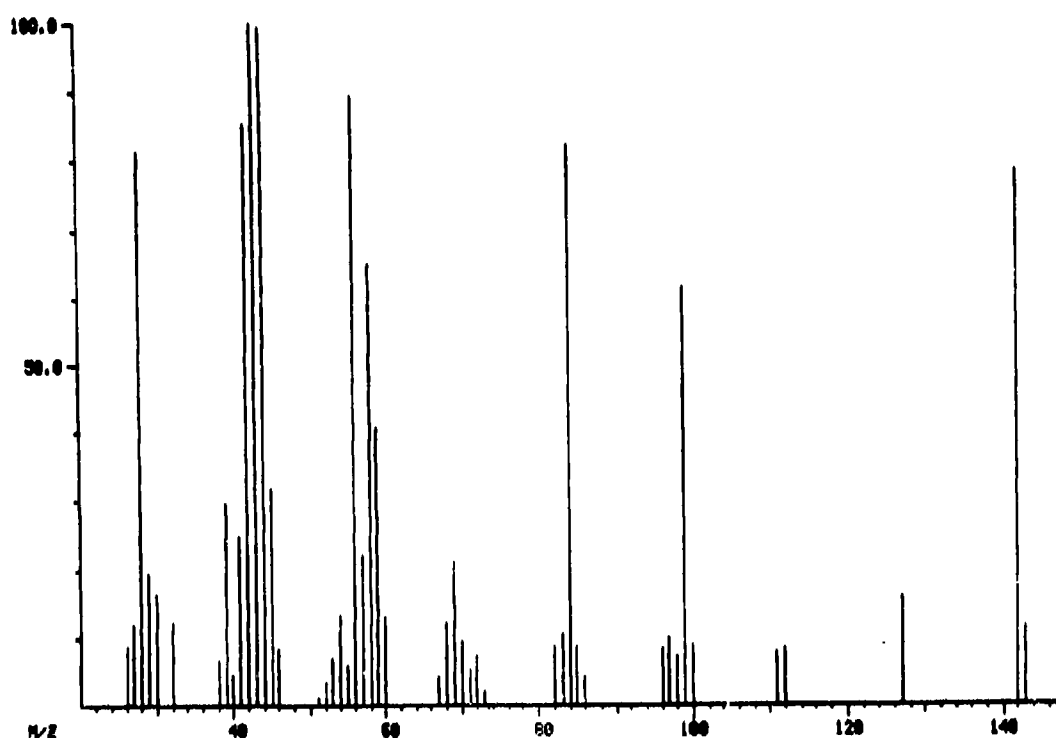


Figure 1. Mass Spectrum of 2-Dimethylhydrazine-4-pentanone

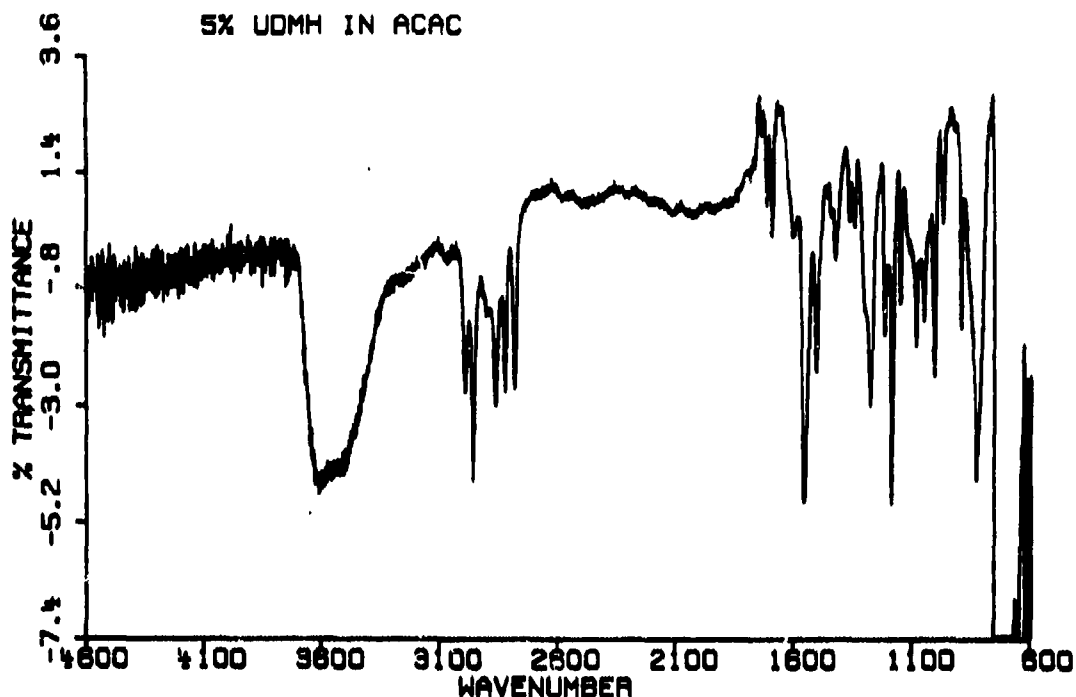


Figure 2. Infrared Spectrum of 2-Dimethylhydrazone-4-pentanone linear for each of the three derivatized hydrazines over nearly three orders of magnitude.

The concentration of 2,4-pentanedione was found to be critical for the complete derivatization of UDMH. A one-percent 2,4-pentanedione concentration was found to produce near-complete derivatization of each of the hydrazines whereas a 5×10^{-3} percent concentration did not allow complete derivatization of UDMH. With the 5×10^{-3} percent 2,4-pentanedione concentration, most of the UDMH apparently decomposed or vaporized when the solution pH was raised above 7; however, the hydrazine and monomethylhydrazine derivatives appeared to be stable under those conditions.

The minimum detectable limits in the soil for each of the hydrazines (which are approximately three standard deviations above the blanks) are 0.1 ppm for HZ, 0.2 ppm for MMH, and 0.5 ppm for UDMH. Note that the minimum detectable limit for TMP is higher than for DMP. This is a reflection of the higher background generally seen near the retention time for TMP. The

minimum detection limit for DMHP is higher than the other two and reflects the lower analytical precision for this species.

CONCLUSIONS

The results of this work can be summarized as follows:

- All available hydrazines (HZ, MMH, and UDMH) can be extracted from contaminated soil using an acidic extraction method.
- This acid extraction method apparently extracts other substances; these substances interfere with some previously reported derivatization methods for hydrazines.
- The derivatization method used in this study creates stable derivatization products that are amenable to analysis by gas chromatography. This method works well for hydrazine, monomethylhydrazine, and, to a lesser extent, unsymmetrical-dimethylhydrazine.
- A derivative of UDMH can be made using a one-percent 2,4-pentanedione concentration.
- Detection limits using this method are 0.1 ppm for HZ, 0.2 ppm for MMH, and 0.5 ppm for UDMH.

REFERENCES

1. Code of Federal Regulations, Section 261, Appendix IX, 1987.
2. Liu, Y.Y., I. Schmelz, and D. Hoffman, "Chemical Studies on Tobacco Smoke-Quantitative Analysis of Hydrazine in Tobacco and Cigarette Smoke," Analytical Chemistry, April 1974, pp. 885 - 889.
3. Wood, G.O. and R.G. Anderson, "Sampling and Analysis of Hydrazines in Air," Paper #136, American Industrial Hygiene Conference, Atlanta, GA, May 17 - 22, 1976.
4. Holtzclaw, J.R., S.L. Rose, J.R. Wyatt, D.P. Rounbehler, and D.H. Fine, "Simultaneous Determination of Hydrazine, Methylhydrazine, and 1,1-Dimethylhydrazine in Air by Derivatization/Gas Chromatography," Analytical Chemistry, December 1984, pp. 2952 - 2956.
5. Selim, S.L. and C.R. Warner, "Residue Determination of Hydrazine in Water by Derivatization and Gas Chromatography," Journal of Chromatography, 1978 (166: 2), pp. 507 - 511.
6. Dee, L.A., "Gas Chromatographic Determination of Aqueous Trace Hydrazine and Methylhydrazine as Corresponding Pyrazoles," Analytical Chemistry, Sept. 1971, pp. 1416 - 1419.
7. Johnson, R.P. and E.L. Miller, "Quantification of Hydrazines and Hydrazones," Proceedings of the 1984 JANNAF Propellant Characterization Subcommittee Meeting, 1984.

LOW PPB LEVEL DETECTION OF TOXIC COMPOUNDS WITH A
FULLY AUTOMATED CO₂ LASER PHOTOACOUSTIC DETECTOR

S. M. Beck, M. L. Takayama, R. L. Corbin and G. L. Loper
Chemistry and Physics Laboratory
The Aerospace Corporation
P. O. Box 92957
Los Angeles, CA 90009

ABSTRACT

Progress towards developing a breadboard CO₂ laser photoacoustic detector capable of monitoring a wide variety of toxic compounds at less than 100 ppb in ambient air is described.

Key achievements include: (1) development of an acoustic frequency tracking device which allows use of a sensitive resonant photoacoustic cell in changing temperature and humidity conditions, (2) development of an electronic spectrum analyzer which provides a means for the computer to scan the CO₂ laser, (3) development of software algorithms which allow efficient and accurate analysis of a gas sample, and (4) actual analysis of laboratory prepared gas mixtures.

The instrument has been demonstrated in a laboratory environment to be capable of automatically and simultaneously monitoring several toxic compounds at low ppb concentrations in laboratory prepared mixtures. The detector was able to detect hydrazine at concentrations as low as five ppb in mixtures containing three other interferent gases at concentrations as high as 600 fold greater.

INTRODUCTION

Laser photoacoustic (PA) detection promises to be a useful technique for monitoring airborne compounds below the 100 parts per billion (ppb) concentration regime.¹⁻³ With the addition of laser wavelength tuning, the technique is capable of analyzing a gas mixture for its component identities and concentrations.^{4,5} This is a critical attribute for toxic vapor monitoring where more than one compound may be of concern. In a scenario where the analyzer is used as a toxic vapor monitor, component analysis reduces the possibility of a false alarm caused by the presence of nontoxic interfering gases. While no such instrument has yet been reported, we review here progress towards development of a CO₂ laser based photoacoustic trace gas analyzer, capable of analyzing in real time, mixtures of gases below 100 ppb in air.

This review is divided into sections, each dealing with a specific aspect of the instrument development. In the first section the principle of operation of a PA gas analyzer is discussed. Subsequent sections deal with the light source, the

PA cell, laser tuning, wavelength verification and computer control of the instrument. Finally, results of recent breadboard instrument tests on laboratory gas mixtures are presented.

RESULTS AND DISCUSSION

PRINCIPLE OF OPERATION

The photoacoustic effect was first discovered by Alexander Graham Bell when he noticed that an amplitude modulated sunbeam striking a solid black surface, produced an audible tone at the modulation frequency. In modern applications of the technique, a laser beam replaces the sunbeam and a sensitive microphone serves as the "ear". A schematic of a typical photoacoustic apparatus is shown in Figure 1. The technique, applied to a gas mixture, works as follows; a laser photon is absorbed by a sample gas molecule, in resonance with the laser wavelength. The photon energy is rapidly converted to heat by collisions of the excited molecule with background molecules. This heat produces a local pressure rise, which propagates outward from the point of photon absorption. If the laser beam is amplitude modulated at an acoustic frequency, the pressure waves which are produced are also periodic and can be detected by a microphone located nearby. The technique is extremely sensitive, capable of detecting gases at concentrations below 1×10^{10} molecules/cm³.

Analysis of gas mixtures containing n components is straightforward. The optical absorption of the gas sample is measured by the PA apparatus at m laser wavelengths where $m \geq n$. From these measurements, and a library of spectral data, a set of linear equations is set up relating the measured absorptions at each wavelength, absorption cross sections for possible constituent gases, and the unknown concentrations of these gases. This coupled set of equations is then solved using matrix algebra, the result being the identity and concentration of each gas in the mixture.

Work has been performed to determine how uncertainties in the measured sample absorbances at the monitoring laser wavelengths, as well as in the cross-section data for the components in the gas mixture, influence the uncertainties in the calculated concentrations of the components. Average concentration errors have been calculated as a function of average errors in the cross sections and absorbances for three hypothetical mixtures containing hydrazine, monomethylhydrazine (MMH), and unsymmetrical dimethylhydrazine (UDMH), and various combinations of three other components. The gases in the mixtures were assumed to be present in equal concentrations. Random errors were then induced in our previously measured cross sections for these compounds and the sample absorbance values predicted from the original cross-section data. This simulation showed that the average concentration errors increase in nearly

a linear manner with an increase in the magnitude of the average error in the cross-section data and sample-absorbance values. For the three hypothetical mixtures, when the random induced errors averaged 5%, the average concentration error was predicted to be less than 10% when 18 or more monitoring wavelengths were used, and less than 20% when as few as six wavelengths were used. The components of a mixture could thus be determined with satisfactory accuracy in cases where the average absorbance and cross-section errors were 5% or less, even when the minimum number of monitoring wavelengths were used.

THE LIGHT SOURCE

The CO₂ laser is an ideal light source for monitoring airborne organic and inorganic compounds because its wavelength is tunable over the 9 μ m and 11 μ m region of the infrared spectrum. This region overlaps strong, structured absorptions for a large number of organic and inorganic compounds. For this reason it has been termed the "finger-print" region of the infrared spectrum and has been used for decades by organic and inorganic chemists for compound identification by standard infrared absorption spectroscopy. In addition, there is an atmospheric transmission window in the 8-12 μ m spectral region, reducing background interferences by water and carbon dioxide.⁶

Figure 2 shows the absorption cross sections at various CO₂ laser wavelengths for several compounds of potential interest. The magnitude of the infrared absorptions provide the CO₂ laser-based PA detector with high sensitivity, while the uniqueness of the CO₂ laser spectral profiles allows specific identification of the various compounds.

The laser itself is a sealed tube RF discharge CO₂ laser, with line tunability provided by a grating and piezoelectric mounted output coupler. The laser is tunable over 70 discrete rotational lines from 9 μ m to 11 μ m, with the strongest lines providing 5 watts of power.

LASER TUNING AND WAVELENGTH VERIFICATION

CO₂ laser wavelength tuning is an essential part of the PA analysis technique. It is also important to verify that the laser is at the correct wavelength, as any error in line identification would produce completely erroneous concentration values.

The laser tuning and wavelength measurement are under computer control. Tuning is provided by a computer controlled stepper motor which tilts the laser grating to the appropriate angle for a given laser line. Optimization of the output power of a given laser line is accomplished by computer monitoring of the laser output wavelength and power while small adjustments

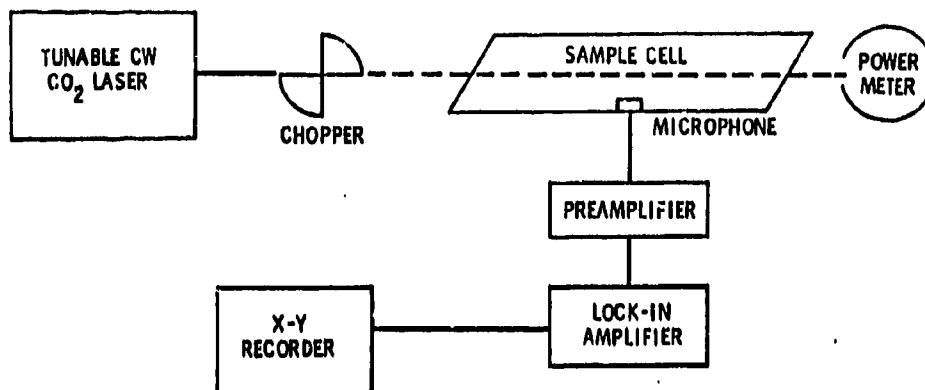


Figure 1. Schematic of a typical photoacoustic apparatus. Light from a line tunable CO_2 laser is amplitude modulated by a mechanical chopper. Absorption of this light by the sample produces a periodic pressure wave in the sample cell which is detected by a microphone. The resulting electrical signal is processed by the detection electronics.

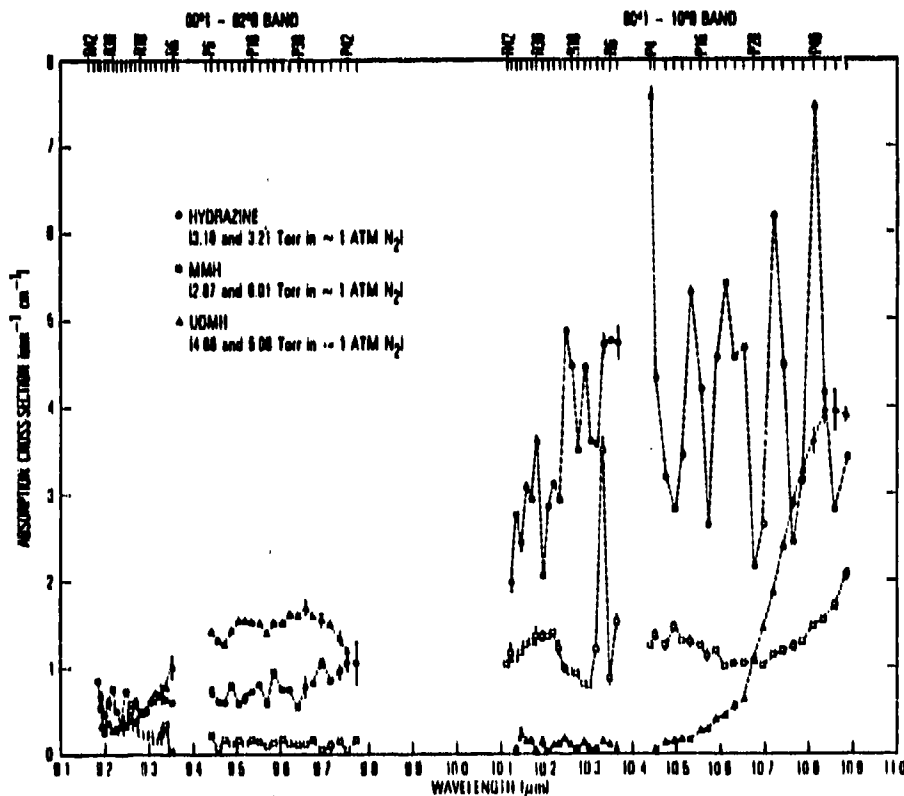


Figure 2. Absorption cross sections at various CO_2 laser wavelengths for hydrazine, monomethylhydrazine (MMH) and unsymmetrical dimethylhydrazine (UDMH). The spectra for these structurally similar molecules can readily be distinguished from each other. Most airborne organic and inorganic molecules display unique spectra in the CO_2 laser wavelength region, providing the photoacoustic technique with generality and specificity.

are made in grating position and piezoelectric voltage by the computer. The time required to tune from one line to another and take a photoacoustic absorption measurement, is about 90 seconds.

The laser wavelength is monitored by a laboratory built grating spectrograph. The laser output is detected by a thermistor array placed at the exit focal plane of the spectrograph. The electrical output of the array is multiplexed and sent to the computer. Ten percent of the CO₂ laser power is split off and sent through the spectrograph, allowing continuous monitoring of the laser wavelength.

THE CELL

Both acoustically resonant and nonresonant PA cells have been reported for use in trace gas detection. The resonant cell has certain advantages which make it an attractive candidate for an actual real time field gas analyzer. Properly designed, it has higher immunity to noise generated by laser light absorbed at the cell windows, and turbulence produced by sample flow. This eliminates the need for a reference cell which may require frequent calibration. Additionally, the resonant cell can have a large volume-to-surface ratio and still maintain high responsivity, thus minimizing the chance for sample loss due to surface adsorption.

Based on the above arguments, we have selected a resonant PA cell for the prototype gas analyzer. The cell, shown in Figure 3 is of the Amer and Garlach design.⁸ It is a cylindrical cavity designed to operate at the frequency of its first radial mode. Laser beam entrance windows and gas ports are located at the nodal positions of this mode, insuring poor coupling between noise produced at these locations and the detection microphone. The microphone which detects the PA signal is mounted at the center of one cylinder face, the position of the maximum pressure amplitude of the first radial mode. Figure 4 shows the cell response versus ethylene concentration in nitrogen. The various noise contributions due to gas flow, window absorption, and ambient and coherent chopper sound are indicated on the figure. The minimum detectable flowing ethylene concentration monitored at the P(14) 10 μ m band CO₂ laser line is 1.8 ppb at 1 watt laser power.

As mentioned above, sample adsorption at cell surfaces can make accurate detection, especially of polar compounds, difficult. The resonant cell's large volume to surface area ratio, and its ability to operate at high sample flow rates help to reduce the problem of adsorption. In addition, however, a large number of experimental tests were performed to evaluate the effectiveness of various cell coating materials in reducing sample adsorption. It was determined from these tests that thin coatings of TFE teflon or paraffin wax, over the cell's metal surface, could completely eliminate loss of either ammonia or

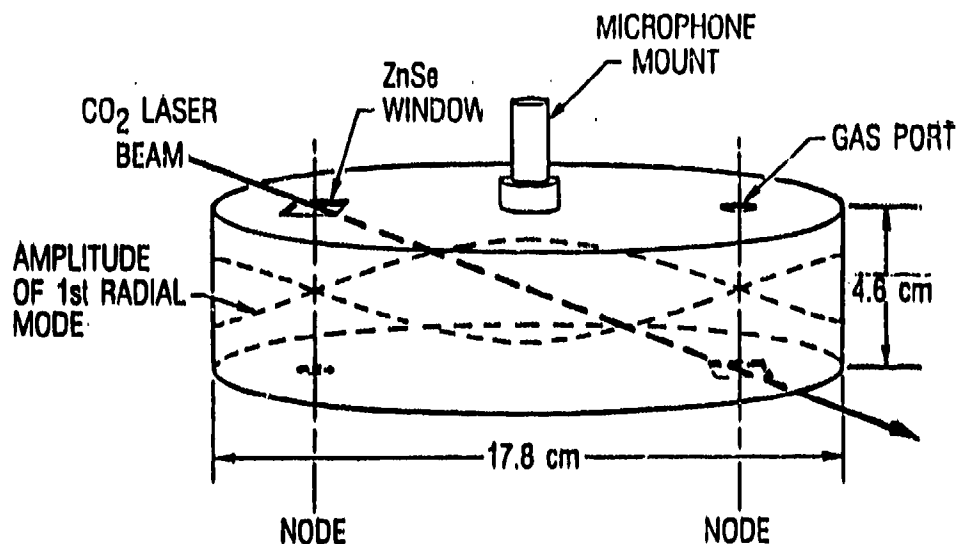


Figure 3. Resonant photoacoustic cell for the prototype gas analyzer. The thin dashed curves represent first radial mode amplitudes of the cell, separated in phase from each other by 180° . The placement of the laser beam entrance windows and gas ports at the node of this mode minimizes coupling between noise generated at these positions and the detected radial pressure wave. The microphone is placed at the point of maximum amplitude of the first radial mode.

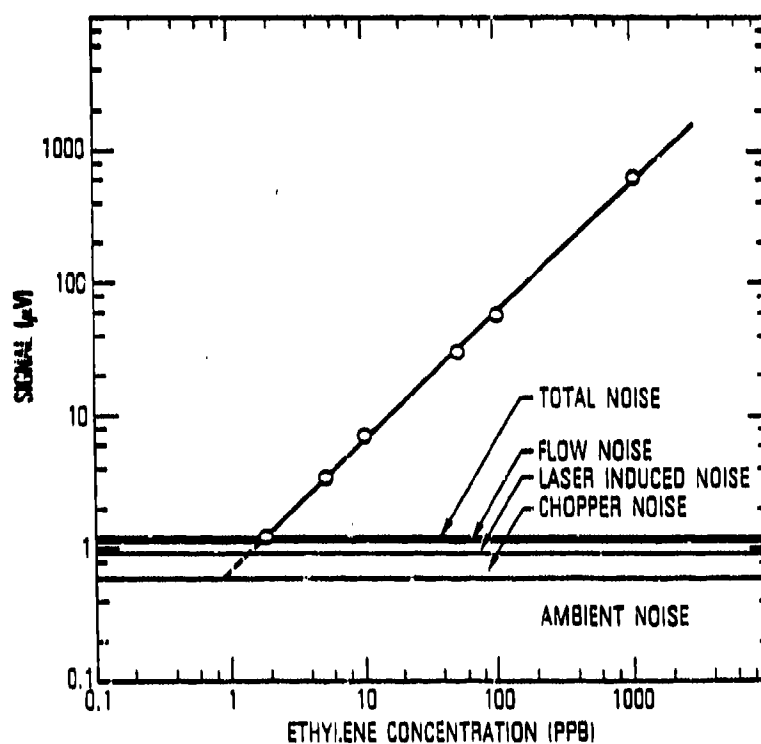


Figure 4. Log-log plot of the resonance cell response versus ethylene concentration in nitrogen. Also shown are the noise floors due to several contributing sources which limit the ethylene detection level to 1.8 ppb at one watt of laser power.

hydrazine by adsorption.² Both of these polar compounds strongly adsorb to metal, glass, or ceramic surfaces.

FREQUENCY TRACKING AND DATA ACQUISITION

In spite of certain inherent advantages described above, the use of the resonant PA cell for field use has been limited by the fact that the cell's response is typically more than 500 times greater at modulation frequencies equal to the cell's acoustic resonance frequency than at slightly different frequencies. This requires that the light modulation frequency be continuously maintained at the cell's acoustic resonance frequency. This is particularly difficult since that frequency is a sensitive function of gas temperature and composition. For a typical cell with a high quality factor ($Q = 500$), driven at a constant frequency, a one degree temperature change translates to a greater than eighty percent drop in cell responsivity.

In order to alleviate this problem, we have developed a novel electronic device that automatically tracks the resonance frequency of the resonant cell under changing temperature and humidity of the gas sample. The device uses the high acoustical bandpass filter properties of the cell itself to detect changes in the acoustic resonance frequency and automatically adjusts the laser light modulator to this frequency to maintain the peak photoacoustic signal. The device also serves as the photoacoustic system's signal processing electronics, eliminating the need for a lock-in amplifier. A block diagram of the tracking/acquisition device is shown in Figure 5. The principle of operation of the device is as follows. A small speaker, placed inside of the resonant cell, is initially made to emit a broad range of acoustic frequencies. The cell resonates preferentially at its acoustic resonance frequency. Acoustic energy is dissipated rapidly in the cell at nonresonant frequencies. The cell microphone thus selectively detects sound at the cell's radial mode resonance frequency. The signal detected by the microphone is fed back into a 34 db input amplifier, through a voltage controlled attenuator (VCA), and through another 34 db output amplifier. The sinusoidal voltage signal v_1 exiting the output amplifier has a frequency equal to the cell's acoustic resonance frequency and drives the speaker. The signal v_1 is also fed into a rectifier to produce a DC voltage V_1 proportional to the amplitude of v_1 . V_1 is compared to an internal DC reference voltage V_{REF} by the VCA driver. The VCA driver produces a DC output voltage V_2 which is proportional to $V_1 - V_{REF}$. The voltage V_2 controls the amount of attenuation produced by the VCA. The portion of the device described so far forms an acousto-electronic loop. The loop oscillates at the particular cell resonance frequency with a small, constant amount of acoustic energy in the cell. The DC output voltage V_2 rapidly adjusts to a constant value K in the absence of any light absorption by the gas in the cell.

Another portion of the device drives a mechanical chopper which modulates the laser light intensity. The signal V_1 , whose frequency is equal to the cell resonance frequency, is phase-shifted by the amount needed to drive the mechanical chopper such that light absorption in the cell occurs in phase with the small acoustic signal produced in the cell by the speaker. Light absorption in the cell increases the magnitude of the signal V_1 giving rise to an increase in its rectified DC signal V_1 . V_2 , which is proportional to $V_1 - V_{REF}$, will then increase so that the amount of attenuation produced by the VCA increases in an attempt to reduce the magnitude of the signal V_1 to the constant, small value it had in the absence of light absorption by the gas sample. The quantity $V_2 \cdot K$ at any time is thus directly proportional to the amount of light absorbed by the gas in the cell.

The performance of the tracking device was tested over a temperature range of -25°C to 57°C , the range relevant to a field environment. Within our ability to measure it, the device tracked the cell's resonant frequency perfectly. The sensitivity for the PA system using the tracking device to acquire the signal compares favorably with the lock-in amplifier results (Figure 4). In both cases the limit to the sensitivity is acoustical noise, not the detection electronics. A systematic increase in the system response of less than 5 percent is observed as the cell temperature is raised from 25°C to 35°C . This change is not due to small temperature induced changes in the ethylene concentration or absorption cross section. More work is needed to fully characterize the origin of this small (< 0.5 percent/ $^{\circ}\text{C}$) responsivity change with temperature. It should be emphasized that this response change is many times smaller than the approximately 80 percent/ $^{\circ}\text{C}$ responsivity change that would occur without the frequency tracking device.

SYSTEM AUTOMATION

The various functions of the PA gas analyzer are controlled by a personal computer. These include laser wavelength tuning, wavelength verification, laser power measurement, zero offset measurement and photoacoustic signal acquisition. The computer also stores a library of absorption cross sections of known compounds and performs the necessary matrix computation to determine the unknown gas concentrations. The computer could also control various flow valves involved in the gas sampling routine. The instrument is autonomous, needing only initial input as to which gases and which laser lines are to be used in the analysis.

GAS MIXTURE ANALYSIS RESULTS

In order to test the ability of the breadboard detector to obtain accurate and reproducible concentrations of gases in mixtures a gas flow and mixing system was assembled. The use of

mass-flow controllers in this system allowed the concentrations of four different gases to be independently varied in nitrogen from low ppb to high ppm values. A sample of this gas mixture was then continuously drawn through the photoacoustic cell. The concentration of any of the gases in the mixture could be quantitatively changed by adjusting the appropriate flow controller.

The four gases chosen for the mixture were hydrazine, methyl bromide, ammonia, and ethylene. Hydrazine was chosen for use in the mixture since it is the most reactive and adsorptive of the hydrazine-fuels. Methyl bromide is widely used as a fumigant. It is among toxic compounds for which improved detection capability is desired by EPA. This compound also was chosen to test the discrimination capability of the instrument. Methyl bromide's spectrum consists of a series of peaks and valleys, that in many instances, are located at the same wavelength positions as peaks and valleys in the spectrum for hydrazine. Ammonia may be present at hydrazine-fuel monitoring locations since it is an important air oxidation product of the hydrazines and it is used as a refrigerant on the Shuttle Transporter. Ethylene is present in typically polluted urban air samples. Seven CO₂ laser lines [10 μ m band lines R(16), R(14), P(14), P(22), P(28), P(30), and P(32)] were selected in order to determine the concentrations of each of these four species in the gas mixtures prepared.

Table I lists the results of five sequential analyses performed on a flowing gas mixture in which the mixture composition was held constant. Any variance in the measured concentrations for these gases reflects instrumental uncertainties and real variances in the gas concentrations. The good repeatability in the measured concentrations here (in all cases less than $\pm 4\%$ standard deviation) indicates the good reproducibility of the technique.

Table II shows results for samples where the concentrations of various components were changed. The first two rows give the results of analyses performed on a mixture of constant composition. The third row shows the results obtained following hydrazine flow termination. The analysis in this case was performed after a several minute delay so that adsorbed hydrazine was completely depleted from the mass flow controller and gas inlet lines. The constant concentrations observed for ethylene, ammonia, and methyl bromide in the first three rows of Table II indicate that the technique can uniquely identify the mixture's components with minimal interference from the other gases present. These results also indicate that the absorption cross-section data used to calculate the concentrations of these four gases have been accurately determined.

The last two rows of Table II show the results of the mixture analysis after the input flows of ethylene, ammonia, and methyl bromide have been reduced by a factor of about two.

Precise control of the flows is difficult so the concentration of each gas does not fall by exactly one-half. The analysis results, however, are in good agreement with the expected concentrations. Reproducibility is also quite good.

The results of several analyses of another mixture in which the ethylene, ammonia, and methyl bromide concentrations were held constant but the hydrazine concentration was varied by changing its flow rate into the gas mixture system are plotted in Fig. 6. Here the measured hydrazine concentration is observed to vary linearly with the hydrazine flow rate set on the mass flow controller. The non-zero intercept and slightly greater than unit slope suggest the presence of small calibration errors in the flow system. Nonetheless, the results shown indicate the accurate detection of hydrazine at concentrations down to below 5 ppb in the presence of 238 ppb of ethylene, 134 ppb of ammonia, and 1.73 ppm of methyl bromide in this mixture. In similar experiments hydrazine was detected in mixtures containing as much as a 600-fold excess of methyl bromide.

TABLE I: Results of Consecutive Mixture Analyses:
Static Mixture Concentrations

RUN	C ₂ H ₄ (ppb)	N ₂ H ₄ (ppb)	NH ₃ (ppb)	CH ₃ Br(ppm)
1.	269	164	270	1957
2.	260	180	255	2036
3.	268	174	275	2003
4.	250	178	280	1976
5.	<u>257</u>	<u>171</u>	<u>269</u>	<u>2003</u>
Ave.	260.8 ±7.9(3.2%)	173.4 ±6.3(4.0%)	269.8 ±6.3(4.0%)	1995 ±9.4(2.7%)

TABLE II: Results of Consecutive Mixture Analyses:
Changing Mixture Concentrations

RUN	C ₂ H ₄ (ppb)	N ₂ H ₄ (ppb)	NH ₃ (ppb)	CH ₃ Br(ppm)
1.	250	82	157	1.80
2.	243	84	155	1.79
N ₂ H ₄ FLOW TERMINATED				
3.	253	0	162	1.76
REDUCED BY ~1/2, C ₂ H ₄ , NH ₃ AND CH ₃ Br CONCENTRATIONS				
4.	121	0	99	1.04
5.	120	0	97	1.02

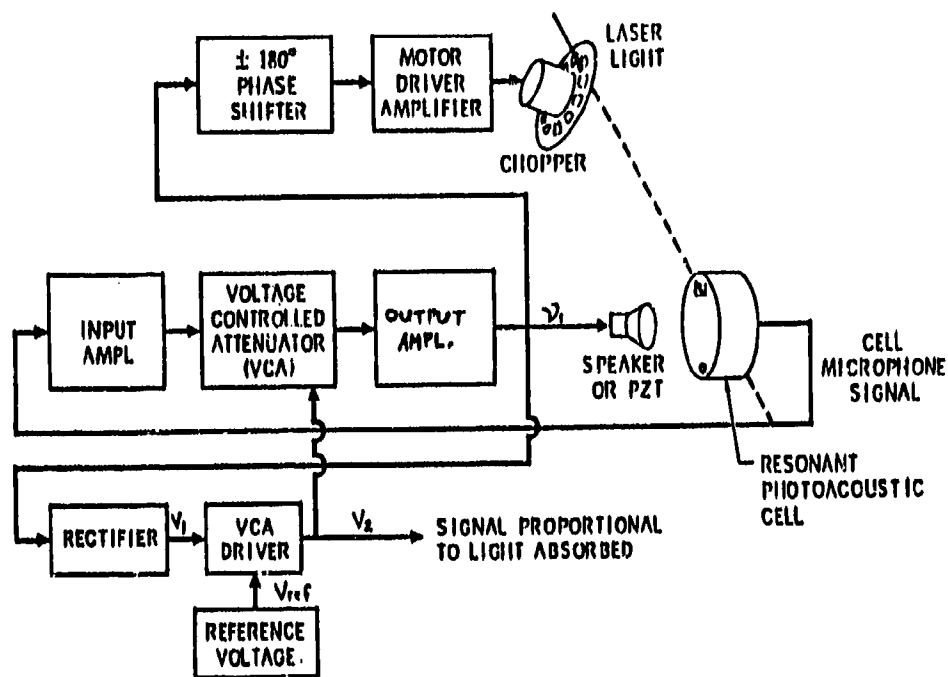


Figure 5. Block diagram of the resonant acoustic frequency tracking and signal acquisition electronics.

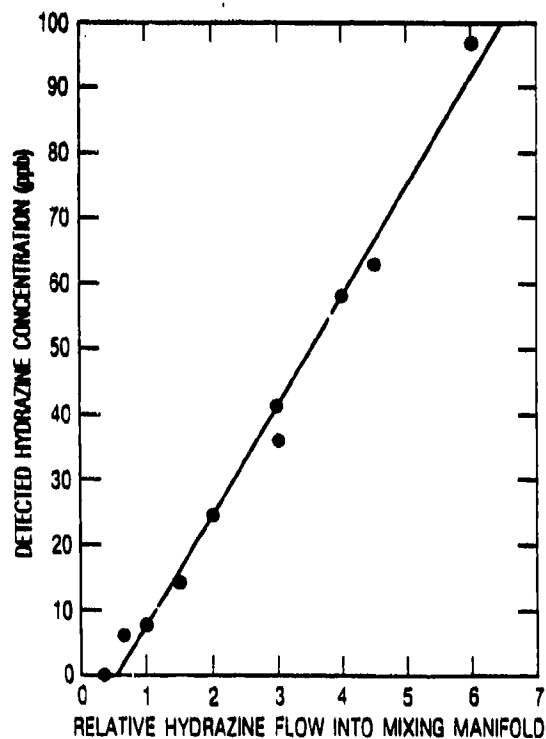


Figure 6. Plot of hydrazine concentration detected by photoacoustic apparatus as a function of the relative flow rate of the hydrazine into the gas mixing manifold. The measurement is in the presence of 238 ppb of acetylene, 134 ppb of ammonia, and 1.7 ppb methyl bromide.

ACKNOWLEDGEMENT

The authors would like to thank Dr. J. A. Gelbwachs for his suggestions and encouragement and Mr. R. A. Clifton for his fine technical assistance.

REFERENCES

1. L. B. Kreuzer, N. D. Kenyon and G. K. N. Patel, Science 177, 347 (1972).
2. S. M. Beck, Appl. Opt. 24, 1761 (1985).
3. G. L. Loper, A. R. Calloway, M. A. Stamps and J. A. Gelbwachs, Appl. Opt. 19, 2726 (1980).
4. G. L. Loper, J. A. Gelbwachs and S. M. Beck, Can. J. Phys. 64, 1124 (1986).
5. B. D. Green and I. I. Steinfeld, Environ. Sci. Technol 10, 1134 (1976).
6. R. A. McClatchey, W. S. Benedict, S. A. Clough, D. E. Burch, R. F. Calfee, K. Fox, L. S. Rothman and J. S. Garing, AFCRL Atmospheric Absorption Line Parameters Compilation. Report No. AFCRL-TR-73-0096, Air Force Cambridge Research Laboratory, Bedford, MA 1973.
7. L. B. Kreuzer, Anal. Chem. 46, 239A (1974); C. F. Dewey, R. D. Kamm, and C. E. Hackett, Appl. Phys. Lett. 23, 633 (1973); E. Max, L. G. Rosengren, Optics Comm. 11, 422 (1974); P. D. Goldan, and K. Goto, J. Appl. Phys. 45, 4350 (1974); G. L. Loper, R. A. Calloway, M. A. Stamps, and J. A. Gelbwachs, Appl. Opt. 19, 2726 (1980).
8. R. Gerlach and N. M. Amer, Appl. Phys. 23, 319 (1980).
9. R. L. Corbin, G. L. Loper, and S. M. Beck to be submitted to Rev. Sci. Inst. (1987).

SECTION VII

TOXICOLOGY

OCCUPATIONAL SAFETY CONSIDERATIONS WITH HYDRAZINE

Lt Col Harvey J. Clewell III, Deputy Director
Toxic Hazards Division

Harry G. Armstrong Aerospace Medical Research Laboratory
Wright-Patterson Air Force Base, Ohio 45433

Major James N. McDougal, PhD
Marilyn E. George
Malvin E. Andersen, PhD

ABSTRACT

Hydrazine is a reducing agent that is most commonly used as a propellant and as an oxygen scavenger in boilers. Hydrazine is extremely irritating and has been demonstrated to produce both acute and chronic toxicity. As a result, the established permissible inhalation exposure limits are very low, and respiratory protection is required whenever vapors are present. Liquid hydrazine penetrates the skin and produces a chemical burn; therefore, some protective measures must also be taken to protect the skin from liquid contact. Often, however, a cumbersome, whole-body protective suit is worn to protect against skin contact with vapor as well. To what extent it is actually necessary to protect skin from vapor penetration had not previously been demonstrated. In an attempt to answer this question, we conducted a study with rats to compare the dermal penetration of hydrazine vapor with inhalation. Pharmacokinetic modeling was used to compare body burdens resulting from these different routes of exposure. The analysis concluded that the vapor concentration during a skin-only exposure would have to be at least 200 times higher than that during inhalation to achieve the same body burden. This type of estimation illustrates the use of predictive toxicology in occupational exposures.

INTRODUCTION

Hydrazine is a hypergolic fuel used in the Titan missile, in space shuttle auxiliary power units, in F-16 aircraft emergency power units, in boiler water as an oxygen scavenger, and in some chemical manufacturing processes. Hydrazine is a polar base with a great affinity for water and is therefore extremely irritating to eyes and mucous membranes. Hydrazine fumes in air and has a characteristic odor similar to that of ammonia. The National Institute for Occupational Safety and Health (NIOSH) has estimated that 90,000 workers could be exposed to hydrazine or hydrazine salts each year (1). When absorbed, hydrazine can rapidly cause convulsions, respiratory arrest, or cardiovascular collapse in humans and laboratory animals (2,3).

A few instances of hydrazine toxicity in humans have been reported. Dermal sensitization after exposure to hydrazine has been cited (4,5). Accidental ingestion of a concentrated aqueous solution of hydrazine by a workman caused prolonged unconsciousness and seizures; however, he was considered reasonably recovered within two weeks (6). Hydrazine toxicity has been fatal in at least one case in which an individual experienced conjunctivitis, nausea, and tremors each time he handled hydrazine. After six months of repeated exposure he was admitted to the hospital and, after three weeks, died despite treatment (7). The autopsy showed areas of granular degeneration of heart muscle, renal tubular necrosis with interstitial hemorrhage, and hepatic necrosis.

In laboratory animals, exposure to hydrazine may produce either immediate toxicity or delayed kidney and liver injury in animals that survive the exposure. Via inhalation, the 4-hr LC50 of hydrazine is 250 ppm for mice and 580 ppm for rats (8). In another study, the 1-hr LC50 in rats was 640 ppm (9). A six-month inhalation study conducted with dogs, monkeys, rats, and mice suggested that effects were dose-related regardless of whether the exposures were intermittent or continuous (10). Long-term intermittent inhalation exposure in rats, mice, hamsters, and dogs demonstrated that rats and hamsters were sensitive to the tumorigenic action of hydrazine (11). Hydrazine has been shown to enter the body via

the skin. In anesthetized dogs, topical application of hydrazine, in the hundreds of milligram per kilogram range, produces detectable blood concentrations within 30 seconds and a chemical burn at the site of application (12). Percutaneous absorption of hydrazine in the rabbit has been shown to occur with anhydrous hydrazine and 70% aqueous solutions of hydrazine (13,14).

These and other studies suggest that hydrazine exposure via the inhalation route or direct contact with skin should be prevented. As a result, very low permissible inhalation exposure limits have been set. For example, the American Conference of Governmental Industrial Hygienists (ACGIH) have recommended a threshold limit value (TLV) for hydrazine of 0.1 ppm. Because of uncertainty concerning the relative importance of skin exposure to hydrazine vapor, it is commonly required that individuals working with hydrazine wear a self-contained protective ensemble to provide full-body protection. To determine whether full body protection against hydrazine vapor is actually necessary, the relative importance of the skin as a route of entry must be estimated. In a recent study using a specially designed dermal vapor exposure chamber (15), we showed that, in rats, hydrazine vapor penetrates skin relatively slowly compared to other chemicals. The purpose of this simulation effort was to estimate a dermal equivalent of the permissible hydrazine inhalation exposure level in order to establish realistic guidelines for ensuring the personal safety of individuals exposed to hydrazine vapor.

METHODS

A pharmacokinetic model for hydrazine exposure in rats, written using the Advanced Continuous Simulation Language (16) on an IBM PC/AT, was used to estimate body burdens and blood concentrations after skin-only and inhalation exposures to hydrazine vapors. The pharmacokinetic description used in this analysis was a modification of the two-compartment model described previously (15), that simplified the body into blood and deep compartments. Regardless of the route of exposure, hydrazine was described as appearing directly in the blood compartment,

the volume of which is 5% of body weight. The deep compartment represents the hydrazine in tissues that is not available for assay. The volume of the deep compartment is 55% of body weight, which is approximately the volume of interstitial plus intracellular fluids. Parameters in the model describing the distribution, binding, and clearance of hydrazine in the animal were established on the basis of intravenous studies (15,17). The parameter estimation was performed using Simusolv (18) on a VAX 8530 to optimize the agreement between the model predictions and the experimental data (Figure 1).

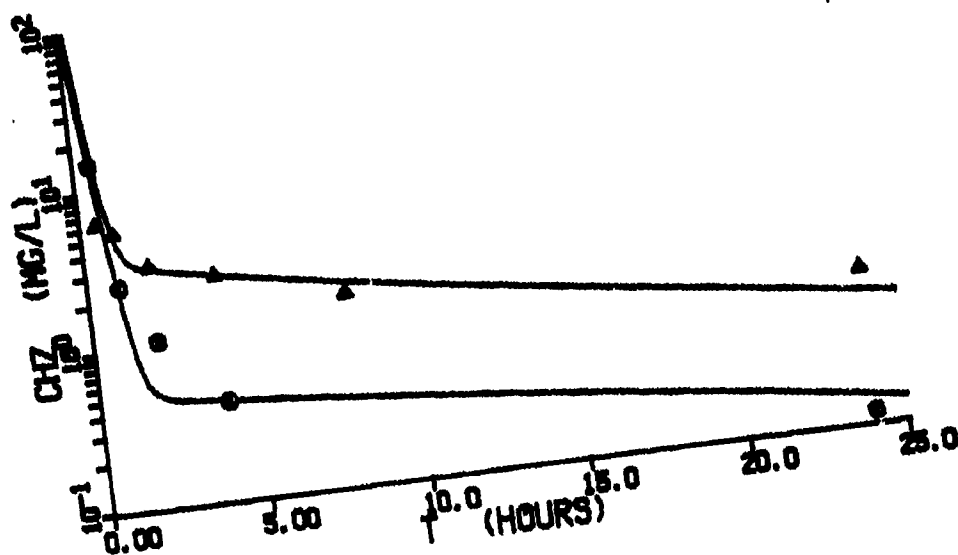


Figure 1. Model-Predicted and Experimental Blood Concentrations for Intravenous Doses of 12 and 6 mg/kg of Hydrazine.

The route-to-route extrapolation capability of the model was validated by comparing its predictions for a 10 ppm inhalation exposure with actual data obtained in our laboratory (17). The comparison between the model predictions and the inhalation data shown in Figure 2 was obtained without any adjustment of the model parameters from those used for the intravenous case.

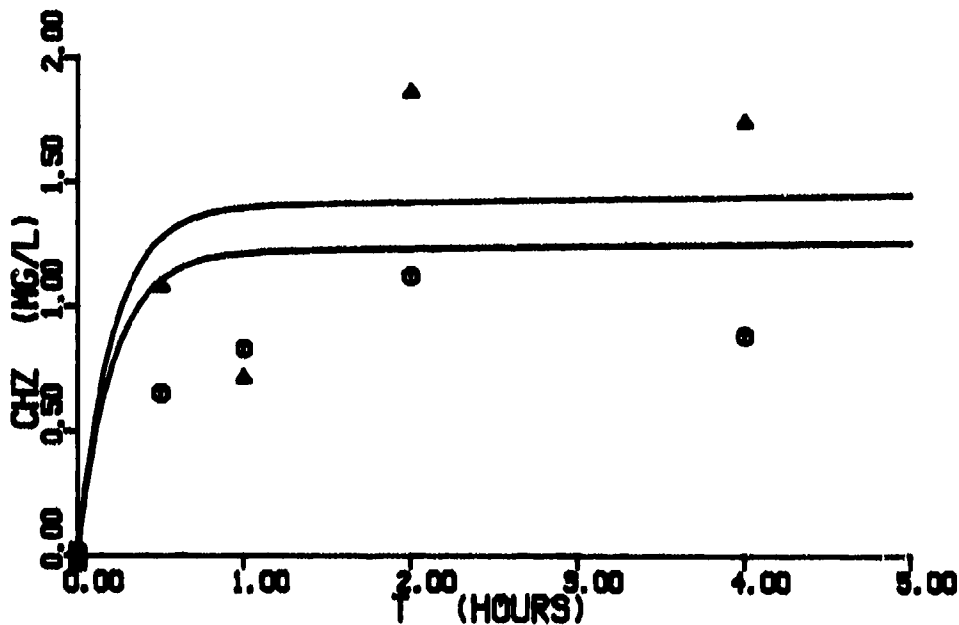


Figure 2. Model-Predicted and Experimental Blood Concentrations for Inhalation Exposures at 10.7 and 9.3 ppm Hydrazine.

The permeability constant for hydrazine vapor in rats was determined by modeling of the skin-only vapor exposure data (Figure 3). The model was then used to simulate 8-hr dermal vapor exposures at increasing hydrazine vapor concentrations until predicted blood concentrations and total body burden of hydrazine matched those achieved in a simulated 8-hr inhalation exposure at the current TLV (0.1 ppm). The equivalent dermal exposure concentration was used to provide an estimate of the recommended dermal exposure limit required to ensure a safe dermal exposure to hydrazine vapor in the presence of respiratory protection.

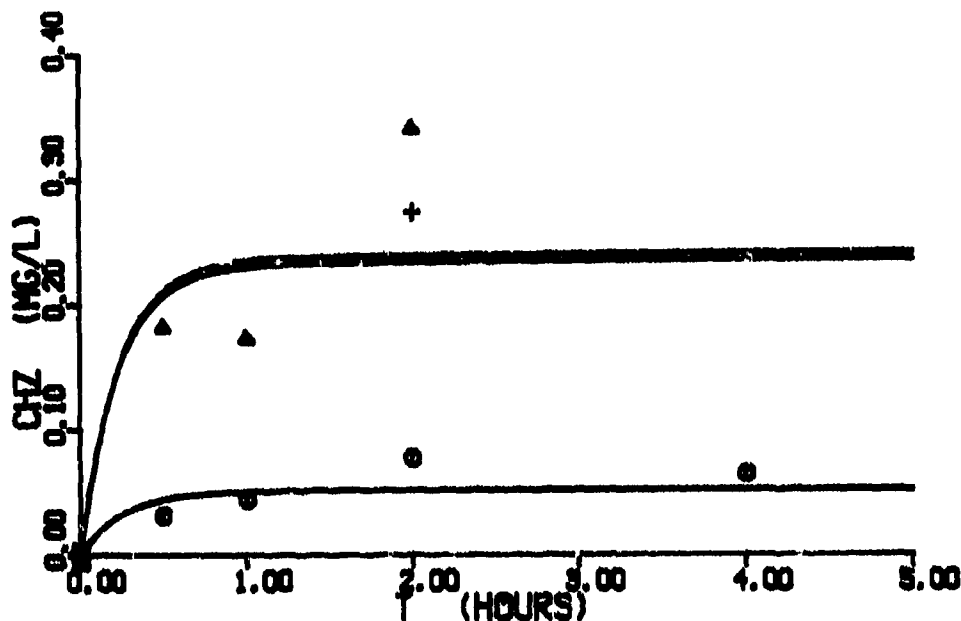


Figure 3. Predicted and Experimental Blood Concentrations for Skin-Only Vapor Exposures at 486, 476, and 105 ppm.

RESULTS AND DISCUSSION

The results of the modeling of intravenous, inhalation, and dermal vapor exposures are shown in Figures 1, 2, and 3, respectively. Based on this analysis, the skin permeation coefficient for hydrazine vapor is approximately 0.06 cm/hr. According to the simulation, a 20 - 30 ppm hydrazine vapor concentration would be required to produce, in a skin-only exposure, the same blood concentrations and body burden of hydrazine as an inhalation exposure at the TLV. That is, it is predicted that more than a 200:1 ratio of dermal-to-inhalation exposure concentrations would be required to produce the same body burden. Thus the modeling suggests that if hydrazine vapor concentrations do not exceed 20 ppm, respiratory protection and protection against liquid contact are all that would be required for safety.

Several assumptions are inherent in estimating this safe skin-only value; among these are the assumptions that this ratio would be similar in humans and rats, that the skin itself is not a significant reservoir for hydrazine, and that there is no direct effect of hydrazine in the skin. Even with these assumptions this estimate is likely to be conservative, and we are currently conducting studies to evaluate the ability of the skin to act as a reservoir and potential target for hydrazine.

This approach for estimating safe skin-only exposure levels could be generally applied to other toxic vapors suspected of causing systemic effects via skin penetration. Provided that vapor permeation coefficients are either known or can be determined, the calculation of equivalent body burden can be used with inhalation TLVs to estimate skin-only values. This approach could provide a method for use by ACGIH in assigning quantitative skin notations.

REFERENCES

- 1 National Institute for Occupational Safety and Health,
Occupational Exposure to Hydrazine, DHEW No. 78-172,
1978.
- 2 Clark, D.A., J.D. Bairrrington, H.L. Bitter, F.L. Coe,
M.A. Medina, J.H. Marrit and W.N. Scott, "Pharmacology
and Toxicology of Propellant Hydrazines," USAF School of
Aerospace Medicine Review, 1968.
- 3 Back, K.C. and A.L. Thomas, "Aerospace Problems in
Pharmacology and Toxicology," Ann. Rev. Pharmacol.,
vol. 10, p. 395, 1970.

- 4 Evans, D.M., "Two Cases of Hydrazine Hydrate Dermatitis Without Systemic Intoxication," Br. J. Ind. Med., vol. 16, p. 126, 1959.
- 5 Hovding, G., "Occupational Dermatitis from Hydrazine Hydrate Used in Boiler Protection," Acta Dermato-Venereologica, vol. 47, p. 293, 1967.
- 6 Reid, F.J., "Hydrazine Poisoning," Br. J. Med., vol. 2, p. 1246, 1965.
- 7 Sotaniemi, E., J. Hirvonen, H. Isomaki, J. Takkanen and J. Kaila, "Hydrazine Toxicity in the Human - Report of a Fatal Case," Ann. Clin. Res., vol. 3, p. 30, 1971.
- 8 Jacobson, K.H., J.H. Clem, H.J. Wheelwright, Jr., W.E. Rinehart and N. Mayes, "The Acute Toxicity of the Vapors of Some Methylated Hydrazine Derivatives," A.M.A. Arch. Ind. Health, vol. 12, p. 609, 1955.
- 9 Comstock, C.C., L.H. Lawson, E.A. Green and F.W. Oberst, "Inhalation Toxicity of Hydrazine Vapor," A.M.A. Arch. Ind. Health, vol. 10, p. 476, 1954.
- 10 Haun, C.C. and E.R. Kinkead, "Chronic Inhalation Toxicity of Hydrazine," Proceedings of the 4th Annual Conference on Toxicology, 1973, p. 351.
- 11 Vernot, E.H., J.D. MacEwan, R.H. Bruner, C.C. Haun, E.R. Kinkead, D.E. Prentice, A. Hall III, R.E. Schmidt, R.L. Eason, G.B. Hubbard and J.T. Young, "Long-term Inhalation Toxicity of Hydrazine," Fundam. Appl. Toxicol., vol. 5, p. 1050, 1985.

- 12 Smith, E.B. and D.A. Clark, "Absorption of hydrazine through canine skin," Toxicol. Appl. Pharmacol., vol. 21, p. 186, 1972.
- 13 Keller, W.C., J.P.F. Murphy, M.E. Andersen and K.C. Back, Percutaneous toxicokinetics of hydrazine and H-70 in the rabbit, AFAMRL-TR-81-13, 1981.
- 14 Keller, W.C., J.P.F. Murphy, R. H. Bruner, M.E. Andersen and C.T. Olson, Toxicokinetics of hydrazine administered percutaneously to the rabbit, AFAMRL-TR-84-035, 1984.
- 15 McDougal, J.N., M.E. George, H.J. Clewell III, M.E. Andersen and D.L. Pollard, "Dermal absorption of hydrazine vapors," 1985 JANNAF Safety and Environmental Protection Subcommittee Meeting, CPTA Publication 436, 1985, p.299.
- 16 Advanced Continuous Simulation Language (ACSL), Mitchell and Gauthier Associates, Inc., Concord, Massachusetts.
- 17 Haddad, T.S., personal communication.
- 18 SimuSolv Computer Program, Dow Chemical Company, Midland, Michigan.

SECTION VIII

RECOMMENDATIONS FOR FUTURE RESEARCH

The concluding session of the conference was a group discussion. Conference participants were asked to give their recommendations for additional research in the general area of the environmental chemistry of hydrazine fuels. Comments were solicited from speakers in each of the five general presentation areas, in turn. After the speaker comments, any additional thoughts from the group as a whole were noted. Comments are summarized below, by session.

It is hoped that these comments will assist both researchers and managers in assessing the need for a continued long-term commitment to an increased understanding of the environmental chemistry of hydrazine fuels.

Gas-Phase Kinetics and Models

- More emphasis is needed on chamber studies which address the fundamental chemical reactions, resulting products, and mechanisms of the reactions of hydrazine fuels in the urban troposphere.
- Toxic products are often formed. These are not well characterized in terms of their eventual fate.
- Understanding reaction rates in 'real' atmospheres is essential if the kinetics of these fuels is to be successfully modeled (i.e., reactions with ozone, oxides of nitrogen, hydroxyl radicals, and other reactive species).
- This implies the need for more fundamental and elementary reaction studies which emphasize homogeneous processes.
- Existing atmospheric dispersion models for toxic materials which include provision for hydrazine fuels, do not, in general, include any atmospheric chemistry in their concentration calculations. This deficiency could be corrected with the proper kinetic studies as described above.
- Such 'second-generation' models would give much more realistic "worst case" concentration profiles and will become a virtual necessity under new, lower exposure criteria.
- From a practical standpoint, most of the large hydrazine storage areas involve concrete or asphalt containment surfaces. More work is needed to characterize the details of interactions of hydrazine vapor with these types of surfaces.

- Similarly, many 'operational' surfaces are not yet well characterized with respect to their effects on the air chemistry of hydrazine fuel vapors.

Soil, Surface, and Matrix Isolation Studies

- During the course of several previous studies, some progress has been made in our understanding of hydrazine and MMH interactions with soils. However, virtually nothing is known about UDMH behavior in soil systems.
- One particular area of limited past research is the chemical degradation products of hydrazine fuels in soil systems. A corollary to this is how these degradation products interact with the colloidal constituents of soils.
- The area of structure/interaction relationships is totally unexplored. From both the perspective of the soil and the hydrazine fuel or its products, this could be a powerful predictor of potential reactions.
- Another generally unknown factor is the effect of biological or microbial activity on the stability of hydrazine fuels in soils.
- Hydrazine is a unique molecule with properties which make it a powerful probe of soil systems when coupled with appropriate spectroscopic instrumentation. Taking advantage of this probe has great potential for new information on the molecular interaction mechanisms of hydrazine fuels in soil systems.
- All possible analytical techniques should be brought to bear on the complex problems of understanding both macro- and microscopic hydrazine fuel - soil interactions.
- An increased understanding of hydrazine fuels - soil interactions can be applied to many other similar chemicals by inference.
- Many more parametric studies are needed to characterize macroscopic interactions: i.e., pH, soil type, aerobic versus anaerobic, etc.

Hydrazine Disposal Studies

- Clearly, in today's heavily regulated environment, studies must be undertaken to completely characterize the components of effluents from treatment systems. Many times only the primary pollutant (i.e., the hydrazine fuel) or its direct treatment product is monitored. Many more intermediates are often formed that have not yet been completely identified.

- The treatment of intermediates must also be directly addressed once their chemical composition is definitely known.
- In analyzing the effectiveness of disposal treatment processes more attention must be paid to material balances. If we cannot account for all of the influent there may be serious deficiencies in either the analysis scheme or the treatment process or both.
- Once acceptable treatment procedures are established, proper protocol must be maintained to protect the safety of emergency or facility personnel.
- The potential utility of gelling agents for use in controlling the spread and evaporation of hydrazine fuel spills should be studied.

Detection and Monitoring

- Market demands, corporate combinations, and other factors have led to a general decline in performance of commercial hydrazine detectors. There do not appear to be any commercially available units which are able to reliably detect hydrazines at currently mandated exposure levels.
- This is a somewhat specialized market and the demand tends to be localized to some Air Force and NASA locations. Therefore, commercial vendors are reluctant to commit major resources to new product development.
- The situation dictates a government-funded research effort to produce the required detectors. Though some such efforts are underway, the feeling is that much more work remains in this area and it will require continued interest and funding.
- All types of monitors are needed: area, point, and dose.
- A resource list for experts in hydrazine detector technology should be compiled. This would give users points of contact for questions like "which detector is best for this situation?" or "which detection scheme would work best under these circumstances?".
- Perhaps those who use hydrazine detectors or published detection schemes would be interested in conducting a series of round-robin tests to compare results between labs.

Toxicology

- Improved toxic effects and toxicokinetic models need to be developed to determine how chemicals affect animals and humans. Scientifically sound models could provide a powerful tool for setting more realistic exposure limits than the current order-of-magnitude estimating techniques.

- There needs to be some mechanism for the periodic reevaluation of the toxicity of chemicals. As exposure recommendation experimental protocol evolves, many chemicals may have their allowed concentration levels significantly altered. Generally, any change in exposure level has substantial implications in either additional costs or substantial savings.